The Effect of Adiponectin and Adiponectin Receptors in Bone

Aneka I Sowman



Supervisors

Prof. James Edwards

Dr Sam Olechnowicz

Nuffield Dept. of Rheumatology, Orthopaedics and Musculoskeletal Sciences

University of Oxford

A thesis submitted for the degree

Doctor of Philosophy

Trinity Term 2019

For Sarala Gramopadhye

For her love and her bravery

Declaration

All the work presented in this thesis is the result of my own work unless otherwise stated and does not constitute part of any other thesis. The work herein described was carried out while I was a graduate student of the Nuffield Department of Orthopaedics, Rheumatology and Musculoskeletal Sciences at the Botnar Research Centre under the supervision of Associate Professor James Edwards and Dr Sam Olechnowicz.

Acknowledgements

I would first like to thank my supervisors, Prof. James Edwards and Dr Sam Olechnowicz, for giving me this opportunity and for their unlimited support and invaluable insight that were so critical for its completion. Your seemingly endless optimism and definitely endless patience are also hugely appreciated.

Thanks go to Dr Sally-Ann Clark for her vast knowledge, guidance and help in the confusing world of FACS, to Neil Ashley for his work preparing and sequencing primary cells, and to Dr Srinivasa Rao for his bioinformatics expertise in the analysis of this sequencing work. Thank you to Dr Jennifer Hill for her help in running the Luminex screens, to Felix Richter for his careful handling of the osmium tetroxide staining, and to Dr Stefan Kluzek for his help and advice with the work on the Chingford Study. Thanks also to Dr Adam Cribbs for making my first foray into research life during my undergraduate years such a positive and motivating experience, and for his insight and help throughout the course of this project.

Huge thanks are due to the extended Edwards' lab group for providing such an enjoyable environment of which to be a part for four years. Particular thanks go to Prof. Claire Edwards, Dr Emma Morris, Dr Beatriz Gámez Molina, Dr Jessica Whitburn, Dr Srinivasa Rao and Dr Christina Turner for their scientific insight, and for always making things better when they could, easier when they couldn't make them better, and funnier when they couldn't make them easier. For every lab meeting discussion and lunchtime piece of cake that it took to get me here, thank you.

Thank you to my fellow residents of Sophie's house, Séverin and Bradley, who made our little flat such a lovely respite from lab life. Thanks also to my DPhil room friends Quitterie and Laura for celebrating and commiserating every high and low of PhD student life with me.

Thank you to my lovely friends who have stuck with me throughout years of my nonsense and continue to make my life such a joy. To Lucy and Emilie, my day one Hughsies, without whom I have never known Oxford and never wish to. To Nat and Alia, who always remind me what being home feels like. And to Alice, who always shows me that all that is needed for happiness is good friends and a cup of tea.

Thank you to Debbie, for her constant and varied supply of books, tea, and gin & tonic as the situation demanded, and to Paul, whose gentle words of perspective were more helpful than perhaps even he realised.

Thanks to my big brother Jon who made doing this look far easier than it turned out to be. Remember when you suggested I should 'just' do a PhD? I do.

Thank you to my parents, Colin and Shubha, for their unfailing love and support. From hand-drawn smiley faces on spelling tests and answering my endless childhood questions about where rain comes, to proof-reading this thesis and encouraging me to ask questions that as yet have no known answer: your support has changed, but your love never has. I appreciate it all.

And finally, thank you to Jonny, for always being the light at the end of the tunnel. The darker it gets, the brighter you shine.

Publications and Achievements

Publications

Sowman A, Sanchez-Santos MT, Hart D, Spector T, Arden NK, Kluzek S, Edwards JE. Serum Adipokines and Bone Mineral Density in a Community-Based Cohort of Middle-Aged Women: A Cross-Sectional and Prospective Study (in preparation for Journal of Clinical Endocrinology and Metabolism, expected 2020)

Morris EV, Suchacki KJ, Hocking J, Cartwright R, **Sowman A**, Gamez B, Lea R, Drake MT, Cawthorn WP, Edwards CM. Myeloma Cell Down-Regulation of Adiponectin in Bone Marrow Adipocytes Promotes Growth and Survival via TNF-alpha (under review at Journal of Bone and Mineral Research, expected 2020)

Gamez B, Morris EV, Olechnowicz SWZ, Webb S, Sowman A, Turner CJ, Edwards CM. Preventative Metformin Treatment Increases Myeloma Tumor Burden and Bone Disease In Vivo (under review at Journal of Hematology and Oncology, expected 2020)

Roberts S, Colombier P, **Sowman A**, Mennan C, Rölfing JHD, Guicheux J, Edwards JR. Ageing in the Musculoskeletal System: Cellular Function and Dysfunction Throughout Life. Acta Orthopaedica, 87 (Suppl 363): 15-25, 2016.

Presentations

Sowman A, Olechnowicz SWZ, Edwards JR. AdipoR1 Deficiency Leads to Low Bone Mass and Increased Bone Marrow Adiposity In Vivo. June 2017, Bone Research Society Meeting, Bristol UK.

Sowman A, Olechnowicz SWZ, Edwards JR. AdipoR1 Deficiency Leads to Low Bone Mass and Increased Bone Marrow Adiposity In Vivo. August 2017, Bone Marrow Adiposity Meeting, Lausanne Switzerland.

Posters

Sowman A, Olechnowicz SWZ, Kluzek S, Arden NK, Edwards JR. Dysregulated Adiponectin Signalling via AdipoR1 Deletion Leads to Bone Loss and Increased Marrow Adiposity In Vivo Through Distinct Local and Systemic Mechanisms and in Contrast to Epidemiological Evidence. September 2019, American Society for Bone and Mineral Research Conference, Orlando Florida.

Sowman A, Sanchez-Santos MT, Hart D, Spector T, Arden NK, Kluzek S, Edwards JE. Serum Adiponectin Concentrations Are Inversely Associated with Bone Mineral Density in a Community-Based Cohort of Middle-Aged Women. June 2018, Bone Research Society Meeting, Winchester UK.

Awards

The Bone Research Society Best Oral Presentation award – for presentation at the Bone Research Society Meeting, Bristol UK, 2017.

The Bone Research Society Best Basic Science Abstract award – for abstract submitted to the Bone Research Society Meeting, Bristol UK, 2017.

The Bone Research Society New Investigator award – for abstract submitted to the Bone Research Society Meeting, Bristol UK, 2017.

Abstract

The adipokine adiponectin exerts many complex endocrine and paracrine biological effects, particularly regulation of insulin sensitivity and glucose homeostasis. Despite bone marrow cells producing the majority of adiponectin, its role in bone accrual and homeostasis remains controversial, with contradictory reports from human and mouse studies. Adiponectin receptors AdipoR1 and AdipoR2 are expressed widely in cells of the bone and bone marrow and signal primarily through activation of AMPK and PPARα. The aim of this project was to characterise further the role of adiponectin in bone using novel mouse models and epidemiological data from a large cohort study.

In the first prospective study of its kind, analysis of a large, population-based cohort of healthy, post-menopausal women revealed adiponectin to be negatively associated, and the leptin to adiponectin ratio to be positively associated, with hip BMD both cross-sectionally and five years prospectively following adjustment for age, BMI and smoking status. Circulating leptin levels did not associate with hip BMD and showed a significant relationship only with prospective lumbar spine BMD. These results indicate adiponectin and the adiponectin to leptin ratio as significant clinical correlates of osteoporotic development and progression.

Female mice deficient in AdipoR1 or AdipoR2 showed significantly retarded bone accrual and accelerated bone loss in middle age as compared with controls as determined by μCT analysis, and in AdipoR1 females, this low bone volume was associated with significant alterations in the biomechanical properties of the bone throughout life. Young female AdipoR1 knockout mice were further characterised by histology, and while osteoblast and osteoclast parameters were unchanged, osmium tetroxide staining showed significantly increased bone marrow adiposity. FACS-based isolation and RNASeq of bone marrow stem cells did not suggest any mechanistic genes for these changes. The altered blood chemistry profile of young female AdipoR1-deficient mice indicated a whole-body alteration in mineral metabolism, although a significant indirect effect on the bone was not conclusively identified. *In vitro* investigation found stimulation of AdipoR1 inhibited the osteogenic potential of a murine pre-osteoblast cell line while knockdown of AdipoR1 stimulated it, in contrast with the *in vivo* findings.

The epidemiological data identifying adiponectin as a negative correlate of BMD suggests adiponectin could represent a valuable candidate for the unmet clinical need of a biomarker of osteoporotic incidence and development. In two pre-clinical murine models, the association between adiponectin and bone volume was positive, although this response was inverted *in vitro*. These results suggest adiponectin has complex effects on the bone, with indirect endocrine effects having a positive effect on bone, and direct local effects negatively regulating bone and bone marrow adipose tissue itself.

List of Abbreviations

4-MUP	4-Methylumbelliferyl phosphate
AdipoR1/2	Adiponectin receptor 1/2
AdipoQ	Adiponectin
AKT	Protein Kinase B
αMEM	Minimum Essential Medium Eagle - alpha modification
ALPL	Alkaline phosphatase
AMPK	AMP kinase
ANOVA	Analysis of variance
APPL1/2	Adaptor protein containing pleckstrin homology domain, phosphotyrosine binding domain and leucine zipper motif 1/2
Atg	Autophagy
BAT	Brown adipose tissue
BFR	Bone formation rate
BMA	Bone marrow adipocytes
BMAT	Bone marrow adipose tissue
BMAT/BV	Bone marrow adipose tissue/bone volume
BMD	Bone mineral density
BMI	Body mass index
BMP	Bone morphogenic protein
BMU	Bone multicellular unit
BSA	Bovine serum albumin
BV/TV	Bone volume/tissue volume

CaMKIIα	Calcium/calmodulin-dependent protein kinase-IIα
cDNA	Complementary deoxyribose nucleic acid
CEBP	CCAAT/enhancer-binding protein
cMAT	Constitutive bone marrow adipose tissue
cMAT/BV	Constitutive bone marrow adipose tissue/bone volume
Col1a1	Collagen type I α-1
DEXA	Dual X-ray absorptiometry
DKK1/2	Dickkopf protein 1/2
DMEM	Dulbecco's Modified Eagle Medium
DMP1	Dentin matrix protein 1
DMSO	Dimethyl sulfoxide
ECL	Enhanced chemiluminescence
EDTA	Ethylenediaminetetraacetic acid
ELISA	Enzyme-linked immunosorbent assay
Enho	Energy homeostasis associated
ER	Endoplasmic reticulum
EtOH	Ethanol
FABP4	Fatty acid binding protein 4
FACS	Fluorescence-assisted cell sorting
FBS	Foetal bovine serum
FGF	Fibroblast growth factor
FMO	Fluorescence minus one
GAL	Galanin
GALR2	Galanin receptor 2

GAPDH	Glyceraldehyde-3-phosphate dehydrogenase
GFP	Green fluorescent protein
GPCR	G-protein coupled receptor
GSK3β	Glycogen synthase kinase-3β
H&E	Haemotoxylin and eosin
HCl	Hydrochloric acid
HDL	High density lipoprotein
HMW	High molecular weight
HRP	Horseradish peroxidase
HSC	Haematopoietic stem cell
IBMX	3-isobutyl-1-methylxanthine
IGF	Insulin-like growth factor
IgG	Immunoglobulin G
IL	Interleukin
IMPC	International mouse phenotyping consortium
IMS	Industrial methylated spirits
IRS	Insulin receptor substrate proteins
Ldoc1	Leucine zipper, down-regulated in cancer-1
L1-4	Lumbar vertebra 1-4
LMW	Low molecular weight
LDLR	Low-density lipoprotein receptor
LRP	Low-density lipoprotein related receptor
MAPK	Mitogen-activated protein kinase
MAR	Mineral apposition rate

MCSF	Macrophage colony stimulating factor
µCT	Micro-computed tomography
MMA	Methylmethacrylate
MMW	Middle molecular weight
(m)RNA	(Messenger) ribonucleic acid
MSC	Mesenchymal stem cell
MSK	Musculoskeletal
NaOH	Sodium hydroxide
NICD	Notch intracellular domain
OCN	Osteocalcin
OPG	Osteoprotegerin
OPN	Osteopontin
PBS	Phosphate buffered saline
PE	Phycoerythrin
PES	Polyethersulfone
PI3K	Phosphatidylinositol 3-kinase
PPAR	Peroxisome proliferator-activated receptor
PTH	Parathyroid hormone
(q)PCR	(Quantitative) polymerase chain reaction
RA	Rheumatoid arthritis
RANK	Receptor activator of nuclear factor (NF) κB
RANKL	RANK ligand
rMAT	Regulated bone marrow adipose tissue
rMAT/BV	Regulated bone marrow adipose tissue/bone volume

RNASeq	RNA sequencing
ROI	Region of interest
RT	Room temperature
Runx2	Runt-related transcription factor 2
shRNA	Short hairpin RNA
siRNA	Small interfering RNA
SNP	Single nucleotide polymorphism
SOST	Sclerostin
TBS	Tris buffered saline
TBST	TBS-tween
TCF	T cell factor
TGFβ	Transforming growth factor-β
TMD	Tissue mineral density
TNFα	Tumour necrosis factor-α
TRAP	Tartrate-resistant acid phosphatase
TZD	Thiazolidinediones
UCP1	Uncoupling protein-1
UV	Ultraviolet
WAT	White adipose tissue

Table of Contents

Declaration ... III

Acknowledgements ... IV

Publications and Achievements ... VI

Abstract ... VIII

List of Abbreviations ... IX

List of Figures ... XIX

List of Tables ... XXIV

CHAPTER 1: INTRODUCTION ... 1

1.1 The bone ... 1

1.1.1 The structure and function of bone ... 2

1.1.2 The cellular components of bone ... 4

1.1.3 The basic multicellular unit and the bone remodelling cycle ... 16

1.1.4 The inorganic components of bone ... 19

1.2 Adipose tissue ... 20

1.2.1 White adipose tissue ... 22

1.2.2 Brown adipose tissue ... 25

1.2.3 Bone marrow adipose tissue ... 27

1.3 Adiponectin ... 33

1.3.1 Structure and circulating levels ... 33

1.3.2 Adiponectin receptors ... 35

1.3.3 Adiponectin in health and disease ... 43

1.4 Adiponectin in the bone ... 46

1.4.1 Human evidence ... 47

1.4.2 Pre-clinical evidence ... 50

1.5 Project aims and hypothesis ... 59

CHAPTER 2: MATERIALS AND METHODS 60

2.1 *In vivo* and *ex vivo* 60

2.1.1 Animal models 60

2.1.2 Genotyping 61

2.1.3 Gross morphology measurements 64

2.1.4 µCT analysis 65

2.1.5 Histomorphometry 68

2.1.6 Biomechanical testing 72

2.1.7 Collection of blood serum and bone marrow plasma 72

2.1.8 Enzyme-linked immunosorbant assays (ELISAs) 73

2.1.9 Luminex assays 74

2.1.10 Bone formation rate 75

2.1.11 Osmium tetroxide staining 77

2.1.12 FACS analysis of bone lining cells 78

2.2 *In vitro* 84

2.2.1 Cell culture and maintenance 84

2.2.2 Alamar Blue assay 86

2.2.3 RNA manipulation 87

2.2.4 Alkaline phosphatase activity assay 91

2.2.5 Protein manipulation 92

2.2.6 Adipocytic differentiation and staining of cell lines 93

2.2.7 Osteoblastic differentiation and staining of cell lines 96

2.2.8 Creation of a stable knockdown cell line 98

2.2.9 Statistical analysis 103

CHAPTER 3: SERUM ADIPOKINES AND BMD: A CROSS-SECTIONAL AND PROSPECTIVE STUDY 104

3.1 Introduction 104

3.1.1 The Chingford 1000 Women Study 105

3.1.2 Osteoporosis 105

3.1.3 Chapter aims and hypothesis 110
3.2 Methods 111
3.2.1 Study design and exclusion criteria 111
3.2.2 Participants 111
3.2.3 Predictor and outcome variables 112
3.2.4 Statistical analysis 113
3.2.5 Testing the assumptions of linear regression 113
3.3 Results 118
3.3.1 Characteristics of participants 118
3.3.2 Cross-sectional association 118
3.3.3 Prospective association 120
3.4 Discussion 122
3.5 Conclusions 126
CHAPTER 4: SKELETAL PHENOTYPING OF ADIPOR1-DEFICIENT AND ADIPOR2-DEFICIENT MICE 127
4.1 Introduction 127
4.1.1 The utility of animal models 127
4.1.2 The International Mouse Phenotyping Consortium 128
4.1.3 µCT analysis of bone microarchitecture 129
4.1.4 Histological analysis of bone cell distribution 131
4.1.5 Three-point bend testing of bone biomechanical properties 132
4.1.6 Chapter aims and hypothesis 133
4.2 Results 134
4.2.1 Gross morphology of AdipoR1$^{-/-}$ mice 134
4.2.2 Bone phenotyping of AdipoR1$^{-/-}$ mice 136
4.2.3 Gross morphology of AdipoR2$^{-/-}$ mice 148
4.2.4 Bone phenotyping of AdipoR2$^{-/-}$ mice 149
4.3 Discussion and conclusions 158

CHAPTER 5: METABOLOMIC, ADIPOGENIC AND TRANSCRIPTOMIC ASSESSMENT OF ADIPOR1$^{-/-}$ FEMALE MICE 166

5.1 INTRODUCTION 166

5.1.1 Blood serum analytes associated with bone and fat phenotypes 166

5.1.2 Bone formation rate analysis 168

5.1.3 Osmium tetroxide staining 168

5.1.4 RNASeq 169

5.1.5 Phenotypic data from the IMPC 169

5.1.6 Chapter aims and hypothesis 170

5.2 RESULTS 170

5.2.1 Analysis of fat- and bone-related blood serum analytes in AdipoR1$^{-/-}$ females 170

5.2.2 The low bone phenotype of young AdipoR1$^{-/-}$ females is coupled with a bone marrow-specific increase in adiposity 176

5.2.3 RNASeq on primary MSCs 184

5.2.4 Bone-extrinsic phenotyping of AdipoR1$^{-/-}$ females 187

5.3 DISCUSSION AND CONCLUSIONS 193

CHAPTER 6: *IN VITRO* MANIPULATION OF ADIPOR1 IN CELLS OF THE BONE MICROENVIRONMENT 204

6.1 INTRODUCTION 204

6.1.1 *In vitro* cell culture and the use of cell lines 204

6.1.2 AdipoRON 205

6.1.3 Gene markers of osteoblastic and adipocytic differentiation 205

6.1.4 Chapter aims and hypothesis 206

6.2 RESULTS 207

6.2.1 Effect of AdipoRON treatment 207

6.2.2 Effect of stable AdipoR1 knockdown 214

6.3 DISCUSSION AND CONCLUSIONS 226

CHAPTER 7: DISCUSSION AND FUTURE DIRECTIONS 232

7.1 Discussion 232

7.2 Directions for future research 237

7.2.1 Characterisation of the clinical utility of adiponectin as a biomarker ..237

7.2.2 Further investigation of the effect of AdipoR1 deletion on the bone....238

7.2.3 Clarifying the effects of *in vitro* culture on cells of the bone microenvironment 240

References 242

List of Figures

Figure 1.1: Structural anatomy of long bones 3

Figure 1.2: Major regulatory pathways involved in osteoblastic and adipocytic differentiation 8

Figure 1.3: Osteoclastic bone resorption 13

Figure 1.4: Bone cell differentiation pathways 15

Figure 1.5: The bone remodelling cycle 18

Figure 1.6: Adipocyte differentiation pathways 32

Figure 1.7: Adiponectin oligomeric complexes 35

Figure 1.8: Schematic representation of key adiponectin signalling pathways 42

Figure 2.1: Representative genotyping gel for mice of the AdipoR1 line 63

Figure 2.2: Trabecular and cortical regions of interest in µCT analysis 67

Figure 2.3: Representative image of ROI for histological analysis 71

Figure 2.4: Representative image of ROI for bone formation rate analysis using calcium staining 77

Figure 2.5: Example gating strategy used to isolate mesenchymal stromal progenitor cells via FACS 82

Figure 2.6: 5µg/ml hexadimethrine bromide provides sufficient transfection efficacy. 100

Figure 2.7: 4µg/ml puromycin is sufficient for 2T3 and ST2 cytotoxicity in 7 days... 101

Figure 3.1: Consort diagram of inclusion of participants in cross-sectional and prospective analyses. 112

Figure 3.2: Normality of predictor variables before and after logarithmic transformation 114

Figure 3.3: Normality of outcome variables 114

Figure 3.4: Linearity between logarithmically transformed predictor and untransformed outcome variables 115

Figure 3.5: Cross-sectional multivariate regression analysis between blood analytes and BMD 119

Figure 3.6: Prospective multivariate regression analysis between blood analytes and BMD 121

Figure 3.7: Summary of Chapter 3 key findings 126

Figure 4.1: Young AdipoR1$^{-/-}$ mice show significantly reduced body weight 134

Figure 4.2: AdipoR1$^{-/-}$ mice show a reduced long bone length 135

Figure 4.3: Female AdipoR1$^{-/-}$ mice show a reduced bone volume at four weeks old. 138

Figure 4.4: Female AdipoR1$^{-/-}$ mice show a reduced bone mineral density 139

Figure 4.5: AdipoR1$^{-/-}$ mice show no changes in cortical thickness 140

Figure 4.6: AdipoR1$^{-/-}$ mice show no significant differences in osteoblast parameters 142

Figure 4.7: AdipoR1$^{-/-}$ mice show few significant differences in osteoclast parameters 143

Figure 4.8: Female AdipoR1$^{-/-}$ mice show significantly increased bone marrow adiposity 145

Figure 4.9: Female AdipoR1$^{-/-}$ mice show significant changes in bone biomechanical properties 147

Figure 4.10: Adult female AdipoR2$^{-/-}$ mice show significantly reduced body weight.. 148

Figure 4.11: Female AdipoR2$^{-/-}$ mice show a reduced long bone length at 52-weeks-old. 149

Figure 4.12: Female AdipoR2$^{-/-}$ mice show a reduced bone volume at four weeks old. 151

Figure 4.13: Young female AdipoR2$^{-/-}$ mice show a reduced bone mineral density ...152

Figure 4.14: AdipoR2$^{-/-}$ mice show no changes in cortical thickness.....153

Figure 4.15: Male AdipoR2$^{-/-}$ mice show significant increase in osteoblast number and surface coverage 155

Figure 4.16: Male AdipoR2$^{-/-}$ mice show significant increase in osteoclast number and surface coverage 156

Figure 4.17: Aged female AdipoR2$^{-/-}$ mice show significantly reduced bone marrow adiposity.....158

Figure 4.18: Summary of Chapter 4 key findings.....165

Figure 5.1: 24-week old AdipoR1$^{-/-}$ females show a significant increase in circulating adiponectin levels.....171

Figure 5.2: Four-week-old AdipoR1$^{-/-}$ female mice show changes to adiponectin oligomeric ratios.....173

Figure 5.3: AdipoR1$^{-/-}$ females showed few significant differences in a screen of fat- and bone-related blood analytes.....176

Figure 5.4: Young AdipoR1$^{-/-}$ females show a significant reduction in bone formation rate....178

Figure 5.5: Young AdipoR1$^{-/-}$ females show increased bone marrow adiposity by osmium staining....180

Figure 5.6: rMAT/BV correlates significantly with total circulating adiponectin in young AdipoR1$^{-/-}$ females....181

Figure 5.7: Young AdipoR1$^{-/-}$ female mice show no significant change in fat depot gross morphology or weight....183

Figure 5.8: Young AdipoR1$^{-/-}$ females show no significant change in bone marrow plasma adiponectin concentration....184

Figure 5.9: RNASeq of primary MSCs....186

Figure 5.10: AdipoR1$^{-/-}$ females show no clear gross morphological changes in a panel of soft tissues....190

Figure 5.11: AdipoR1$^{-/-}$ females show significant differences in blood chemistry....191

Figure 5.12: AdipoR1$^{-/-}$ females show no further evidence of chronic kidney disease (CKD) or hypoparathyrodism....193

Figure 5.13: Summary of Chapter 5 key findings....203

Figure 6.1: AdipoRON-treated 2T3 and ST2 cells show dose-dependent toxicity by Alamar Blue assay....208

Figure 6.2: AdipoRON-treated 2T3 and ST2 cells show few significant changes in relative AdipoR1 or AdipoR2 gene expression by qPCR analysis....209

Figure 6.3: AdipoRON-treated 2T3 cells show significantly reduced expression of some osteoblast-related genes....211

Figure 6.4: AdipoRON-treated ST2 cells show significantly altered expression of some osteoblast- and adipocyte-related genes 212

Figure 6.5: AdipoRON-treated 2T3 cells show significantly reduced alkaline phosphatase activity 213

Figure 6.6: AdipoRON-treated 2T3 cells show no significant difference in mineralisation capacity 214

Figure 6.7: Lentiviral knockdown of AdipoR1 expression does not significantly affect AdipoR2 expression in 2T3 or ST2 cells 216

Figure 6.8: Lentiviral knockdown of AdipoR1 expression does not significantly affect cell viability by Alamar Blue assay 217

Figure 6.9: AdipoR1 knockdown is maintained in 2T3s during osteoblastic differentiation 219

Figure 6.10: AdipoR1 knockdown in 2T3 cells is associated with altered relative expression of some osteoblast-related genes at baseline and during osteoblastic differentiation 221

Figure 6.11: AdipoR1 knockdown in ST2 cells is associated with increased relative expression of osteoblast-related genes at baseline 223

Figure 6.12: AdipoR1 knockdown in 2T3 cells increases mineralisation capacity but AdipoR1 knockdown in ST2 cells has no conclusive effect on adipogenic potential ... 225

Figure 6.13: Summary of Chapter 6 key findings 231

List of Tables

Table 1.1: Summary of pre-clinical evidence on the role of adiponectin in bone.....59

Table 2.1: µCT output bone parameters.....67

Table 2.2: Steps of automated tissue processing.....69

Table 2.3: Table of ELISAs.....74

Table 2.4: Table of antibodies used in fluorescence-assisted cell sorting (FACS) of primary bone marrow stem cells.....81

Table 2.5: Table of primer sequences.....88

Table 2.6: shRNA constructs used in the production of AdipoR1 knockdown cell lines. 99

Table 2.7: Packaging plasmids used in the production of AdipoR1 knockdown cell lines. 99

Table 3.1: Breusch-Pagan test to assess validity of homoskedasticity assumption 116

Table 3.2: No significant interactions exist between predictor and confounder variables at the hip or spine.....117

Table 3.3: Baseline characteristics of participants included in cross-sectional and prospective study.....118

1

Introduction

1.1 The bone

The bone is specialised connective tissue composed of organic and inorganic components that interact to fulfil the basic functions of the skeleton: providing structural support and permitting locomotion, protecting the vital organs, maintaining mineral homeostasis and providing a suitable environment for haematopoiesis[1]. Considered for many years a static tissue, the bone is now understood to be highly dynamic, undergoing turnover throughout life to maintain a constant bone mass while providing the strength and stiffness needed to withstand loading and the flexibility and ductility necessary for shock absorption and fracture prevention[2]. This turnover is coordinated by the tightly regulated interaction between bone-forming osteoblasts and bone-resorbing osteoclasts within the bone multicellular unit. Bone marrow adipocytes have been observed for decades, but the role of adipocyte-related factor signalling in bone accrual and homeostasis has only recently begun to be investigated and the bone marrow is now considered an important biological component of bone.

1.1.1 The structure and function of bone

During development, the skeleton forms via two crucial processes: endochondral ossification, in which the cartilage is replaced by bone via the apoptosis of the resident chondrocytes and infiltration by blood vessels, osteoblast progenitors and osteoclasts to form a marrow cavity and lay down mineralised bone, and intramembranous ossification, in which bone is laid down directly by osteoblasts without a cartilaginous scaffold[3]. Some of the bones of the skull and part of the clavicle form by intramembranous ossification while the rest of the skeleton, including the axial and appendicular skeleton and the other bones of the skull, form by endochondral ossification[3]. Longitudinal bone growth occurs at the growth plates and in humans finishes when these growth plates close at puberty[2], although growth of mice long bones continues beyond sexual maturity at 6 weeks of age[4]. Conversely, appositional bone growth to permit changes in bone shape in response to altered mechanical stresses[2] and turnover and remodelling both occur throughout life via intramembranous ossification (**Section 1.1.3**).

Mineralised bone can be divided into cortical and trabecular bone which differ in their structure and function. Cortical bone, which accounts for around 80% of bone in the adult human skeleton, surrounds the diaphysis of the long bones and has an outer periosteal surface and an inner endosteal surface[1]. Structurally, cortical bone is primarily made up of lamellar bone, in which cylindrical units that contain blood vessels and occasionally nerves are surrounded by concentric layers of bone matrix (lamellae) forming harversian systems or osteons[5,6] (**Figure 1.1**). This dense and highly ordered structure makes cortical bone strong and suitable for its mechanical load-bearing role. Trabecular bone constitutes around 20% of bone and forms a honeycomb-like network of plates and rods interspersed within the marrow compartment[1]. Its relatively low density makes trabecular bone less strong than cortical bone, but its structure permits shock absorption through force distribution to reduce fracture risk associated with

weight bearing[6]. Trabecular bone volume is likely to be a more sensitive indicator of changes in loading and unloading or in bone formation and/or resorption, likely due to its proximity to cells of the bone marrow, a higher metabolic rate and a turnover rate 3-10 times more rapid than cortical bone[5,6].

Woven bone can be found in both cortical and trabecular bone. Primarily observed in childhood before being replaced by lamellar bone, woven bone is also observed during the initial stages of fracture healing and is exemplified by a fast turnover rate and disordered, irregular appearance as compared with lamellar bone.

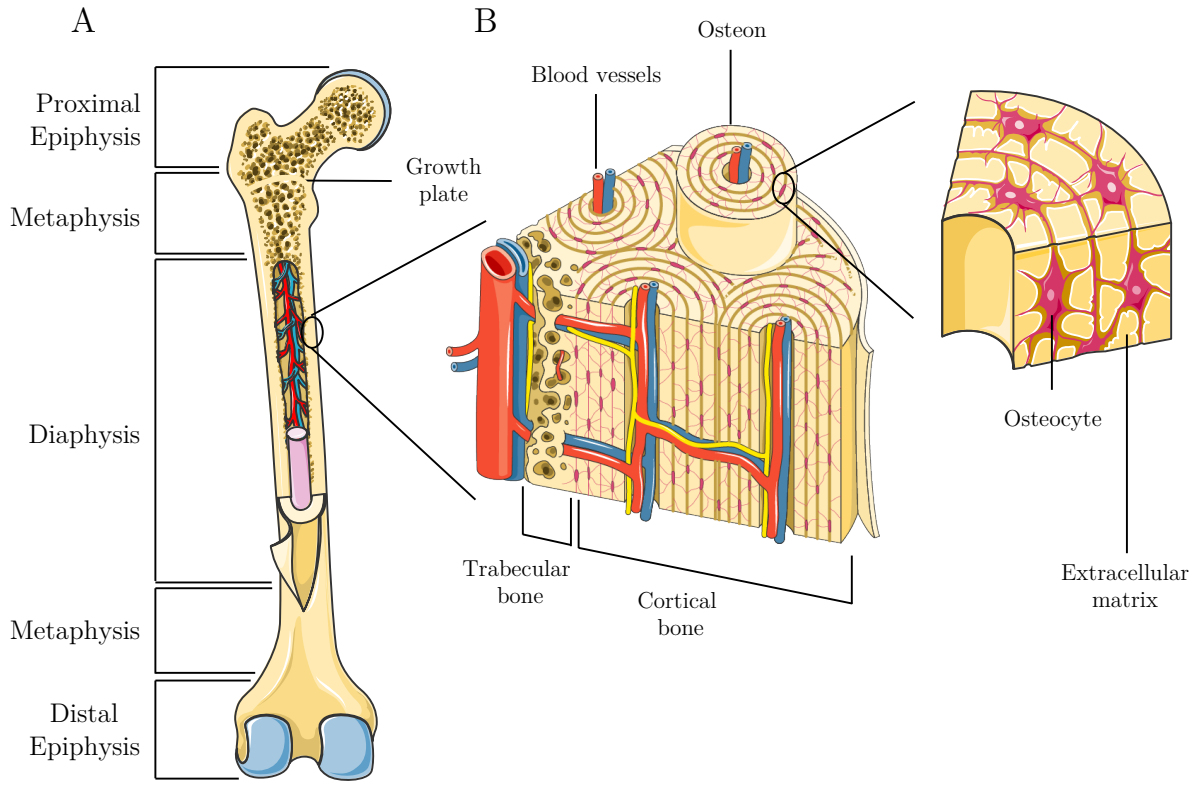


Figure 1.1: Structural anatomy of long bones. (**A**) Diagram of the anatomy of a whole long bone showing the distribution of cortical and trabecular bone. (**B**) Detailed structure of a segment of the diaphysis, showing the concentric lamellae of the osteon. Figure adapted from Smart Servier Medical Art.

1.1.2 The cellular components of bone

Three major cell types exist within the calcified bone and are responsible for its development and maintenance throughout life: bone-forming osteoblasts, bone-resorbing osteoclasts, and bone-sensing osteocytes. Bone marrow adipocytes exist within the bone marrow cavity and have been explored as significant regulators of energy metabolism; these are discussed in **Section 1.2.3**. A diagram of bone cell differentiation is provided in **Figure 1.4**.

1.1.2.1 Osteoblasts

Comprising approximately 5% of total resident cells of the calcified bone[7], osteoblasts are cuboidal, single nucleic cells responsible for the formation of bone via deposition and subsequent mineralisation of the extracellular organic matrix, called osteoid, which is composed primarily of collagenous proteins[8,9]. Their morphology reflects their protein synthesis activity, with fully differentiated osteoblasts containing large quantities of rough endoplasmic reticulum, mitochondria and golgi apparatus[1,6]. Highly active during embryonic skeletal formation and growth, osteoblast activity during adulthood is restricted to situations of defect repair or matrix depletion[10].

Osteoblasts are derived from mesenchymal stem cells (MSCs) (**Section 1.1.2.4**), multipotent cells that exist on the endosteal surface and within the bone marrow[7] capable of differentiating to osteoblasts, adipocytes, myoblasts or chondrocytes[10]. Runx2 (or Cbfα1) is the master regulator of osteogenic differentiation: its overexpression is sufficient for osteoblastic differentiation of bone marrow stromal cells and bone formation both *in vitro* and *in vivo*[11] and its *in vivo* deletion inhibits mineralisation completely, with the entire skeleton remaining cartilagenous[12]. Osterix (Osx) is an additional transcription factor critical for osteoblastogenesis that is a target of Runx2: Osterix-

knockout mice show normal Runx2 expression but inhibited osteoblast differentiation and bone formation, whereas Runx2-deficient mice show no Osterix[13], showing that Osterix lies downstream of Runx2. Runx2-mediated signalling is associated with the activation of osteoblast-specific genes, including osteopontin, type I collagen and osteocalcin[14]. Many factors associated with altering osteoblastic differentiation do so via regulation of Runx2 expression. Wnt/Notch signalling is the best studied of these factors, some of which are summarised in **Figure 1.2**.

The paracrine glycoprotein Wnt can signal through several possible pathways. Canonical Wnt signalling involves the regulation of proteasomal degradation of the transcription factor β-catenin. In the absence of Wnt ligands, β-catenin is sequentially phosphorylated by a protein complex involving glycogen synthase kinase-3β (GSK3β) and casein kinase-1 (Ck-1), targeting it for degradation. Wnt signalling permits formation of a multiprotein receptor complex involving Frizzled receptor, low-density lipoprotein related receptor-5 (Lrp5) and Lrp6 and the recruitment of dishevelled (Dvl) and Axin. Ultimately, this protein complex prevents β-catenin degradation, permitting its accumulation in the cytoplasm and subsequent translocation to the nucleus where it enhances gene expression by interacting with DNA-bound T-cell factor (TCF) to prevent its interaction with Groucho, a transcriptional repressor[15]. This results in altered gene expression, including direct upregulation of Runx2 gene expression[16]. Wnt signalling is held in balance by inhibitors: the binding of Notch to its ligand Jagged promotes β-catenin degradation and promotes expression of Hey1, an inhibitor of Runx2 transcription[17], and Dickkopf proteins 1 and 2 (Dkk1 and Dkk2) and sclerostin act to inhibit Wnt signalling via Lrp5/6[18,19]. The importance of the contribution of Wnt signalling to skeletal homeostasis is evidenced by the significant disturbances in skeletal development observed in mouse models deficient in proteins of the Wnt signalling pathway[20,21] and the observed association between Lrp5 mutation and high bone mass in humans[22].

The skeletal effects of Wnt signalling via non-canonical pathways are less well defined, mediated by signalling molecules involving mitogen-activated protein kinase (MAPK) and calcium/calmodulin-dependent protein kinase-IIα (CaMKIIα)[23]. Interestingly, unlike mice deficient in ligands of the canonical Wnt pathway which showed no change in bone marrow adiposity, heterozygous mice deficient in the non-canonical Wnt ligand Wnt5a showed a significant increase in bone marrow adiposity and a concurrent reduction in osteoblastogenesis[24]. This direct interaction was found to be mediated by non-canonical Wnt signalling transcriptionally inducing Runx2 expression and repressing PPARγ expression; this was mediated via the phosphorylation of a histone lysine methyltransferase that inactivates PPARγ through histone methylation[24]. This work has established Wnt5a as a determinant of MSC fate.

Bone morphogenic proteins (BMPs), cytokines of the TGFβ superfamily, can moderate Runx2 expression via cell surface receptor binding activating effector SMADs, which translocate to the nucleus to regulate target gene transcription via cofactor binding. Pro-osteogenic BMP2 and BMP4 can induce osteoblastic differentiation of uncommitted progenitor cells both *in vitro* and *in vivo* via upregulation of Runx2 transcription and acting as cofactors to regulate transcription of its target genes[10,25]. BMP2 signalling has further pro-osteogenic effects via SMAD-mediated induction of interleukin-11 (IL-11) expression, which is believed to suppress Wnt inhibitors Dkk1 and Dkk2. Interestingly, IL-11 expression is stimulated by parathyroid hormone (PTH) and mechanical stress[26]; the effects of PTH within the bone are discussed in more depth in **Section 1.1.4**. BMPs are produced by osteoblasts in a positive feedback loop[7], but these pro-osteogenic effects of BMP2 and BMP4 are held in balance by their antagonist, Noggin[25].

Following Runx2 activation and commitment to the osteogenic line, osteoblastic differentiation occurs in three stages[10]. Initially cells continue to proliferate, expressing early indicators of osteoblastic development including fibronectin and osteopontin. Cells

then begin to differentiate, increasing alkaline phosphatase expression and producing osteoid. The collagen secreted by osteoblasts is in a precursor state which is extracellularly processed to produce mature type I collagen molecules, which are then assembled into ordered, cross-linked collagen fibrils that provide the bone with a very high tensile strength[27]. Aside from collagen, osteoblasts produce several proteins that become incorporated into the bone matrix, including osteocalcin (OCN) and osteonectin which constitute nearly half of the non-collagenous proteins of bone and are essential for correct calcification of the matrix by osteoblasts[14,27]. Mineralisation of the osteoid matrix, which represents the third stage of osteoblastic differentiation, involves the deposition of hydroxyapatite crystals to provide bone with its resistance to compression, and in combination with type I collagen produces strength and durability within the skeleton[27]. The production of osteoid determines bone volume, whereas its subsequent mineralisation determines its density[14].

Details of the mechanisms of osteoblastic mineral deposition, including the exact transporters responsible for ion movement, are still unknown, with some citing lack of consistency in the model used to investigate osteoblastic differentiation and function as the reason for a fragmented understanding[10], but diseases of mineralisation have been used to elucidate the central mechanisms. The osteon (**Figure 1.1**) forms the multicellular structure in which mineralisation is considered: an extended network of mineral-embedded osteocytes and bone surface osteoblasts are joined by gap junctions in order to surround entirely the unmineralised bone matrix and thus establish local control of extracellular ion composition and pH buffering[27]. These groups of active osteoblasts are distinguishable histologically. Sources of calcium and phosphate are required for mineralisation to occur. The molecular mechanism by which calcium is transported from the extracellular fluid to the unmineralised bone matrix is not fully understood, but sodium-calcium exchangers expressed by osteoblasts are likely

involved[28]. Phosphate is produced locally by alkaline phosphate from pyrophosphate; while other mechanisms of phosphate production might be involved, the key role played by alkaline phosphatase is demonstrated by the severe osteopenia, impaired mineralisation and increased fracture incidence in an alkaline phosphatase knockout mouse model[27,29]. Phosphate, calcium and water together in the alkaline environment yield hydroxyapatite, a calcium-phosphate compound, and H^+ ions, which must be actively removed from the local environment in order to maintain the high pH levels[27,30].

Active osteoblasts are estimated to have a lifespan in humans of around 3 months[14], after which they undergo one of three cell fates: they may die by apoptosis or become entombed in the bone matrix as osteocytes (see **Section 1.1.2.2**). Alternatively, osteoblasts may remain on the bone surface as quiescent bone lining cells, which reside in areas without ongoing bone formation or resorption[7].

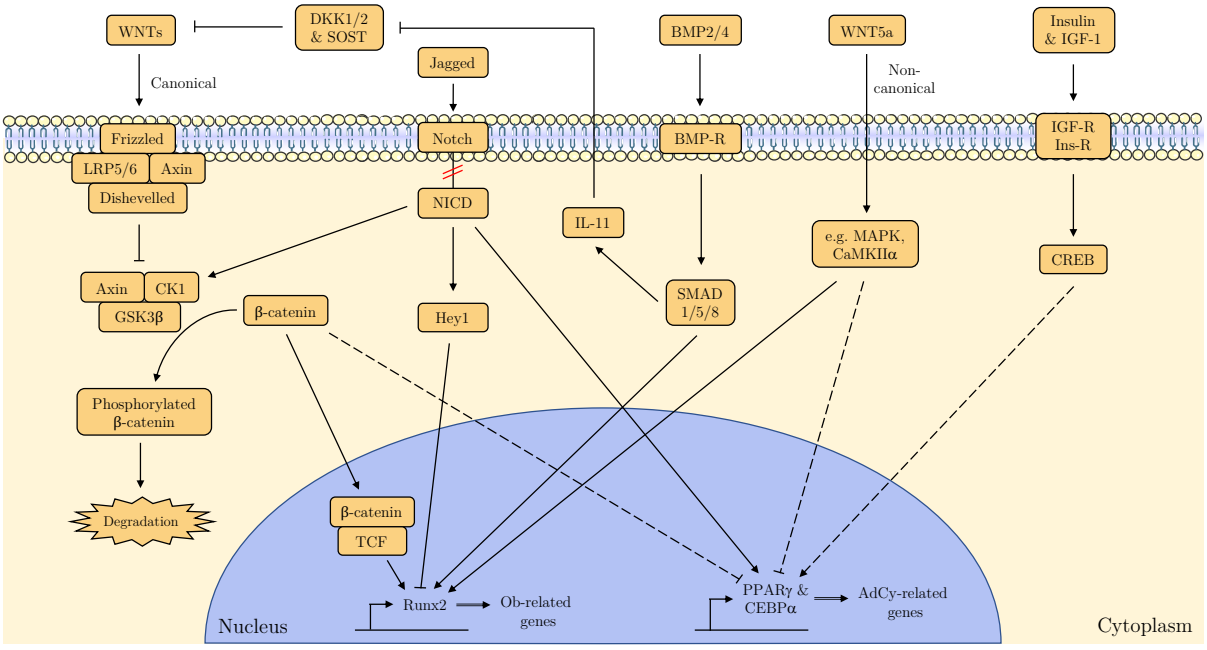


Figure 1.2: Major regulatory pathways involved in osteoblastic and adipocytic differentiation. Runx2 is the main transcriptional regulator for osteoblast differentiation while PPARγ and CEBPα are the key regulators of adipocytic differentiation. Many of the regulatory pathways involved in differentiation regulate the transcription of these key genes. The activation of canonical Wnt signalling stabilises β-catenin allowing its translocation to the nucleus where it promotes Runx2 transcription and inhibits

PPARγ and CEBPα expression. The signalling of Notch, DKK1/2 and SOST all inhibit canonical Wnt signalling. Non-canonical Wnt signalling is mediated by many downstream regulators and van also promote osteoblast differentiation and prevent adipocytic differentiation. BMP2/4 signalling upregulates Runx2 expression both directly and indirectly via IL-11-mediated suppression of Wnt inhibitors. Insulin/IGF-1 signalling is complex, acting to promote adipocyte formation and inhibit osteoclastogenesis. Arrowheads indicate activation pathways; bluntheads indicate inhibitory pathways. Broken lines indicate indirect signalling. LRP5/6: lipoprotein related receptor-5/6; CK1: casein kinase-1, GSK3β: glycogen synthase kinase-3β; DKK1/2: Dickkopf protein 1/2; SOST: sclerostin; NICD: Notch intracellular signalling domain; TCF: T-cell factor; IL-11: interleukin-11; BMP: bone morphogenic protein; BMP-R: BMP receptor; MAPK: mitogen-activated protein kinase; CaMKIIα: calcium/calmodulin-dependent protein kinase-IIα; IGF-1: insulin-like growth factor-1; IGF-R: IGF receptor; Ins-R: insulin receptor; CREB: cyclic AMP (cAMP) response element-binding protein; PPARγ: peroxisome proliferator-activated receptor-γ; CEBPα: CCAAT/enhancer-binding protein-α.

1.1.2.2 Osteocytes

It is estimated approximately 15% of osteoblasts eventually become encased in the bone matrix where they become terminally differentiated osteocytes[9]. Immature osteocytes resemble osteoblasts, displaying large quantities of rough endoplasmic reticulum and golgi apparatus, but with reduced cytoplasm as they mature and become more deeply entombed within the bone[6]. This maturation process is associated with a reduction in alkaline phosphatase expression and an increase in osteocalcin and casein kinase II expression[31].

Despite representing over 90% of cells present within the mineralised bone, likely due to their longevity of up to a decade[31], the function of osteocytes remained unknown and relatively unexplored for many years; research only in the last 20 years has begun to uncover their functional roles within the bone. Osteocytes have long cytoplasmic processes that allow contact with adjacent cells, including bone-forming cells[8], and they are now considered key regulators of bone maintenance and surveillance due to their significant interconnectivity and distribution throughout the bone matrix[32]. Osteocytes positively regulate bone formation via their high expression of dentin matrix protein 1 (DMP1), a critical mediator in mineralisation of bone and dentin[33], but inhibit bone

formation by Wnt/β-catenin signalling inhibition and promote bone resorption by upregulating osteoclastogenesis via their high expression of sclerostin and RANKL respectively[34,35]. They are also acknowledged to respond to mechanical stress: the osteoporosis at baseline and protection against unloading-induced bone loss in 10-week-old C57Bl/6 mice following inducible and targeted osteocyte deletion suggests these cells play a key role in bone homeostasis under normal load conditions and in mechanotransduction and bone responses to changes in loading[36].

1.1.2.3 Osteoclasts

Osteoclasts are large, multinucleated cells originating from mononucleic cells of the haematopoietic lineage and are the only known cell type capable of resorbing bone[1,7]. Their high energy resorption activity is reflected by their intracellular components, which include many mitochondria and acidic vacuoles containing acid phosphatases and other lysosomal enzymes but little endoplasmic reticulum and golgi apparatus, suggesting large quantities of protein are not synthesised or exported[37].

Osteoclastic differentiation from haematopoietic precursor cells is critically dependent on the AP-1 transcription factor complex: mice deficient in AP-1 complex component c-Fos show significant osteopetrosis and an increased bone marrow macrophage number due to inhibited osteoclastic differentiation that was rescued following ectopic c-Fos expression[38]. The AP-1 complex regulates transcription of genes essential for osteoclastic development, in particular promoting the expression of nuclear factor-activated T cells c1 (NFATc1), a master regulator of osteoclastic differentiation[39]. Forced overexpression of NFATc1 in c-Fos-deficient cells rescued the inhibition of osteoclastic differentiation, highlighting NFATc1 as a regulatory of osteoclastogenesis downstream of c-Fos[39]. c-Fos signalling also promotes expression of receptor activator of nuclear factor (NF) κB

(RANK) on osteoclastic precursors[40]. The axis between RANK, its TNF-related cytokine ligand RANK ligand (RANKL), and the RANK decoy receptor osteoprotegerin (OPG) is a key regulator of osteoclastogenesis and holds a crucial role in the coupling between osteoclasts and nearby osteoblasts and stromal cells, which is discussed further in **Section 1.1.3**.

The binding of RANKL and the growth factor macrophage colony stimulating factor (M-CSF) to their receptors, RANK and cFMS respectively, on osteoclast precursor cells on the bone surface is necessary and sufficient for osteoclastic lineage allocation and maturation[41,42], stimulating their proliferation and inhibiting their apoptosis[7]. Osteoclast maturation is associated with the expression of osteoclast-specific genes, including cathepsin K and tartrate-resistant acid phosphatase (TRAP), which is used in histological stains to identify osteoclasts. Conversely, the binding of OPG to RANKL neutralises its pro-osteoclastic effects[42]. The OPG/RANKL/RANK axis is regulated by many factors, balancing the pro-resorptive activities of PTH, vitamin D and TNF with the anti-osteoclastic effects of factors such as oestrogens and BMPs to prevent insufficient or excessive bone resorption[42]. Recently developed anti-osteoporotic drugs seek to manipulate this axis to stimulate new mineralised bone formation rather than solely prevent its resorption as by bisphosphonates: teriparatide, a recombinant human PTH analogue, and Denosumab, a human monoclonal anti-RANKL antibody, both significantly reduce osteoporotic fracture rates and represent an important new line in anti-osteoporotic intervention[43,44].

The resorption of calcified bone by mature osteoclasts involves the dissolution of the hydroxyapatite crystals formed during mineralisation followed by the proteolytic cleavage of the organic component of the bone, primarily collagen[41] (**Figure 1.3**). Bone resorption occurs in an isolated compartment formed by attachment of the mature osteoclast to the bone surface via sealing zones comprised of integrins, which induces

cytoskeletal reorganisation that polarises the resorptive machinery of the cell towards the bone interface and forms an actin ring surrounding the bone-adjacent ruffled border characteristic of active osteoclasts[37,41]. Proteolytic enzymes including cathepsin K and TRAP are transported across the ruffled border for bone matrix degradation. Hydrochloric acid (HCl) for the acidification of the extracellular space and subsequent mineral dissolution is created in a two-step process: cytoplasmic carbonic anhydrase converts carbon dioxide and water into bicarbonate and protons and the bicarbonate ions are removed from the cell in exchange for chloride ions via a cell surface transporter. Protons and chloride ions are transported into the extracellular space by a proton pump and chloride channel respectively. Matrix degradation releases degraded bone matrix proteins and inorganic minerals like calcium which are subsequently removed via transcytosis[37,41].

Observation and quantification of the resorptive pits can be used in functional studies of osteoclasts[45]. Osteoclasts are relatively short-lived cells with an average lifespan in humans of around 2 weeks, after which time they die by apoptosis and are removed by phagocytes. Interestingly, this apoptosis has been shown to be promoted by oestrogen *in vitro* and in murine models *in vivo*, suggesting its clinical relevance in age-related bone loss in women following the menopause[46].

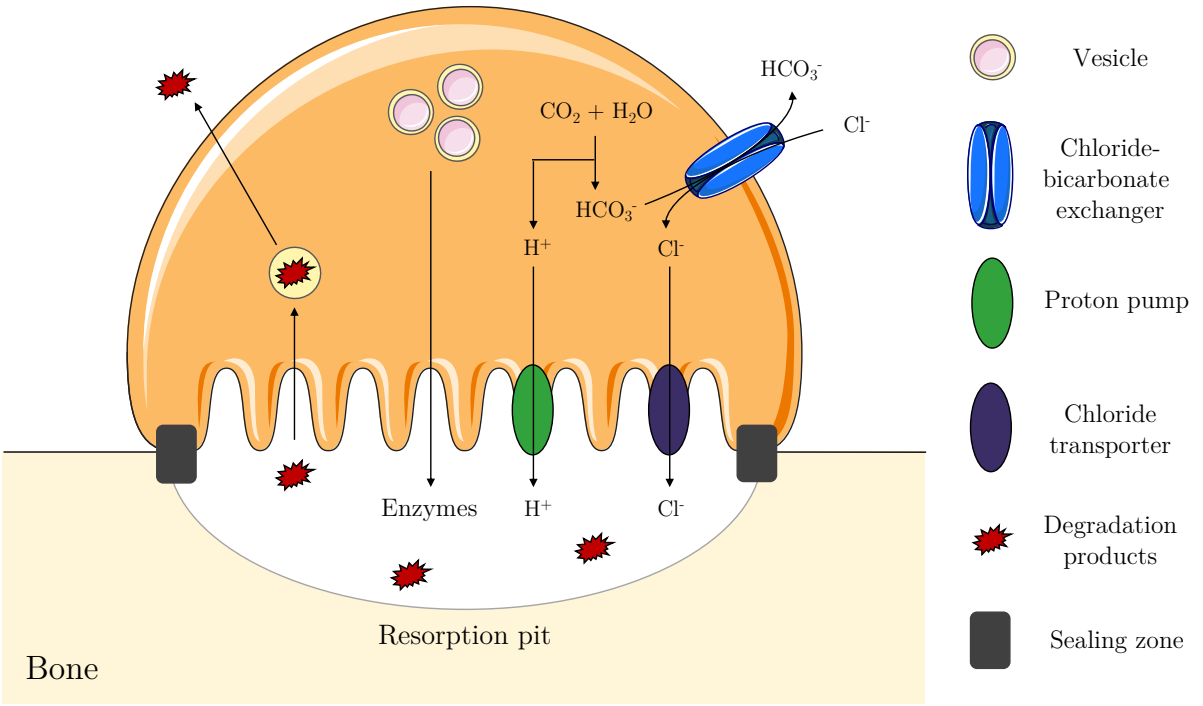


Figure 1.3: Osteoclastic bone resorption. Mature osteoblasts resorb bone by forming an isolated compartment using sealing zones. Proteolytic enzymes are released into this space from vesicles. Cytosolic carbonic anhydrase produces protons and chloride ions are moved into the cell via a cell surface exchanger. Protons and chloride ions produce hydrochloric acid in the extracellular space for mineral dissolution. Waste products are removed from the cell via transcytosis. Figure adapted from Smart Servier Medical Art.

1.1.2.4 Mesenchymal stem cells

The bone marrow consists of a heterogenous population of cells. Its main function has long been considered the provision of a microenvironment for haematopoiesis: hematopoietic stem cells (HSCs) reside within the bone marrow and give rise to all cells of the blood cell lineage[47]. In the 1960s, the existence within the bone marrow of a rare (approximately 1 in 10,000 cells) precursor cell population distinct from the HSC that gave rise to the osteoblasts and fibroblasts was demonstrated[48]. These cells became termed mesenchymal stem cells (MSCs)[49] and there is significant evidence to suggest that they exhibit the classic features associated with stemness: they are multipotent and capable of differentiating to osteoblasts, adipocytes, myoblasts or chondrocytes[10], they

show self-renewal capacities[50], and they show lineage priming in which the cell expresses a subset of genes associated with the cell lineages to which it can commit: the master differentiation regulators Runx2 (osteoblastic), PPARγ (adipogenic) and Sox9 (chondrocytic) were all observed to be expressed in undifferentiated MSCs[51].

In vitro culture has been a mainstay of MSC research due to the lack of a robust and reproducible cell surface marker profile by which to identify MSCs, with research instead selecting MSCs by their ability to adhere to plastic[52]. However, it has been observed that the prominence of *in vitro* assay systems to study MSC differentiation could impair the reliability and reproducibility of results due to differences in isolation techniques and culture conditions coupled with the non-physiological aspects of *in vitro* culture[52,53]; indeed, primary MSCs have been observed to show changes in their cell surface marker profile following *in vitro* culture, suggesting removal from the bone marrow microenvironment has significant phenotypic and possibly functional effects[54]. The search for a cell surface marker profile that defines MSCs is ongoing, with recent work identifying an MSC hierarchy, in which early, intermediate and mature osteo-progenitors are defined in primary mouse bone marrow by their cell surface marker profile and show distinct *in vivo* effects alongside their ability to support HSCs[55].

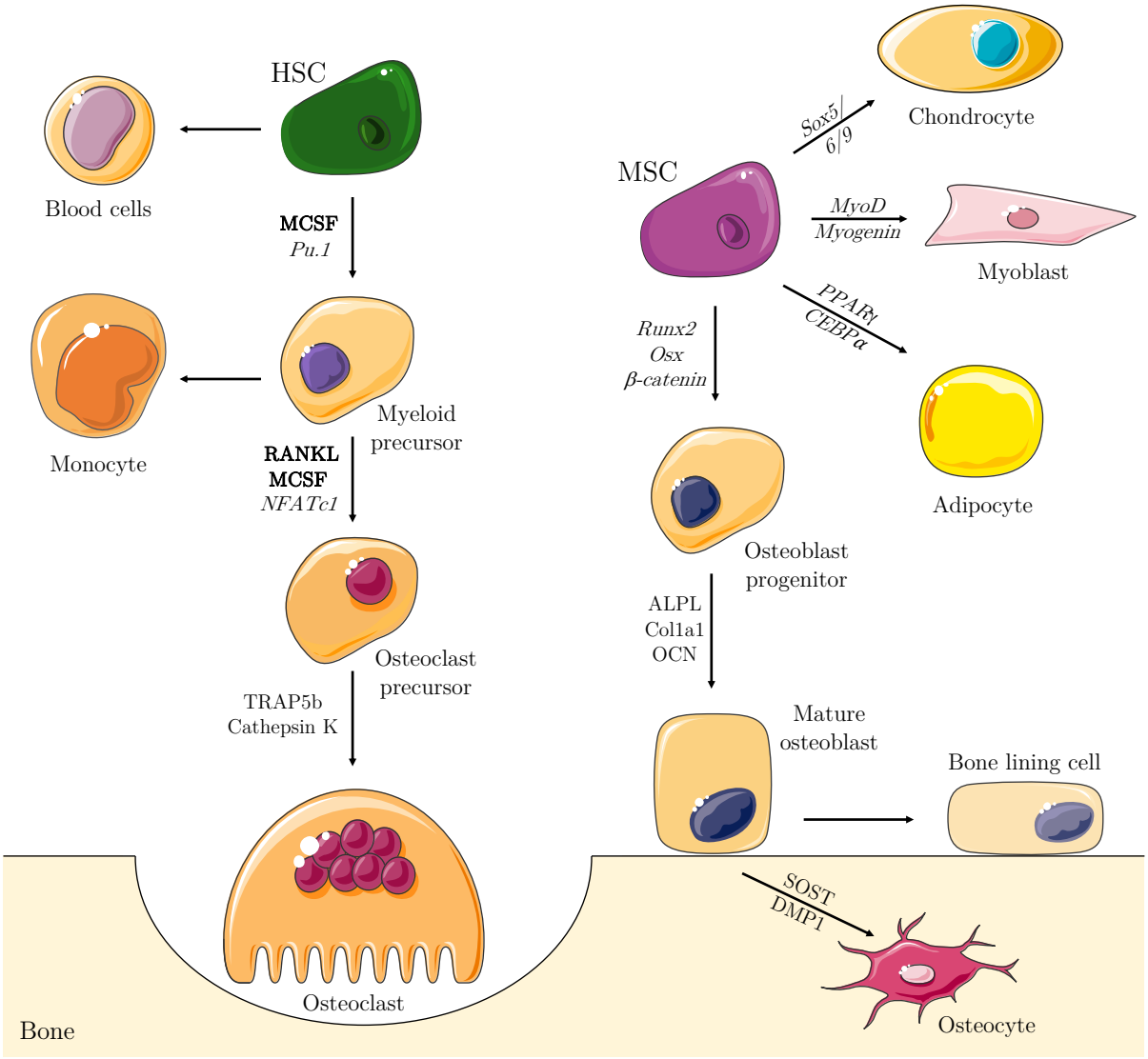


Figure 1.4: Bone cell differentiation pathways. Haematopoietic stem cells are the source of all blood cells and can differentiate to a myeloid precursor cell, which in turn can differentiate to monocytes and osteoclasts. Mesenchymal stem cells can differentiate into chondrocytes, myoblasts, adipocytes or osteoblasts; mature osteoblasts can further differentiate into osteocytes embedded in the bone or bone lining cells which line the bone surface. Some key proteins expressed by cell types are indicated. Italics indicates key transcriptional regulators and bolding indicates key cytokine regulators necessary for that differentiation stage. HSC: haematopoetic stem cell; MSC: mesenchymal stem cell; Osx: osterix; ALPL: alkaline phosphatase; Col1a1: collagen type I α-1; OCN: osteocalcin; SOST: sclerostin; DMP1: dentin matrix protein-1. Figure adapted from Smart Servier Medical Art.

1.1.3 The basic multicellular unit and the bone remodelling cycle

The resorption of old or damaged bone to be replaced by new bone is called bone remodelling and continues throughout life, with around 10% of bone replaced annually in order to maintain biomechanical strength and prevent accumulation of microdamage[1,56]. Bone resorption by osteoclasts and bone formation by osteoblasts are not independent processes; they are closely linked temporally and spatially to ensure a balance between the two maintains a constant bone mass. Many disorders of the adult skeleton, including osteoporosis in advancing age, can be attributed at least in part to an imbalance between bone formation and resorption during remodelling[57]. The importance of this coupling is demonstrated by Runx2 knockout mice, which display a lack of osteoclastic development alongside the failure of osteoblastic development[12].

Bone turnover is orchestrated within the basic multicellular unit (BMU) of bone, which comprises osteoblasts and osteoclasts alongside blood vessels, nerves and connective tissues[14]. It is estimated that the adult human skeleton has 1-2 million of these temporary biological structures active at any given time, moving through cortical bone or across the surface of trabecular bone[14,41]. Within the active BMU, sequential stages occur to permit remodelling: activation, resorption, reversal, formation and quiescence (**Figure 1.5**).

The BMU has an average lifespan of 6-9 months[14], significantly longer than the lifespan of the cells it comprises. This necessitates recruitment and activation of progenitor cells both at the initiation of the BMU and during its lifespan. The exact mechanisms by which the BMU is initially recruited to the site of bone remodelling are not well understood, but osteocyte apoptosis due to microdamage or changes in biomechanical loading is considered to play a key role in recruitment of osteoclast precursors from the

vasculature closely associated with the BMU[58–60]. The death of osteocytes is also associated with a loss of their baseline inhibition of osteoclast precursor development, permitting the differentiation of the latter into mature osteoclasts which can resorb the adjacent bone[58]. Full osteoclastic differentiation is reliant on RANKL and M-CSF signalling from osteoblasts which respond to osteocytic signals[41,60,61]; aside from osteoblasts, osteocytes[35], synovial fibroblasts[62] and immune T cells[63] of the bone microenvironment have also been identified as capable of producing RANKL to affect osteoclastogenesis. Upregulation of chemokine monocyte chemoattractant protein-1 (MCP1) expression by osteoblasts also serves to recruit osteoclast precursors to the area for resorption[61].

Following bone resorption, there exists a poorly understood reversal phase before bone formation commences, estimated to last up to 5 weeks in healthy humans[64] during which "reversal cells" of an unclear phenotype cover the newly exposed bone surface following osteoclastic resorption and clear it of collagen remnants in order to prepare it for deposition of new bone by osteoblasts[61].

Active osteoclastic resorption of bone in turn activates osteoblastic differentiation and activity, although the exact mechanisms by which this occurs remain controversial. The release of growth factors such as TGFβ and insulin-like growth factor I (IGF-I) from the resorbed bone matrix has long been understood to increase bone formation via recruitment of MSCs to the area[65]; the existence of these released factors was demonstrated in the early 1980s by the *in vitro* stimulation of bone formation following application of conditioned media taken from cultures of actively resorbing osteoclasts[60,66]. However, the preservation of osteoblasts and their activity in mice and human models lacking functional osteoclasts suggests osteoblasts can differentiate and function without these matrix-derived signals[61] and that coupling signals could be produced by the osteoclasts themselves. Despite the proposal of some osteoclast-derived coupling

mechanisms, including via osteoclast secretion of sphingosine 1-phosphate to recruit osteoblasts and promote their maturation and survival[67], the relative importance of these cell-to-cell mechanisms remains uncertain, particularly given both physical and temporal limitations: the lack of space within the BMU and the lengthy reversal phase between resorption and formation both likely limit physical contact between these cell types. Thus, the exact mechanisms of osteoclastic regulation of osteoblastic activity remain unknown, although it has been observed that activated osteoblasts cause the apoptosis of activated osteoclasts via their upregulation of factor associated suicide ligand (FasL) and subsequent binding to the receptor Fas on osteoclasts[68]. Following bone formation, the bone becomes covered once again with bone lining cells and remains in quiescence.

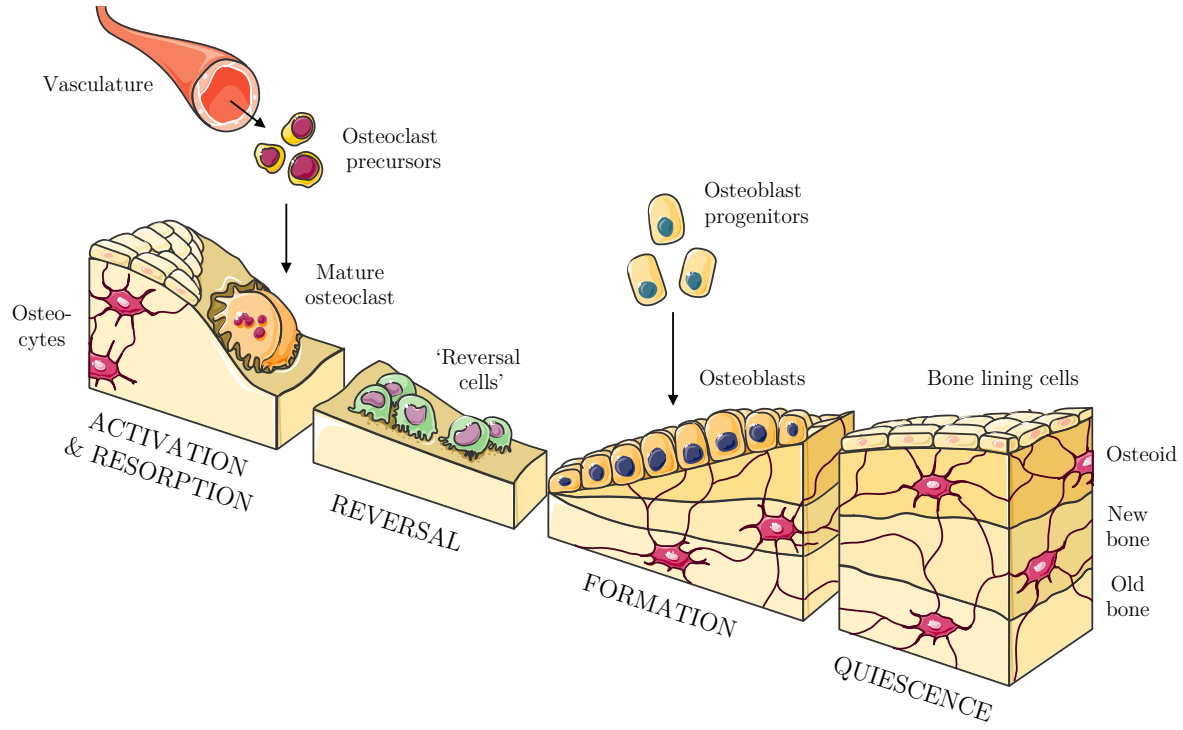


Figure 1.5: The bone remodelling cycle. Osteoclast precursors recruited from the vasculature are recruited and activated to resorb bone. 'Reversal cells' of an undetermined phenotype prepare the newly exposed bone surface for bone formation by osteoblasts which develop from osteoblast progenitors in a process tightly coupled with osteoclastic development and activity. Quiescent bone surface is covered in bone lining cells. Figure adapted from Smart Servier Medical Art.

1.1.4 The inorganic components of bone

While growing children have a net positive intake of calcium and phosphate as they are incorporated into growing bones during mineralisation and hydroxyapatite formation, a series of regulatory mechanisms in healthy adults balance the calcium and phosphate content of the body such that their intake in the diet is matched by their excretion through the kidneys[69]. The bone represents a large storage of these ions and thus is critical in buffering the blood phosphate and calcium levels, but its participation is not passive: bone cells produce hormones which actively affect mineral homeostasis.

Parathyroid hormone (PTH), fibroblast growth factor-23 (FGF-23) and the physiologically active form of vitamin D, calcitriol (otherwise known as 1,25 dihydroxyvitamin D_3) regulate calcium and phosphate levels and each other in the PTH-vitamin D-FGF23 axis. PTH is produced by the parathyroid gland in response to hypocalcaemia and generally acts to increase levels of calcium and phosphate in the blood: it promotes their reabsorption in the kidney and their release from the bone matrix by stimulating bone resorption. The actions of calcitriol directly oppose this: following its synthesis in the kidneys from an inactive form of vitamin D, it acts to inhibit calcium and phosphate absorption from the GI tract and reabsorption in the kidney and inhibits PTH secretion. FGF-23 is produced by osteocytes in the bone and its secretion is augmented by PTH; it acts to reduce PTH and calcitriol secretion. Together, this axis provides stable calcium and phosphate levels in the blood and maintains a store of these minerals in the bone[69].

Disruption of this axis can lead to problems with the bone following mineral leaching; in particular, metabolic bone disease is an important clinical aspect of chronic kidney disease[70]. A reduction in kidney function is associated with hyperphosphatemia due to inadequate phosphate excretion in the urine coupled with a reduction in blood calcium

levels due to impaired renal calcitriol production[71]. A compensatory increase in PTH secretion in response to hypocalcaemia leads to secondary hyperparathyroidism in patients with CKD, leading to osteodystrophy characterised by abnormally high levels of bone resorption[72] and an increased fracture risk in patients[70].

1.2 Adipose tissue

Excess energy is stored for future needs in the form of fat; in mammals, fat storage occurs in adipose tissue which resides in several depots around the body[73]. Adipose tissue efficiently deposits energy in the form of triglycerides, increasing lipid droplet size and resulting in adipose expansion[74]. These triglycerides can either be taken up from the environment via the action of lipoprotein lipase (LPL) on the vascular endothelium of adipose tissue, which hydrolyses circulating triglycerides to non-esterified fatty acids to permit their uptake into the cell via fatty acid transporters such as CD36 and fatty acid transport protein-1 (FATP1), or they can be produced *de novo* via a lipogenesis pathway following uptake of glucose from the environment[75]. When energy demands exceed energy supply, triglycerides are lipolysed to glycerol and free fatty acids which move through the blood to regulate whole body energy balance[74]. Adipose tissue is now considered to have significant biological roles besides fat storage and has been described as the body's largest endocrine organ[76], secreting many factors including cytokines, known as adipokines, which act systemically to regulate metabolism and inflammation[74].

Although many cell types like hepatocytes, muscle cells and immune cells can accumulate some lipid, adipocytes are defined by their large lipid droplets for triglyceride storage and the expression of adipocyte-specific markers. In mammals there are two main types of adipocytes which are histologically and functionally distinct: white and brown, which are the primary cell types in white adipose tissue (WAT) and brown adipose

tissue (BAT) respectively. Historically, WAT has been the best studied adipose tissue, due to its volume and ready availability in humans and mice alike, and much of the biological understanding of adipose tissue is based on the study of WAT. In recent years, bone marrow adipocyte tissue (BMAT) has become considered a distinct third category of adipose tissue (differentiation pathways summarised in **Figure 1.6**).

All adipocytes are derived from MSCs, but a precise understanding of the intermediary stages between MSCs and fully differentiated adipocytes is lacking due to the absence of well-defined expression markers to define each stage. It is now understood that white and beige adipocytes (**Section 1.2.1**) derive from a MYF5-negative subset of MSCs, whereas MYF5-positive cells represent a common progenitor cell for both brown adipocytes and myocytes[77] with expression of transcriptional factor PRDM16 regulating this fate decision[78], making brown adipocytes more closely related to myocytes than white adipocytes. Following this split, the adipogenic differentiation pathways remain similar, driven by peroxisome proliferator-activated receptor-γ (PPARγ) and CCAAT/enhancer-binding protein-α (CEBPα) which *in vivo* and *in vitro* investigation has established as key regulators in the adipogenic transcriptional cascade.

PPARγ is the master adipocytic differentiation regulator and has been demonstrated to be necessary for adipocytic differentiation: assessment of its *in vivo* role in fat development has been hindered by lack of a viable knockout model, but the absence of any significant contribution of PPARγ-null cells to adipose tissue development in mice chimeric for wild type and PPARγ-null cells demonstrates an important *in vivo* effect on adipogenesis[79]. Indeed, its forced expression in fibroblasts is sufficient to induce their adipocytic differentiation[80], and its adenovirus-mediated *in vitro* ablation following adipocytic differentiation prevents maintenance of the differentiated state, reducing lipid accumulation and the expression of adipogenic markers[81]. CEBPα can induce adipocytic genes alongside PPARγ: forced expression of PPARγ in CEBPα-deficient fibroblasts is

sufficient to restore their capacity for lipid accumulation and expression of adipogenic markers, but the reverse is not true, with expression of CEBPα unable to rescue the phenotype of PPARγ-null cells[82]. Interestingly, PPARγ and CEBPα are able to promote the expression of each other in a positive feedback loop[82].

Many of the same pathways regulate MSC osteoblastic and adipogenic lineage commitment and differentiation; in adipocytic differentiation, these pathways converge on altering expression of PPARγ and CEBPα or their transcriptional co-factors (**Figure 1.2**). Overexpression of Wnt10b in the bipotential mouse stromal ST2 cell line promotes osteoblastogenesis while blocking adipogenesis[83], while loss of Notch signalling in a mouse white fat cell line, 3T3-L1, impaired adipogenesis and induced differentiation inhibitor expression[84], although the development of adipocytes in Notch-deficient mice suggests activation of Notch signalling is not required for adipogenic differentiation *in vivo*[85]. The effects of BMP signalling are more complex, with low concentrations of BMP2 stimulating adipogenesis, but higher concentrations favouring chondrocyte and osteoblast development[86]. Insulin or insulin-like growth factor 1 (IGF1) can signal via a number of mechanisms to promote adipogenesis, including promoting phosphorylation of cyclic AMP (cAMP) response element-binding protein (CREB) which in turn promotes PPARγ and CEBPα expression[87]. Increased expression of PPARγ and CEBPα leads to upregulated expression of adipocyte-related genes, including adiponectin, fatty acid binding protein-4 (FABP4) and fatty acid synthase (FASN)[88].

1.2.1 White adipose tissue

White adipocytes are primarily evolved for energy storage with the majority of the cytoplasmic space taken up with a single unilocular lipid droplet, but they also show a very high endocrine activity[89]. In mid 1980s, Cook *et al* identified the first adipose-

specific secreted proteins: lipoprotein lipase, responsible for triglyceride hydrolysis, and adipsin, a serine protease of the alternative complement pathway[90,91]. Despite this, it was not until the positional cloning of leptin in 1994[92] that white adipose tissue (WAT) began to be considered a significant endocrine organ. Of the adipokines identified to date[93], adiponectin (see **Section 1.3**) and leptin remain the best studied.

Leptin is produced by adipocytes in approximate proportion to their triglyceride content, thus circulating levels of leptin reflect body energy stores and body mass index (BMI). Leptin enters the bloodstream and acts at its receptor which is highly expressed in the feeding and energy expenditure centres of the brain and in peripheral tissues. Leptin has effects associated with satiety and high energy levels, including inhibiting appetite, increasing insulin sensitivity in the muscle, liver and pancreas by reducing their intracellular lipid content, and promoting growth[74,93,94]. Leptin negatively regulates bone mass centrally via hypothalamic stimulation of sympathetic tone[95,96], and peripherally, it acts to increase bone turnover and bone density with subcutaneous injection of leptin rescuing the impaired bone formation observed in leptin-deficient mice[97] and early *in vitro* work suggested a direct effect on MSC lineage commitment[98]. More recent work has utilised mice in which the leptin receptor (LepR) was conditionally ablated from limb bone marrow stromal cells but not from the axial skeleton or hypothalamic neurons in order to characterise better the bone-specific peripheral effects of leptin signalling. Jak2/Stat3 signalling was identified as mediating the increased osteogenesis, reduced adipogenesis and improved fracture healing time in these LepR knockout models, and these mice were found to be resistant to high-fat diet-induced increases in adipogenesis, reflecting the simultaneous local and systemic effects of leptin[99].

Several immunomodulatory factors are produced by WAT; for many, adipose-resident immune and epithelial cells represent the main source of production rather than the adipocytes[74]. Despite this, TNFα is secreted from adipocytes and stromo-vascular cells

and interleukin 6 (IL6) is secreted by many cell types including adipocytes and immune cells. These proinflammatory cytokines have been identified as having significant effects on the bone; as compared with high-fat diet wild type controls, high-fat diet TNFα knockout mice are reported to show increased trabecular bone volume and reduced body weight, BMSC PPARγ expression and osteoclast number and activity[100]. Similarly, high-fat diet IL6 knockout mice showed increased lipid metabolism dysregulation and increased trabecular bone volume as compared with high-fat diet wild type controls[101]. This amelioration of an obesity-induced phenotype in both models suggests a negative impact of these proinflammatory modulators on the bone and a positive effect on adipogenesis. *In vitro* work has provided evidence of direct local effects: TNFα-mediated modulation of the β-catenin pathway in a mouse pre-adipocyte cell line, 3T3-L1[102] and IL6-mediated modulation of BMP signalling pathways in human MSCs have been observed[103]. The relationship between these cytokines and bone is particularly important given that their circulating levels are proportional to BMI and are thus increased significantly in obesity. TNFα and IL6 have been linked with obesity-related insulin resistance with suggested mechanisms including increasing fatty acid release by adipocytes and reducing adiponectin synthesis[104,105].

Given its observed roles in inflammation, insulin resistance, glucose regulation and satiety, it is unsurprising that WAT has primarily been studied in the context of obesity and diabetes, a particularly interesting clinical paradigm given that obesity is often associated with resistance to the satiety-related effects of the increased circulating leptin levels which leads to a feedback cycle of increasing weight gain[106].

Interestingly, white adipose tissue can be further subdivided to visceral fat, including mesenteric, gonadal and epicardial, which is very uniform in its cell population of adipocytes, and subcutaneous fat, which is suggested to have a heterogenous mix of large unilocular adipocytes mixed with clusters of smaller multilocular adipocytes[76,107]. These

smaller adipocytes found within subcutaneous white adipose tissue are termed beige adipocytes as they are white adipocytes that show brown-like characteristics including uncoupling protein 1 (UCP1) expression (see **Section 1.2.2**) and they represent a plastic thermoregulatory mechanism with their numbers increased following prolonged cold exposure in a process known as the 'browning' of white fat[107,108]. Visceral and subcutaneous fat show distinct metabolic properties and have distinct contributions to obesity-related morbidity: transplantation of subcutaneous fat in mice has been shown to protect against obesity-induced metabolic dysregulation including improved hepatic insulin sensitivity, whereas removal of this fat exaggerated obesity-induced dysregulation[109]. Although this paradigm has yet to be directly examined in humans, this study suggests WAT distribution, rather than overall fat mass, can affect development of obesity and its comorbidities[76].

1.2.2 Brown adipose tissue

Unlike WAT which is highly evolutionarily conserved from invertebrates to humans, brown adipose tissue (BAT) is unique to mammals and is primarily involved in non-shivering thermogenesis[73,110]. BAT depots are located intra-scapullarly in mice and in the neck and supraclavicular region in humans[111]. BAT is particularly active in neonates following its rapid activation at birth, thought to confer an evolutionary advantage for survival in cold environments and during the cold stress of birth[110]. Brown adipocytes are characterised by the expression of UCP1 which is located in the inner mitochondrial membrane and collapses the mitochondrial electron gradient in order to generate heat rather than adenosine triphosphate (ATP)[74,76]. This energy expensive function is fuelled by fatty acids produced by intracellular lipolysis and is reflected in brown adipocyte histology: they display multilocular lipid droplets and an abundance of mitochondria

that give the tissue its distinctive colouring and a thermogenic potential up to 300 greater than any other tissue[108,110,112]. Proliferator-activated receptor γ coactivator 1-α (PGC1α) is a critical regulator of the BAT thermogenic response to cold exposure[113].

Aside from thermoregulation, BAT is an active secretory tissue, a function overlooked for many years. While capable of producing only very low levels of adipokines and inflammatory cytokines traditionally associated with WAT, including leptin and adiponectin, BAT has a distinct secretory profile of 'batokines', a term used to distinguish these BAT-derived factors from WAT-derived factors[108]. Several of the batokines identified to date act in a paracrine or autocrine fashion that affect the formation or function of BAT, reflecting its role in altering thermogenesis in response to environmental changes. For example, nerve growth factor (NGF) expression by BAT increases its innervation, and therefore induction of thermogenesis by sympathetic nervous system stimulation, in response to cold exposure in mice[114]. Similarly, BAT-derived vascular endothelial growth factor A (VEGFA) promotes BAT vascularisation: BAT-specific VEGFA overexpression leads to increased thermogenesis following increased vascularisation and UCP1 expression[115], and fat-specific VEGFA-knockout mice show inhibited vascularisation and thermogenesis of BAT[116]. Other factors associated with autocrine or paracrine regulation of BAT include prostaglandins, endocannabinoids and fibroblast growth factor (FGF) 23 and 2[108].

Although the exact mechanisms defining the relationship between obesity and BAT are yet to be elucidated, BAT generally seems to be associated with protection against obesity, perhaps unsurprising given its key role in lipolysis and the expenditure of energy. BAT activity is significantly reduced in morbidly obese individuals[117] and BAT-resident immune cells are primarily associated with an anti-inflammatory phenotype except under obesogenic conditions, in which secretion of proinflammatory cytokines TNFα, monocyte chemoattractant protein-1 (MCP-1) and IL1 have been observed[108].

1.2.3 Bone marrow adipose tissue

The presence of bone marrow adipocytes (BMAs) has been noted for more than a century, but only within recent years has the biological relevance of bone marrow adipose tissue (BMAT) been investigated, before which BMAs were considered inert space-fillers. Despite significant research interest over the past few years, an understanding of their origin, differentiation and function remains significantly underdeveloped as compared with WAT and BAT from which it is considered a distinct tissue despite expression of WAT-related phenotypes, including adiponectin secretion and a unilocular lipid droplet, and BAT-related phenotypes, including UCP1 expression and being responsive to cold exposure[111,118,119]. Lineage-tracing experiments have determined that BMAs are derived from MSCs, but MSCs distinct from those that give rise to WAT and BAT populations[120], suggesting they are derived from bone-resident MSCs, but further clarification is still lacking.

At birth, the marrow cavities contain active haematopoietic and osteogenic tissue known as red bone marrow which is progressively replaced throughout childhood with fatty marrow known as yellow marrow; in humans, the marrow of peripheral bones is completely converted to yellow marrow, whereas the central bones of the pelvis and lumbar vertebrae retain some red marrow throughout life. By age 25, approximately 70% of human bone marrow is BMAT, with its accumulation slowing but continuing throughout life after this point[121,122].

The majority of BMAs exist within the long bones (tibia, femur and humerus) which has historically presented practical difficulties for its study, particularly given the small size of bone in mice, a preferred model organism in biological research. Consequently, the development of osmium tetroxide staining to allow visualisation of BMAs via osmium dissolution into the fat and subsequent imaging by standard X-ray micro-computed

tomography (μCT) within the last decade has revolutionised the field and permitted a more in depth understanding of BMAT than was previously possible by histological examination alone[122].

Utilisation of osmium staining permitted the same group that pioneered its use to define two distinct forms of MAT less than a year later which they termed constitutive (cMAT) and regulated (rMAT)[118]. They identified adipocytes in rMAT as disperse within the proximal tibial region and their volume to be significantly reduced in 4- and 56-week-old C3H mice following 21 days of cold exposure. Conversely, they found cMAT to be highly concentrated adipose tissue that appears early in the postnatal period in the distal skeleton, including the hands, feet and distal tibia. cMAT does not support haematopoiesis, resembles WAT in its histology, and is generally unaffected by systemic challenges known to affect bone marrow adiposity, including cold exposure, with later evidence proving their higher resistance to lipolytic stimuli than rMAT cells[118,123]. Its development appears to be conserved between inbred mouse lines, unlike rMAT formation, which is highly variable between lines, and rMAT showed a significantly lower unsaturated fatty acid content as compared with cMAT. Interestingly, investigation using polymerase I and transcript release factor (PTRF)-deficient mice revealed a specific inhibition of rMAT formation with a relative preservation of cMAT in the distal tibia, suggesting these forms of BMAT could be of distinct lineages and/or regulated by distinct differentiation pathways, although this is yet to be confirmed[118,124].

It is interesting to note that some physiological situations, including osteoporosis[125], diabetes[126], chemotherapy[127] and anorexia nervosa[128], that are associated with increased bone marrow adiposity show a concurrent reduction in bone volume, possibly suggesting alterations in lineage commitment from osteoblastic to adipocytic. An exception is obesity, which is associated with increased bone marrow adiposity but no reduction in bone volume, possibly due to a counteracting increase in biomechanical loading of the

joints[129]. The increase in both BMAT and the contribution of BMAT to total body fat in anorexia nervosa patients seems counterintuitive but is possibly mediated via the endocrine effects associated with its secretion of adiponectin (see **Section 1.3**), and caloric restriction is now a common laboratory method for increasing bone marrow adiposity in mouse models[128].

BMAT has been identified as the largest contributor in the body to circulating adiponectin levels[128] and many of its endocrine effects are mediated through the action of adiponectin (see **Section 1.3**). Aside from adiponectin, BMAT produces leptin, which acts centrally and peripherally as discussed in **Section 1.2.1**, but its relative contribution to total circulating leptin as compared with WAT secretion is yet to be fully established. Many effects of the secretory profile of BMAs have been identified as having local effects on other cells of the bone microenvironment.

The effect of BMAs on haematopoiesis is not clearly understood. It has been observed that in areas of the mouse skeleton in which adipocytes are enriched, the activity of HSCs and HSC progenitors was greatly reduced as compared with HSCs and progenitors from regions of the skeleton in which adipocytes are scarce, and the increased BMAT following induction of a high fat diet was associated with a reduced number of haematopoietic precursor cells and a shift in differentiation from the lymphoid to myeloid compartments[130]. However, it was also observed that lipoatrophic A-ZIP/F1 mice, or mice treated with a PPARγ inhibitor to block adipogenesis, BMAT formation was inhibited but haematopoietic recovery was observed following irradiation so that the physiological role of BMAs in regulating haematopoiesis remains unclear[130]. In contrast, others have shown PPARγ agonist troglitazone-induced adipocytes support haematopoietic cells *in vitro*[131]. The reasons underlying these discordant results is unknown, but transplantation studies have provided evidence that a hierarchy exists in pre-adipocytic cells with some reducing haematopoietic precursor numbers but others

supporting haematopoietic regeneration[132], suggesting further investigation is needed in order for meaningful interpretation of results regarding the effect of BMAs on haematopoiesis.

In vitro treatment of differentiating osteoclasts with adipocyte conditioned media enhances osteoclast formation and increases expression of genes associated with osteoclast-driven bone remodelling, including cathepsin K, suggesting a positive regulation of osteoclasts by adipocytes[133]. Cells expressing preadipocyte factor-1 (Pref-1) have been observed to express RANKL; these double-positive cells are capable of inducing osteoclastogenesis from bone marrow macrophages and their numbers are increased in ageing mice[134]. An observed reduction in bone marrow adiposity following inhibition of osteoclast resorptive activity by bisphosphonate administration suggests a reciprocal regulation by osteoclasts on adipocytes[135], strengthened by evidence that *in vitro* bisphosphonate treatment suppresses MSC adipogenesis and enhances osteoblastogenesis[136]. A direct or indirect mechanism behind this observation has not yet been investigated but warrants further investigation given the traditional view that bisphosphonates exert their effects solely through inhibition of osteoclastic function.

Osteoblasts and adipocytes are generally considered to be inversely regulated given their shared progenitor cell. Co-culture of human osteoblasts with differentiating pre-adipocytes or pre-adipocyte conditioned media led to reduced mineralisation and alkaline phosphatase expression, but these effects were ameliorated by addition of a fatty acid synthase inhibitor, suggesting adipocytic inhibition of osteoclast formation is mediated at least in part via fatty acid lipotoxicity[137]. Pre-adipocytes have also been observed to secrete the Wnt inhibitor secreted frizzled-related protein-1 (sFRP1) which promotes MSC adipocytic differentiation over osteoblastic[138]. Recent *in vitro* co-culture work has suggested the transfer of RNA from human MSC-derived adipocytes to osteoblasts through extracellular vesicles identified to contain pro-adipocytic transcriptions,

including PPARγ, leptin and CEBPα and anti-osteoblastic miRNAs, although the exact nature of these extracellular vesicles and their existence and biological significance *in vivo* is yet to be established[139].

BMAs secrete some inflammatory mediators similar to WAT: under steady-state conditions, BMAT has been characterised to have significantly higher expression of pro-inflammatory cytokines including TNFα and IL6 as compared with WAT[140]. Interestingly, high-fat diet-induced obesity increased expression of these cytokines in WAT while it was reduced in BMAT[141], highlighting dissimilar inflammatory responses between these two tissues.

In summary, BMAT remains relatively understudied, comprising only around 0.25% of publications concerning adipose tissue as of 2016[142], but is now appreciated as a distinct tissue that is a highly active component of the bone microenvironment, mediating the activity of other cell types to influence bone architecture in response to external cues.

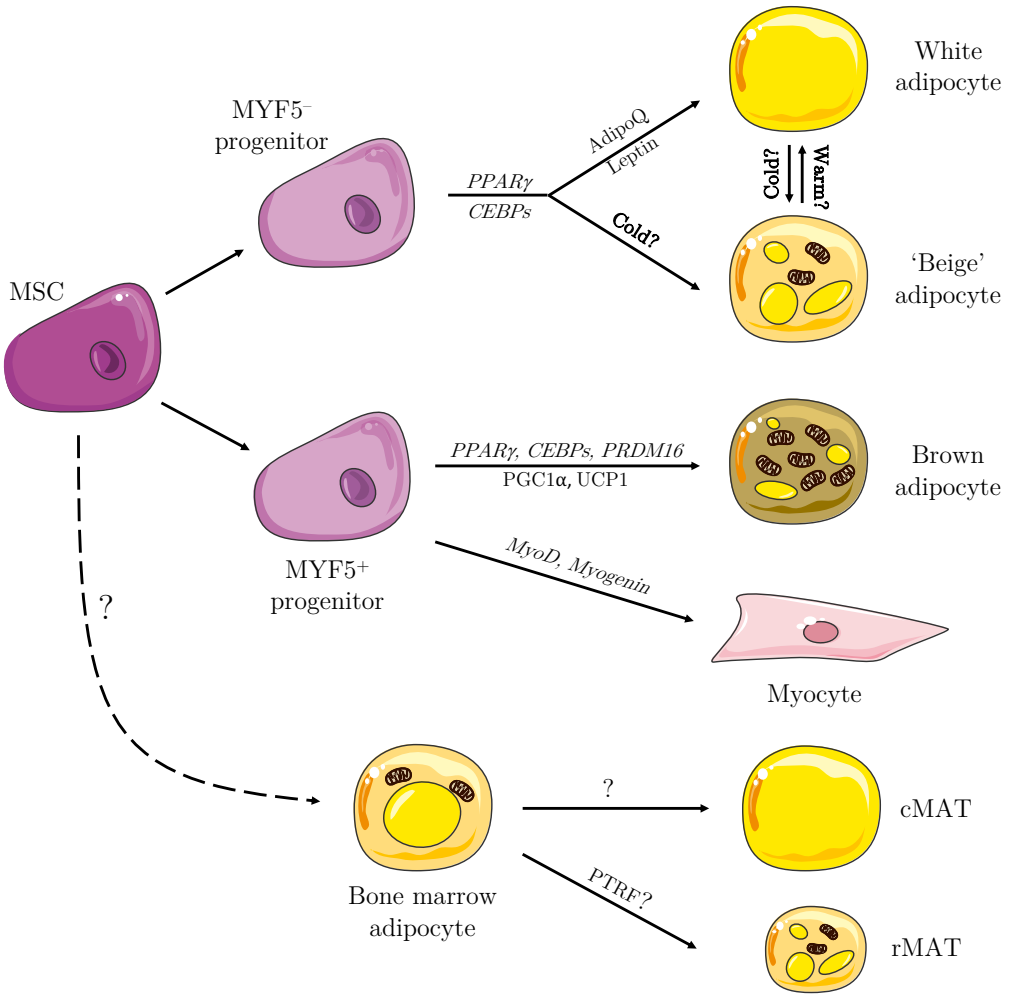


Figure 1.6: Adipocyte differentiation pathways. All adipocytes derive from mesenchymal stem cells (MSC). MYF5⁻ progenitors give rise to white and 'beige' adipocytes, while brown adipocytes and myocytes derive from MYF5⁺ progenitors. The origin of bone marrow adipocytes and the factors regulating their subsequent differentiation to cMAT and rMAT remain poorly characterised. Some key proteins expressed by cell types are indicated. Italics indicates key transcriptional regulators necessary for that differentiation stage and bolding indicates conditions thought to promote that pathway. AdipoQ: adiponectin; PGC1α: proliferator-activated receptorγ coactivator 1-α; UCP1: uncoupling protein-1; PTRF: polymerase I and transcript release factor; cMAT: constitutive marrow adipose tissue; rMAT: regulated marrow adipose tissue. Figure adapted from Smart Servier Medical Art.

1.3 Adiponectin

The first published description of adiponectin came in 1995 following sequencing of pre-adipocytic mouse 3T3-L1 cells during which the expression of a novel secretory protein that the authors named Acrp30 (adipocyte complement-related protein of 30kDa) was found to increase over 100-fold following adipocytic differentiation[143]. Shortly afterwards, three independent groups published work identifying the same protein via sequencing of a pre-adipocytic cell line[144], sequencing of primary human fat tissue obtained from female patients at surgery[145], and via its gelatin binding-mediated purification from human serum[146]. These groups termed the newly identified protein AdipoQ, apM1 (adipose most abundant gene transcript 1) and GBP28 (gelatin-binding protein of 28kDa) respectively, leading to some years of crosstalk within the field before the nomenclature adiponectin/AdipoQ was accepted. Adiponectin is now known to be a signalling molecule primarily secreted by adipocytes that exerts complex endocrine and paracrine effects.

1.3.1 Structure and circulating levels

Adiponectin is a 30kDa protein of 244 amino acids in humans and 247 amino acids in mice[147]. In both species, it consists of four domains: a C1q-like globular carboxy-terminal domain, an N-terminal signal peptide responsible for translocation to the endoplasmic reticulum (ER), a short collagenous domain and a short domain commonly referred to as the variable region due to lack of easily recognisable structural motifs that is involved in adiponectin oligomerisation[147,148]. Adiponectin closely resembles complement-related C1q in its primary amino acid sequence and subunit domain structure, but X-ray crystallography has revealed structural homology with TNFα, perhaps suggesting an evolutionary link between the two[149].

Adiponectin does not circulate in the blood in its 30kDa monomeric state, instead forming trimeric homo-oligomers likely due to the interfacing regions of individual monomers forming a highly hydrophobic interior[148]. Despite this, the globular C1q domain of adiponectin generated from proteolytic cleavage of full-length adiponectin is found naturally in serum and has been shown to be biologically active[147,150]. Trimeric adiponectin is termed low molecular weight adiponectin (LMW) and forms the basic building block of adiponectin; it can further oligomerise to form middle molecular weight (MMW) hexamers and high molecular weight (HMW) multimers, including dodecamers and 18-mers (**Figure 1.7**), all of which are found naturally in the serum[148,151,152].

Formation of these larger oligomers is reliant on formation of a disulphide bond between LMW adiponectin oligomers at a cysteine (position 36 in humans and position 39 in mice) which exists in a highly conserved sequence of six amino acids in the variable region[147,148]: substitution of this cysteine for alanine results in adiponectin that is unable to oligomerise beyond trimers[153]. Endoplasmic reticulum (ER) chaperones including Ero1L-α and DsblA work with ERp44, a protein-disulphide isomerase located in the ER-Golgi intermediate compartment that acts as the critical ER chaperone in controlling the oligomerisation state of adiponectin[154]. ERp44 retains oxidised LMW and MMW adiponectin, but not HMW adiponectin, in a pH-dependent manner, and reduces them to reduced LMW adiponectin, thus facilitating disulphide bond formation for the assembly of HMW complexes before secretion[154]. Further modification of adiponectin determines the serum half-life of adiponectin, which is usually around 75 minutes before clearance mediated primarily by the liver[155]: O-linked glycosylation of threonine residues within the N-terminal by sialic acids determines the half-life of adiponectin by modulating its clearance from the bloodstream[156], although the exact mechanism by which it does this remains uncertain.

The extent to which these oligomeric forms interconvert extracellularly *in vivo* remains unclear: *in vitro*, HMW adiponectin can be converted to hexamers following a reduction in pH of the solution to 6 or below (14, 34, 40) and extracellular conversion of hexamers to trimers has been described via an extracellular redox system[157], but fluorescently labelled recombinant adiponectin injected into mice revealed no significant interconversion occurs *in vivo*[158] which is supported by evidence from human subjects[159] suggesting their ratios at secretion are critical in determining their circulating ratios.

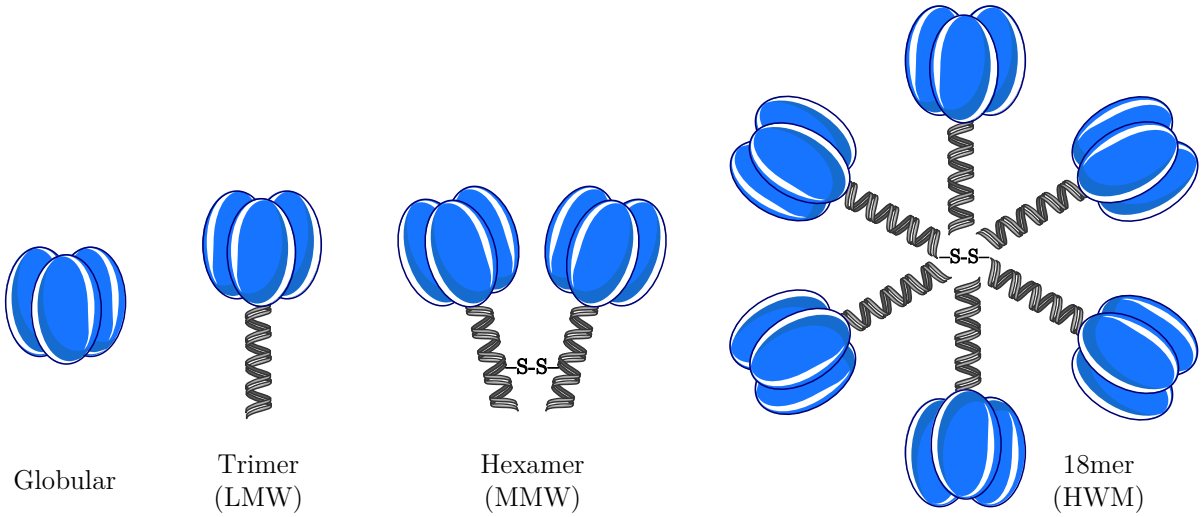


Figure 1.7: Adiponectin oligomeric complexes. 30kDa monomeric adiponectin forms low molecular weight (LMW) trimers which can further oligomerise by the formation of disulphide bonds (indicated by S-S) to form middle molecular weight (MMW) hexamers or high molecular weight (HMW) multimers, including 18mers. Proteolytic cleavage of full-length adiponectin produces globular adiponectin. Figure adapted from Smart Servier Medical Art.

1.3.2 Adiponectin receptors

Adiponectin signals through two cell surface receptors, adiponectin receptor 1 (AdipoR1) and adiponectin receptor 2 (AdipoR2), the distribution and activities of which were first described following their expression cloning nearly 10 years after the first published description of adiponectin[150].

1.3.2.1 Structure and distribution

AdipoR1 and AdipoR2 are significantly homologous (67% amino acid identity) integral membrane proteins that show an inverse topology to G-protein coupled receptors (GPCRs), with seven transmembrane domains but an internal N-terminus and an extracellular C-terminus[152]. Both receptors are highly evolutionarily conserved: structural homologues of the receptors are found in yeast[160], and human and mouse AdipoR1 and AdipoR2 share 96.8% and 95.25% identity respectively[161]. The original paper in which these receptors were cloned found the highest expression of AdipoR1 to be in the muscle and of AdipoR2 to be in the liver[150], but further work has identified them both to be ubiquitously expressed throughout the body[162,163], including in human osteoblasts[164] and adipose tissue[165].

1.3.2.2 Signalling

Activation of AMP kinase (AMPK) and PPARα were identified as two main intracellular signalling outcomes of adiponectin receptor signalling in the original paper that first cloned AdipoR1 and AdipoR2; AdipoR1 signalling is more significantly associated with AMPK activation, where PPARα activation was more significantly associated with AdipoR2 activation[150,166]. A significant cross-over in signalling of AdipoR1 and AdipoR2 exists such that they cannot be delineated independent of each other; the shared outcomes of AdipoR1 and AdipoR2 signalling is highlighted by the association of single nucleotide polymorphisms (SNPs) in the human AdipoR1 and AdipoR2 genes, as well as the adiponectin gene itself, with reduced insulin sensitivity[167,168]. This is likely due in part to their association with the same intracellular binding protein, adaptor protein containing pleckstrin homology domain, phosphotyrosine binding domain and leucine zipper motif 1 (APPL1), which has been

identified as playing a key role in mediating the effects of adiponectin signalling: suppression of APPL1 expression in cultured skeletal muscle cells reduced adiponectin-induced glucose uptake and GLUT4 translocation, whereas its overexpression enhanced these adiponectin-induced actions[169], and whole-body APPL1-knockout mice show impaired adiponectin signalling[170]. Adiponectin receptor signalling is summarised in **Figure 1.8**.

APPL2, an APPL1 isoform that shares 54% amino acid sequence homology with APPL1, has been suggested as a negative regulator of adiponectin signalling in a reciprocal relationship with APPL1: *in vitro* in C2C12 mouse myotube cells, APPL2 bound directly to AdipoR1 or AdipoR2 to prevent receptor-APPL1 interaction via competitive inhibition and sequestered APPL1 by the formation of heterodimers which dissociated upon stimulation by adiponectin, insulin or TZDs[171]. *In vivo*, mice with skeletal muscle-specific deletion or overexpression of APPL2 show enhanced or reduced skeletal muscle insulin sensitivity and glucose uptake respectively[172].

Mechanistically, upon adiponectin signalling, APPL1 mediates the translocation of liver kinase B1 (LKB1) from the nucleus, where it exists under basal conditions, to the cytoplasm where it can activate AMPK[173]. AMPK acts a major energy-sensing coordinator in the cell and has many diverse effects upon its activation, including indirect inhibition of NFκB-mediated inflammation[174], increased fatty acid oxidation via inhibition of acetyl-coenzyme A carboxylase (ACC) which mediates the rate limiting step in fatty acid synthesis[175], and direct phosphorylation and activation of the insulin receptor to potentiate insulin signalling[176]. Adiponectin-mediated AMPK phosphorylation is reduced in cultured skeletal muscle myotubes of obese or type II diabetic patients as compared with healthy controls, suggesting impaired adiponectin receptor signalling and subsequently impaired adiponectin action in these individuals[177].

APPL1 also mediates crosstalk between the adiponectin and insulin signalling pathways in an AMPK-independent manner. APPL1 forms a complex with insulin receptor substrate proteins 1 and 2 (IRS1/2); following adiponectin- or insulin-stimulated APPL1 phosphorylation, this APPL1/IRS1/2 complex is recruited to the insulin receptor where it potentiates insulin-related effects via the PI3K/AKT signalling pathway. Biological effects of insulin signalling include lipogenesis, gluconeogenesis and translocation of glucose transporter GLUT4 to the cell membrane in peripheral tissues in order to increase glucose uptake[178] and APPL1-deficient mice show significantly impaired insulin and glucose tolerance[170]. In this way, adiponectin exerts insulin-sensitising effects, reducing circulating glucose levels without altering insulin levels[179]. This provides a mechanistic insight into the observed positive relationship between circulating adiponectin levels and insulin sensitivity[180].

APPL1 expediates phosphorylation and activation of kinases of the p38 MAPK pathway by tethering p38 MAPK with its upstream activating kinases, including TGFβ-activated kinase 1 (TAK1) and mitogen-activated protein kinase kinase 3 (MKK3)[181]. p38 MAPK has diverse biological roles including regulating inflammation, apoptosis and cellular differentiation[182]; its activation following adiponectin receptor signalling increases fatty acid oxidation and glucose uptake in C2C12 mouse myotubes with this effect blocked following application of a p38 MAPK-specific inhibitor[150].

Adiponectin receptor signalling is associated with increased expression and activation of PPARα, which in turn upregulates acetyl CoA oxidase (ACO) and uncoupling proteins to promote fatty acid oxidation and energy expenditure[150]. Aside from its roles in energy regulation, activation of PPARα is associated with anti-inflammatory effects as demonstrated by PPARα-knockout mice, which show a prolonged inflammatory response when challenged with a pro-inflammatory factor[183]. Interestingly, *in vivo* stimulation of PPARα with a PPARα agonist led to significantly increased AdipoR1

and AdipoR2 expression in the WAT of obese diabetic mice, suggesting a positive feedback loop between adiponectin receptor signalling and expression[184].

Despite the crossover in the signalling pathways, AdipoR1 and AdipoR2 have been identified as having some distinct effects. One report found revascularisation following chronic hind limb ischemic surgery in 9- to 11-week-old male AdipoR2 knockout mice was significantly attenuated, whereas AdipoR1 deficient mice showed no significant difference in blood flow recovery as compared with wild type mice; this same study identified significant metabolic dysfunction in high-fat diet AdipoR1 knockout mice, whereas AdipoR2 knockout mice appeared protected from weight gain and obesity-induced metabolic dysfunction[185]. A similar study identified 15- to 32-week-old male AdipoR1 knockout mice as having increased body weight and reduced glucose tolerance as compared with wild type controls, whereas AdipoR2 knockout mice were lean and resistant to high fat diet-induced obesity[186]. In a mouse model of diabetes, skeletal muscle expression of AdipoR1 was found to be significantly reduced as compared with lean controls whereas hepatic AdipoR2 expression was not altered by diabetes or obesity[187]. Similarly, AdipoR1 or AdipoR2 expression in the skeletal muscle of obese mice was unchanged as compared with lean controls, but AdipoR2 expression was decreased in the adipose tissue[188]. These results suggest tissue- and receptor-specific involvement in disease.

It is likely that these differential effects are mediated at least in part by the distinct affinities of the different oligomeric complexes for binding to and eliciting downstream signalling from AdipoR1 and AdipoR2. In the original paper in which the adiponectin receptors were cloned, these differential effects were noted in C2C12 mouse myotube cells: siRNA-mediated suppression of AdipoR1 expression greatly reduced globular adiponectin binding but had little effect on full-length adiponectin binding, whereas siRNA knockdown of AdipoR2 reduced binding of both globular and full-length

adiponectin. In accordance with this, siRNA knockdown of AdipoR1 in C2C12 myotubes significantly reduced PPARα ligand activity, fatty acid oxidation and glucose uptake following treatment with globular adiponectin but showed no effect on these outcomes following full-length adiponectin treatment[150]. Similarly, others have shown that incubation of primary rat muscle cells with trimeric adiponectin increased AMPK phosphorylation and activation, but the same response was not elicited following treatment with MMW or HMW adiponectin complexes[153]. These data underpin the current understanding that AdipoR1 is a high-affinity receptor for globular and LMW adiponectin and a low-affinity receptor for MMW and HMW adiponectin, whereas AdipoR2 is an intermediate-affinity receptor for both large oligomeric and globular adiponectin. The potential clinical significance of these varied responses to the different adiponectin oligomeric complexes is discussed in **Section 1.3.3**. Interestingly, the authors found globular and full-length adiponectin both increased AMPK and ACC phosphorylation in C2C12 myotubes, whereas in hepatocytes, full-length adiponectin alone elicited these outcomes, suggesting tissue-specific effects of adiponectin receptor signalling, likely reflecting the tissue-specific variation in the level of AdipoR1 and AdipoR2 expression[150].

More recent *in vitro* experimentation in HEK293AD cells, a derivative of the commonly used human embryonic kidney (HEK) 293 cell line, has identified the formation of homo- and heteromeric complexes by AdipoR1 and AdipoR2 in resting conditions and the subsequent dissociation of these complexes in response to adiponectin. The heteromers were found to dissociate faster than the homomers, and cells which favoured heteromer formation showed delayed activation of AMPK as compared with cells with predominantly homomers, suggesting differential signalling properties between different complexes[189]. However, whether these complexes are observed *in vivo* and the biological significance of any effect they may have remains unknown.

MMW and HMW forms of adiponectin, but not trimeric or globular, have been identified to bind cell surface T-cadherin[190] leading to its possible consideration as a third adiponectin receptor, but the biological function and significance of its interaction with adiponectin remains uncertain. T-cadherin knockout mice show a significant increase in circulating adiponectin levels, particularly HMW adiponectin, and have altered revascularisation and cardioprotection during ischemia-reperfusion injury[191,192], but osteoblast-specific deletion of T-cadherin led to no significant bone phenotype[96] and the key phenotypic aspects of an adiponectin knockout mouse are recapitulated in AdipoR1/AdipoR2 double knockout mice[166]. Together, these data suggest a limited biological role for T-cadherin in mediating the effects of adiponectin *in vivo*, particularly given its lack of an intracellular signalling domain[161], and its contribution to adiponectin signalling pathways remains unknown, so AdipoR1 and AdipoR2 were considered the adiponectin receptors for study in this work. However, it has been postulated that T-cadherin could act as a co-receptor for an as yet unidentified signalling receptor, likely AdipoR1 and/or AdipoR2, through which it could mediate and fine-tune adiponectin signalling[190]. Given the remaining confusion surrounding the role of adiponectin signalling in bone, this possibility warrants further investigation, since it could help to contextualise currently discordant results.

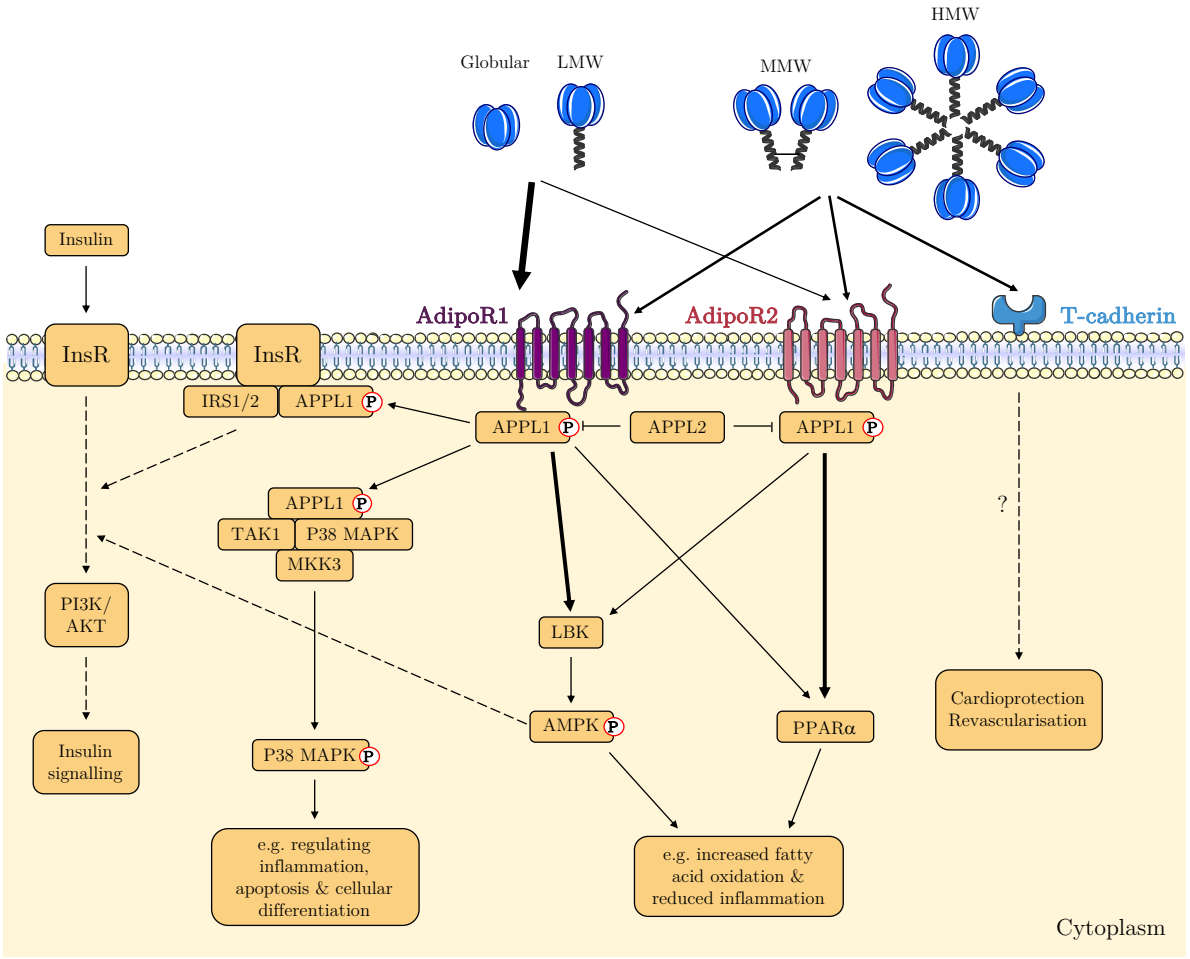


Figure 1.8: Schematic representation of key adiponectin signalling pathways. Cell surface receptors AdipoR1 and AdipoR2 are bound by extracellular adiponectin and associate intracellularly with adaptor protein APPL1 to trigger downstream signalling mediated by APPL2. APPL1 mediates AdipoR1/2 crosstalk with and stimulation of with the insulin signalling pathway to augment responses including lipogenesis and glucose uptake primarily via the PI3K/AKT pathway. AdipoR1 preferentially binds globular and LMW adiponectin and is most associated with LBK activation and cytosolic translocation to enable AMPK activation by phosphorylation. AdipoR2 is an intermediate-affinity receptor for globular and large oligomeric adiponectin and is most associated with activation of PPARα pathways. APPL1 expediates activation by phosphorylation of p38 MAPK by tethering it to its upstream regulators including TAK1 and MKK3. MMW and HMW adiponectin can bind to T-cadherin which lacks an intracellular signalling domain, and the mechanisms by which it mediates cardioprotection and revascularisation remain unknown. Arrowheads indicate activation pathways; bluntheads indicate inhibitory pathways. Broken lines indicate indirect signalling. Thicker arrows indicate potency of binding or effect. LMW/MMW/HMW: low/middle/high molecular weight adiponectin; AdipoR1/2: adiponectin receptor 1/2; InsR: insulin receptor; PI3K: phosphatidylinositol 3-kinase; AKT: protein kinase B; IRS1/2: insulin receptor substrate proteins 1/2; APPL1/2: adaptor protein containing pleckstrin homology domain, phosphotyrosine binding domain and leucine zipper motif 1; TAK1: TGFβ -activated kinase 1; p38 MAPK: p38 mitogen-activated protein kinase; MKK3: mitogen-activated protein kinase kinase 3; LBK: liver kinase B1; PPARα: peroxisome proliferator-activated receptor-α. Adapted from Smart Servier Medical Art.

1.3.3 Adiponectin in health and disease

Adiponectin is primarily produced by BMAT[128] and is the most abundantly expressed adipokine in the blood, accounting for 0.01% of total plasma protein[146]. A significant sexual dimorphism is known to exist in its circulating levels: cohorts of healthy men and women with an average age of around 50 years had average circulating adiponectin concentrations of around 7.1 and 12.3µg/ml respectively[193] possibly due to the generally higher BMAT content in women than men[124]. Despite this, age represents a significant independent positive variable in adiponectin levels in both men and women as levels rise throughout life, with women showing a particularly large increase in adiponectin levels at the menopause considered to be due to several menopause-associated factors, including altered oestrogen levels, fat redistribution and increased BMAT[124,194–196]. Adiponectin has been linked with longevity, with the children of centenarians identified to have significantly increased adiponectin levels, suggesting heritability of genetic protection[197]. Interestingly, a role for adiponectin in longevity is supported by mice in which adiponectin is transgenically overexpressed: as well as the previously noted protection from high-fat diet-induced weight gain and shortened lifespan, these mice show a significantly increased lifespan on conventional low-fat chow as well[198].

Adiponectin has been observed to be reduced in several pathological states, including type II diabetes[199], coronary artery disease[200] and anorexia nervosa[201], sparking interest in its potential as a protective adipokine against the development of metabolic syndrome[202]. Indeed, its circulating levels have been identified as negative indicators of development of type II diabetes and hypertension[203,204] and single nucleotide polymorphisms (SNPs) in the adiponectin gene locus 3q27 have been associated with diabetes and cardiovascular disease development[205,206].

Despite its cell of origin, it has been observed for many years that adiponectin circulating levels are significantly reduced in obesity[207]. This seemingly paradoxical relationship is now understood to be a reflection of the complex obesity-induced adipose dysfunction, including mitochondrial dysfunction, ER stress, and the sustained low-grade inflammation and production of pro-inflammatory cytokines like TNFα which directly inhibit adiponectin transcription[208,209]. Accordingly, patients with rheumatoid arthritis (RA) had significantly reduced serum adiponectin levels as compared with age-, sex- and BMI-matched healthy controls. Interestingly, however, this relationship persisted regardless of disease activity: a reduced circulating adiponectin concentration was observed in both newly diagnosed RA patients and those in clinical remission[210]. This is perhaps explained by the observation that the proportion of LMW adiponectin correlates negatively more significantly with disease activity in RA patients than total circulating adiponectin[211].

Evidence exists to suggest that the ratio between LMW, MMW and HMW adiponectin, rather than total circulating adiponectin, is associated with other pathological states. The contribution of HMW adiponectin to total circulating levels was found to be significantly reduced in obese patients as compared with controls[212]; an independent study of type II diabetes corroborated an inverse association of HMW proportion of total adiponectin with BMI and also identified a positive relationship between LMW proportion and duration of diabetes[213], and an increased HMW contribution is observed in patients with chronic obstructive pulmonary disease (COPD) as compared with healthy controls[214]. The contribution of HMW to total circulating adiponectin, rather than a change in total adiponectin concentration itself, has been shown to correlate with thiazolidineione (TZD)-mediated improvement in insulin sensitivity *in vivo* suggests that alteration in oligomeric ratios is a clinically relevant consideration[215].

While exact mechanistic explanations for these alterations in oligomeric ratios in pathogenic states are still lacking, two papers from the same group show that succination, defined as *S*-(2-Succinyl)cysteine formation following reaction of Krebs cycle intermediate fumarate with cysteine residues in protein, of adiponectin blocks its multimerization: adipocytes cultured *in vitro* in high glucose medium and the adipose tissue of diabetic mice both show increased succination. This suggests that increased succination of adiponectin due to Kreb cycle intermediate accumulation could underly the reduced circulating adiponectin concentration and increased LMW contribution observed in diabetes[213,216,217]. Equally, pre-clinical data shows that while female mice show a significantly higher contribution of HMW to total circulating adiponectin at baseline than males, the ratio of HMW adiponectin is significantly reduced in both males and females following exogenous insulin administration and restored following normalisation of insulin levels, suggesting the observed differences in obesity are due at least in part to altered insulin levels[218]. Aside from these proposed mechanisms, it is likely that these alterations in multimeric distribution in pathological conditions is due at least in part to the distinct affinities of the different oligomeric complexes for AdipoR1 and AdipoR2 binding as discussed in **Section 1.3.2.2**.

Insulin resistance is the most well-documented phenotype of adiponectin knockout mice[219–221]; this phenotype is rescued upon virus-mediated adiponectin expression[222] and is recapitulated in AdipoR1/AdipoR2 double knockout mice[166]. Alongside insulin resistance, these mice show increased TNFα expression in adipose tissue mRNA[222] and increased neointimal formation[219], highlighting the anti-inflammatory and anti-atherogenic effects of adiponectin. Ablation of adiponectin expression also reduced responsiveness to TZDs suggesting adiponectin is at least in part responsible for mediating the anti-diabetic effects of these drugs[220].

A more recent tool available for investigating the biological effects of adiponectin is AdipoRON. AdipoRON is an orally bioavailable small molecule agonist of the adiponectin receptors. First described in 2013[223], it has been shown to bind to both adiponectin receptors, although with a slightly higher affinity for AdipoR1 (K_D=1.8µM) than AdipoR2 (K_D=3.1µM), and has been characterised to show similar effects to adiponectin, including activation of the AMPK and PPARα pathways[223] at concentrations upwards of around 10µM. In the original paper describing AdipoRON in 2013, its effects on insulin resistance and glucose intolerance were reported[223]. Since then, research on the effects of AdipoRON in diabetes-related systems has continued, where it has been found to have positive effects in reducing pathology[224,225], unsurprising given the body of research supporting a role of adiponectin in these systems. The majority of this work has been performed *in vivo*, possibly because AdipoRON represented the first orally bioavailable adiponectin receptor agonist, increasing the plausibility of *in vivo* investigation. *In vitro*, 5-100µM AdipoRON inhibited human aortic vascular smooth muscle cell proliferation, DNA synthesis and cyclin D1 expression via AMPK-dependent and AMPK-independent suppression of phosphorylation of mTOR and its downstream targets[226], 20µmol/L AdipoRON prevented myostatin-induced upregulation of fatty acid synthesis and downregulation of insulin activity in a mouse hepatic cell line[227], and 0-100µM AdipoRON activated AMPK and p38 MAPK to elicit survival signals and increased mitochondrial dysfunction through mitochondrial calcium overload and ERK1/2 activation in a human pancreatic cancer cell line[228].

1.4 Adiponectin in the bone

Evidence on the role of adiponectin and its receptors in bone remains controversial and inconclusive, likely due to variation in experimental design and the complex nature of

adiponectin signalling[229]. Large human cohorts remain the most clinically relevant source of information, but pre-clinical *in vitro* and *in vivo* studies provide an opportunity for causative and mechanistic understanding of the activity and effect of adiponectin in bone, although misleading results following contamination of recombinant adiponectin with lipopolysaccharide has contributed to confusion in this area[229].

1.4.1 Human evidence

Clinical studies investigating the relationship between circulating adiponectin and bone health most often define the latter by BMD of the hip or lumbar spine by DEXA scanning, but major osteoporotic fracture occurrence or serum bone turnover markers are variously used. The majority of these studies have made use of healthy women, particularly around or after menopause and often compared with pre-menopausal women, reflecting their status as a high-risk group for osteoporotic development.

In some cohorts of post-menopausal women, adiponectin has been identified as a negative correlate of BMD following adjustment for age, BMI and other confounding factors[230–232], whereas other reports suggest no significant correlation exists between the two variables[233,234]. Interestingly, one study concluding no significant relationship exists between adiponectin and BMD used a cohort of pre- and post-menopausal women adjusted for age but not for menopausal status[235]. Evidence from other studies suggest this could be a significant confounding factor: one study in a cohort of Chinese women found a positive correlation between adiponectin and bone turnover markers in post-menopausal women but not pre-menopausal women, and another study noted that the significant negative relationship between adiponectin and BMD in a mixed cohort of pre- and post-menopausal women was significantly strengthened in post-menopausal women alone, but was non-significant in pre-menopausal women, suggesting adjustment

for menopausal status is critical in understanding this relationship. Similarly, age and ethnic background should also be considered when interpreting conflicting results: one report in healthy pre- and post-menopausal women found a significant negative relationship between total BMD and adiponectin levels when stratified for menopausal status, but this did not persist significantly following further adjustment for age[196], while another study identified a significant negative correlation between adiponectin and BMD in Caucasian women that was not present in Hispanic women[236].

This relationship in healthy men has been less well-studied but shows similar results: men with the highest adiponectin levels in a cohort of over 3,000 men and women showed a significantly increased risk of fracture as compared with those in the lowest adiponectin concentration tertile following adjustment for confounders including sex, age, BMI and race[234], while analysis of elderly men found a significant negative correlation between adiponectin and BMD, although interestingly no significant effect on fracture risk was noted in this cohort[231].

The effect of diseases known to affect adiponectin concentration on this correlation is poorly studied, but one study found the negative correlation persisted in both men and women with type II diabetes and that higher adiponectin levels were significantly associated with increased fracture risk at any major osteoporotic site[237], and in a separate cohort of type II diabetics, both total and HMW adiponectin were negatively associated with BMD and positively with moderate or severe vertebral fracture occurrence in middle-aged men but not post-menopausal women following adjustment for confounders including age, duration of diabetes and BMI[238]. This negative correlation was also reported in wheelchair-bound men with chronic spinal cord injury and in the BMD of the distal radius in men with chronic kidney disease undergoing haemodialysis, although this was not observed to be significant at the lumbar spine, suggesting site specificity[239,240].

Most of the studies carried out on the role of adiponectin in the bone has been in middle-aged and elderly populations, reflecting the fact that osteoporosis is an age-related disease. However, the negative correlation between adiponectin and BMD has been identified in young women with anorexia nervosa[241], and one study of a mixed cohort of over 7,500 male and female children found a significant inverse relationship of BMD and bone area with circulating adiponectin persisted pre- or early pubertally (mean age 9.9 years old) and late pubertally (mean age 15.5 years old), suggesting adiponectin is perhaps involved in bone mass accrual in childhood as well as bone loss associated with old age or disease[242]. A similar study found no association between adiponectin and BMD in pre-pubertal girls, perhaps attributable to an underpowered study design of only 48 girls[243]. Finally, the reductions in total body, spine and hip BMD in morbidly obese women twelve months after bariatric surgery were found to be significantly positively associated with circulating adiponectin concentration following adjustment for body composition parameters, leading the authors to conclude adiponectin increase could have an independent action on BMD in these patients[244].

These studies provide evidence that adiponectin concentration is likely a negative correlate of BMD in human cohorts, but conflicting results have been reported and many questions remain to be resolved. In particular, correlative human studies of this kind cannot provide causative information on the observed relationships, so it remains unknown whether reduced BMD is a consequence of increased adiponectin levels or vice versa, or whether they are independently regulated by as yet unidentified confounding factors. Some evidence for a causative effect of adiponectin on bone is provided by the negative association of a haplotype in the adiponectin gene with lumbar spine BMD in a cohort of Chinese postmenopausal women[245] and the similar negative association of two AdipoR1 SNPs, but no AdipoR2 SNPs, with lower lumbar spine BMD in a cohort

of postmenopausal Korean women[246]. The use of pre-clinical studies can provide insight to the direct effect of adiponectin on the bone.

1.4.2 Pre-clinical evidence

Pre-clinical studies making use of *in vivo* mouse models or *in vitro* cell culture have also provided conflicting evidence on the role of adiponectin in the bone, with conflicting *in vitro* and *in vivo* results sometimes presented in the same paper. A summary of this section is provided in **Table 1.1**.

One of the first descriptions of the bone phenotype of adiponectin knockout mice came in 2006, where C57Bl/6-derived 8-week-old male mice in which adiponectin had been globally deleted or transgenically overexpressed in the liver were found to have no significant bone phenotype[247]. The group explained this by carrying out *in vitro* investigation: following confirmation that adiponectin and its receptors were all expressed in the osteoblasts, osteoclasts, bone marrow cells and bone marrow macrophages of the wild type mice, it was demonstrated that cultured bone marrow cells from the adiponectin deficient mice showed a reduced osteogenic capacity as compared with wild type cells, prompting the group to speculate a positive effect of adiponectin on bone formation in a local environment. Conversely, addition of recombinant adiponectin to cultured wild type bone marrow cells significantly inhibited osteogenesis, suggesting a direct inhibitory endocrine effect of circulating adiponectin on bone formation; taken together, it was concluded that this demonstrated opposing local and systemic effects of adiponectin which together produced no bone phenotype *in vivo*[247].

Shortly after this first report, Cornish *et al* also reported distinct *in vitro* and *in vivo* effects of adiponectin in the bone[248]. An increased trabecular bone volume and number was identified in 14-week-old male C57Bl/6 global adiponectin knockout mice, although

this was non-significant in 8- and 22-week-old mice; these alterations in bone volume were associated with reduced bone fragility and were concluded to suggest a negative effect on bone volume systemically. However, *in vitro*, treatment with recombinant full-length adiponectin dose-dependently increased the osteogenic potential of primary rat and human osteoblasts and inhibited the osteoclastogenesis of primary rat bone marrow cells, suggesting a direct positive effect on bone formation. The authors concluded, similar to the original 2006 paper, that adiponectin acts to stimulate osteoblasts and inhibit osteoclasts directly but acts indirectly *in vivo* to suppress overall bone volume[248]. Interestingly, several years later, the same group published in the same journal reporting that eight- to 37-week-old female C57Bl/6 global adiponectin knockout mice showed reduced whole-body BMD, cortical thickness and trabecular bone volume and concluding a positive effect of adiponectin on bone density in contrast to their previous conclusions[249]. While no explanation was proposed for these contradictory findings, it is likely that a significant sexual dimorphism[250] could explain this at least in part, including in the age-related bone loss of C57Bl/6J mice, in which the phenotype is more pronounced in female mice than males[251], highlighting the need for age and sex matching for meaningful interpretation of results.

Some pre-clinical reports have identified a positive relationship between adiponectin and bone volume in *in vivo* models in contrast to human epidemiological data. Femurs of three-day-old luciferase-tagged C57Bl/6 wild type mice were isolated and explanted into the back muscles of C57Bl/6 eight- to 10-week-old wild type or adiponectin knockout mice before their harvest and analysis 4 weeks later to observe the effect of acute changes in adiponectin signalling to the bone microarchitecture[252]. The bone explants in adiponectin deficient mice were observed to have reduced trabecular volume and cortical thickness and increased osteoclast number, suggesting lack of adiponectin retards bone growth. *In vitro*, adiponectin treatment of RAW264.7 cells, an immortalised mouse

macrophage cell line, reduced their osteoclastic survival, proliferation and differentiation. Together, these data were concluded to suggest that adiponectin inhibits bone resorption, in contrast to previous findings, although the sex of these animals was not reported making contextualisation of the results difficult[252].

Overexpression of adiponectin has also provided evidence of a positive effect of adiponectin in bone. Eight-week-old male C57Bl/6 mice treated with an adenovirus expressing full length mouse adiponectin and culled 14 days later showed increased trabecular bone mass and reduced osteoclast number and serum bone resorption markers. This was supported by reduced osteoclastic capacity of mouse bone marrow macrophages and human mononuclear cells and increased alkaline phosphatase expression and mineralisation of MC3T3-E1 mouse osteoblastic cells following *in vitro* treatment with adiponectin[253]. Similarly, 12-week-old C57Bl/6 male mice transgenically overexpressing full-length human adiponectin in the liver showed increased bone volume and bone formation rate, although no change in osteoclast number or osteoclastic serum markers were observed[254]. These overexpression models support a positive systemic effect of adiponectin on bone. This is supported by the observed increased bone volume in 20-week-old diet-induced obesity diabetic mice and adiponectin knockout mice treated for two weeks with adiponectin receptor agonist AdipoRON[255].

Interestingly, eight- and 56-week old female and eight-week old male FVB-derived mice transgenically overexpressing porcine AdipoR1 showed increased bone volume and trabecular number, with serum osteocalcin and OPG levels elevated significantly in the 8-week-old females. *In vitro* knockdown of AdipoR1 reduced MC3T3 and bone marrow stem cell mineralisation and expression of osteoblast-related genes[256]. This suggests that the positive effect of adiponectin on bone microarchitecture and bone cells observed in adiponectin overexpression models is recapitulated by overexpression of AdipoR1 and thus that its effects are mediated at least in part via this receptor. However, male 12-

week-old C57Bl/6J:129/Sv mice with an osteoblast-specific deletion of AdipoR1, AdipoR2, AdipoR1/AdipoR2 or T-Cadherin have been reported to cause no significant bone phenotype[96], warranting further investigation.

Alongside these reports suggesting a positive effect for adiponectin signalling in bone, however, discordant results suggesting the opposite conclusion exist. It was reported in 2013 that C57Bl/6-derived 16- to 18-week-old female mice in which adiponectin had been globally deleted showed no significant change in BMD as compared with wild type controls, but they were protected from the ovariectomy-induced bone loss experienced by the controls[257]. It was demonstrated that bone marrow stem cells from adiponectin deficient mice showed increased proliferation and osteoblastic differentiation as compared with controls, suggesting a role for adiponectin in accelerating post-menopausal osteoporosis via inhibition of bone marrow stem cell osteogenic potential[257]. Two separate reports on 12-week-old male adiponectin knockout mice on a pure or mixed C57Bl/6 background identified increased BMD, bone volume and fewer osteoclasts than age-matched controls[96,258]. Equally, eight- and 16-week-old female FVB mice transgenically overexpressing full-length adiponectin have been found to show significantly reduced femur BMD and maximum load to breakage and reduced peak load during spine compression testing[259]. These results suggest an inhibitory role for adiponectin in bone mass accrual and/or maintenance in contrast to the finding of the previously described models, but aligning more significantly with the overall findings of the epidemiological studies described in **Section 1.4.1**.

In summary, the *in vivo* effect of adiponectin in the bone of pre-clinical models remains uncertain, with evidence for both an anabolic and a catabolic role reported. Some considerations, including age and sex, have been mentioned. Further, a variety of inbred mouse lines have been used to study adiponectin in the bone: while several studies use the C57Bl/6 strain, transgenic overexpression models tend to make use of FVB or FVB

hybrid mice, a popular choice in transgenic work due to the prominent pronuclei present in the fertilised egg[260], and one mixed models during explant procedures[252]. Baseline differences in bone architecture and volume in different mouse lines should be taken into account when interpreting and comparing results; for example, C57Bl/6 mice show a particularly low bone density as compared with other in-bred mouse lines[261], such that direct comparison between mouse lines may not be reliable. It is also hypothesised that environmental factors, including differences in the fat content of the standard mouse chow used and the provision or lack of exercise wheels could affect adiponectin concentrations in laboratory mice[262] and subsequent interpretation of bone phenotype. All of these factors justify study of the relationship between adiponectin and bone volume in a mouse model in which these factors are controlled as much as possible.

Alongside consideration of these experimental inconsistencies, it is likely that a dual action of adiponectin, with opposing effects centrally and peripherally, underlies some of these discordant results. Strong evidence suggests that adiponectin regulates bone mass negatively when acting locally, promoting osteoblast death and inhibiting osteoblast function, but positively regulates bone mass centrally, promoting bone mass accrual by crossing the blood brain barrier and acting to inhibit the sympathetic nervous system in the neurons of the locus coeruleus in the brain, which express both AdipoR1 and T-cadherin[96]. This systemic effect appears to counteract the effect of leptin on bone mass via the sympathetic nervous system partially[96] and the opposing nature of the local and systemic effects of adiponectin must be taken into account when interpreting *in vivo* and *in vitro* evidence.

In 2004, it was reported that adiponectin and its receptors are expressed in primary human osteoblasts, suggesting for the first time that adiponectin could mediate effects on the bone directly as evidenced by the increased proliferation of murine osteoblasts following treatment with recombinant mouse adiponectin[164]. A comprehensive

understanding of the pathways induced in bone cells during adiponectin signalling is still lacking[229], but two independent studies have since reported that adiponectin stimulated proliferation, differentiation and mineralisation of murine osteoblastic MC3T3-E1 cells via activation of AMPK[263] and primary human osteoblasts via activation of MAPK signalling[264], both of which were mediated via AdipoR1 signalling. Adiponectin has been described to promote BMP2 expression in cells of the human MG-63 osteoblast cell line via AdipoR1 activation of AMPK[265] and via Cox2 signalling in bone marrow stem cells and murine mesenchymal progenitor C3H10T1/2 cells, where increased osteogenesis was also observed[266]. APPL1 has been identified as a critical mediator of these *in vitro* responses, with its inhibition associated with loss of adiponectin-induced upregulation of Runx2 and osteocalcin expression and increased mineralisation in primary human bone marrow stem cells from the jaw[267]. One recently published paper found adiponectin receptor agonist AdipoRON dose-dependently inhibited osteoclastogenesis of RAW264.7 cells and primary bone marrow macrophages and promoted osteogenesis and mineralisation *in vitro*[255]. Together, these data provide evidence that *in vitro*, adiponectin has a positive effect on bone formation.

However, recombinant adiponectin has also been reported to induce RANKL and inhibit OPG expression in human osteoblasts in an AdipoR1- and p38MAPK-dependent manner; these pre-treated osteoblasts stimulated osteoclastogenesis of peripheral blood mononuclear cells (PBMCs) in indirect, but not direct, co-culture, suggesting AdipoR1/MAPK signalling promotes osteoclastic activity via modulation of the RANKL/OPG axis[268]. Similarly, adiponectin signalling has been described as a negative regulator of osteoblast proliferation and a promoter of osteoblastic apoptosis, mediated in an AMPK-independent, PI3K-dependent manner, leading to the phosphorylation of AKT and the subsequent phosphorylation, and thus inhibition, of transcription factor

FoxO1[96]. Overall, pre-clinical evidence *in vitro* supports a positive role of adiponectin in bone formation, with *in vivo* results less clear.

Pre-clinical evidence suggesting a positive role of adiponectin in bone

Publication	*Main findings*	*Main conclusions*
Naot, D. *et al.* Endocrinology (2016)[249]	Eight- to 37-week-old female C57Bl/6 AdipoQ gKO mice → reduced BMD, cortical thickness and trabecular BV.	AdipoQ has a positive effect on BV *in vivo*
Tu, Q. *et al.* J. Biol. Chem. (2011)[252]	Femurs of three-day-old C57Bl/6 WT mice explanted into of eight- to 10-week-old WT or AdipoQ gKO mice → explants in AdipoQ gKO mice showed reduced BV, cortical thickness and increased Oc number. AdipoQ-treated RAW264.7 cells → reduced Oc survival, proliferation & differentiation.	AdipoQ has a positive effect on bone growth *in vivo* and *in vitro*
Oshima, K. *et al.* Biochem. Biophys. Res. Commun. (2005)[253]	AdipoQ tOE in eight-week-old male C57Bl/6 mice → increased BV and reduced Oc number and serum bone resorption markers. AdipoQ-treated BMMs → reduced osteoclastic capacity *in vitro*. AdipoQ-treated MC3T3-E1 mouse Ob cells → increased ALPL expression and mineralisation.	AdipoQ has a positive effect on bone growth *in vivo* and *in vitro*
Mitsui, Y. *et al.* MSK Disord. (2011)[254]	AdipoQ tOE in 12-week-old C57Bl/6 male mice → increased BV and BFR.	AdipoQ has a positive effect on BV *in vivo*
Wu, X. *et al.* J. Dent. Res. (2019)[255]	AdipoRON treatment of 20-week-old diet-induced obesity diabetic mice and AdipoQ gKO mice → increased BV. AdipoRON-treated RAW264.7 cells and primary BMMs *in vitro* → inhibited osteoclastogenesis and increased osteogenesis and mineralisation.	Activation of AdipoRs has a positive effect on BV*in vivo* and *in vitro*
Lin, Y. Y. *et al.* Bone (2014)[256]	Porcine AdipoR1 tOE in eight- and 56-week old female and eight-week old male FVB-derived mice → increased BV, trabecular number and serum OCN and OPG. AdipoR1 KD in MC3T3 mouse Ob cells and BMSCs *in vitro* → reduced mineralisation and Ob-related gene expression.	AdipoQ mediates its positive effects on bone *in vivo* and *in vitro* via AdipoR1

Publication	*Main findings*	*Main conclusions*
Kanazawa, I. *et al.* BMC Cell Biol. (2007)[263]	AdipoQ-treated MC3T3 mouse Ob cells *in vitro* → increased proliferation, differentiation and mineralisation via AMPK activation downstream of AdipoR1.	AdipoQ positively regulates BF via stimulation of Obs via AdipoR1
Luo, X. H. *et al.* Exp. Cell Res. (2005)[264]	AdipoQ-treated primary human Obs *in vitro* → increased proliferation, differentiation and mineralisation via MAPK activation downstream of AdipoR1.	AdipoQ positively regulates BF via stimulation of Obs via AdipoR1
Huang, C. Y. *et al.* J. Cell. Physiol. (2010)[265]	AdipoQ-treated human MG-63 Ob cell line *in vitro* → increased BMP2 expression via AMPK activation downstream of AdipoR1.	AdipoQ positively regulates BF via stimulation of Obs via AdipoR1
Hyun, W. L. *et al.* Stem Cells (2009)[266]	AdipoQ-treated BMSCs and C3H10T1/2 murine mesenchymal progenitor cells *in vitro* → increased osteogenesis via Cox2 signalling.	AdipoQ positively regulates BF via stimulation of Obs via Cox2 signalling
Pu, Y. *et al.* J. Dent. Res. (2016)[267]	Inhibition of APPL1 expression *in vitro* → loss of AdipoQ-induced upregulation of Runx2 and OCN and mineralisation in primary human BMSCs.	AdipoQ positively regulates BF via stimulation of Obs via APPL1
Pre-clinical evidence suggesting a negative or uncertain role of adiponectin in bone		
Shinoda, Y. *et al.* J. Cell. Biochem. (2006)[247]	gKO or tOE of AdipoQ in C57Bl/6-derived 8-week-old male mice → no bone phenotype. AdipoQ KO BM cells → reduced osteogenic potential *in vitro*. AdipoQ-treated WT BM cells → reduced osteogenic potential *in vitro*.	AdipoQ has positive local and inhibitory endocrine effects on bone which together produce no *in vivo* phenotype

Publication	*Main findings*	*Main conclusions*
Williams, G. A. *et al.* Endocrinology (2009)[248]	14-week-old male C57Bl/6 AdipoQ gKO mice → increased BV and reduced bone fragility. AdipoQ-treated primary rat and human Obs *in vitro* → inhibited osteogenic potential.	AdipoQ has positive local effects on bone but acts indirectly to inhibit overall BV
Kajimura, D. *et al.* Cell Metab. (2013)[96]	AdipoQ gKO in 12-week-old C57Bl/6J:129/Sv male mice → increased BMD, BV and biomechanical properties due to increased BFR following reduced Ob death increased Oc function. AdipoQ tOE 12-week-old C57Bl/6J:129/Sv male mice → reduced BV due to reduced Ob number. AdipoQ gKO in 36-week -old C57Bl/6J:129/Sv male mice → reduced BMD and BV due to reduced number and proliferation of Obs and increased bone resorption. Ob-specific KO of AdipoR1, AdipoR2, AdipoR1/AdipoR2 or T-Cadherin in 12-week-old C57Bl/6J:129/Sv male mice → no bone phenotype.	AdipoQ regulates bone volume positively locally but negatively indirectly via central inhibition of sympathetic tone: it inhibits FoxO1 activity in a PI3K-dependent manner in Obs rather than acting locally through known AdipoRs in the bone
Wang, F. *et al.* PLoS One (2013)[257]	AdipoQ gKO in C57Bl/6-derived 16- to 18-week-old female mice → no significant change in BMD, but protection from ovariectomy -induced bone loss. AdipoQ gKO BMSCs *in vitro* → increased proliferation and Ob differentiation.	AdipoQ could accelerate post-menopausal osteoporosis via inhibition of bone marrow stem cell osteogenic potential
Wang, Q. *et al.* Endocrine (2014)[258]	AdipoQ gKO in 12-week-old male C57Bl/6 mice → increased BMD and BV and reduced Oc number.	AdipoQ has a negative effect on bone volume *in vivo*
Ealey, K. N. *et al.* Exp. Biol. Med. (2008)[259]	. AdipoQ tOE in eight- and 16-week-old female FVB mice → reduced BMD and increased bone fragility.	AdipoQ has a negative effect on bone volume *in vivo*
Luo, X. H. *et al.* J. Bone Miner. Res. (2006)[268]	AdipoQ-treated Obs → induced RANKL and inhibited OPG expression in an AdipoR1- and p38MAPK-dependent manner; stimulated PBMC osteoclastogenesis in indirect co-culture.	AdipoQ/AdipoR1/MAPK negatively regulates BV via Oc/RANKL/OPG.

Table 1.1: Summary of pre-clinical evidence on the role of adiponectin in bone. *In vivo* and *in vitro* findings are summarised. BV: bone volume; (g)KO: (global) knockout; tOE: transgenic overexpression; AdipoQ: adiponectin; BMD: bone mineral density; WT: wild type; Ob: osteoblast; Oc: osteoclast; BMMs: bone marrow macrophages; ALPL: alkaline phosphatase; BF(R): bone formation (rate); AdipoRs: adiponectin receptors; OCN: osteocalcin; RANKL: receptor activator of nuclear factor (NF) κB ligand; OPG: osteoprotegerin; KD: knockdown; BMSCs: bone marrow stem cells.

1.5 Project aims and hypothesis

This project aimed to clarify further the relationship between adiponectin and bone. It was hypothesised that adiponectin signalling via its receptors AdipoR1 and AdipoR2 has a direct biological effect on the bone but that further characterisation of this effect in a range of biological settings is needed since conflicting evidence exists. Therefore, this thesis aimed to:

- Determine the cross-sectional and five-year prospective association of circulating adiponectin concentration with BMD at the hip and spine in a cohort of middle-aged women.
- Investigate the role of adiponectin in bone by characterising the bone phenotype of mouse models globally deficient in AdipoR1 or AdipoR2.
- Characterise the whole-body phenotype of young AdipoR1-deficient mice in order to begin characterisation of the mechanism of action of adiponectin in bone.
- Recapitulate the adiponectin knockout phenotype *in vitro* to permit mechanistic investigation.

2

Materials and Methods

All reagents were purchased from Sigma unless otherwise stated.

2.1 *In vivo* and *ex vivo*

2.1.1 Animal models

Animal acquisition

Male and female wild type (AdipoR1$^{+/+}$ and AdipoR2$^{+/+}$) mice and mutants globally deficient in adiponectin receptor 1 (AdipoR1$^{-/-}$) or adiponectin receptor 2 (AdipoR2$^{-/-}$) were obtained from MRC Harwell (Oxfordshire, UK) where they were produced as part of The International Mouse Phenotyping Consortium (IMPC), a global phenotyping project. Mice were of the C57BL/6N inbred line and the promoter-driven cassette containing the LacZ insert and LoxP-flanked critical region in exon 4 of the AdipoR1 or AdipoR2 gene was introduced via micro-injection. The targeting vector used in the creation of these animals is available online at http://www.mousephenotype.org. More information on the IMPC and its phenotyping pipeline can be found in **Section 4.1.2**.

Animal ethics

All animals were maintained in conditions in accordance with the Animal (Scientific Procedures) Act 1986 and the guidelines of the University of Oxford, and all procedures were approved by the Home Office under project licence 30/2996. Animals were maintained in individually ventilated cages under controlled temperature (19-23°C) and light (12h light, 12h dark cycle) with *ad libitum* access to water and chow. The colony was maintained with litters produced by pairs of heterozygous animals and subsequent genotyping of pups. Breeding females were retired at six months of age or following the birth of their sixth litter.

Schedule 1

Schedule 1 procedures were used to sacrifice and confirm death in all animals. Animals were anaesthetised by intraperitoneal injection of sodium pentobarbitone before exsanguination via cardiac puncture. Dislocation of the neck confirmed death.

2.1.2 Genotyping

2.1.2.1 Materials

NaOH/EDTA solution

EDTA powder was dissolved in 25mM NaOH to a final concentration of 0.2mM.

Tris.HCl

Tris.HCl was dissolved in distilled water and pH adjusted to 5.5 using 1M NaOH before dilution with more distilled water to a final concentration of 40mM.

TAE buffer

Trizma base, dihydrate EDTA and glacial acetic acid were dissolved in distilled water and pH adjusted to pH 8.4-8.6 using 1M NaOH before further dilution with distilled water to 1L giving final concentrations of 0.04M, 0.002M and 0.02M respectively.

Agarose gel

Gels were made at 1% or 2% agarose (w/v). Agarose was dissolved in 1x TAE buffer by gentle warming. After slight cooling, ethidium bromide (1:20,000) or Invitrogen SYBR Safe™ DNA Gel Stain (Thermo Fisher Scientific, 1:10,000) was added and mixed gently before the gel was poured and left to set.

2.1.2.2 Methods

Designing primers for in-house genotyping

Phenotyping requires the use of three primers; the loss or inclusion of the critical region will determine which product is produced. Using one reverse primer targeting a sequence downstream of the critical region, one forward primer targeting a sequence in the middle of the critical region, and one forward primer targeting a sequence in the LoxP region upstream of the critical region, one of two products will be produced: a product formed between the primer in the centre of the critical region and the reverse primer, indicating no knockout has occurred, or a product formed between the upstream LacZ primer and the reverse primer, indicating a knockout allele. By ensuring these two potential products are 100bp or more different in their size, genotyping is possible by determination of product size; presence of both products indicates heterozygosity.

The targeting vector used in the creation of these animals and the LacZ forward primer targeting a sequence upstream of the critical region provided by the original creators of this line are available online at http://www.mousephenotype.org. The other two primers were designed using a primer design website (https://primer3plus.com). An 800bp region surrounding the LoxP site was copied into the website and candidate primer pairs are generated. Based on factors including self-anneal capacity and melting point, candidate primer pairs were selected. The selected primers had a product length of 806bp (AdipoR1$^{+/+}$) and 579bp (LacZ) and are listed in **Table 2.5.** An example genotyping gel is shown in **Figure 2.1**.

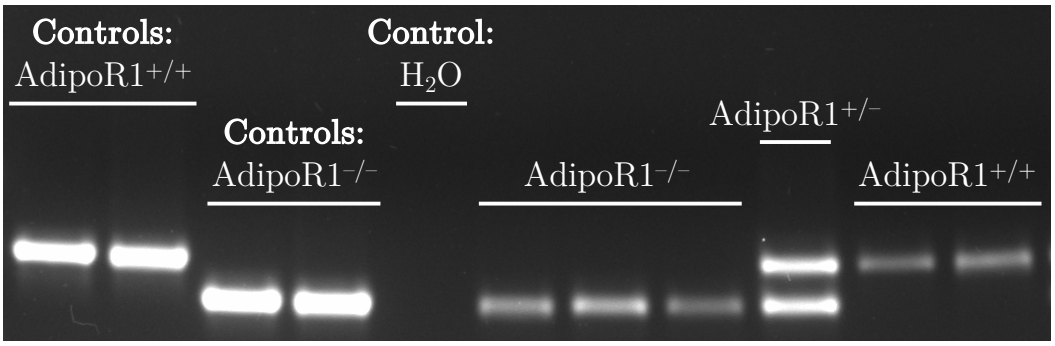


Figure 2.1: Representative genotyping gel for mice of the AdipoR1 line. Each gel was run with at least two AdipoR1$^{+/+}$, two AdipoR1$^{-/-}$ and one negative control. The larger product indicates presence of the wild type gene whereas presence of the smaller product indicates presence of the LacZ insert. Presence of a double band indicates heterozygosity.

Internal genotyping:

Earclips were placed in 75µl 25mM NaOH/0.2mM EDTA and run in the thermocycler at 90°C for 60 minutes, then held at 15°C until ready to proceed. 75µl 40mM Tris.HCl (pH 5.5) was added to the resulting supernatant which together were diluted 1:20 with distilled water for use in PCR. The three genotyping primers were diluted together to a final concentration of 5µM each. Per reaction, 5µl BioMix Red (Bioline), 2.5µl water, 0.5µl primer mix and 2µl diluted DNA were combined and run in the thermocycler: 95°C for 2 minutes followed by 40 cycles of 95°C (30 seconds), 60°C (30 seconds), 72°C (1

minute). Samples were held at 72°C for 10 minutes and 4°C indefinitely before being run with 1x TAE buffer on an ethidium bromide or SYBR™ Safe™ DNA Gel Stain agarose gel. Gels were visualised using a UV documentation system (UVITEC, Cambridge, UK) (**Figure 2.1**).

External genotyping:

Earclips were sent to Transnetyx Inc. (Cordova, TN, USA) for external genotyping. Results were returned within 72 hours.

2.1.3 Gross morphology measurements

Body weight

Animals were weighed immediately before sacrifice on scales precise to 0.1g.

Measurement of tibial length

The leg bones were cleaned of soft tissue and gently dearticulated at the knee joint. Calipers precise to 0.01mm were used to measure the distance from the articular surface to the fibular notch.

Measurement of humeral length

The arm bones were cleaned of most soft tissue and gently dearticulated at the elbow joint. Calipers precise to 0.01mm were used to measure the distance from the humerus head to the distal articulating surface.

Inguinal white adipose tissue and interscapular brown adipose tissue weight

Inguinal white adipose tissue and interscapular brown adipose tissue were both excised and weighed at cull on scales precise to 0.001g.

2.1.4 µCT analysis

Micro-computed tomography (micro-CT or µCT) is a standard imaging tool commonly used for the visualisation and quantification of bone structure in a three-dimensional and highly accurate manner that can be used both *in vivo* and *ex vivo* in pre-clinical models. µCT scanning involves sequential X-ray scanning of the sample to build a three-dimensional reconstruction of it. Further discussion of the theory behind µCT scanning can be found at **Section 4.1.3**.

Preparation of bones and µCT scanning

Leg bones were excised at cull and gently dearticulated at the knee joint before being cleaned of soft tissue while keeping the tibia intact. Tibiae were placed in 10% neutral-buffered formalin for at least 48 hours for fixation and were subsequently washed in 1x phosphate buffered saline (PBS) before being wrapped in wet tissue and ParafilmM and placed in a small plastic tube to prevent dehydration and movement during scanning.

Bones were placed vertically in a high-resolution µCT scanner (SkyScan 1172, BRUKER, Belgium) for scanning. The parameters used for scanning were 0.5mm aluminium filter, isometric resolution of 8.79µm per pixel, voltage 37kV, current 228µA and 0.1 degrees rotation with 4 frame averaging. All parameters were kept consistent for every bone scanned.

Image reconstruction and analysis

After scanning, 3D image stacks were submitted to the reconstruction programme NRecon (v1.6.9.4, BRUKER). During reconstruction, scans underwent smoothing (9), ring artefact reduction (13) and beam hardening (40%); all parameters were kept consistent for every bone analysed. Following reconstruction, the trabecular and cortical regions of interest (ROI) were defined vertically for each bone using CTAn software (v1.16.4.1, BRUKER): the trabecular ROI began directly under the growth plate and extended down 200 frames; the cortical ROI began 200 frames below the end of the trabecular ROI and extended down 200 frames (**Figure 2.2**). Trabecular bone was delineated from cortical bone within the trabecular ROI by a free-hand contouring method; this same method was used to remove artefacts from both ROIs. These parameters defined the three-dimensional volumes of interest VOIs for analysis.

The threshold values of µCT analysis were chosen to be between 60 and 255 for trabecular bone and between 100 and 255 for cortical bone. Bone parameters were calculated using the in-built batch manager three-dimensional analysis software BATMAN (v2.3.2.0, BRUKER) and are listed in **Table 2.1**.

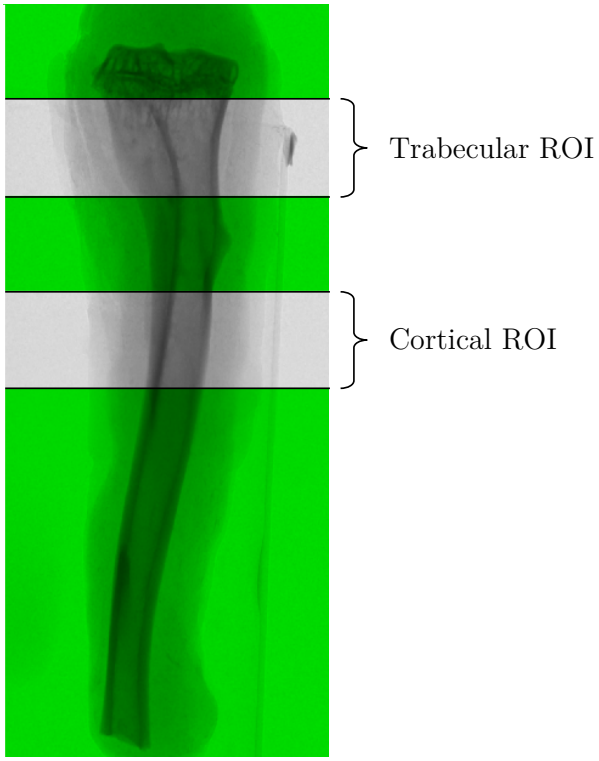


Figure 2.2: Trabecular and cortical regions of interest in µCT analysis. Once bones were fully reconstructed, the trabecular and cortical regions of interest (ROIs) were defined. The trabecular ROI began directly under the growth plate and extended down 200 frames; the cortical ROI began 200 frames below the end of the trabecular ROI and extended down 200 frames.

Parameter (unit)	VOI	Description
Bone volume (BV/TV) (%)	Trabecular	Bone volume as a proportion of the total VOI
Trabecular spacing (pixels)	Trabecular	Average distance between trabeculae
Trabecular thickness (pixels)	Trabecular	Average thickness of trabeculae
Trabecular number (/pixel)	Trabecular	Average number of trabeculae per area of VOI
Bone mineral density (BMD) (AU)	Trabecular	Arbitrary measure of bone mineral density
Cortical thickness (pixels)	Cortical	Average thickness of bone in the cortical VOI
Tissue mineral density (TMD) (AU)	Cortical	Arbitrary measure of tissue mineral density

Table 2.1: µCT output bone parameters. Following analysis, bone volume, trabecular spacing, thickness and number and bone mineral density were acertained from the trabecular VOI. Cortical thickness and tissue mineral density were acertained from the cortical VOI.

2.1.5 Histomorphometry

2.1.5.1 Materials

EDTA decalcification solution

EDTA was dissolved in distilled water and pH adjusted to 7.4 with NaOH before further dilution to a final concentration of 10% (w/v).

TRAP staining basic incubation media

15.2g sodium acetate trihydrate (.3H2O), 11.4g L-(+) tartaric acid and 2.8ml glacial acetic acid were dissolved in 800ml distilled water and pH adjusted to 4.7-5.0 using 5M NaOH before being made up to 1L with distilled water and stored at room temperature.

Napthol solution

100mg napthol was dissolved in 5ml 2-ethoxyethanol and used immediately.

Pararosaniline dye

1g pararosaniline was dissolved in 20ml 2M HCl by gentle warming before filtration and used within 2 weeks.

Sodium nitrate

1g sodium nitrate was dissolved in 25ml distilled water and used within 2-3 days.

2.1.5.2 Methods

Preparation of slides

Long bones were placed in 10% neutral-buffered formalin for at least 48 hours for fixation before 10-12 days decalcification in 10% (w/v) EDTA solution. Decalcified bones were placed in the automated tissue processor (Leica) for dehydration and defatting by submersion in a sequence of ethanol and xylene concentrations (**Table 2.2**). Processed bones were embedded in paraffin wax and cut on a microtome at 5µM. Slides were dried at 37°C overnight before staining.

Reagent	Duration (minutes)
Formalin (100%)	60
Ethanol (70%)	45
Ethanol (100%)	45
IMS (100%)	60
IMS (100%)	60
IMS (100%)	60
Ethanol/xylene (50%/50%)	60
Xylene (100%)	60
Xylene (100%)	60
Xylene (100%)	60
Paraffin wax (100%)	75
Paraffin wax (100%)	75
Paraffin wax (100%)	75

Table 2.2: Steps of automated tissue processing. Decalcified bones were moved sequentially through alcohols to xylene to paraffin wax to prepare them for paraffin embedding. IMS: industrial methylated spirit.

Hydration and dehydration of slides

Slides were deparaffinised and hydrated by successive immersion in histoclear (2x 3 minutes), 100% EtOH (wash), 100%/90%/80%/70% EtOH (2 minutes each) before being washed in running water and immersed in distilled water (2 minutes). After staining, slides were dehydrated by successive immersion in distilled water (wash), 70%/80%/90%/100%/100% EtOH (1 minute each). Slides were washed well in histoclear twice until no evidence of water remained before being mounted with a glass coverslip and left to dry for at least 24 hours at room temperature before use.

H&E staining

Deparaffinated hydrated slides were shaken to remove excess water then placed in pre-filtered (Grade 1 filtration paper, Whatman, GE LifeSciences) Harris haemotoxylin (2 minutes) and rinsed in running tap water until the water ran clear. Slides were submerged in aqueous eosin for 1 minute before dehydration and mounting. In this preparation, dehydration in 70% EtOH was skipped to avoid removal of the eosin.

Tartrate-resistant acid phosphatase (TRAP) staining

Hydrated slides were immersed in substrate solution (5ml napthol solution added to 500ml basic incubation media warmed to 42°C) for 30 minutes. The colour solution was made immediately before use: 10ml pararosaniline and 10ml sodium nitrate solution were mixed and stood for 2 minutes before being added to 500ml basic incubation media warmed to 42°C. Slides were moved from the substrate solution directly into the colour solution and left at room temperature for 5-10 minutes, or until the colour had developed sufficiently. Slides were rinsed in distilled water placed briefly in pre-filtered (Grade 1 filtration paper, Whatman, GE LifeSciences) Harris haemotoxylin (10-15 seconds) and

then washed well in running water for 2 minutes, or until the water runs clear. Slides were dehydrated and mounted.

Determining cellular parameters histologically

The area under the tibial growth plate, excluding any areas of cortical bone, was analysed in all cases for the determination of osteoblastic, osteoclastic and adipogenic parameters (**Figure 2.3**). This area corresponded to approximately 4 fields of view at 10x magnification and approximately 2mm under the growth plate. All histological analysis was performed using Osteomeasure (Osteometrics, USA) (BX51 Olympus, Japan).

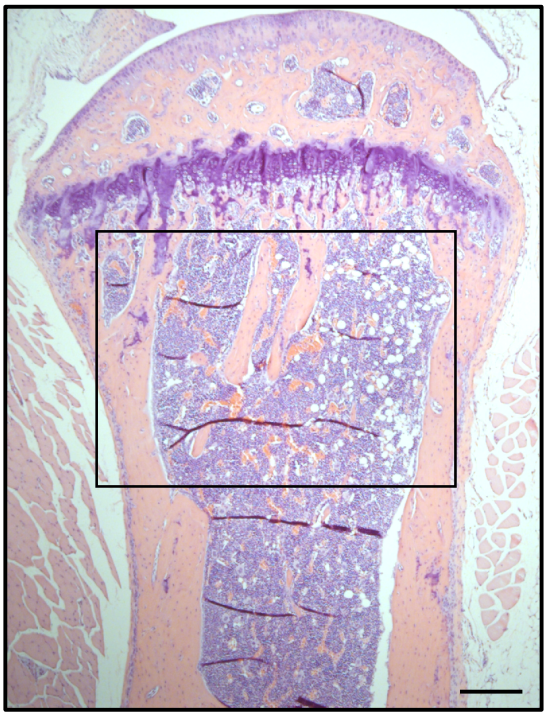


Figure 2.3: Representative image of ROI for histological analysis. Representative image of an H&E-stained mouse tibia with the region of interest for analysis indicated by a box. Scale bar: 250µm.

2.1.6 Biomechanical testing

Humeri were frozen in PBS after harvesting. When thawed for analysis, bones were cleaned of as much soft tissue as possible and placed in the same orientation each time. Force until breakage was applied to the centre of the long bone shaft and measured using an Instron machine. Contact with the bone was ensured before force was applied to confirm correct positioning of the bone and accurate recording of bone deformation. All raw data was recorded using in-built BlueHill Universal Software (Instron, MA, US).

2.1.7 Collection of blood serum and bone marrow plasma

Blood serum

Following exsanguination, blood was collected in a Microvette® 500 Z-gel separation column (Sarstedt). Tubes were centrifuged (10,000g, 5 minutes, RT) to allow separation of serum from blood cells. Cells were discarded; collected serum was flash frozen in liquid nitrogen before long-term storage at –80°C. Repeated freeze-thaw cycles were avoided where possible.

Bone marrow plasma

Legs were disconnected at the hip joint and the feet and all soft tissue removed from the femur and tibia. The epiphyses of the femur and tibia were removed to expose the central cavities before the bones, with openings facing downwards, were placed into a small, perforated centrifugation tube. This tube was subsequently placed into a larger centrifugation tube containing 500µl PBS. Samples were centrifuged (full speed, 2 minutes, RT) resulting in a pellet of bone marrow cells and bone marrow plasma diluted

in PBS. Bone marrow plasma was flash frozen in liquid nitrogen before long-term storage at –80°C. Repeated freeze-thaw cycles were avoided where possible.

2.1.8 Enzyme-linked immunosorbant assays (ELISAs)

Enzyme-linked immunosorbent assays (ELISAs) involve quantification of analyte concentration by making use of antibodies specific to the analyte and antibodies conjugated to enzymes which can facilitate a quantifiable colour change reaction. ELISAs can be direct, indirect, sandwich or competitive. Sandwich ELISAs involve capturing the analyte of interest between two antibodies: the specific capture antibody attached to the plate, and the enzyme-linked detection antibody. Addition of a substrate to this enzyme produces a colour change reaction which is quantified by absorbance and is positively correlated with the concentration of analyte in the sample. Competitive ELISAs involve addition of sample or standard to a plate coated with a detection antibody specific for the analyte alongside a known concentration of enzyme-linked substrate. The analyte in the sample or standard competes with the enzyme-linked substrate for limited binding space. Addition of a substrate to this enzyme produces a colour change reaction which is quantified by absorbance and is negatively correlated with the concentration of analyte in the sample: the higher the concentration of analyte in the sample, the more successfully it outcompetes binding of the enzyme-linked substrate.

ELISAs were performed as per manufacturer's instructions and were read on a microplate reader (FLUOstar Omega, BMG LabTech, Germany). Where a suggested sample dilution factor was given, samples were diluted accordingly, otherwise a pilot test was performed to determine optimal sample dilution. All ELISAs used are listed in **Table 2.3**.

Analyte	Sample	ELISA type	Company (Cat. No.)	Dilution
Total adiponectin	Blood serum	Sandwich	R&D Systems (MRP300)	1:2000
Calcitriol	Blood serum	Competitive	Aviva Systems Biology (OKEH02542)	1:10*
Sclerostin	Blood serum	Sandwich	R&D Systems (MSST00)	1:2
Osteocalcin	Blood serum	Sandwich	Novus Biologicals (NBP2-68151)	1:7.5*
Total adiponectin	Bone marrow plasma	Sandwich	R&D Systems (MRP300)	1:1500*

Table 2.3: Table of ELISAs. ELISAs were performed as per manufacturer's instructions. Sample dilution was performed as suggested where available and pilot tests to determine optimal sample dilution were performed where necessary (*).

2.1.9 Luminex assays

Luminex Assays (R&D Systems) allow analysis of multiple blood serum analytes simultaneously using a system of magnetic colour-coded beads. A standard curve is run for each of the analytes to allow absolute analyte concentration to be determined.

Color-coded beads are pre-coated with analyte-specific capture antibodies that bind to the analyte in the sample or standard before a biotinylated detection antibody specific to the analyte binds to the analyte forming an antigen sandwich. Once phycoerythrin (PE)-conjugated streptavidin is added, it binds the biotin on the detection antibodies to produce a fluorescent signal proportional to analyte concentration. Plates are run on a Luminex MAGPIX Analyzer (R&D Systems) which magnetically holds the beads in a monolayer on the bottom of the plate. Here, two spectrally-distinct light-emitting diodes (LEDs) illuminate the beads: one identifies the analyte detected based on the colour of the bead, and one determines the magnitude of the PE-derived signal to allow quantification of analyte concentration.

Luminex plates were set up as per manufacturer's instructions. Within analytes, samples from four-week-old and 52-week-old animals were run on the same plate to allow direct comparison and avoid inter-plate variation. All samples were diluted as per

manufacturer's instructions and analytes were grouped on plates according to dilution factor and biological compatibility.

Reading of the plates on the Luminex MAGPIX Analyzer was performed externally by Dr Jennifer Hill (Oxford Vaccine Group). Plate set up and data processing were performed in-house.

2.1.10 Bone formation rate

2.1.10.1 Materials

Calcein was dissolved in 1x PBS and adjusted to pH 7 using 1M NaOH and 1M HCl before further dilution with 1x PBS to a final concentration of 2mg/ml. After filter-sterilisation through a polyethersulfone (PES) membrane with a 0.2µM pore size (Corning), it was protected from light and used within two hours.

2.1.10.2 Methods

Calcein is a calcium-binding dye that becomes incorporated during bone formation and as such will be removed from samples upon decalcification, necessitating use of undecalcified spines embedded in plastic resin for bone formation rate quantification.

Calcein treatment of animals and preparation of spines

Animals were injected intraperitoneally with 100µl 2mg/ml filter-sterilised calcein on day 1 and day 4 before cull on day 5 or 6. Excised spines were fixed in 10% neutral-buffered formalin for at least 72 hours before soft tissue was removed to expose the lumbar vertebrae and vertebral discs.

Preparation of slides

Spines were prepared using a modified version of the methylmethacrylate (MMA) embedding protocol outlined previously[269]. In brief, spines were fixed in 10% neutral-buffered formalin for at least 48 hours before dehydration by submersion in 70% (2 days) and 100% ethanol (3x 1 day). Dehydrated spines were infiltrated with the plastic embedding mixture in three steps, each for 3 days: solution I consisted of 120ml MMA, 70ml butyl methacrylate, 10ml methyl benzoate and 2.4ml polyethylene glycol 400; solution II contained 200ml solution I with 1g wet benzoyl peroxide; solution III contained 200ml MMA solution I with 2g wet benzoyl peroxide. Solutions II and III were filtered through calcium chloride to remove water before use. Spines were embedded in glass vials in the embedding mix: 200ml monomer mix III at 4°C plus 800µl *N*,*N*-dimethyl-*p*-toluidine to catalyse polymerisation. Sealed glass vials were stored at –20°C for 3 days to set and the blocks removed and washed in water before use.

Cutting, mounting and visualising slides

Spine blocks were cut to 5-6µm thickness on a microtome with a diamond-edged cutting blade. A cutting solution of 7% ethanol in water with 1ml of detergent added was used to soften the cutting surface. Cut samples were placed on glass microscope slides and covered in plastic film before being stacked in a vertical clamp for pressing (37°C, 3-4 days). One lumbar (L1-4) vertebra, excluding any area of cortical bone, was analysed per mouse, with vertebral arms visible on both sides to ensure correct orientation and were visualised under light and fluorescence microscopy (BX40, Olympus, Japan) to quantify bone volume and the fluorescent bone labelling respectively (**Figure 2.4**). Bone labelling was quantified using Osteomeasure (Osteometrics, USA) as single- or double-labelled, which indicate mineral apposition rate and bone formation rate respectively.

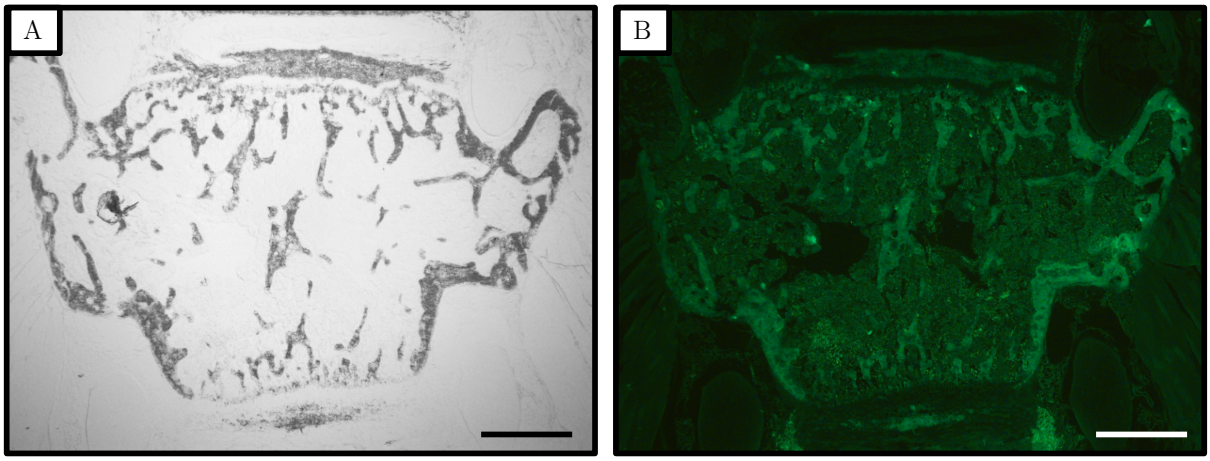


Figure 2.4: Representative image of ROI for bone formation rate analysis using calcium staining. Representative (**A**) brightfield and (**B**) fluorescence images of the region of interest during bone formation rate analysis. One lumbar (L1-4) vertebra was analysed per mouse with the vertebral arms visible each side to ensure correct orientation. Scale bar: 500µm.

2.1.11 Osmium tetroxide staining

Osmium tetroxide (OsO_4) is soluble in fat and creates a black precipitate easily detectable by µCT scanning due to the presence of a heavy metal. Before its dissolution in fat, osmium tetroxide is acutely toxic necessitating all work to be performed in a designated fume hood and all waste disposed under corn oil. All preparation, staining and subsequent µCT analysis was performed by Felix Richter of the Kennedy Institute of Rheumatology, Oxford, UK.

Tibiae were disassociated from the femur and cleaned of any soft tissue before being fixed in 10% neutral-buffered formalin overnight. Once rinsed in running water for 40 minutes to remove excess formalin, bones were decalcified in pH 7.4 10% EDTA (4°C, 10-14 days, solution changed every 3 days) before washing and storage in Sörensen's buffer (81 mM KH_2PO_4, 19 mM $Na_2HPO_4{\cdot}7H_2O$, pH 7.4) at 4°C.

Decalcified bones were stained in a 1% Osmium Tetroxide solution (Agar Scientific) (24-48 hours, RT) before excess stain was removed by transferral to fresh Sörensen's buffer

(2x a day, 3 days). Stained bones were embedded in a 1% (w/v) agarose solution to prevent movement or dehydration during µCT scanning (SkyScan1172): voltage 90V, current 200µA, capture size small, field of view 20mm and scan technique 4.5 minutes with a 0.5mm aluminium filter and 2 frame averaging. All parameters were kept consistent for every bone scanned. Data was processed on Analyzer 12.0 software. The threshold windows were optimised to discriminate cortical bone from BMAT: bone 3800-5499 and BMAT 5500-maximum. Thresholds were kept consistent for every bone processed.

2.1.12 FACS analysis of bone lining cells

2.1.12.1 Materials

Preparation buffer

5% FBS (v/v) in PBS was filter-sterilised through a 0.2µm PES membrane (Corning) before use.

Analysis buffer

EDTA was dissolved in 5% FBS in PBS (v/v) to a final concentration of 2mM and filter-sterilised through a 0.2µm PES membrane (Corning) before use.

DNase I solution

Bovine pancreas DNase I (Sigma, Cat. No. 260913) was dissolved in sterile water to produce a stock of 1000 units/µl. 10µl aliquots were stored at –20°C. 990µl PBS was

added to one aliquot to make DNase working solution (10units/µl) immediately prior to use. Unused working solution was discarded.

Collagenase I/DNase I solution

Collagenase I (Cat No. LS004196, Worthington, NJ, USA) was dissolved in preparation buffer to a final concentration of 3mg/ml. Working DNase solution was added to a final concentration of 200units/ml. Collagenase I/DNase I solution was filter-sterilised through a 0.2µm PES membrane (Corning) before being warmed to 37°C and protected from light at all times.

Smart-Seq2 buffer (provided by Dr Neil Ashley)

0.4% (v/v) Triton X-100 containing 2units/µl RNase inhibitor, $4x10^7$ dilution of ERCC spike-in control (a preformulated mix of 92 transcripts), 2.5mM dNTPs (ThermoFisher) and 2.5µM oligo (Oligo-dT30VN). 100 FACS-sorted cells were sorted directly into 4µl of this buffer and immediately placed on dry ice before storage at –80°C until further processing.

2.1.12.2 Methods

Isolation of bone lining cells

All bone lining cell preparation was performed in aseptic conditions using sterile equipment and reagents. Leg bones were extracted and cleaned of soft tissue. Both ends of each bone were removed to expose the central cavity which was flushed to remove all bone marrow using preparation buffer through a 19g needle. The flushed bone was cut into small fragments which were pelleted by centrifugation (100g, 1 minute, 4°C). Bone

fragments were incubated in Collagenase 1/DNase solution (37°C, 30 minutes, regular agitation, light protected) before pelleting again (100g, 1 minute, 4°C). The Collagenase I/DNase I solution containing detached cells was removed to a new 50ml falcon tube on ice via a 70µM cell strainer. Bone fragments underwent a second Collagenase 1/DNase incubation (37°C, 30 minutes, regular agitation, light protected). Following centrifugation (100g, 1 minute, 4°C), detached cells were added via a 70µM cell strainer to the same 50ml falcon tube now containing all collected bone lining cells.

Antibody staining

Bone lining cells were pelleted by centrifugation (300g, 5 minutes, 4°C) and resuspended in 1.5ml analysis buffer. A small fraction of cells was reserved for fluorescence-minus-one (FMO) control staining and all cells were pelleted again (300g, 5 minutes, 4°C). Samples were resuspended in 50µl TruStain FcX™ antibody (anti-CD16/CD32 to reduce non-specific antibody binding to widely expressed Fcγ receptors) (BioLegend) and FMO cells were resuspended in 25µl TruStain FcX™ antibody (4°C, 15 minutes, light-protected). Subsequently, 50µl complete antibody mix was added to samples while 25µl FMO antibody mix was added to FMO cells. Sample/antibody mixes were vortexed briefly before incubation (4°C, 15 minutes, light-protected). Stained samples were washed and resuspension in analysis buffer. Single-stained controls, using anti-mouse Igκ and negative control BD™ CompBeads were also prepared: one drop of positive beads and one drop of negative beads were added to single antibody samples and incubated (4°C, 15 minutes, light-protected). Beads were subsequently washed and resuspended analysis buffer. 7AAD viability stain was added to all samples, excluding the 7AAD FMO, immediately before analysis.

Target	Fluorochrome	Dilution	Company	Clone
CD45	AF700	1:50	BioLegend	30-F11
CD31	APC	1:200	BioLegend	390
Ter119	PECy5	1:600	BioLegend	TER-119
ALCAM/CD166	PE	1:10	Invitrogen	eBioALC48
Sca1	FITC	1:200	BioLegend	D7
CD106	BV650	1:20	BD Biosciences	429 (MVCAM.A)
Dead cells	7AAD	1:100	BD Biosciences	

Table 2.4: Table of antibodies used in fluorescence-assisted cell sorting (FACS) of primary bone marrow stem cells. All antibodies are anti-mouse rat IgG and were protected from light at all times during preparation and staining to prevent fluorochrome bleaching.

FACS

FACS and all optimisation of gating strategy was performed by Dr Sally-Ann Clark (Weatherall Institute of Molecular Medicine, Oxford, UK). The gating strategy employed was taken from a recent Nature Communications paper in which the authors identified mesenchymal stromal progenitor cells defined as $CD45^{-}Ter119^{-}CD31^{-}CD166^{-}Sca1^{+}CD106^{-}$ [55]. Gating was based on FMO controls; an example gating strategy is shown in **Figure 2.5**. 100 $CD45^{-}Ter119^{-}CD31^{-}CD166^{-}Sca1^{+}CD106^{-}$ cells were sorted directly into Smart-Seq2 buffer and flash frozen before storage at –80°C until use.

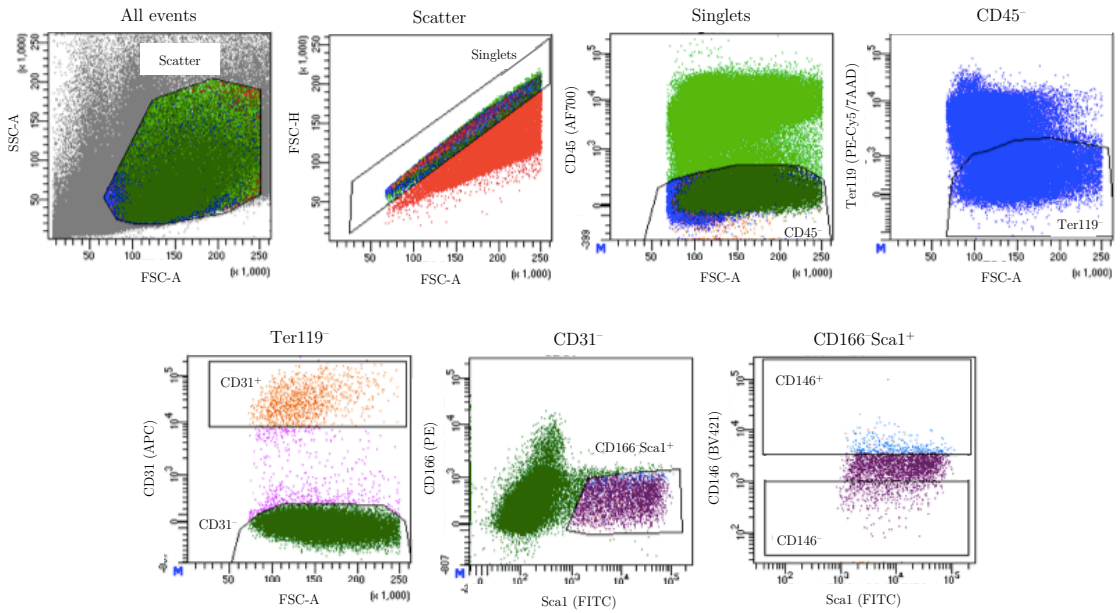


Figure 2.5: Example gating strategy used to isolate mesenchymal stromal progenitor cells via FACS. Representative plots showing the full gating strategy for isolation of CD45⁻Ter119⁻CD31⁻CD166⁻Sca1⁺CD106⁻ mesenchymal stromal progenitor cells from mouse bone lining cells. Gating strategy taken from Hu *et al*, 2016[55].

Smart-Seq2 and RNASeq

Amplification of RNA by the Smart-Seq2 protocol and RNASeq were performed by Dr Neil Ashley (Weatherall Institute of Molecular Medicine, Oxford, UK). Amplification was performed according to the published Smart-Seq2 protocol[270]. In short, RNA was reverse transcribed before PCR pre-amplification of cDNA. The cDNA product was quality purified via magnetic bead cleaning before quality checking and quantification. cDNA was Tagmented to fragment and add barcodes and adaptors to it before undergoing PCR to enrich adaptor-ligated fragments. Samples were purified, quality checked and quantified again and pooled to a final concentration of 2-10nM per pool before RNASeq (Illumina HiSeq2000) with 25 million reads per sample (75bp single-end reads).

Bioinformatics

Bioinformatics from the RNASeq was performed by Dr Srinivasa Rao (Botnar Research Centre, Oxford, UK). Total counts from the sequencing were normalised to the size of the library before differentiation expression between samples was analysed in R by alignment to the reference mouse genome version GRCm38 using STAR version 2.5.3a. Expression variance between experimental replicates was then plotted, along with a volcano plot and heatmap of up- or downregulated genes. All packages used for this analysis are widely available in R.

2.2 *In vitro*

2.2.1 Cell culture and maintenance

2.2.1.1 Materials

Water

Nanopure water (type I) from a MilliQ water system was used for all procedures and preparations and autoclaved before use.

Phosphate Buffered Saline (PBS)

Five PBS tablets were dissolved in 1L MilliQ water to produce 1x PBS. PBS was autoclaved before use.

Cell lines

2T3 mouse pre-osteoblastic cells were obtained from the American Type Culture Collection (ATCC). ST2 mouse bone marrow-derived stromal cells were obtained from the Riken Cell Bank (Tsukuba, Japan). Cells were mycoplasma tested regularly.

Basic media

Dulbecco's Modified Eagle's Medium (DMEM) and Minimum Essential Medium Alpha (MEMα) were purchased from Gibco, UK. All culture medium was stored at 4°C.

Media supplements

Heat-inactivated foetal bovine serum (FBS) (LabTech) was stored at –80°C, or in 50ml aliquots at –20°C, and used at a final concentration of 5% (v/v) or 10% (v/v). Penicillin/Streptomycin and L-glutamine (Gibco, UK) were stored at –20°C in 5ml aliquots. Penicillin/Streptomycin was supplied at 10,000 units/ml penicillin and 10mg streptomycin/ml and used at a final concentration of 100 units penicillin and 100µg streptomycin/ml (1% v/v). L-Glutamine was supplied at 200µM and used at a final concentration of 2µM (1% v/v).

AdipoRON

AdipoRON was dissolved in DMSO to a final concentration of 50mM and stored in 50µl aliquots at –20°C until use.

2.2.1.2 Methods

Maintenance of cell lines

Murine 2T3 and ST2 cell lines and human HEK293T cell line were maintained in DMEM supplemented with 10% FBS, 1% Penicillin/Streptomycin and 1% L-glutamine. All cell lines were incubated in T25 or T75 flasks (Corning) at 37°C in 5% CO_2. At confluency, approximately every 3-4 days, cells were washed in 1x PBS and incubated with pre-warmed 0.25% Trypsin-EDTA (Gibco) at 37°C until cell detachment. Pre-warmed media was added to neutralise the trypsin and the cells were collected in a non-adherent polythene tube before subsequent seeding into new flasks or plates.

Cell counting

10µl detached cells were mixed well with 10µl 0.4% Trypan Blue solution and added to a BioRad cell counting slide. The slide was inserted into the automated cell counter (BioRad) for quantification of cell number and live fraction. Cells were not used if the live fraction was below 90%.

Freezing and thawing cells

Cells were grown to 80-100% confluency and collected by trypsinisation before being pelleted (400rpm, 5 minutes). The pellet was resuspended in freeze mix (10% (v/v) DMSO, 90% (v/v) FBS, prepared fresh each use) and aliquoted into CyroTube™ cryovials (ThermoFisher Scientific). Cells were cooled to –80°C at a rate of approximately 1°C per minute in a Mr Frosty™ Freezing Container (ThermoFisher) before transfer to liquid nitrogen for long-term storage. To thaw cells for use, the cryovials were placed in a polystyrene box for 5 minutes to thaw naturally. Thawed cells were added to pre-warmed growth media and pelleted (400rpm, 5 minutes) before resuspension in fresh growth medium and transferral to a T25 or T75 flask and incubation at 37°C overnight for recovery.

2.2.2 Alamar Blue assay

The Alamar Blue assay is used to determine cell viability. It contains resazurin, a cell-permeable, non-fluorescent blue compound which is reduced within cells to resorufin, a red compound that fluoresces strongly. Healthy cells maintain a reducing environment causing a strong colour change; therefore, negative effects on cell viability reduce colour-change.

Resazurin sodium salt was dissolved in sterile PBS to a final concentration of 50mg/ml. This stock was stored at –20°C in 1ml aliquots. To make the working solution, the stock was diluted in sterile PBS to a final concentration of 1mg/ml and stored at 4°C.

After the desired treatment time, 10µl working solution was added to 96 well plates containing 100µl of growth medium without changing the media. The plate was incubated at 37°C for 3 hours before fluorescence was read (544/590) on a microplate reader (FLUOstar Omega, BMG LabTech, Germany) to quantify the colour change reaction. Results were standardised to their own untreated control with the background reading accounted for by normalising against cell-free wells containing Alamar Blue.

2.2.3 RNA manipulation

2.2.3.1 Materials

All primer sequences used for PCR are provided in **Table 2.5**. Primer sequences were derived from previously published sequences or designed using The Basic Local Alignment Search Tool (BLAST). For primer design, the sequence of the gene of interest was found using the NCBI Gene database and copied to Primer3Plus to find primer pair sequences. These primers were designed for specificity based on exclusion of primers with undesirable characteristics: high melting points (52-58°C ideal, excluded over 65°C), high tendency for hairpin formation, undesirable length (18-22bp ideal) or unusual GC content (40-60% ideal, with similarity between the forward and reverse primer).

Target	Primer sequence
AdipoR1	F: TAACCTGGCTGATAACGGGC
	R: TCAAGGCGTGGCTTTGTTTG
AdipoR2	F: GCCTTCCCTAGGCCGATAAC
	R: ATGCCCAAAGGCTCTCAGTC
Runx2	F: TATGGAGTGCTGCTGGTCTG
	R: CCCAGCCACCTTTACCTACA
ALPL	F: GCTGATCATTCCCACGTTTT
	R: CTGGGCCTGGTAGTTGTTGT
Osteopontin	F: AGCCACAAGTTTCACAGCCACAAGG
	R: CTGAGAAATGAGCAGTTAGTATTCCTGC
Collagen1α	F: CACCCTCAAGAGCCTGAGTC
	R: GTTCGGGCTGATGTACCAGT
Osteocalcin	F: GCTACCTTGGAGCCTCAGTC
	R: GGCGGTCTTCAAGCCATACT
PPARγ	F: CTGACGGGGTCTCGGTTG
	R: AACCATGGTAATTTCAGTAAAGGGT
CEBPα	F: CAGAGGATGGTTTCGGGTCGCT
	R: TAGACGCACCGAGTCCGGCT
Adiponectin	F: AGACCTGGCCACTTTCTCCTCATT
	R: AGAGGAACAGGAGAGCTTGCAAGA
GAPDH	F: TCAACAGCAACTCCACTCTTCCA
	R: ACCCTGTTGCTGTAGCCGTATTCA
AdipoR1 (genotyping)	F: TCTCTTCAGTGCGGTTTCCC
LacZ (genotyping)	F: CCAGTTGGTCTGGTGTCA
AdipoR1 (genotyping)	R: GGCTTCTTGGAGCTAGGCAA

Table 2.5: Table of primer sequences.

2.2.3.2 Methods

RNA extraction

All RNA extraction was performed using an RNeasy Mini Kit (QIAGEN, UK) as per the manufacturer's instructions. Briefly, cells were washed once in 1x PBS before addition of Buffer RLT lysis buffer supplemented with 10µl/ml β-mercaptoethanol for denaturation of natural RNases. The lysate was mixed with one volume of 70% ethanol and transferred to an RNeasy Mini spin column where the RNA specifically binds to the silica membrane during centrifugation (15 seconds, >8000g). The membrane was washed 3 times (15 seconds, >8000g) by centrifugation with Buffer RW1 once and Buffer RPE twice. The spin column centrifuged (1 minute, full speed) to dry the membrane before 30-50µl RNase-free water was used to elute the RNA (1 minute, >8000g). RNA samples were placed at –20°C for short-term storage or –80°C for long-term storage.

RNA quantification

The concentration of the RNA was established using Nanodrop® spectrophotometer ND-1000 v3.8.1 (ThermoFisher Scientific) at absorbance at 260nm. Purity of the sample was also established: a 260/280nm absorbance ratio below 2.0 can suggest genomic DNA contamination and a 260/230nm absorbance ratio above 2.0-2.2 can suggest chemical contamination from the extraction process. Abnormal values in these fields led to exclusion of the sample where necessary.

Making a cDNA library

Where necessary, samples underwent a DNase cycle to remove contaminating genomic DNA. 1µg RNA, 1µl DNase reaction buffer (PrimerDesign) and 1µl Precision DNase

were made up to 10µl using RNase-free water and placed in the thermocycler (30°C for 10 minutes, 55°C for 5 minutes, 4°C indefinitely). 20µl Precision Reverse Transcription Premix 2 (PrimerDesign) or 20µl RNase-free water as a no reverse transcription control was added; this was placed in the thermocycler (42°C for 20 minutes, 72°C for 10 minutes, 4°C indefinitely). If desired, cDNA samples were diluted to a total volume of 60µl or 100µl with RNase-free water before storage at –20°C; all samples run in the same experiment were diluted identically.

qPCR

qPCR was carried out in 96- or 384-well MicroAmp™ Optical reaction plates (Applied Biosystems) with a total volume per well of 10µl. All reactions were performed using Fast SYBR Green PCR Master Mix (Applied Biosystems). SYBR Green binds to double stranded DNA and subsequently emits green light at about 550nm; fluorescence increases exponentially as DNA replication takes place, allowing quantification of gene expression. For comparative CT, a pilot experiment was run to confirm that the efficiencies of the target gene and endogenous control amplifications were approximately equal before comparisons between CT values were performed to produce a measure of gene expression relative to expression of the glycolysis enzyme glyceraldehyde-3-phosphate dehydrogenase (GAPDH) as a housekeeper gene.

In each well, 5µl SYBR Green Master Mix (Applied Biosystems), 4µl RNase-free water, 1µl cDNA sample and 1µl primer mix were combined. This primer mix contained forward and reverse primers, each to a final concentration of 5µM, providing a final working concentration of 500nM each. Each sample was plated in triplicate to allow calculation of average fold change. The plate was sealed and spun well before being placed in a ViiA™ 7 Real-Time PCR System (ThermoFisher).

2.2.4 Alkaline phosphatase activity assay

2.2.4.1 Materials

Tris base

Tris base was dissolved in 0.1% (w/v) BSA in distilled water to a final concentration of 50mM, pH 8.0.

4-Methylumbelliferyl phosphate (4-MUP)

4-Methylumbelliferyl phosphate (4-MUP) was dissolved in absolute ethanol to a final concentration of 10mM; this 100x stock was stored in the dark at –20°C. Immediately before use, stock was further diluted in 50mM Tris to produce a 100µM working solution.

2.2.4.2 Methods

This alkaline phosphatase activity assay used 4-MUP, a substrate metabolised by alkaline phosphatase to produce the fluorescent product methylumbelliferone. Fluorescence readings quantify alkaline phosphatase activity.

Cells in a 96-well plate were washed once in PBS before addition of 50µl CelLytic M (15 minutes, RT, gentle shaking). 10µl of the cell lysate was removed and plated in a white opaque 96 well plate. 100µl 1x 4-MUP was added to the plate and fluorescence read immediately at 360nm excitation/450nm emission on a microplate reader (FLUOstar Omega, BMG LabTech, Germany) to allow calculation of alkaline phosphatase activity levels relative to control.

2.2.5 Protein manipulation

2.2.5.1 Materials

Tris-buffered saline (TBS)

10x TBS solution was diluted with distilled water and stored at room temperature (RT).

TBS-Tween20 (TBS-T)

1ml Tween20 was added to 1L 1x TBS and stored at RT.

2.2.5.2 Methods

Serum samples were diluted with PBS appropriately: 1:300 for serum from young animals and 1:600 for serum from adult animals. Diluted samples were mixed with appropriate volumes of 4x sample buffer (Invitrogen) and loaded directly without boiling for protein denaturation. Pre-cast gels were used for all western blots (4-20% PROTEAN® TGX polyacrylamide gels, BioRad). Gels were loaded into an electrophoresis chamber (BioRad) and samples loaded into the gel lanes before gels were run at 100-120V for approximately 1 hour using TGS running buffer (BioRad) and the Precision Plus Protein™ Kaleidoscope™ Pre-stained Protein Standard (BioRad) as a size standard. Once run, the gel was transferred to a PVDF membrane (Trans-Blot® Turbo™ Transfer System, BioRad).

After transfer, the membrane was immediately blotted with Ponceau S to stain all protein to provide an indication of loading volume via albumin staining. The stained membrane was imaged by scanning before all Ponceau S was removed with excess water and the membrane was blocked using 5% (w/v) BSA in 1x TBS-T (1 hour, RT). The

blocked membrane was probed with an anti-adiponectin primary antibody (Cat. No. ab3455, Abcam) diluted 1:1000 in 5% (w/v) BSA in 1x TBS-T (90 minutes at RT or overnight at 4°C). The membrane was subsequently washed with TBS-T (3x 5 minutes) and incubated with an horseradish peroxidase (HRP)-linked anti-rabbit secondary antibody (Cat. No. 7074S, Cell Signaling Technology) diluted 1:5000 in 5% (w/v) BSA in 1x TBS-T (1 hour, RT). After washing, the membrane was visualised using Clarity Western ECL Substrate (BioRad) in a chemiluminescence and UV documentation system (UVITEC, Cambridge, UK). Densitometry analysis was performed using ImageJ. In the absence of a quantifiable loading control, relative values only were produced

2.2.6 Adipocytic differentiation and staining of cell lines

2.2.6.1 Materials

Dexamethasone

Dexamethasone was dissolved in absolute ethanol to 1mM before filter-sterilisation through a 0.2µm PES membrane (Corning), storage at –20°C and use at a final concentration of 1µM.

IBMX

3-isobutyl-1-methylxanthine (IBMX) was dissolved in DMSO to 0.5M. This stock was filter-sterilised through a 0.2µm PES membrane (Corning), stored at –20°C and used at a final concentration of 0.5mM.

Indomethacin

500µl indomethacin was dissolved in absolute ethanol to 50mM as needed. This was filter-sterilised through a 0.2µm PES membrane (Corning), stored at –20°C and used at a final concentration of 0.2mM.

Insulin

Sterile insulin solution was purchased from Sigma and used at a final concentration of 10µg/ml.

Oil Red O

Oil Red O stock solution was prepared by dissolving 300mg Oil Red O in 100% isopropanol and stored at RT. For the working solution, 3 parts stock solution to 2 parts water were mixed and filtered through Grade 1 filtration paper (Whatman, GE LifeSciences) before use within one hour.

2.2.6.2 Methods

Differentiation

Cells were seeded at $5x10^4$/ml in basal DMEM media. A total volume of 2ml in a 6 well plate or 1ml in a 24 well plate was used. 24 hours later, the media was replaced with the same base media supplemented with 1µM dexamethasone, 0.5mM IBMX, 0.2mM indomethacin and 10µg/ml insulin. On day 4, the media was replaced with base media supplemented with 10µg/ml insulin only. On day 7, the media was replaced with the

base media alone before analysis on day 8. The differentiation media was prepared fresh before immediate use, and media on undifferentiated controls was replaced each time.

Oil Red O staining

Oil Red O is a fat-soluble dye. It is minimally soluble in the organic solvent in which the stock solution is prepared, and its solubility is reduced even further once mixed with the water to produce the working solution causing its preferential movement to association with the lipids within tissue sections, clearly and specifically staining them red as compared with surrounding tissue and leaving adipocytes with easily quantifiable stained lipid droplets.

Following differentiation, cells were washed twice with 1x PBS before fixation in 10% formalin (30 minutes, RT). Following two washes with distilled water, cells were permeabilised by immersion in 60% isopropanol (5 minutes, RT) and covered in pre-filtered working solution Oil Red O (15 minutes, RT, gentle shaking) before unincorporated dye was removed by washing. Wells were imaged by light microscopy (Eclipse TE300, Nikon, Japan) and staining quantified via ImageJ densitometry analysis. Images were RGB stacked and thresholded to 60 and above; any staining above this threshold contributed to the total area covered to provide a readout of adipocytic coverage (%).

2.2.7 Osteoblastic differentiation and staining of cell lines

2.2.7.1 Materials

β-glycerophosphate

β-glycerophosphate was dissolved in the base media for osteoblastic differentiation to 50mM. This stock was filter-sterilised through a 0.2µm PES membrane (Corning) and stored at –20°C before use at a final concentration of 5mM.

Dexamethasone

The stock of dexamethasone produced in **Section 2.2.6.1** was further diluted in the base media for osteoblastic differentiation to 1µM and stored at –20°C in 1ml aliquots before use at a final concentration of 1nM.

L-ascorbic acid

L-Ascorbic acid (Sigma) was dissolved in distilled water to 50mM and filter-sterilised through a 0.2µm PES membrane (Corning). Stock was stored at –80°C before use at a final concentration of 75µM.

Alizarin Red S

Alizarin Red S was dissolved in distilled water and pH adjusted to 4.1-4.3 before further dilution to a final concentration of 40mM and storage at room temperature. Immediately before use, it was filtered through Grade 1 filtration paper (Whatman, GE LifeSciences).

2.2.7.2 Methods

Differentiation

Cells were seeded at 5x10^4/ml in basal DMEM media. A total volume of 2ml in a 6 well plate or 1ml in a 24 well plate was used. 24 hours later, the media was replaced with base differentiation media (MEMα with 5% (v/v) FBS, 100units/ml penicillin/streptomycin) supplemented with 20mM β-glycerophosphate, 1nM Dexamethasone and 75µM L-ascorbic acid. The media was replaced every 3 days with fresh differentiation media prepared each time and the base media on undifferentiated controls replaced each time. Analysis took place between day 8 and day 16.

Alizarin Red S staining

Alizarin Red S staining is used to identify calcium deposits, which together form a complex in a chelation process resulting in a bright red stain which can be imaged and quantified.

Following differentiation, cells were washed once with 1x PBS before fixation in 10% formalin (15 minutes, RT). Following two washes with distilled water, fixed cells were stained with pre-filtered Alizarin Red S solution (30 minutes, RT, gentle shaking) beore unincorporated dye was removed with washing. Wells were scanned and imaged by light microscopy (Eclipse TE300, Nikon, Japan).

Stain was extracted with 10% acetic acid (30 minutes, RT, gentle shaking) before the well contents, including the cell layer, was collected, vortexed briefly and heated (85°C, 10 minutes, tubes sealed). Following centrifugation (15 minutes, 20,000g), 200µl of the supernatant was added to 75µl 10% ammonium hydroxide, and 50µl/well of this sample was plated in triplicate in a 96 well plate. Standards of alizarin red concentration,

produced by 1:2 serial dilutions of the 4mM stock with water, were also plated in triplicate. The plate was read at absorbance 405nm on a microplate reader (FLUOstar Omega, BMG LabTech, Germany) to allow Alizarin Red quantification.

2.2.8 Creation of a stable knockdown cell line

2.2.8.1 Materials

Agar

3.5% (w/v) agar was prepared in MilliQ water by gentle warming before sterilisation by autoclaving.

Ampicillin

Ampicillin Sodium Salt was dissolved in water to 100mg/ml in sterile conditions before storage at –20°C.

Vegitone LB Broth

2% (w/v) Vegitone LB Broth was prepared in MilliQ water before sterilisation by autoclaving.

shRNA constructs and packaging vectors

shRNA constructs (**Table 2.6**) and packaging plasmids (**Table 2.7**) were bought or acquired as detailed.

shRNA	Cat. No.	Depositing lab	Source	Hairpin sequence
pLKO.1 puro (empty vector)	8453	Bob Weinberg	AddGene	None
Scrambled (1)	1864	David Sabatini	Gift from Oppermann group	CCTAAGGTTAAGTCGCCCTCGCTCG AGCGAGGGCGACTTAACCTTAGG
Scrambled (2)	1864	David Sabatini	AddGene	CCTAAGGTTAAGTCGCCCTCGCTCG AGCGAGGGCGACTTAACCTTAGG
AdipoR1	TRCN00 00249149	N/A	Merck	CCGGGGGATTGCTCTACTGATTAT GCTCGAGCATAATCAGTAGAGCAA TCCCTTTTTG

Table 2.6: shRNA constructs used in the production of AdipoR1 knockdown cell lines.

Plasmid	Cat. No.	Depositing lab	Source
psPAX2	12260	Didier Trono	AddGene
pMD2.G	12259	Didier Trono	Add Gene

Table 2.7: Packaging plasmids used in the production of AdipoR1 knockdown cell lines.

Puromycin

Puromycin was dissolved in MilliQ water to 1mg/ml before storage at –20°C. Puromycin was added to complete media; puromycin media was prepared fresh each time.

2.2.8.2 Methods

Preparatory work

2T3 and ST2 cells were treated with a GFP-containing pLKO-puromycin plasmid and 5-20µg/ml hexadimethrine bromide (Polybrene®), a cationic polymer used to increase the efficiency of transfection that works by reducing the charge repulsion between the

cell surface sialic acid moieties and the infecting virions, for 3 days to check their transfection capacity. Transfection was visualised under fluorescence microscopy (Eclipse TE300, Nikon, Japan) (see **Figure 2.6**).

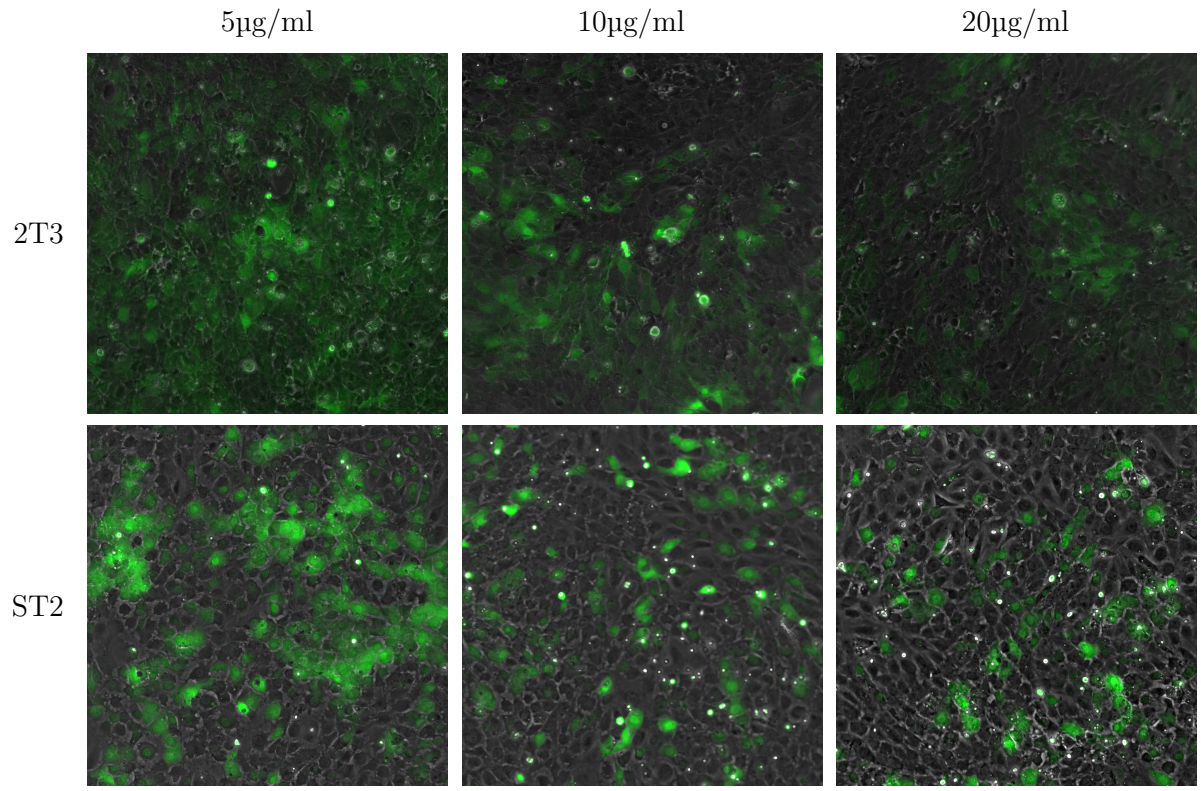


Figure 2.6: 5µg/ml hexadimethrine bromide provides sufficient transfection efficacy. 2T3 and ST2 cells were plated with varying concentrations of hexadimethrine bromide and a pLKO-puromycin plasmid containing GFP. Fluorescence was visualised 3 days after transfection. 5µg/ml was determined to facilitate sufficient transfection efficacy, particularly given the noted toxicity associated with higher concentrations of hexadimethrine bromide. Representative composite images shown.

2T3 and ST2 cell lines were treated for 7 days at varying concentrations of puromycin (0-8µg/ml) with media changes every other day to test their sensitivity to puromycin. Viability was determined by Alamar Blue assay; a cell viability of below 5% at day 7 was considered sufficient for selection, so 4µg/ml was selected for both cell lines (**Figure 2.7**).

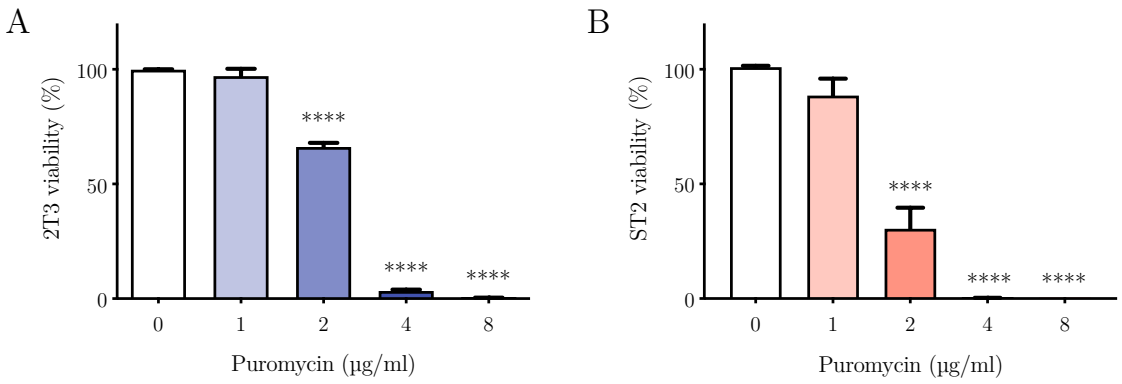


Figure 2.7: 4µg/ml puromycin is sufficient for 2T3 and ST2 cytotoxicity in 7 days. (**A**) 2T3 and (**B**) ST2 cells were treated for 7 days with puromycin-supplemented media after which viability was determined by Alamar Blue. Significant reductions in viability were seen from 2µg/ml in both lines. Less than 5% viability after 7 days defined sufficient toxicity, so a final concentration of 4µg/ml was decided for selection in both cell lines. One-way ANOVA, N=3 (biological replicates), data presented as mean+SD, ****=p≤0.0001.

Amplification of bacterial stock

Mouse MISSION® shRNA bacterial glycerol stock was ordered from Sigma; the shRNA is constructed within a TRC2-pLKO-puro vector which contains a bacterial ampicillin resistance gene and has been transformed into ampicillin-resistant *E. coli*. Stock was stored at –80°C. An empty vector and a scrambled vector were also used (**Table 2.6**).

All bacterial work was performed in aseptic conditions. For each vector, a sterile pipette tip was dipped into the stock and streaked across a 3.5% agar plates containing 100mg/ml ampicillin. Seeded plates were placed upside-down in the incubator (18-24 hours, 37°C). One colony from each plate was added to 250ml 2% (w/v) Vegitone LB Broth (Fluka Analytical) containing 100µg/ml ampicillin (20 hours, 37°C, vigorous shaking). Where necessary, glycerol stocks for long term storage were prepared by adding 700µl of each overnight bacterial broth to 300µl glycerol, flash freezing and storing at –80°C.

Plasmid purification and quantification

Broth was centrifuged (3200g, 30 minutes, 4°C) before shRNA plasmid purification using the EndoFree Plasmid Maxi Kit (QIAGEN) as per the manufacturer's instruction. Briefly, pelleted bacteria were lysed and filtered to remove materials like genomic DNA, proteins and cell debris. Lysates were mixed with Buffer ER to remove endotoxins and incubated (4°C, 30 minutes) filtered and washed twice with Buffer QC. The DNA was eluted in Buffer QN before precipitation in isopropanol and pelleting (3200g, 60 minutes, 4°C). The pellet was washed in 5ml 70% endotoxin-free ethanol (3200g, 20 minutes, 4°C) and subsequently air-dried before being dissolved in 500µl endotoxin-free Buffer TE and stored in 100µl aliquots at –20°C. Plasmid DNA concentration and purity were assessed (Nanodrop® spectrophotometer ND-1000 v3.8.1, absorbance 280nm, ThermoFisher Scientific).

Lentiviral packaging

A second-generation packaging system was used to produce lentiviruses. This system is designed to prevent the production of replication-competent lentiviruses by necessitating two separate plasmids and a permissive cell line to provide the packaging genes necessary for virus production: psPAX2 contains retroviral genes Gag, Pol, Rev and Tat which produce viral structural proteins and essential regulatory elements; PMD2.G contains retroviral gene Env, a gene encoding an envelope protein essential for packaging of the virus; the cell line used for co-transfection, HEK293T, expresses viral genes E1 and E3.

HEK293T cells were cultured to around 90% confluency in 10cm dishes and were moved to antibiotic-free DMEM (10% FBS, 1% L-glutamine) 30 minutes before transfection. 10µg of the shRNA construct, 5µg psPAX2 and 5µg PMD2.G were mixed well in 500µl OptiMEM (Gibco). Separately, 30µl Lipofectamine 2000 (Invitrogen) was mixed well in

500µl OptiMEM. These were combined by inversion as soon as possible and incubated together (20 minutes, RT) before the total volume of 1ml was added to the 10cm dish and incubated (37°C, 3 days). Cells transfected with the GFP-containing plasmid were checked for fluorescence before the supernatant was collected from all plates and the virus concentrated using Lenti-X concentrator (Clontech) as per the manufacturer's instructions. The virus was resuspended in 1ml growth media and flash frozen in 200µl aliquots before storage at –80°C.

Transfection of target cells

One 200µl aliquot of virus mixed with hexadimethrine bromide to a final concentration of 5µg/ml (**Figure 2.6**) was added to each well of a 6 well plate containing 2T3 and ST2 cells for 3-4 days. Transfected cells were subsequently selected for 4 weeks using 4µg/ml puromycin-supplemented media (**Figure 2.7**) and were passaged as needed to prevent over-confluency that would reduce selection efficiency, after which they were considered selected, but growth media was still supplemented with puromycin to apply a continued selective pressure. Knockdown efficacy was determined by qPCR.

2.2.9 Statistical analysis

Statistical analysis performed in Chapter 3 is outlined in **Section 3.2.4**. All statistical analyses for Chapters 4, 5 and 6 were performed in GraphPad Prism 7 except for analysis of RNASeq data in Chapter 5 which was performed by Dr Srinivasa Rao in R. The statistical test used is denoted in each figure legend. Statistical significance is defined as $p \leq 0.05$.

3

Serum Adipokines and BMD: A Cross-Sectional and Prospective Study

3.1 Introduction

As the global population ages, the increased bone fragility of osteoporosis represents a growing health problem worldwide, but the development of early interventions to prevent its progress has been limited. Despite the identification of several osteoporosis risk factors, research still seeks a successful biomarker of osteoporotic development or progression to permit earlier clinical intervention. The work in this chapter aimed to assess the fat-derived adipokines leptin, adiponectin and their ratio (the leptin/adiponectin ratio, LAR) as cross-sectional and prospective markers of bone mineral density (BMD) in a large cohort of middle-aged women.

3.1.1 The Chingford 1000 Women Study

The Chingford 1000 Women Study is a population-based cohort of middle-aged women recruited from a general practice in North London in 1988-1989 when the women were aged 45-65 years old. 1003 women were initially signed up to the study with baseline analysis in 1988-1989. Since this date, analysis has been carried out annually, with a wide variety of information gathered at each time point, including medication use, medical history and smoking status. This cohort has previously been shown to be representative of middle-aged women in England[271].

3.1.1.1 Study ethics

This study was approved by the Outer North East London Research Ethics Committee (formerly Barking & Havering and Waltham Forest RECs, LREC 96), and each participant provided written consent before the commencement of the study. The Chingford Cohort resource was created in 2013 after approval by South Central – Oxford A Research Ethics committee to allow ongoing data maintenance, sample collection and analysis (REC reference number: 13/SC/0156).

3.1.2 Osteoporosis

Osteoporosis is defined as low bone mass and resulting in increased bone fragility and fracture risk and is estimated to affect over 200 million people worldwide[272]. The financial and social burden of its incidence is set to increase worldwide as average life expectancies continue to increase globally: in 2010, the prevention, treatment and long-term care of fractures associated with osteoporosis cost the EU an estimated €37 billion[273].

3.1.2.1 Risk factors

Factors known to be associated with risk of bone deterioration and development of osteoporosis include age, sex, smoking status, and long-term use of corticosteroids; the risk associated with these factors is reflected in their inclusion in the NICE guidelines for assessment for fragility fracture risk[274]. In particular, post-menopausal women represent a particularly high-risk group for osteoporotic development due to loss of the protective action of oestrogen in bone health[275]. Meanwhile, other factors are known to be associated with osteoporotic development without the establishment of a direct causative link, including weight. It has long been considered that the increased biomechanical loading associated with increased weight can protect bones from fracture[276], but whether a biological association exists alongside the biomechanical consideration is yet to be fully established.

3.1.2.2 Clinical diagnosis and management

Osteoporosis is often a silent disease with no obvious symptoms until fractures occur. It is defined by the World Health Organisation (WHO) as a T score of -2.5 or less as determined by dual energy x-ray densitometry (DEXA) scanning[277]. T scores are a standardised measure of BMD as compared with the expected BMD of a healthy 30-year-old, and a score of below -2.5, indicating a BMD more than 2.5 standard deviations below the expected value, is the critical threshold for osteoporosis diagnosis[277]. Fragility fractures of the hip, spine or wrist are also considered a diagnostic indicator for osteoporosis, particularly if occurring in a person of a high-risk group[278]. This is reflective both of T-scores by DEXA providing no information on the physical strength of the bone and its propensity for fracture, a key determinant in the definition of osteoporosis,

and of the typically late diagnosis of osteoporosis, with pre-symptomatic diagnosis being uncommon.

Following diagnosis, management can be split broadly into pharmacological and non-pharmacological interventions. Bisphosphonates are a family of drugs that inhibit bone resorption and are considered the first line treatment for slowing the progression of osteoporosis. Despite some consideration of adverse effects including osteonecrosis of the jaw[279], bisphosphonates significantly reduce the risk of vertebral, non-vertebral and hip fractures[280]. Calcium or vitamin D supplements may also be recommended, as might hormone replacement therapy (HRT) for women with early-onset menopause. Non-pharmacological interventions include increased exercise and balance programmes to increase fitness and reduce the risk of falls[281].

3.1.2.3 Biomarkers for osteoporotic development

There remains an unmet clinical need to identify methods by which to predict osteoporosis development and to track changes in bone health in order to allow pre-symptomatic intervention in high-risk individuals. This would reduce fracture incidence rates and the financial cost of osteoporotic fracture management.

DEXA scanning is currently the gold-standard of osteoporosis diagnosis, but it makes use of large, heavy and expensive equipment and exposure to radiation, practically limiting its accessibility and use as a method to track changes in bone density. Biomarkers have the potential to provide cheap, reliable and non-invasive readouts of bone health in the clinic; biomarkers that can predict future changes in bone health would be particularly valuable clinically. This is highlighted by studies that show hip fractures are associated with a significantly increased mortality rate for at least one year after the event, a reduced quality of life and reduced independence in patients[282]. While

bisphosphonates have enjoyed significant success at reducing fracture rate, the need for early and effective intervention to prevent osteoporotic development is now more urgent than ever: earlier diagnosis or observation of risk will result in better prevention, management and treatment.

To date, many bone turnover-related proteins have been suggested for use as biomarkers in osteoporosis development with the bone formation marker procollagen type 1 N-terminal polypeptide (P1NP) showing the most promise for development for use in the clinic[283]. The utility of serum adipokines as biomarkers is now being considered.

3.1.2.4 Serum adipokines and osteoporosis: current evidence

Adipokines are produced by adipose tissue and have widely varied biological effects (discussed further in **Section 1.2**). Their high concentrations in the blood coupled with readily available methods of quantification make them good potential biomarkers.

3.1.2.4.1 Leptin

Leptin is primarily involved in energy homeostasis[284] and is produced by white adipose tissue, explaining its well-established positive correlation with BMI. Increased BMI is also associated with bone mass preservation, with obese individuals preserving bone mass well, and the low circulating levels of leptin in anorexia nervosa patients correlating with low bone mass and increased fracture risk[284]. These observed correlations are likely due, at least in part, to the altered biomechanical loading of the joints, but this does not fully explain the relationship, as demonstrated by a significant positive relationship persisting between leptin and bone volume in these anorexia nervosa following adjustment for BMI[285]. The widely varying levels of circulating leptin in healthy individuals following

BMI adjustment suggest the involvement of genetic and environmental factors, and the relationship between leptin and BMD is still not understood with conflicting results produced from previous human studies[286]. The presence of a profound sexual dimorphism in leptin levels[287] is suggested to underly some of these conflicting results, justifying the use of a single-sex cohort representative of high osteoporotic risk groups.

3.1.2.4.2 Adiponectin

Unlike leptin, circulating concentrations of adiponectin correlate more closely with age than BMI: in a group of pre- and post-menopausal women, only age, fasting insulin resistance index and circulating leptin levels were found to be significantly correlated with circulating adiponectin levels[196]. It is suggested this is due to bone marrow adipocytes, rather than white adipose tissue, being the main producer of adiponectin[128]. The literature surrounding the relationship between circulating adiponectin levels and BMD in human cohorts has provided some conflicting results a discussed in **Section 1.4.1**. Some have found a negative correlation between the two[230,288]: in a systematic review of 59 studies of healthy men and women evaluated for at least one adipokine and BMD or fracture risk, adiponectin was found to be negatively correlated with BMD, and high adiponectin levels could be predictors of high vertebral fracture risk in men[289]. Conversely, other studies have found no association between adiponectin and bone mass[196,233,235], although significant sex-specific effects have again been noted[234]. This warrants further investigation in a single sex, high-risk group.

3.1.2.4.3 LAR

The leptin to adiponectin ratio (LAR) has been suggested as a clinical predictor of disease and has been used in assessing risk of metabolic disease in post-menopausal

women[290], proved a significant correlate of abdominal obesity in coronary heart disease patients[291] and was an independent risk factor for endometrial cancer risk in post-menopausal women[292]. A recent study in a population-based cohort of 365 healthy middle-aged men and women in the UK identified not only a significant negative association between adiponectin and baseline lumbar spine and femoral neck BMD in these participants but also a significant positive association between LAR and baseline lumbar spine and femoral neck BMD, suggesting its potential for use as an osteoporosis development biomarker alongside or independent of adiponectin[293].

3.1.3 Chapter aims and hypothesis

The work in this chapter aimed to assess the relative contributions of adiponectin, leptin and the LAR to bone health as determined by DEXA analysis of BMD at the hip and lumbar spine cross-sectionally and prospectively in a large population-based cohort of middle-aged women. The Chingford 1000 Women cohort provided an excellent basis for this study due to the high-risk status of postmenopausal women in osteoporosis development, the sexual dimorphisms present in previous studies of a similar nature, and the longitudinal collection of data coupled with the population-based structure of the study which permitted meaningful prospective study of the development of a disease that can remain asymptomatic for many years.

Based on previously published evidence regarding the relationship between BMD and circulating adiponectin concentration (reviewed in **Section 1.4.1**), it was hypothesised that a negative relationship between these two variables would be observed in this cohort. It was further hypothesised that site-specific relationships may be observed, strengthening this study design with respect to the clinical usefulness and applicability of its findings.

3.2 Methods

3.2.1 Study design and exclusion criteria

In this study, the associations of circulating adiponectin and leptin levels and their ratio (LAR) with BMD at the hip and lumbar spine (L1-L4) were assessed cross-sectionally and prospectively. The analysis carried out at year 10 forms the baseline for this study, with prospective analysis performed between years 10 and 15. Self-reported questionnaires were used to assess presence of potential confounders that could not be assessed in clinic, including smoking status, medication use and diagnosis of other musculoskeletal conditions. These confounding medical diagnoses included rheumatoid arthritis, psoriatic arthritis, gout, Paget's disease, polio, cerebral palsy and chronic inflammatory demyelinating neuropathy.

3.2.2 Participants

Of the 808 participants for whom data was recorded at year 10 of follow-up, participants were excluded from cross-sectional analyses on the basis of missing any pertinent data (n=39), a confounding medical diagnosis (n=22), or due to use of a confounding medication for another condition (n=3). This resulted in the inclusion of 744 participants in cross-sectional analyses. Of these 744 participants, 538 (72%) were included for prospective analyses. Exclusions were due to participants being deceased to follow-up (n=98), missing data (n=91) or a confounding medical diagnosis (n=17) (**Figure 3.1**).

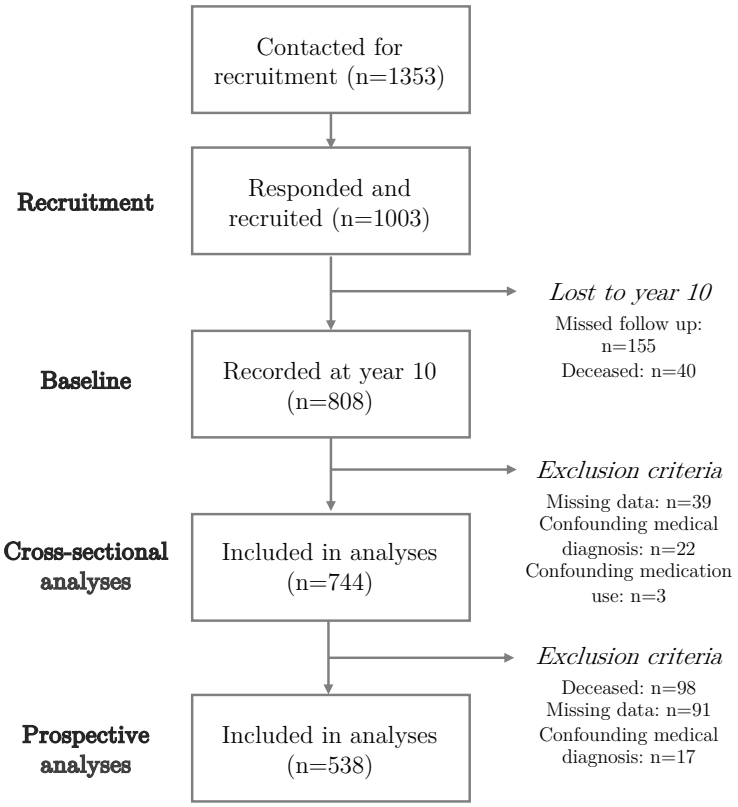


Figure 3.1: Consort diagram of inclusion of participants in cross-sectional and prospective analyses. Of the 1353 women contacted for recruitment from a large GP practice in North London, 1003 were recruited. Of the 808 women who were included in baseline analysis, 744 women went on to be included in cross-sectional analysis, and 538 women were further analysed in prospective study. Women were excluded due to missing information, deceased, diagnosis of a confounding medical condition, or use of a confounding medication.

3.2.3 Predictor and outcome variables

All blood collection and subsequent analysis of serum adiponectin and leptin concentration was performed by the Chingford Study team. Blood samples were drawn following eight hours fasting and stored at -45°C until analysis. The Quantikine® ELISA kit (R&D Systems, USA) determined adiponectin concentration. Leptin concentrations were determined by a combination of immunoassays. The leptin to adiponectin ratio (LAR) was calculated by dividing a participant's leptin concentration by their adiponectin concentration to give a value of arbitrary units. Logarithmically-transformed

leptin, adiponectin and LAR values were used as the predictor independent variables in analyses; transformation ensured normal distribution (**Figure 3.2**).

All DEXA scans were performed by the Chingford Study team. Total hip and lumbar spine (L1-4) BMD was determined by DEXA scanning (QDR 1000, Hologic, USA) at 10 and 15 years of follow-up. BMD at the hip and spine at year 10 were used as the outcome variables for cross-sectional analyses; the change in BMD at these locations for each participant between years 10 and 15 of follow-up, referred to as "delta BMD", were used as the outcome dependent variables in prospective analyses.

3.2.4 Statistical analysis

For each of the three predictor variables, 4 linear regression analyses were performed. These analyses sequentially adjusted for each of the confounder variables: age, BMI and smoking status. Model 1: unadjusted; model 2: adjusted for age; model 3: adjusted for age and BMI; model 4: adjusted for age, BMI and smoking status. Models 1 and 4 are referred to as univariate and multivariate analyses respectively throughout this chapter. All statistical analysis was performed using STATA (Version 15, StataCorp, College Station, TX, USA).

3.2.5 Testing the assumptions of linear regression

Linear regression analyses are used to predict the value of the outcome variable based on the value of the predictor variable. The conclusions drawn from these analyses are valid only if the assumptions underpinning the regression testing are met. Continuous data for the predictor and outcome variables (blood analytes and hip and spine BMD respectively) in these analyses meet the first two assumptions.

3.2.5.1 Normality

Predictor and outcome variables must be normally distributed during linear regression. Predictor variables adiponectin, leptin and the LAR conformed to assumption of normality following logarithmic transformation (**Figure 3.2**). Outcome variables were all normally distributed without transformation (**Figure 3.3**).

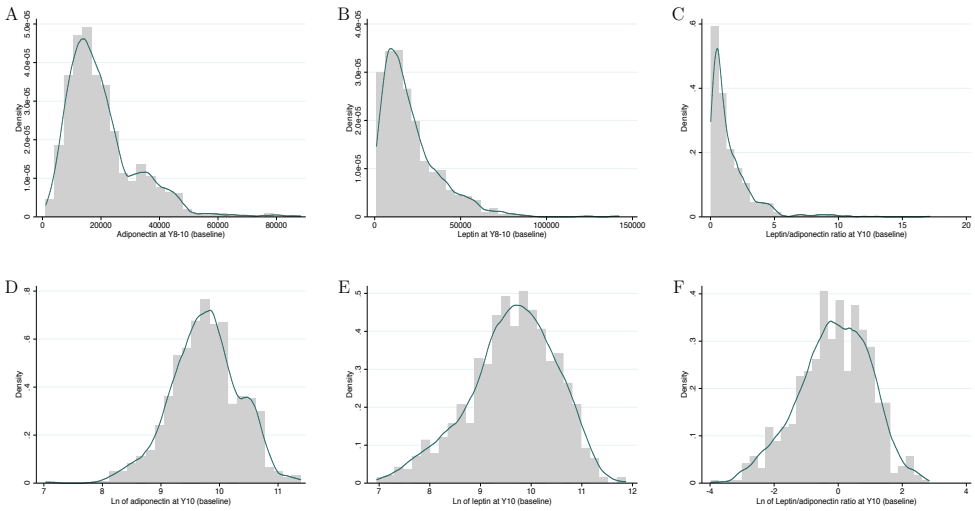


Figure 3.2: Normality of predictor variables before and after logarithmic transformation. Baseline (**A**, **D**) adiponectin, (**B**, **E**) leptin and (**C**, **F**) LAR (**A**-**C**) before and (**D**-**F**) after logarithmic transformation to produce normality.

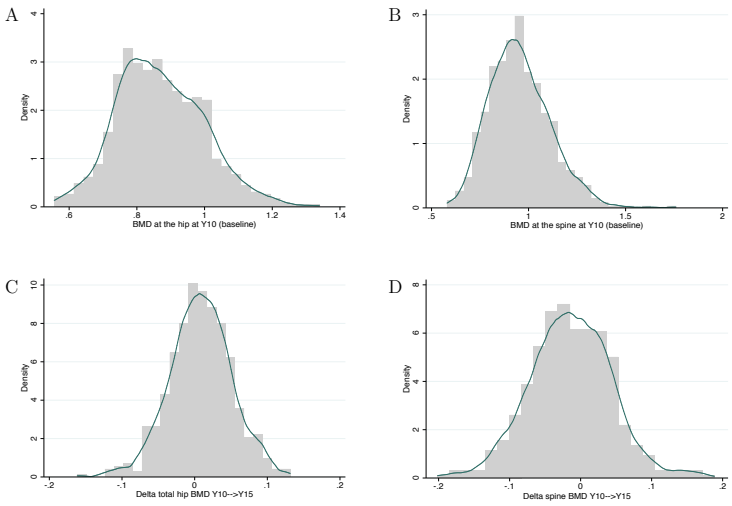


Figure 3.3: Normality of outcome variables. Baseline BMD at (**A**) the hip and (**B**) spine and delta BMD at (**C**) the hip and (**D**) spine all conformed to normal distribution without transformation.

3.2.5.2 Linearity

Linear regression assumes a linear relationship between the predictor and outcome variables. This assumption was met for all logarithmically transformed predictor variables against all outcome variables (**Figure 3.4**).

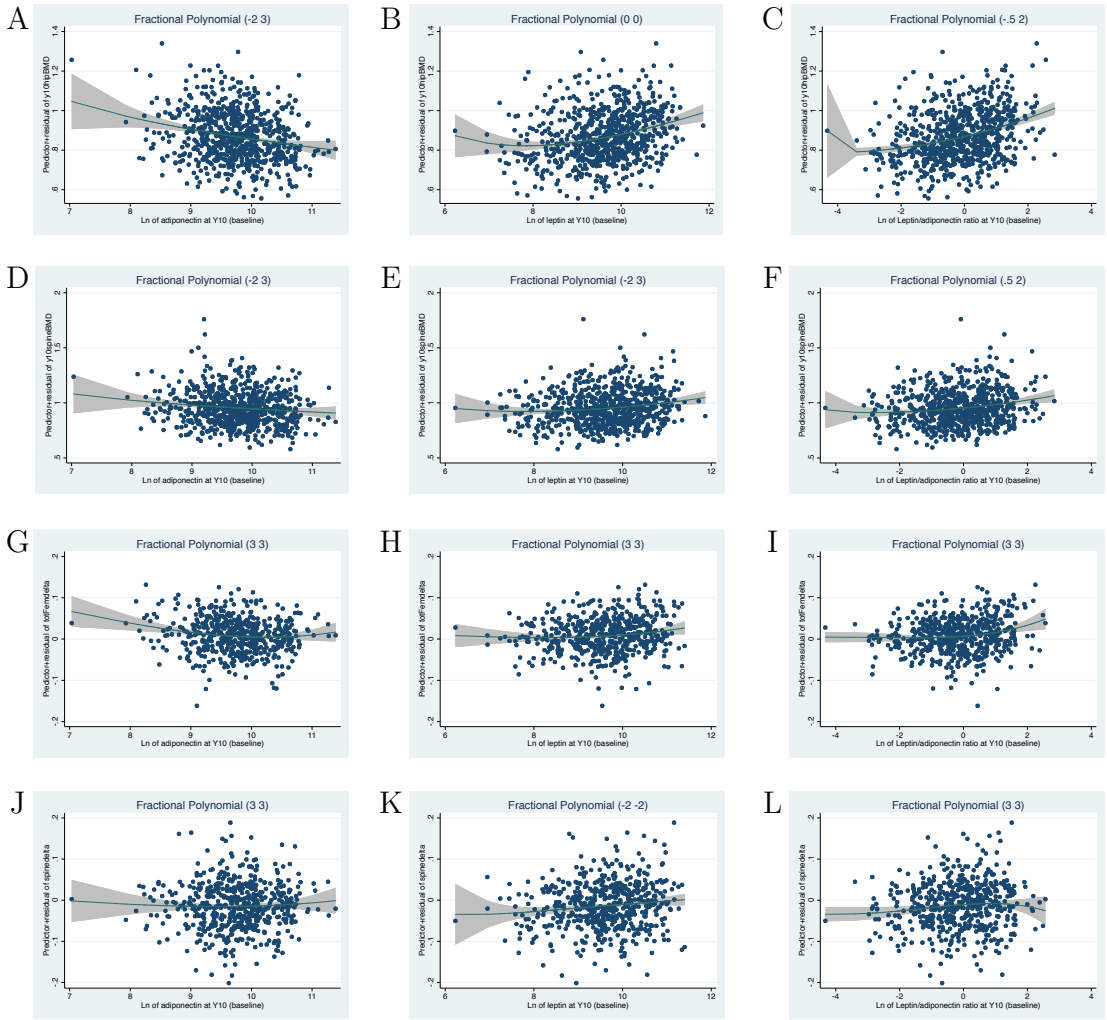


Figure 3.4: Linearity between logarithmically transformed predictor and untransformed outcome variables. Linear relationships are observed for (**A-C**) cross-sectional hip, (**D-F**) cross-sectional spine, (**G-I**) prospective hip and (**J-L**) prospective spine analyses for (**A**, **D**, **G**, **J**) adiponectin, (**B**, **E**, **H**, **K**) leptin and (**C**, **F**, **I**, **L**) the LAR.

3.2.5.3 Homoskedasticity

Homoskedastic data has equal residuals or errors across the dataset; heteroskedasticity occurs when changes in the value of the predictor variable significantly changes the error of the associated outcome value. In a large dataset, heteroskedasticity is often linked with sample size: at the extreme range of the predictor variable, fewer samples often leads to larger associated errors, unlike the errors associated with predictor values situated in the middle of the normality curve, where larger sample sizes often produce more uniform errors.

The assumption of homoskedasticity can be assessed visually in **Figure 3.4**, or it can be quantified using the Breusch-Pagan test (**Table 3.1**). This test found significant heteroskedasticity in several of the analyses performed in this study, both in univariate and multivariate analyses. The increased heteroskedasticity observed in multivariate analyses is likely linked to the smaller sample size. To account for the significant heteroskedasticity observed, robust standard errors were used throughout all analyses.

		Cross-sectional (n=743)		**Prospective (n=537)**	
		Univariate	**Multivariate**	**Univariate**	**Multivariate**
Hip	Adiponectin	0.050 *	0.0254 *	0.0337 *	0.0025 **
	Leptin	0.3452	0.1417	0.0256 *	0.0036
	LAR	0.04211	0.0883	0.0039 **	0.0028 **
Spine	Adiponectin	0.1331	0.6198	0.4987	0.0073 **
	Leptin	0.3727	0.3859	0.0612	0.0445
	LAR	0.1437	0.4584	0.0533	0.0510

Table 3.1: Breusch-Pagan test to assess validity of homoskedasticity assumption. Univariate analysis (model 1) unadjusted; multivariate analysis (model 4) adjusted for age, BMI and smoking status. Data presented as p value; p≤0.05 shows significant heteroskedasticity exists within the dataset; *=p≤0.05, **=p≤0.01.

3.2.5.4 Interactions

Interaction effects occur when the effect of the predictor variable on the outcome variable changes depending on the value of one or more variables thought to be independent from the variables as interest. Regression analysis found no significant interactions between the three predictor variables (adiponectin, leptin and the LAR) and the three confounding variables (age, BMI and smoking status) (**Table 3.2**).

	Adiponectin		**Leptin**		**LAR**	
	Hip	**Spine**	**Hip**	**Spine**	**Hip**	**Spine**
Age	0.592	0.929	0.0929	0.550	0.850	0.568
BMI	0.787	0.901	0.122	0.799	0.337	0.701
Smoking status	0.164	0.984	0.883	0.875	0.447	0.891

Table 3.2: No significant interactions exist between predictor and confounder variables at the hip or spine. Data presented as p value; significance defined as $p \leq 0.05$.

3.3 Results

3.3.1 Characteristics of participants

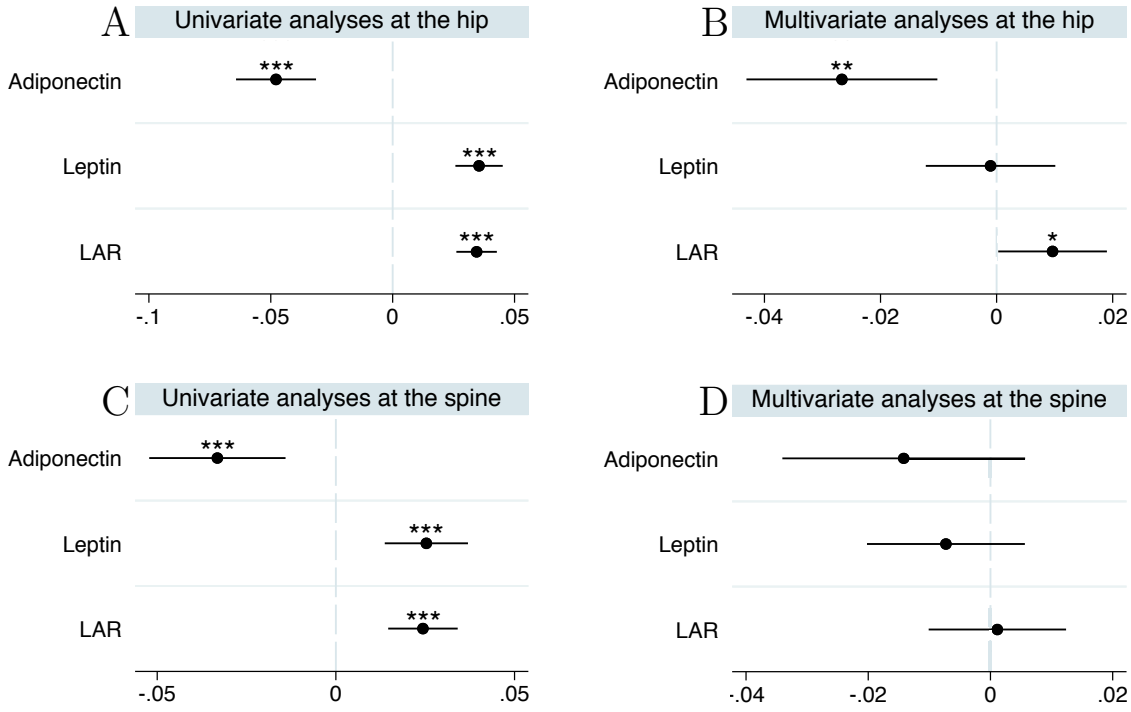
The baseline characteristics of the included participants are displayed in **Table 3.3**.

Parameter	Cross-sectional (n=744)	Prospective (n=538)
Adiponectin (ng/ml)	20128 (11842)	20192 (11839)
Leptin (pg/ml)	20850 (17194)	20022 (15883)
LAR (AU)	1.514 (1.778)	1.448 (1.565)
Age (years)	62.5 (5.9)	61.7 (5.66)
BMI (kg/m²)	26.7 (4.5)	26.6 (4.3)
Smoking (%)	102 (13.7)*	Not available
Total hip BMD (g/cm²)	0.869 (0.128)	0.874 (0.125)
Spine (L1-L4) BMD (g/cm²)	0.955 (0.157)	0.957 (0.147)

Table 3.3: Baseline characteristics of participants included in cross-sectional and prospective study. Data presented as mean (standard deviation); *=data presented as number (% of total).

3.3.2 Cross-sectional association

In cross-sectional analysis (**Figure 3.5**), adiponectin was significantly negatively correlated with hip BMD before (p=0.000, **Figure 3.5A**) and after (p=0.002, **Figure 3.5B**) adjustment for age, BMI and smoking status, with the LAR significantly positively associated with hip BMD (p=0.044 after adjustment, **Figure 3.5B**). Both of these predictors explained a large proportion of these interactions after adjustment (27.7% and 26.8% respectively, **Figure 3.5E**). Leptin failed to correlate significantly with cross-sectional hip or spine following adjustment for BMI (model 3, **Figure 3.5E**). None of the three predictor variables correlated significantly with lumbar spine BMD cross-sectionally following BMI adjustment (model 3, **Figure 3.5C-E**).



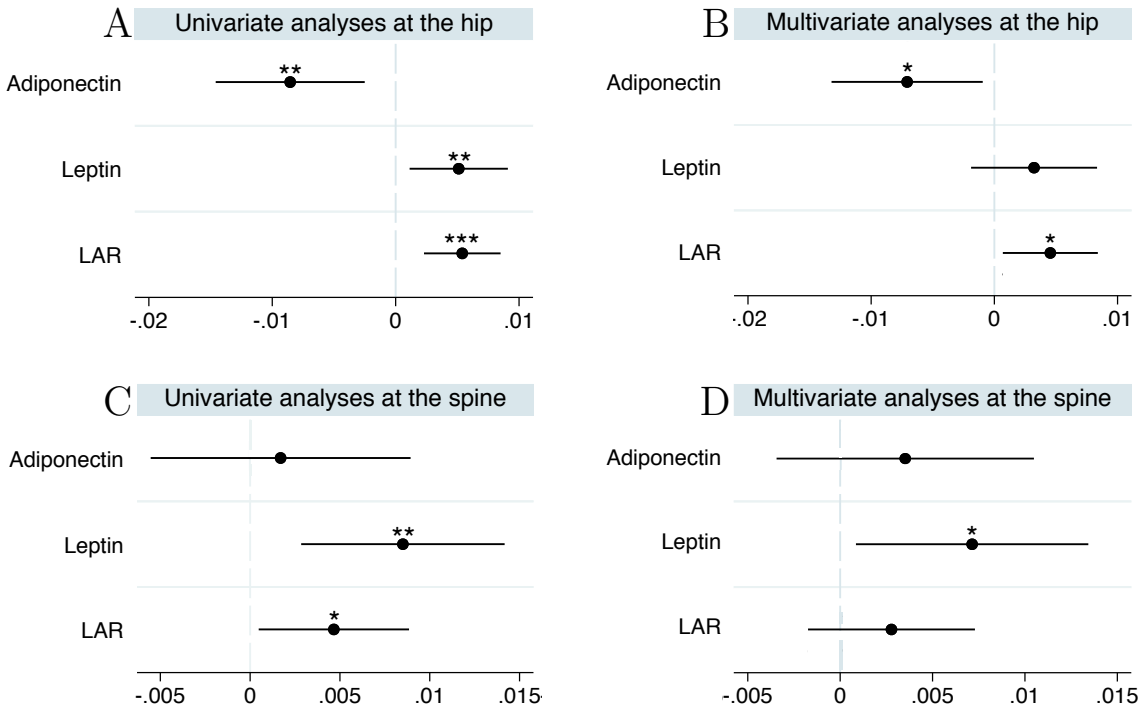
E

		Model 1: univariate	Model 2	Model 3	Model 4: multivariate
Hip	*Adiponectin*	0.000 (0.048) ***	0.000 (0.137) ***	0.002 (0.276) **	0.002 (0.277) **
	Leptin	0.000 (0.058) ***	0.000 (0.154) ***	0.881 (0.263)	0.855 (0.263)
	LAR	0.000 (0.091) ***	0.000 (0.182) ***	0.045 (0.267) *	0.044 (0.268) *
Spine	*Adiponectin*	0.001 (0.015) ***	0.001 (0.056) ***	0.147 (0.123)	0.161 (0.123)
	Leptin	0.000 (0.020) ***	0.000 (0.062) ***	0.257 (0.122)	0.268 (0.122)
	LAR	0.000 (0.030) ***	0.000 (0.071) ***	0.831 (0.121)	0.840 (0.121)

Figure 3.5: Cross-sectional multivariate regression analysis between blood analytes and BMD. Association between BMD at (**A**, **B**) the hip and (**C**, **D**) spine and serum concentrations of adiponectin, leptin and the LAR. (**A**, **C**) Univariate analyses: unadjusted; (**B**, **D**) multivariate analyses: adjusted for age, BMI and smoking status. (**A-D**) Data presented: coefficient of analysis with 95% confidence intervals. (**E**) Data presented as P value (R^2). Model 1 (univariate analyses): unadjusted; model 2: adjusted for age; model 3 adjusted for age and BMI; model 4 (multivariate analyses): adjusted for age, BMI and smoking status. *=p≤0.05; **=p≤0.01; ***=p≤0.001

3.3.3 Prospective association

In prospective analyses (**Figure 3.6**), adiponectin was significantly negatively correlated with delta hip BMD before (p=0.006, **Figure 3.6A**) and after (p=0.024, **Figure 3.6B**) adjustment for age, BMI and smoking status, with the LAR significantly positively associated with delta hip BMD (p=0.022 after adjustment, **Figure 3.6B**), despite the relative contribution of these predictors to these interactions after adjustment being low (2.5% and 2.6% respectively, **Figure 3.6E**). As with cross-sectional analysis, leptin did not correlate significantly with BMD at the hip after adjustment (**Figure 3.6B**), but it did correlate significantly positively with delta spine BMD even following adjustment for BMI (**Figure 3.6D-E**). Leptin was the only predictor variable to correlate with delta spine BMD after adjustments in these analyses and explained over 9% of the observed relationship (**Figure 3.6E**); this was the only analyses in this study for which leptin proved a significant predictor of outcome following full adjustment.



E

		Model 1: univariate	Model 2	Model 3	Model 4: multivariate
Hip	*Adiponectin*	0.006 (0.014) **	0.006 (0.012) **	0.018 (0.024) *	0.024 (0.025) *
	Leptin	0.012 (0.011) **	0.013 (0.013) *	0.229 (0.016)	0.216 (0.019)
	LAR	0.000 (0.021) ***	0.001 (0.023) **	0.019 (0.024) *	0.022 (0.026) *
Spine	*Adiponectin*	0.642 (0.000)	0.721 (0.076)	0.410 (0.084)	0.325 (0.086)
	Leptin	0.003 (0.016) **	0.004 (0.090) **	0.028 (0.090) *	0.026 (0.093) *
	LAR	0.030 (0.008) *	0.027 (0.083) *	0.205 (0.086)	0.228 (0.087)

Figure 3.6: Prospective multivariate regression analysis between blood analytes and BMD. Association between BMD at (**A**, **B**) the hip and (**C**, **D**) spine and serum concentrations of adiponectin, leptin and the LAR. (**A**, **C**) Univariate analyses: unadjusted; (**B**, **D**) multivariate analyses: adjusted for age, BMI and smoking status. (**A-D**) Data presented: coefficient of analysis with 95% confidence intervals. (**E**) Data presented as P value (R^2). Model 1 (univariate analyses): unadjusted; model 2: adjusted for age; model 3 adjusted for age and BMI; model 4 (multivariate analyses): adjusted for age, BMI and smoking status. *=p≤0.05; **=p≤0.01; ***=p≤0.001

3.4 Discussion

Previous work on the association between adipokines and BMD has provided conflicting results. Post-menopausal women are a high-risk group for osteoporosis development and its incidence is associated with significant morbidity and associated mortality after osteoporotic fracture. There is a strong and unmet clinical need to identify reliable, cheap and accessible biomarkers of osteoporotic development risk and progression to permit earlier intervention and better management in this group.

To our knowledge, the study presented here is one of the first to evaluate the association of circulating adipokine levels with cross-sectional and prospective changes in hip and lumbar spine BMD across a five-year follow-up. Performing this study in a large cohort of post-menopausal women representative of women in the UK increases its clinical relevance and it is hoped it will add to the body of knowledge about the applicability of adipokines as biomarkers for risk of osteoporosis development and contribute to better clinical diagnosis and management of bone deterioration in age for this high-risk group.

Throughout these analyses, varying models were used for successive adjustment to take confounding variables age, BMI and smoking status into account. These are factors known to have direct influences in BMD, making their inclusions in these analyses essential for transferral to the clinic. In multivariate analyses models 2, 3 and 4, the correlations persisted after adjustment for age, particularly important in post-menopausal women whose BMD decline is accelerated as compared to pre-menopausal women. This highlights the importance of age-matched studies and provides strength to studies with a cross-sectional and prospective design.

In line with similar previously published studies[229] and the original hypothesis, circulating adiponectin levels at baseline were found to be negatively correlated with total hip BMD cross-sectionally and the change in hip BMD to follow-up after

adjustment for confounders; after the same adjustment, the LAR was shown to be a positive correlate of hip bone density both cross-sectionally and prospectively. A study using participants from the Twins UK study similarly found negative correlations between circulating serum adiponectin and BMD in women of a much wider age range than studied here (18-81 years)[294], supporting the applicability of adiponectin as a biomarker.

In most cases, leptin lost its significant association with the outcome variable following adjustment for BMI, an unsurprising observation given leptin's production by white adipose tissue and its positive correlation with weight. Despite this, leptin was the only correlate of five-year changes in lumbar spine BMD after full adjustment explaining nearly 10% of the observed effect, with none of the predictor variables correlating significantly with cross-sectional lumbar spine BMD.

As hypothesised, these data suggest adipokine correlations with BMD and changes in BMD are site-specific, an important issue for translation to the clinic that warrants further investigation. Cross-sectionally, both adiponectin and the LAR explained over a quarter of the observed interactions at the hip, strongly supporting the idea that adipokines could be valuable potential biomarkers. This is particularly pertinent given that one is a positive correlate and one a negative correlate; their combination as markers could provide a very powerful readout of bone health and deterioration.

The frequent and repeated DEXA scans of the Chingford study provide a useful resource for longitudinal observations of bone density. DEXA scans and their results are still the gold-standard for an osteoporosis diagnosis preceding fragility fracture[295], thus making this study and its conclusions about the use of adipokines as predictive biomarkers of osteoporosis development and progression immediately clinically relevant. However, fracture occurrence is an important clinical outcome of osteoporosis diagnosis and management, and tools are now available to predict future fracture risk[296]. Correlating

circulating adipokine levels with fracture occurrence should be considered an essential next step for this work to begin to define whether the observed correlation is causative, and longer longitudinal studies should also be considered.

This study is limited by the scope of data collected by the Chingford Study, and thus there remain confounding factors, either unknown or unmeasured, which could not be accounted for in the current analysis. Additionally, the study population, homogenous in its sex, age, race and geographical location cannot provide causative information between circulating adipokine concentrations and bone mineral density, nor can the data provide insight into any mechanistic link between these variables. While no current explanation is available for the discordant results previously observed in other studies, several routes for further investigation could be explored to better define the role of adipokines in bone health.

This study makes use of total circulating adiponectin, but the differential effects of the downstream signalling associated with the different oligomeric forms of adiponectin, likely due to their distinct affinities for AdipoR1 and AdipoR2, should be considered[150] (**Section 1.3.2.2**) due to its known clinical relevance: the circulating ratio of these complexes has been associated with several pathological states, including obesity[212], chronic obstructive pulmonary disease (COPD)[214] and coronary heart disease in type II diabetics[297]. It is possible that investigating the relative ratios of these oligomers in a large cohort could present a clearer picture of the role of adiponectin as a biomarker; the ready availability of detection methods that permit the identification of these varying oligomer sizes makes this a practical and attractive potential avenue for further investigation before translation to the clinic is possible.

Another consideration in the use of total circulating adiponectin is that adiponectin concentrations are significantly increased within the bone microenvironment since bone marrow adipocytes are significant producers of adiponectin[128]. Its relatively high

concentration in the bone marrow niche alongside pre-clinical observations that both adiponectin and its receptors are expressed by osteoblasts and osteoclasts suggest adiponectin has local effects as well as systemic endocrine effects[164]. It is likely these autocrine or paracrine effects could be missed in an analysis of whole blood concentrations, a particularly interesting point in light of pre-clinical observations that suggest the ratio between adiponectin concentrations in the bone marrow plasma and concentrations in the blood changes with age[164]. Together, this previous work alongside this study provide a strong rationale for further, more detailed investigation; in particular, study of local adiponectin concentrations should be considered.

A final consideration for the work presented in this chapter is that no genetic material was available for analysis, thus preventing assessment of expression of AdipoR1 and AdipoR2. An understanding of changes in receptor expression is fundamental to interpreting the results of changing adiponectin levels, particularly since level of AdipoR1 and AdipoR2 expression is tissue-specific[150]. Future work could seek to evaluate the effect of osteoporosis and age on AdipoR1 and AdipoR2 expression in primary samples from human cohorts.

These observations suggest that current interpretations of the data could be further clarified by understanding signalling at the cellular level. Despite this need for further understanding, the results presented in this study are nonetheless an exciting and clinically relevant step forward in investigating biomarkers for osteoporosis diagnosis and progression.

3.5 Conclusions

In conclusion, this study identified a strong negative correlation between adiponectin and hip BMD in a large cohort of postmenopausal women both cross-sectionally and five-year prospectively; similar positive correlations were observed between the LAR and hip BMD. These data strongly suggest a clinical benefit of using adiponectin concentration and the LAR in osteoporosis management as cheap, non-invasive and readily available biomarkers of its incidence and development with an aim to addressing the outstanding clinical need for better prediction of osteoporosis risk in an ageing population (**Figure 3.7**).

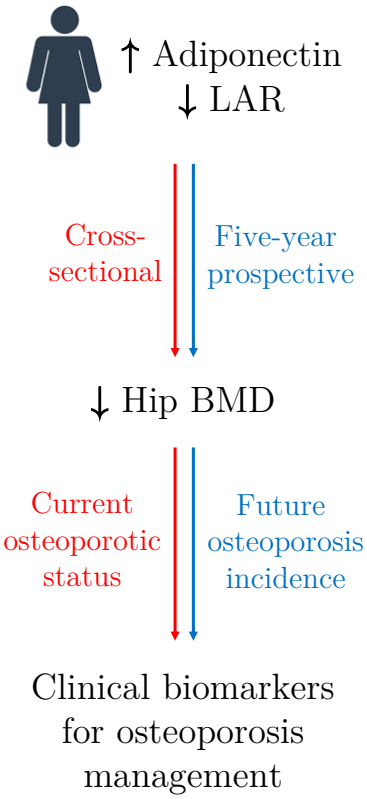


Figure 3.7: Summary of Chapter 3 key findings. Hip BMD correlated negatively with circulating adiponectin concentration and positively with the LAR both cross-sectionally (red) and five years prospectively (blue) in the post-menopausal women of the Chingford Study. The utilisation of these correlations as biomarkers of current osteoporotic status and future risk of osteoporotic development respectively is suggested and represents a novel management option for osteoporosis care in this high-risk group.

4

Skeletal Phenotyping of AdipoR1-Deficient and AdipoR2-Deficient Mice

4.1 Introduction

4.1.1 The utility of animal models

In the previous chapter, data collected from a large human cohort was used to begin to assess the relationship between adiponectin and bone health. Human data undoubtedly remains the most clinically relevant source of information; however, it presents several practical limitations, including length of study and lack of data on some potentially confounding parameters due to insufficient ethical justification for their collection or lack of control over environmental or genetic variables. Equally, researchers are often limited due to the use of data collected in non-hypothesis-driven cross-sectional studies meaning that the data is not specifically designed for subsequent use in a particular study, inevitably leading to missing parameters. For these reasons, animal models form an

invaluable line of scientific investigation, permitting control and analysis of parameters beyond those measurable in human subjects.

While no animal model can perfectly recapitulate human physiology or disease processes, the suitability of mice as a model animal for scientific investigation has been well established due to their genetic and physiological similarities with humans[298] and their favourable practical capacities, such as their small size, large average litter size, and short lifespan[299]. Humans and mice show similar bone biology, homeostasis and age-related bone loss, and the use of mouse models has been instrumental in the discovery of key regulators of human bone health, such as RANKL[4,300]. The popularity of mouse models combined with the advent of advanced genetic techniques permitting targeted gene manipulation has led to the development of large databases of genetic, genomic and phenotypic mouse information[301]. International efforts to phenotype mutant mouse models continue, including by the International Mouse Phenotyping Consortium (IMPC).

4.1.2 The International Mouse Phenotyping Consortium

The International Mouse Phenotyping Consortium (IMPC) is a global project that aims to create and phenotype a null mouse mutant of every protein-coding gene in the mouse genome in order to assess the function of each gene. Following their creation, the animals are offered publicly to any interested research party. The phenotyping screen carried out before their general release assesses hundreds of parameters, covering all major physiological systems including respiratory, cardiovascular, neurological and reproductive, along with broader observations of mortality, ageing and general behaviour. This data is publicly available online[302,303]. As of 2018, 8,000 genes had been phenotyped and published online, representing more than a third of the mouse genome[304];

all animals used in IMPC studies are of the C57Bl/6N line, a commonly used inbred and immunocompetent derivative of the C57Bl/6 line originally developed by The Jackson Laboratory founder Clarence Cook Little in 1921[305]. The AdipoR1$^{-/-}$ and AdipoR2$^{-/-}$ mice studied in this thesis are products of this IMPC hypothesis-generating project. During IMPC phenotypic screening, AdipoR1$^{-/-}$ mice were identified to have significant alterations in their blood chemistry profile (see **Chapter 5**) and increased red blood cell distribution width as compared with sex-matched controls. A significantly reduced body length was also observed in male AdipoR1$^{-/-}$ mice only. The most significant phenotype associated with ablation of AdipoR1 involved the eye: AdipoR1$^{-/-}$ mice showed decreased corneal and retinal thickness and a recent paper confirms the role of AdipoR1 in the eye and vision[306]. Screening of AdipoR2$^{-/-}$ mice identified a significantly reduced grip strength and limb grasping in male mice only, with no significant phenotype associated with female AdipoR2$^{-/-}$ mice in any of the parameters tested.

To date, close examination of the bone phenotype of these mice has not been reported. Skeletal phenotypic evaluation involves assessment of whole-body characteristics, bone morphology measurements, histomorphometric analysis and the biomechanical properties of long bones[307]. These techniques are not performed during routine phenotypic screening due to their relative difficulty and time-consuming nature.

4.1.3 µCT analysis of bone microarchitecture

Three-dimensional micro-computed tomography (µCT) analysis was used in this chapter to quantify bone microarchitecture. Unlike clinical CT scanning, in which an X-ray source is rotated slowly around the scanned object, µCT scanning involves incremental rotation of the scanned object inside a scanner along a single rotational axis until one full rotation has been completed. At each rotational position, X-rays pass through the

material to a detector. The partial attenuation of the X-rays by the calcified bone creates a series of two-dimensional images of the object which are subsequently reconstructed into a three-dimensional image[308]. X-ray absorption is directly related to the mineral density of bone and is not perturbed by other tissues surrounding the bone or within the bone marrow; therefore, the varying relative densities of distinct bone areas permit high resolution reconstructions to be produced and quantified.

µCT scanning has been implemented regularly in the bone biology field since its introduction in the late 1980s by Feldkamp and Goldstein[309,310] before which bone microarchitecture was evaluated by histology. µCT analysis holds significant advantages over histological analysis for this purpose given its objectivity and removal of subjective assessment and its ability to assess the whole bone rather than a two-dimensional section. Use of the same analysis and reconstruction settings permits direct, objective and quantitative comparison of results between cohorts and the difference in their relative densities permits separate analysis of trabecular and cortical areas as desired (**Figure 2.2**).

In this chapter, µCT scanning is used to determine trabecular parameters including bone volume as a fraction of total tissue volume (BV/TV) (**Sections 4.2.2.1.1 and 4.2.4.1.1**), relative bone mineral density (BMD) (**Sections 4.2.2.1.2 and 4.2.4.1.2**) and cortical thickness and relative tissue mineral density (TMD) (**Sections 4.2.2.1.3 and 4.2.4.1.3**). Analysis was performed on the tibia which is a commonly used site of trabecular and cortical parameter evaluation by µCT acknowledged to provide a representative reflection of BMD and bone volume[311].

4.1.4 Histological analysis of bone cell distribution

Histological analysis permits visual study of bone structures and has been a cornerstone of bone phenotyping for many years. Unlike µCT, histology allows identification and quantification of cell type and distribution. The full histological process including staining protocols is outlined in **Section 2.1.5**.

Haematoxylin and eosin (H&E) staining is a common non-cell-specific stain used for gross morphological identification. Haematoxylin is dark purple in colour and stains nucleic acids, whereas eosin, pink in colour, stains proteins non-specifically[312]. In H&E-stained sections, bone appears pale pink, making trabecular structures distinguishable from the surrounding purple bone marrow. Histological identification of osteoclasts is performed by staining of tartrate-resistant acid phosphatase (TRAP). TRAP-positive osteoclasts are stained red with sections counter-stained with nuclear stain haematoxylin for easier visualisation of the bone environment and of the multinucleated nature of these cells.

In this chapter, histomorphometric analysis of H&E-stained sections was used to identify and quantify osteoblast number and relative coverage of the trabecular bone surface and adipocyte number and size (**Figure 4.6, Figure 4.8, Figure 4.15** and **Figure 4.17**). TRAP-stained sections were analysed for identification and quantification of osteoclast number and relative coverage of the trabecular bone surface (**Figure 4.7** and **Figure 4.16**).

4.1.5 Three-point bend testing of bone biomechanical properties

Bones are load bearing, making analysis of their biomechanical properties imperative to the interpretation of a skeletal phenotype. In clinical settings, the health of bones is defined by their ability to maintain their physical properties, a failure to do so ultimately leading to fracture. Therefore, skeletal bone phenotyping must include assessment of bone integrity and pattern of deformation to fracture. Several forms of biomechanical testing exist, including application of tension, shear or torsion stresses. However, the small size of rodent bones is a limiting factor in choice of test, and thus bend testing is most frequently applied[313].

Bend testing is typically carried out on unfixed long bones with the femur, humerus and tibia all representing well-established sites for mechanical testing in murine models[314]. Different skeletal sites have been observed to produce slight variations in skeletal property measurements, making use of the same bone, cleaned of any soft tissue, in the same orientation for each mouse essential for production of comparable results[313]. Three-point bend testing involves placement of the long bone on two vertical supports and application of a single downward force to the centre of the bone until fracture with a force transducer attached; given the application of this force to the middle of the bone shaft, it is likely that results reflect the properties of cortical bone rather than trabecular[314]. From the force transducer recordings, load displacement curves are produced displaying the pattern of bone deformation and breakage by plotting bone extension against applied load.

Maximum load to fracture indicates the overall integrity of the bone and is distinct from load at break due to significant deformation of the bone before breakage. Extension at break is considered to be negatively correlated with bone brittleness, with reduced

extension to break suggesting increased bone brittleness. Energy at break describes the energy required for fracture and is a descriptor of bone toughness. The elastic modulus indicates the resistance of the bone against an applied force and the force needed for displacement to occur. This is calculated from the initial slope of the curve as the bone bends with applied pressure and is referred to as bone stiffness; it is closely linked to bone mineralisation[313].

In this chapter, three-point bend testing is used to determine the biomechanical properties of the humeri of four-, 24- and 52-week-old AdipoR1$^{-/-}$ female mice as compared with age- and sex-matched controls (**Section 4.2.2.3**).

4.1.6 Chapter aims and hypothesis

It was hypothesised that making use of mouse lines in which the adiponectin receptor AdipoR1 or AdipoR2 had been globally ablated, leaving adiponectin and the other receptor intact, could clarify the role of adiponectin and its receptors in the bone since the bone phenotype of these mice remains uncharacterised. Specifically, based on previously published work (reviewed in **Section 1.4.2**), it was hypothesised that global deletion of AdipoR1 or AdipoR2 would result in a reduced bone volume, and age- and sex-specific effects were expected.

A study design that included AdipoR1$^{-/-}$ and AdipoR2$^{-/-}$ male and female mice at young (four weeks old), adult (24 weeks old) and aged (52 weeks old) timepoints was chosen to allow study of any potential sex- or age-related skeletal phenotypes in a paradigm controlled as much as possible for inter-mouse line variation and environmental confounders. The work presented in this chapter aims to characterise the skeletal phenotype of AdipoR1$^{-/-}$ and AdipoR2$^{-/-}$ mice by assessing key phenotypic features, with focus narrowing on females of the AdipoR1 line for biomechanical testing.

4.2 Results

4.2.1 Gross morphology of AdipoR1$^{-/-}$ mice

4.2.1.1 Young AdipoR1$^{-/-}$ mice show a reduced body weight

Phenotyping of the AdipoR1$^{-/-}$ mouse line began with assessment of whole-body morphology. No gross abnormalities, including general behaviour, failure to thrive or changes in gait, were observed, with AdipoR1$^{-/-}$ mice behaviourally indistinguishable from AdipoR1$^{+/+}$ littermates. A significantly reduced body weight was observed in both male (**Figure 4.1A**) and female (**Figure 4.1B**) AdipoR1$^{-/-}$ mice at four weeks old with no significant difference in body weight in older animals.

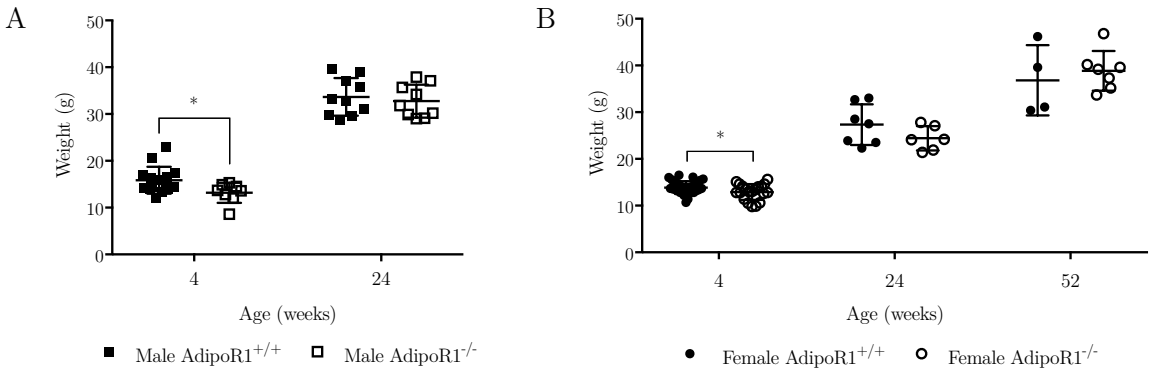


Figure 4.1: Young AdipoR1$^{-/-}$ mice show significantly reduced body weight. (**A**) Four-week-old male AdipoR1$^{-/-}$ mice, but not 24-week-old AdipoR1$^{-/-}$ male mice, show a significantly reduced body weight as compared with age-matched AdipoR1$^{+/+}$ controls. (**B**) Four-week-old female AdipoR1$^{-/-}$ mice, but not 24- or 52-week-old AdipoR1$^{-/-}$ female mice, show a significantly reduced body weight as compared with age-matched AdipoR1$^{+/+}$ controls. Data presented as mean±SD. Unpaired t-test, *=p≤0.05.

4.2.1.2 AdipoR1$^{-/-}$ mice show reduced long bone length

Long bones were measured at cull to determine whether a reduced body weight was associated with reduced long bone length. Tibial length was defined as the distance between the articular surface and the fibular notch and humerus length was defined as the distance from the head of the humerus to the distal articulating surface. Both measurements were precise to 0.01mm. As compared with age- and sex-matched controls, four-week-old male AdipoR1$^{-/-}$ mice showed a significantly reduced tibial length but no statistically significant difference was observed by 24 weeks of age (p=0.068) (**Figure 4.2A**). Female AdipoR1$^{-/-}$ mice showed significantly reduced tibial (**Figure 4.2B**) and humerus (**Figure 4.2C**) length at 52 weeks of age, with no significant difference observed at younger ages.

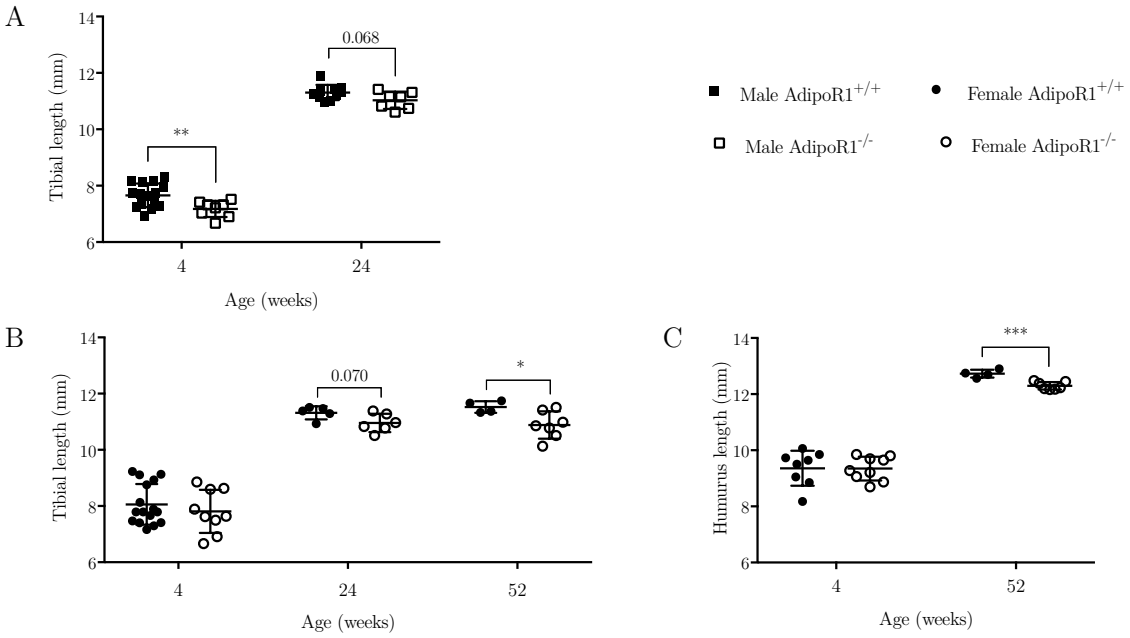


Figure 4.2: AdipoR1$^{-/-}$ mice show a reduced long bone length. (**A**) Male AdipoR1$^{-/-}$ mice show a significantly reduced tibial length at four weeks of age as compared with age-matched AdipoR1$^{+/+}$ controls with significance lost by 24 weeks of age. (**B**) 52-week-old female AdipoR1$^{-/-}$ mice show a significantly reduced tibial length as compared with age-matched AdipoR1$^{+/+}$ controls with no significant difference found at four weeks old or 24 weeks old (p=0.07). (**C**) 52-week-old female AdipoR1$^{-/-}$ mice show a significantly reduced humerus length as compared with age-matched AdipoR1$^{+/+}$ controls with no significant difference found at four weeks old. Data presented as mean±SD. Unpaired t-test, *=p≤0.05; **=p≤0.01; ***=p≤0.001.

4.2.2 Bone phenotyping of AdipoR1$^{-/-}$ mice

4.2.2.1 Bone microarchitecture by µCT of AdipoR1$^{-/-}$ mice

4.2.2.1.1 Young female AdipoR1$^{-/-}$ mice show reduced bone volume and altered trabecular parameters

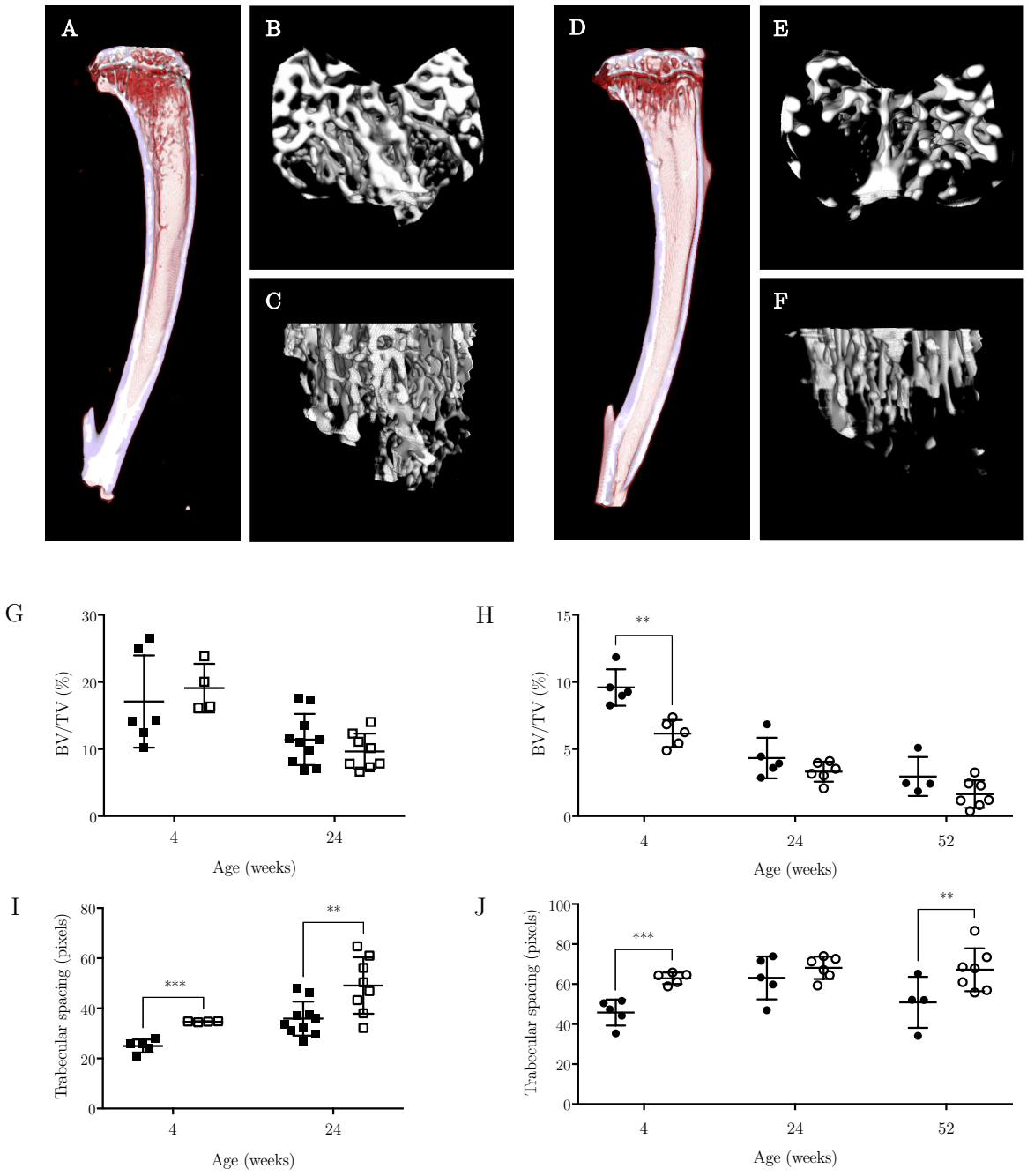
µCT analysis provides comprehensive, objective analysis of bone content (**Section 4.1.3**). Trabecular and cortical areas (**Figure 2.2**) for each bone were analysed with the same parameters each time as described in **Section 2.1.4**. This permits direct comparison of bone volume between groups to provide insights into bone accrual and loss across the ages studied.

Analysis of the trabecular areas of control AdipoR1$^{+/+}$ (**Figure 4.3A-C**) and AdipoR1$^{-/-}$ (**Figure 4.3D-F**) was performed in male mice at four and 24 weeks of age (**Figure 4.3G, I, K and M**) and in female mice at four, 24 and 52 weeks of age (**Figure 4.3H, J, L and N**).

In male AdipoR1$^{-/-}$ mice, no significant differences in BV/TV (**Figure 4.3G**), trabecular thickness (**Figure 4.3K**) or trabecular number (**Figure 4.3M**) were observed at either age studied as compared with age- and sex-matched controls. However, trabecular spacing, denoting the space between trabeculae, was significantly increased in both 24- and 52-week-old AdipoR1$^{-/-}$ males (**Figure 4.3I**).

At four weeks of age, female AdipoR1$^{-/-}$ mice consistently showed a low bone phenotype as compared with age-matched AdipoR1$^{+/+}$ controls: BV/TV (**Figure 4.3H**) and trabecular number (**Figure 4.3N**) were both significantly reduced with trabecular spacing (**Figure 4.3J**) increased. These data are suggestive of a retarded rate of bone accrual in these young animals as compared with controls. By 24 weeks of age, this low bone phenotype was no longer present, with AdipoR1$^{-/-}$ female mice showing no

significant bone phenotype as compared with AdipoR1$^{+/+}$ controls. Only trabecular spacing was significantly altered in the AdipoR1$^{-/-}$ animals at 52 weeks old, increasing significantly as compared with age-matched AdipoR1$^{+/+}$ controls (**Figure 4.3J**), suggesting a small bone loss phenotype may be present. Trabecular thickness remained unchanged in AdipoR1$^{-/-}$ female mice at all ages studied (**Figure 4.3L**).



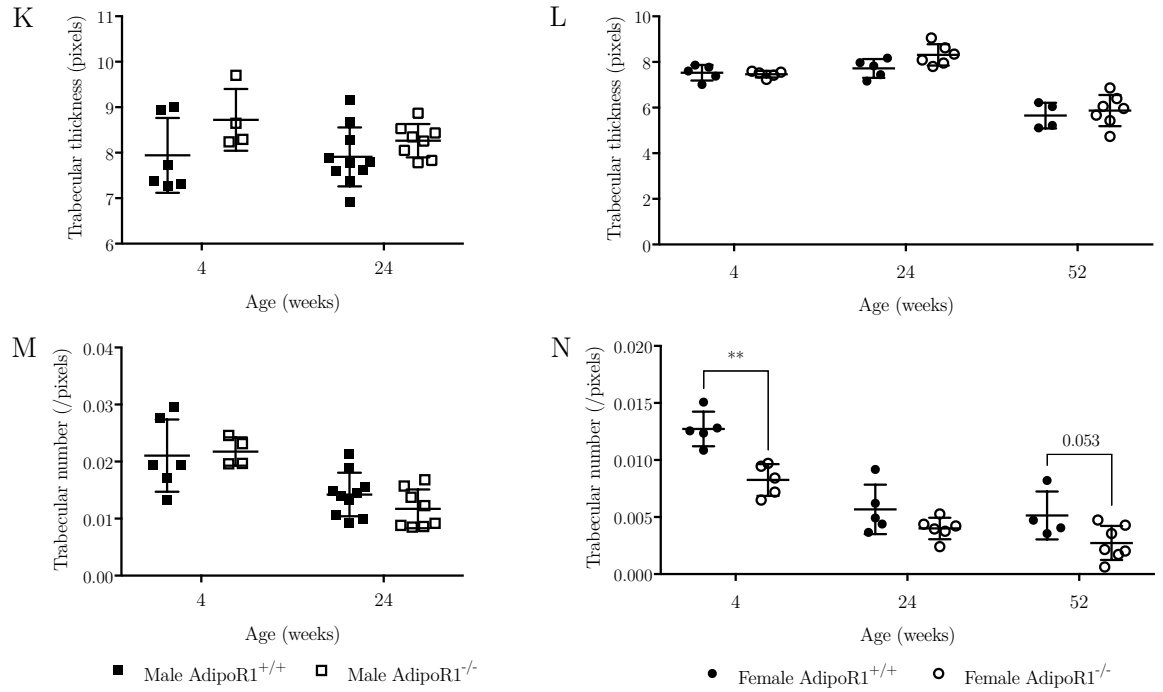


Figure 4.3: Female AdipoR1$^{-/-}$ mice show a reduced bone volume at four weeks old. (**A-F**) Representative reconstruction images of four-week-old female (**A-C**) AdipoR1$^{+/+}$ and (**D-F**) AdipoR1$^{-/-}$ mice (**A, D**) tibiae with (**B, E**) top-down and (**C, F**) side-on views of the trabecular area. (**G, I, K, M**) Male AdipoR1$^{-/-}$ mice show (**I**) significantly increased trabecular spacing at four and 24 weeks old as compared with age-matched AdipoR1$^{+/+}$ controls with no significant change in (**G**) BV/TV, (**K**) trabecular thickness or (**M**) trabecular number. (**H, J, L, N**) Female AdipoR1$^{-/-}$ mice at four weeks old show (**H**) reduced BV/TV, (**J**) increased trabecular spacing and (**N**) reduced trabecular number as compared with age-matched AdipoR1$^{+/+}$ controls, with (**J**) increased trabecular spacing present at 52 weeks old. (**L**) No significant changes in trabecular thickness of females were observed at any age studied. Data presented as mean±SD, N=4-10 (biological replicates). Unpaired t-test, **=p≤0.01; ***=p≤0.001.

4.2.2.1.2 Female AdipoR1$^{-/-}$ mice show reduced bone mineral density

While µCT analysis is primarily used to obtain data on bone structure, it can be used as an accurate measure of bone mineral density (BMD)[311]. The attenuation coefficient describes the attenuation of a single beam per given thickness of a material; if compared to a density control, it is possible to convert this coefficient to absolute mineral density. Here, the arbitrary value of mineral density is given due to lack of a suitable density control. Despite this, identical scanning parameters used during and between batches renders the relative values useable as relative estimates of mineral density.

Male AdipoR1$^{-/-}$ mice showed no change in their bone mineral density as compared with age-matched AdipoR1$^{+/+}$ controls (**Figure 4.4A**). In contrast, AdipoR1$^{-/-}$ female mice showed significantly reduced bone mineral density at four and 52 weeks of age as compared with age-matched AdipoR1$^{+/+}$ controls. 24-week-old female mice showed the highest bone mineral density of all the female mice but no significant genotype-related phenotype (**Figure 4.4B**).

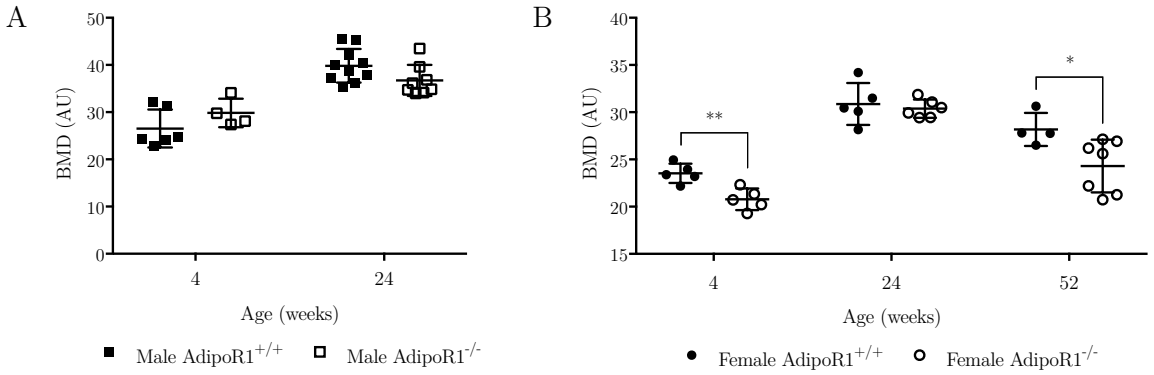


Figure 4.4: Female AdipoR1$^{-/-}$ mice show a reduced bone mineral density. µCT analysis provides relative mineral density measurements. (**A**) Male AdipoR1$^{-/-}$ mice show no changes in bone mineral density four or 24 weeks old. (**B**) Female AdipoR1$^{-/-}$ mice show significantly reduced bone mineral density as compared with age-matched AdipoR1$^{+/+}$ controls at both four and 52 weeks of age. Data presented as mean±SD, N=4-10 (biological replicates). Unpaired t-test, *=p≤0.05; **=p≤0.01.

4.2.2.1.3 AdipoR1$^{-/-}$ mice show no change in cortical thickness or tissue mineral density

Tissue mineral density (TMD) differs from BMD in that it is calculated from the average attenuation value of the bone tissue only rather than including attenuation from non-bone components like the bone marrow which is included in BMD analysis[311]. This is performed by analysis of the cortical ROI (**Figure 2.2**). In this way, TMD more accurately identifies changes in cortical density.

Analysis of cortical bone by µCT revealed no significant differences in the cortical thickness (**Figure 4.5C, D**) or TMD (**Figure 4.5E, F**) of four- or 24-week old male (**Figure 4.5C, E**) or four-, 24- or 52-week-old female AdipoR1$^{-/-}$ mice (**Figure 4.5D, F**) as compared with age- and sex-matched controls.

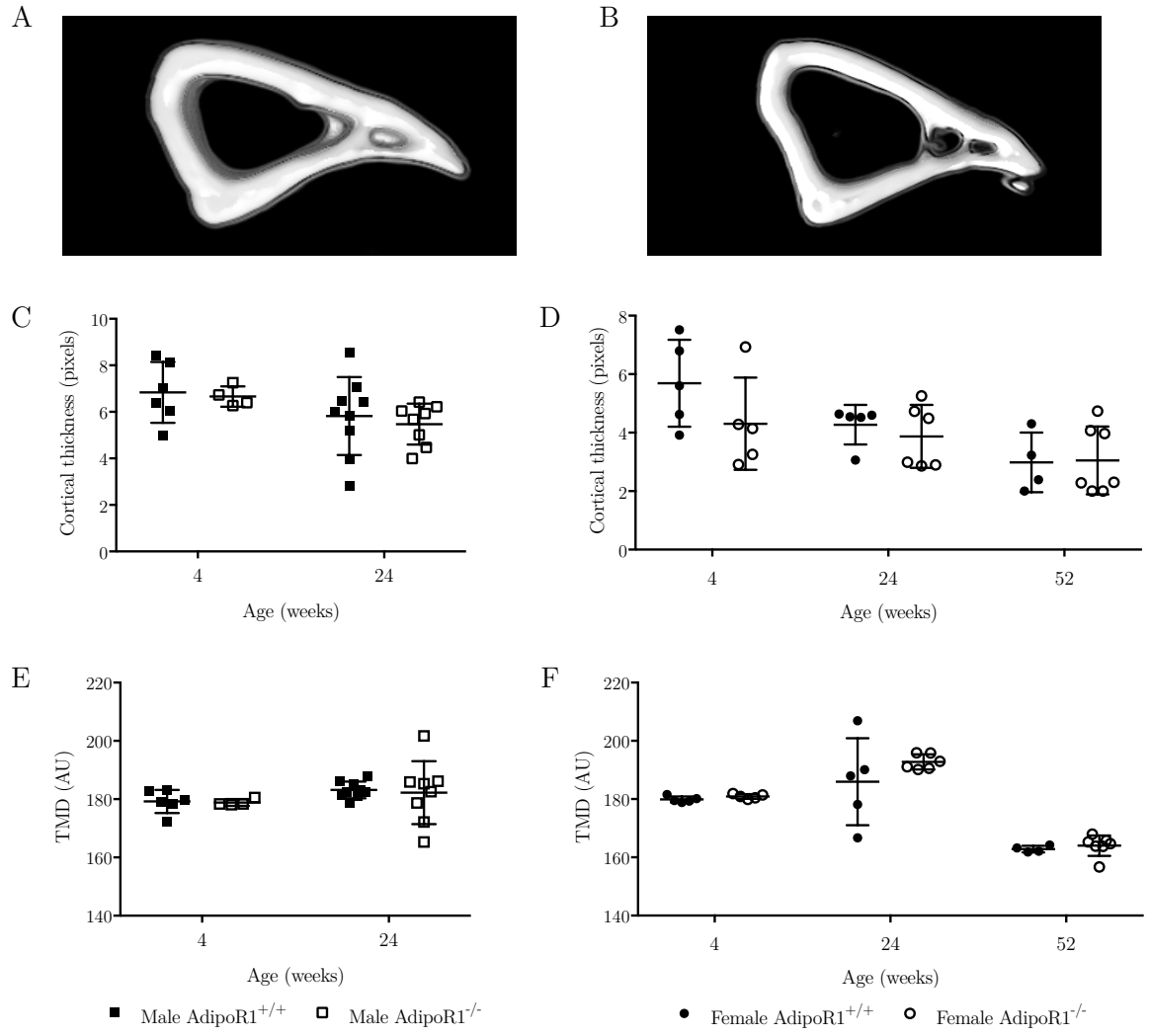
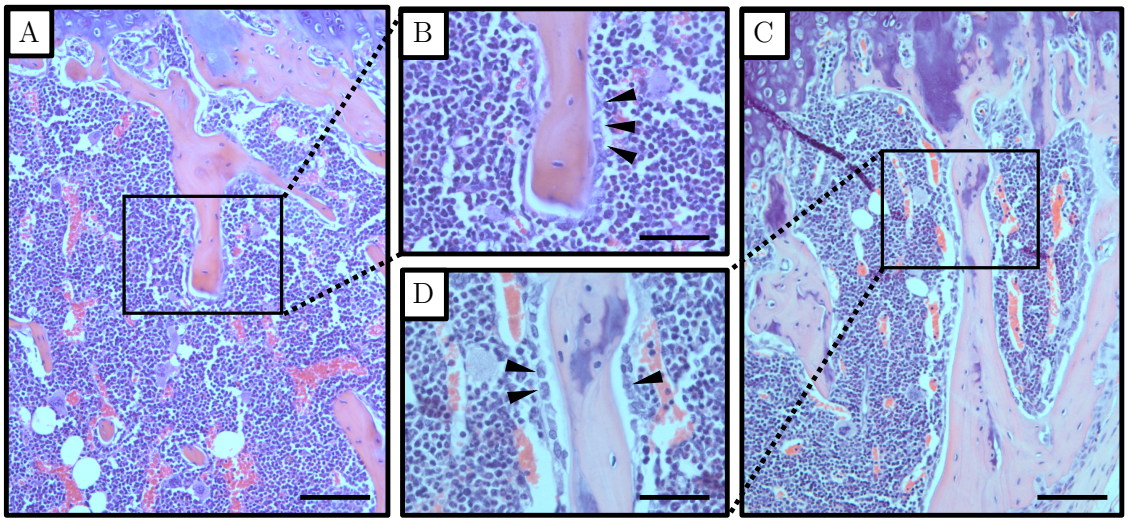


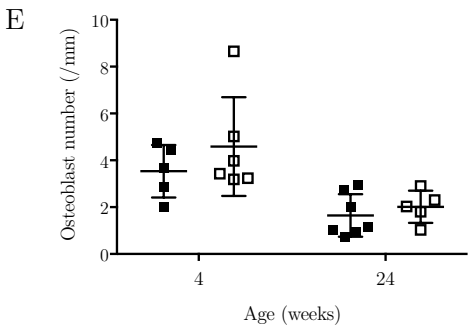
Figure 4.5: AdipoR1$^{-/-}$ mice show no changes in cortical thickness. Representative reconstruction images of four-week-old female (**A**) AdipoR1$^{+/+}$ and (**B**) AdipoR1$^{-/-}$ cortical tibial bone. (**C, E**) Male and (**D, F**) female AdipoR1$^{-/-}$ mice show no significant change in (**C, D**) cortical thickness or (**E, F**) tissue mineral density (TMD) as compared with age-matched AdipoR1$^{+/+}$ controls. Data presented as mean±SD, N=4-9 (biological replicates). Unpaired t-test, significance defined as $p \leq 0.05$.

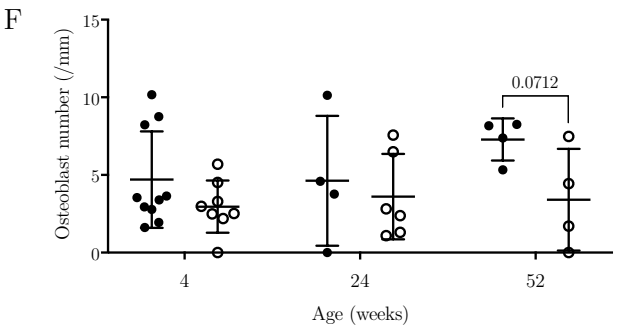
4.2.2.2 Cellular distribution of AdipoR1$^{-/-}$ mice by histology

4.2.2.2.1 AdipoR1$^{-/-}$ mice show no significant changes in osteoblast parameters

Osteoblasts are histologically identifiable on the bone surface in H&E-stained sections by their characteristic square or rectangular morphology coupled with their tendency to appear in groups or lines forming a multicellular unit working to form new bone (**Figure 4.6A-D**). Osteoblasts were counted per millimetre of trabecular bone, and average osteoblast surface was measured as a proportion of trabecular bone surface. The area analysed is shown in **Figure 2.3**. No significant changes in osteoblast number (**Figure 4.6E, F**) or proportion of bone surface coverage (**Figure 4.6G, H**) were observed in male (**Figure 4.6E, G**) or female (**Figure 4.6F, H**) AdipoR1$^{-/-}$ mice at any age studied.







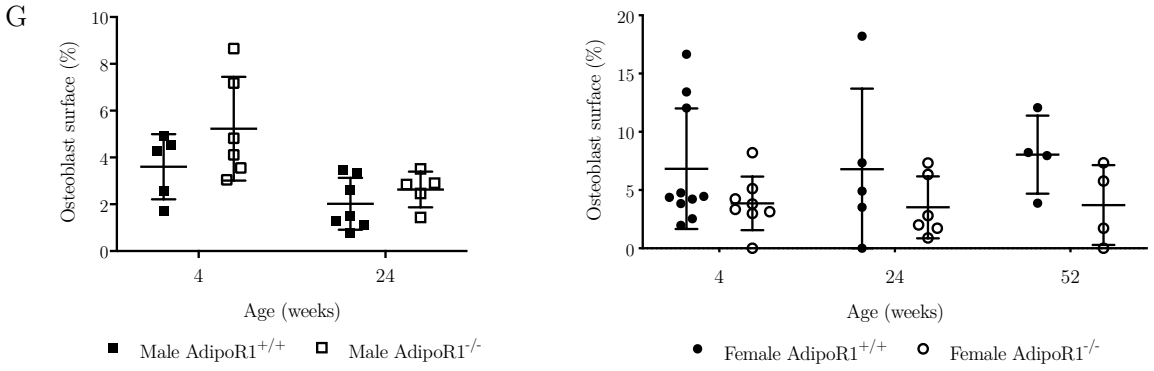


Figure 4.6: AdipoR1$^{-/-}$ mice show no significant differences in osteoblast parameters. (**A-D**) Representative H&E-stained sections of four-week-old female (**A, B**) AdipoR1$^{+/+}$ and (**C, D**) AdipoR1$^{-/-}$ mice with osteoblasts indicated by arrows. (**E, G**) four- and 24-week-old male AdipoR1$^{-/-}$ mice and (**F, H**) four-, 24- and 52-week-old females show no significant differences in osteoblast number or surface coverage as compared with age-matched AdipoR1$^{+/+}$ controls. Scale bar (**A, C**) 200µm, (**B, D**) 100µm. Data presented as mean±SD, N=4-10 (biological replicates). Unpaired t-test, significance defined as $p \leq 0.05$.

4.2.2.2.2 AdipoR1$^{-/-}$ mice show few significant changes in osteoclast parameters

Osteoclasts are histologically identifiable as large, multinucleated cells stained red in TRAP-stained sections and are often found by the growth plate in young mice in which the growth plate is still open (**Figure 4.7A-D**). Unlike osteoblasts, osteoclasts do not work in groups and are often well-dispersed throughout the bone. Osteoclasts were counted per millimetre of trabecular bone, and average osteoclast surface was measured as a proportion of trabecular bone surface. The area analysed is shown in **Figure 2.3**. Male AdipoR1$^{-/-}$ mice showed no significant change in osteoclast number as compared with age-matched AdipoR1$^{+/+}$ controls (**Figure 4.7E**), but a significant increase in osteoclast surface relative to total trabecular bone surface was observed in four-week-old AdipoR1$^{-/-}$ males as compared with age-matched AdipoR1$^{+/+}$ controls (**Figure 4.7G**). No significant changes in osteoclast number (**Figure 4.7F**) or proportion of bone surface coverage (**Figure 4.7H**) was observed female AdipoR1$^{-/-}$ mice at any age studied.

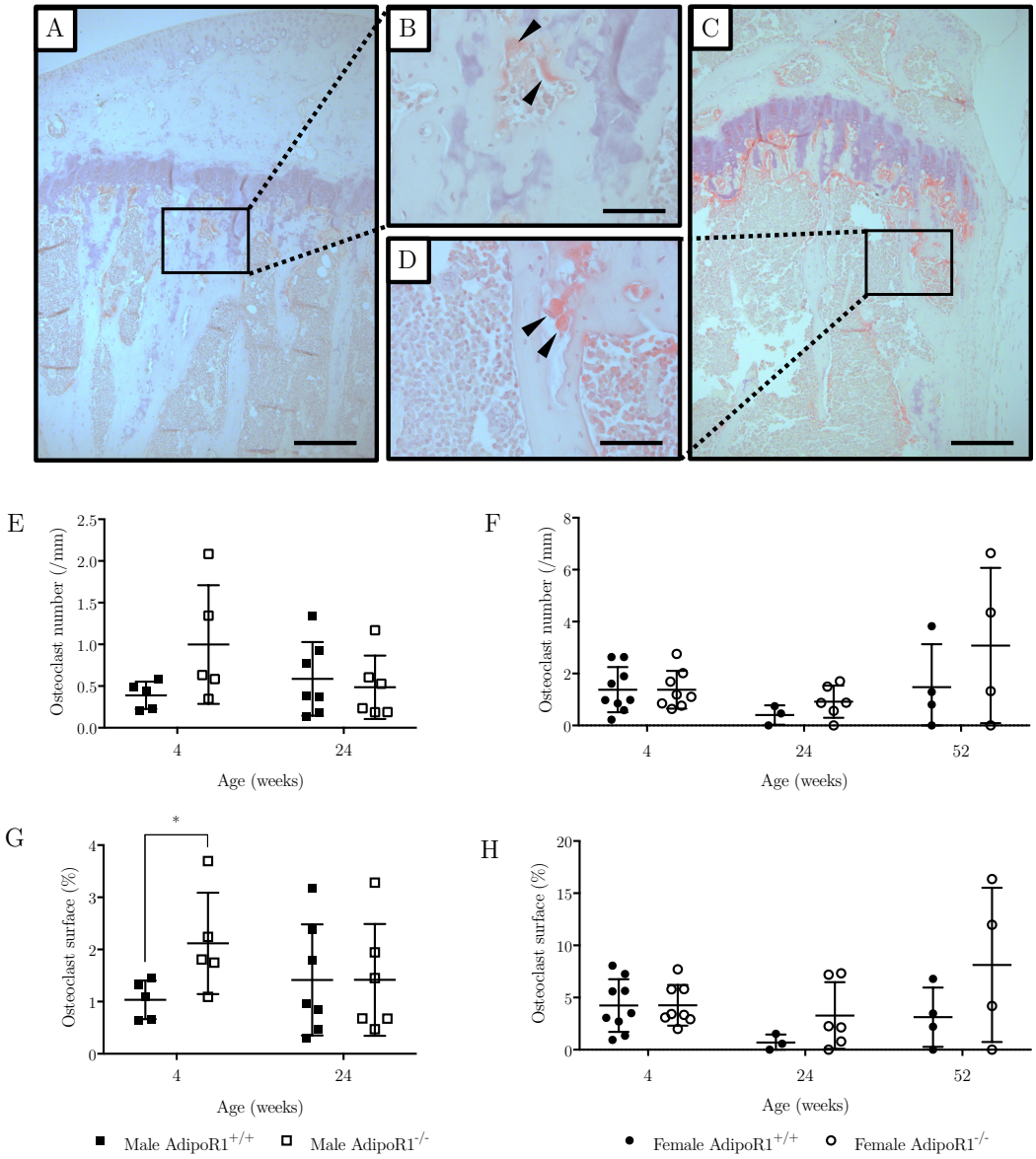
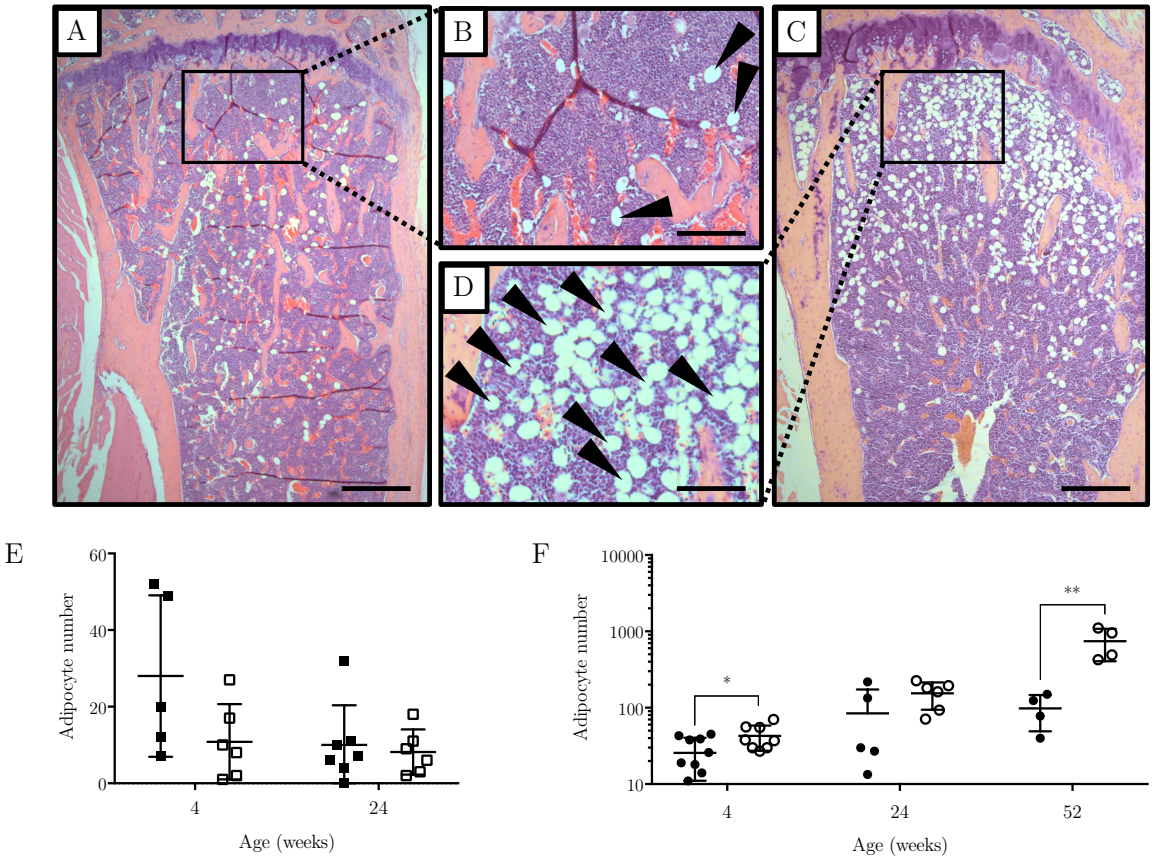


Figure 4.7: AdipoR1$^{-/-}$ mice show few significant differences in osteoclast parameters. (**A-D**) Representative H&E-stained sections of four-week-old female (**A, B**) AdipoR1$^{+/+}$ and (**C, D**) AdipoR1$^{-/-}$ mice with osteoclasts indicated by arrows. (**E, G**) Four-week-old male AdipoR1$^{-/-}$ mice show a significant increase in osteoclast surface relative to total trabecular bone surface as compared with age-matched AdipoR1$^{+/+}$ controls with no significant change in osteoclast number. (**F, H**) Four-, 24- and 52-week-old females show no significant differences in osteoclast number or surface coverage as compared with age-matched AdipoR1$^{+/+}$ controls. Scale bar (**A, C**) 200µm, (**B, D**) 100µm. Data presented as mean±SD, N=3-9 (biological replicates). Unpaired t-test, *=p≤0.05.

4.2.2.2.3 Female AdipoR1$^{-/-}$ mice show increased bone marrow adiposity

Adipocytes within the bone marrow are active producers of many cell signalling molecules, including adiponectin. Histologically, they present as empty spaces or 'ghosts' due to defatting during tissue processing and are easily distinguishable from surrounding cells in H&E-stained sections (**Figure 4.8A-D**). Adipocytes were counted and average perimeter calculated as a measure of average adipocyte size. The area analysed is shown in **Figure 2.3**. Male AdipoR1$^{-/-}$ mice showed no significant differences in bone marrow adiposity as compared with age-matched AdipoR1$^{+/+}$ controls (**Figure 4.8E, G**). Female AdipoR1$^{-/-}$ mice showed an age-associated increase in adiposity and significantly increased adipocyte number (**Figure 4.8F**) and size (**Figure 4.8H**) at four- and 52-weeks-old as compared with age-matched AdipoR1$^{+/+}$ controls but no significant adiposity phenotype at 24 weeks old.



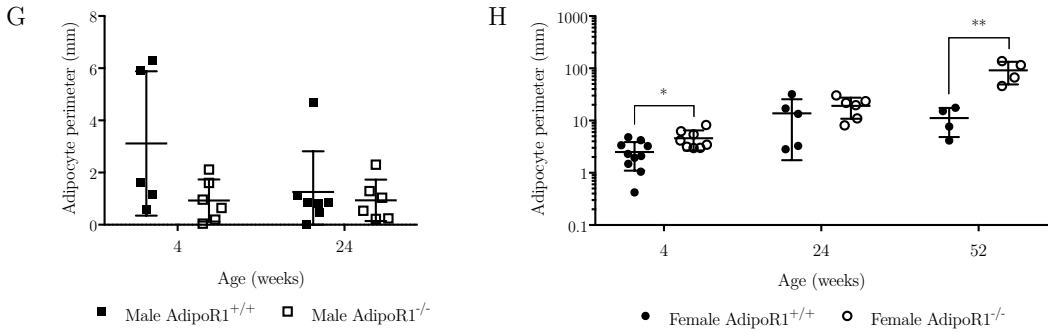


Figure 4.8: Female AdipoR1$^{-/-}$ mice show significantly increased bone marrow adiposity. (**A-D**) Representative H&E-stained sections of four-week-old female (**A, B**) AdipoR1$^{+/+}$ and (**C, D**) AdipoR1$^{-/-}$ mice with adipocytes indicated by arrows. (**E, G**) Male AdipoR1$^{-/-}$ mice show no significant differences in bone marrow adipocyte number or size at four weeks or 24 weeks as compared with age-matched AdipoR1$^{+/+}$ controls. (**F, H**) Female AdipoR1$^{-/-}$ mice have significantly increased bone marrow adiposity with increased adipocyte number and average size as compared with age-matched AdipoR1$^{+/+}$ controls at age four weeks and 52 weeks but show no significant phenotype at 24 weeks. Scale bar (**A, C**) 200µm, (**B, D**) 100µm. Data presented as mean±SD, N=4-10 (biological replicates). Unpaired t-test, *=p≤0.05; **=p≤0.01.

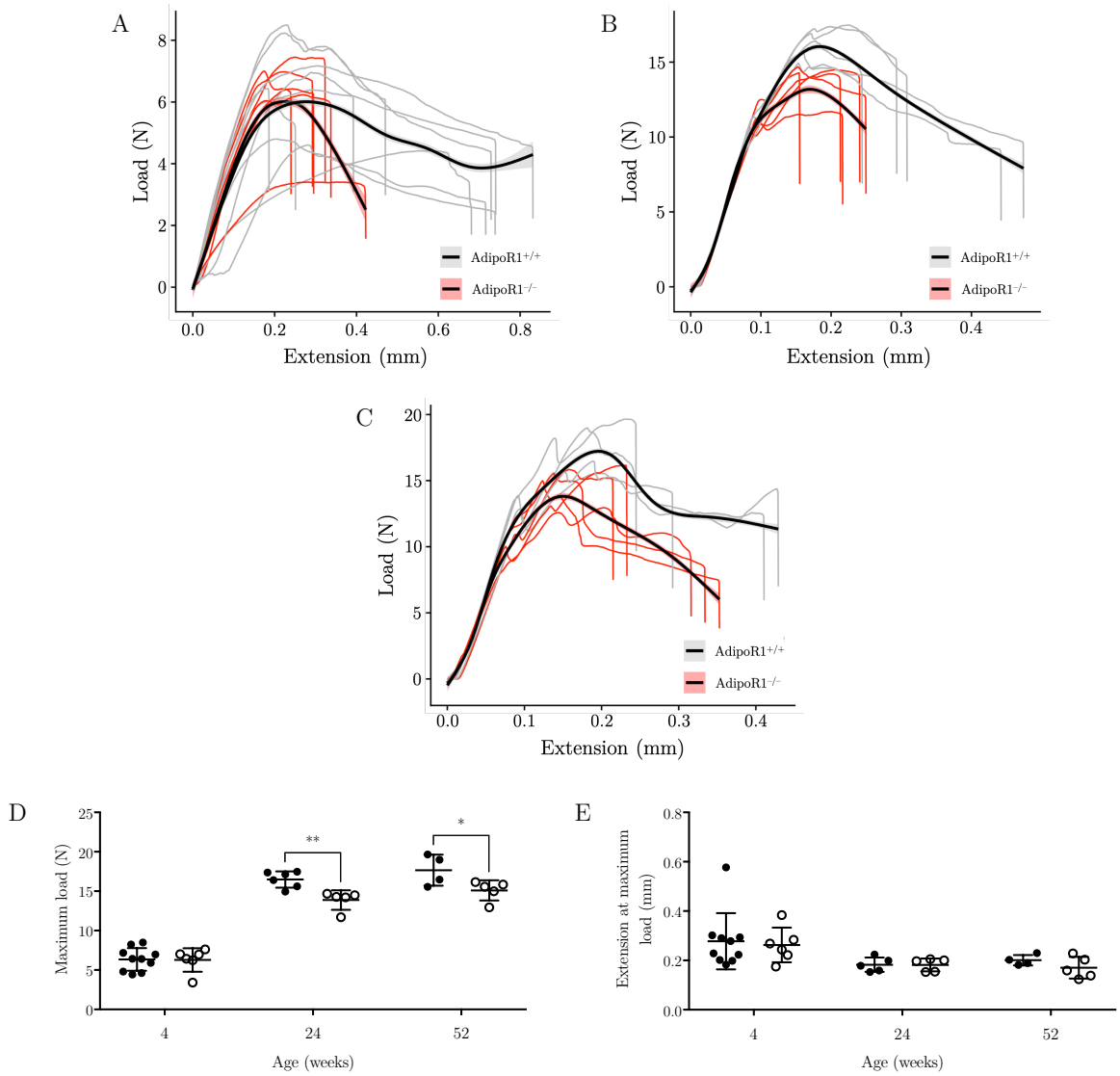
4.2.2.3 AdipoR1$^{-/-}$ is associated with significant changes in the biomechanical properties of female mice

Three-point bend testing is used to assess the biomechanical properties of bones by recording their deformation and ultimate fracture under a force applied vertically to the middle of a long bone cleaned of all supportive soft tissue.

Humeri from AdipoR1$^{+/+}$ and AdipoR1$^{-/-}$ female mice were tested by a three-point bend test at four, 24 and 52 weeks of age. Load-displacement curves were produced during testing displaying individual and average (bolded line) response of four-week-old (**Figure 4.9A**), 24-week-old (**Figure 4.9B**) and 52-week old (**Figure 4.9C**) AdipoR1$^{+/+}$ (grey) and AdipoR1$^{-/-}$ (red) humeri to an applied pressure by plotting load against bone extension.

Adult AdipoR1$^{-/-}$ mice aged 24- and 52-weeks old showed significantly reduced maximum load to breakage (**Figure 4.9D**) but with no significant change at any age in extension at this maximum load (**Figure 4.9E**). Load at break of AdipoR1$^{-/-}$ mice was non-

significantly changed for all ages tested (**Figure 4.9F**) but extension at break was significantly reduced in AdipoR1$^{-/-}$ animals at four- and 24-weeks-old (**Figure 4.9G**). Energy at break was significantly reduced in AdipoR1$^{-/-}$ animals for all ages tested (**Figure 4.9H**). No significant changes in the elastic modulus was observed at any age tested (**Figure 4.9I**).



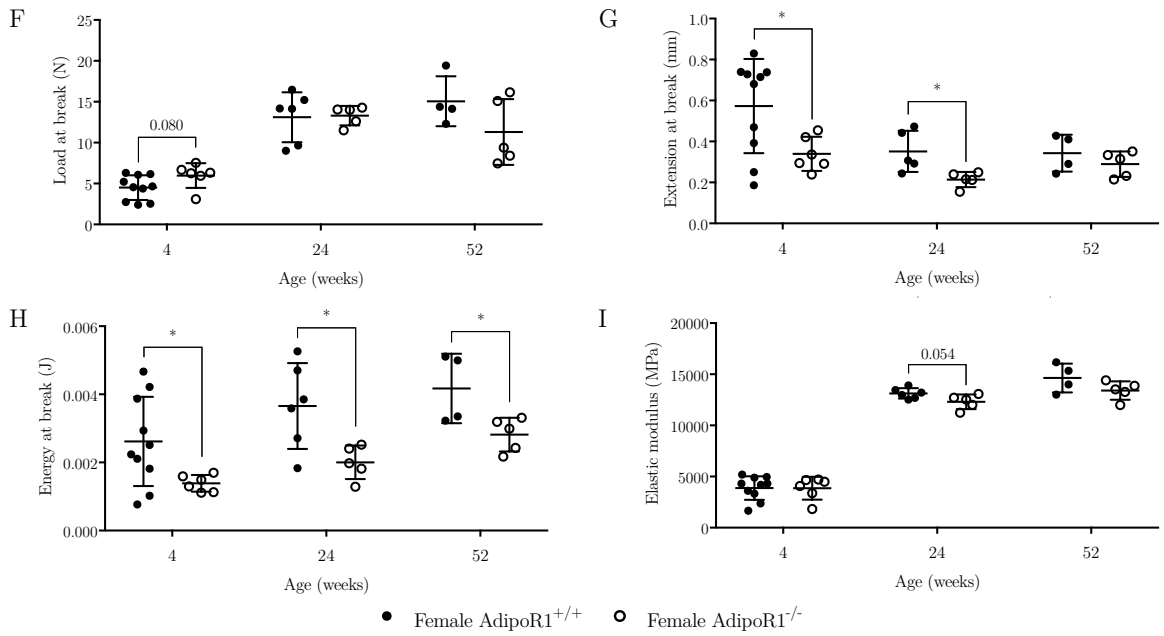


Figure 4.9: Female AdipoR1$^{-/-}$ mice show significant changes in bone biomechanical properties. (**A-C**) Load displacement curves of individual and averaged (bolded with SEM) of (**A**) four-week-old, (**B**) 24-week-old and (**C**) 52-week-old female AdipoR1$^{+/+}$ (grey) and AdipoR1$^{-/-}$ (red) humeri during three-point bend testing. (**D**) Maximum load to breakage was significantly reduced in adult AdipoR1$^{-/-}$ mice as compared with age-matched AdipoR1$^{+/+}$ controls although (**E**) extension at maximum load was not significantly altered at any age. (**F**) No significant change in load at break was observed in any age group studied but (**G**) extension at break was significantly reduced in four- and 24-week-old mice as compared with age-matched AdipoR1$^{+/+}$ controls. (**H**) Energy at break was significantly reduced in AdipoR1$^{-/-}$ mice of all ages as compared with age-matched AdipoR1$^{+/+}$ controls. (**I**) No significant difference in AdipoR1$^{-/-}$ bone elasticity was observed in any age group. Data presented as mean±SD, N=4-10 (biological replicates). Unpaired t-test, *=p≤0.05, **=p≤0.01.

4.2.3 Gross morphology of AdipoR2$^{-/-}$ mice

4.2.3.1 Female AdipoR2$^{-/-}$ mice show a reduced body weight

Whole-body morphology assessment of AdipoR2$^{-/-}$ mice revealed no gross abnormalities such as failure to thrive and AdipoR2$^{-/-}$ mice were behaviourally indistinguishable from AdipoR2$^{+/+}$ littermates. No significant changes in body weight were observed in male AdipoR2$^{-/-}$ mice at 24 weeks old (**Figure 4.10A**), but female AdipoR2$^{-/-}$ mice showed a significantly reduced body weight as compared with age-matched female AdipoR2$^{+/+}$ mice at both 24- and 52-weeks-old (**Figure 4.10B**).

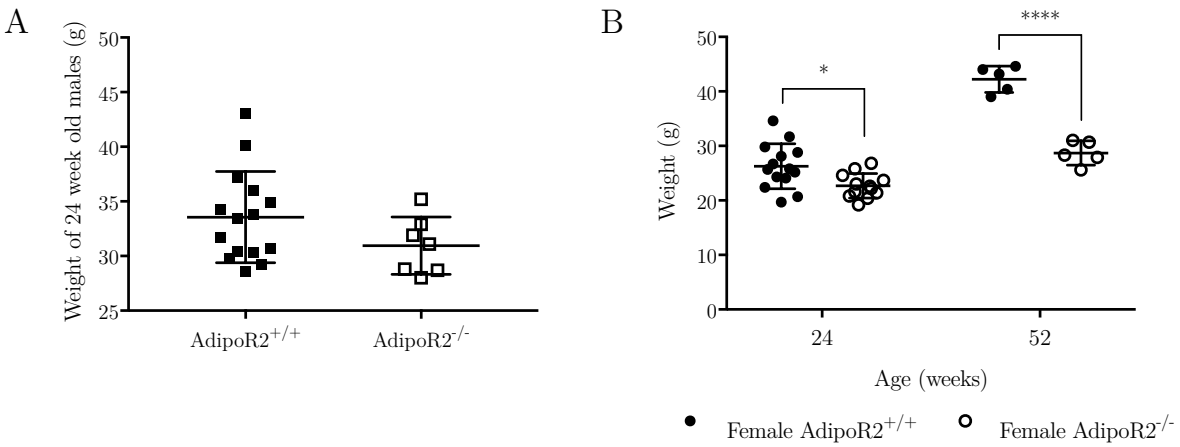


Figure 4.10: Adult female AdipoR2$^{-/-}$ mice show significantly reduced body weight. (**A**) 24-week-old AdipoR2$^{+/+}$ male show no change in body weight as compared with age-matched AdipoR2$^{+/+}$ controls. (**B**) 24- and 52-week-old female AdipoR2$^{-/-}$ mice show a significantly reduced body weight as compared with age-matched AdipoR2$^{+/+}$ controls. Data presented as mean±SD, N=5-15 (biological replicates). Unpaired t-test, *=p≤0.05, ****=p≤0.0001.

4.2.3.2 Aged female AdipoR2$^{-/-}$ mice show a reduced tibial length

Male AdipoR2$^{-/-}$ mice showed no significant change in tibial length as compared with age-matched AdipoR2$^{+/+}$ males at four or 24 weeks old (**Figure 4.11A**). Female AdipoR2$^{-/-}$ mice showed significantly reduced tibial length at 52 weeks of age, with no significant difference observed at younger ages (**Figure 4.11B**).

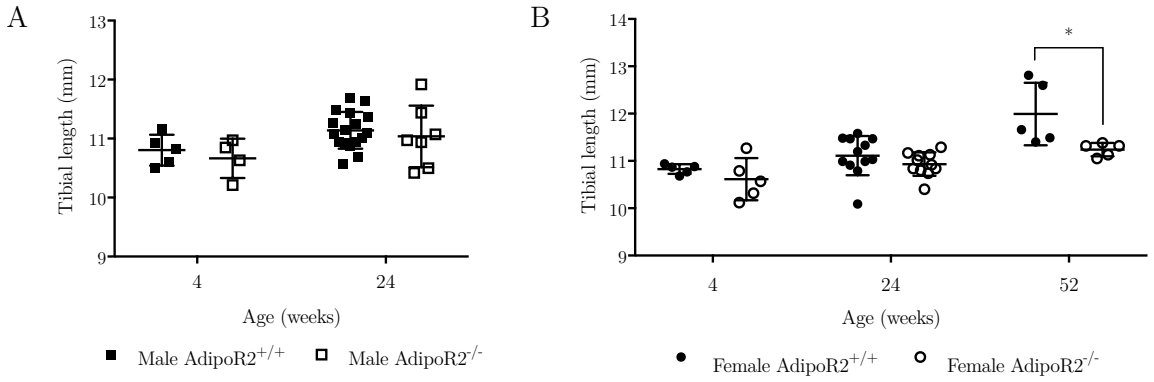


Figure 4.11: Female AdipoR2$^{-/-}$ mice show a reduced long bone length at 52-weeks-old. (**A**) Male AdipoR2$^{-/-}$ mice no significant difference in tibial length at four- or 24-weeks-old as compared with age-matched AdipoR2$^{+/+}$ controls. (**B**) 52-week-old female AdipoR2$^{-/-}$ mice show a significantly reduced tibial length as compared with age-matched AdipoR2$^{+/+}$ controls with no significant difference in tibial length at four weeks old or 24 weeks old. Data presented as mean±SD, N=5-15 (biological replicates). Unpaired t-test, *=p≤0.05.

4.2.4 Bone phenotyping of AdipoR2$^{-/-}$ mice

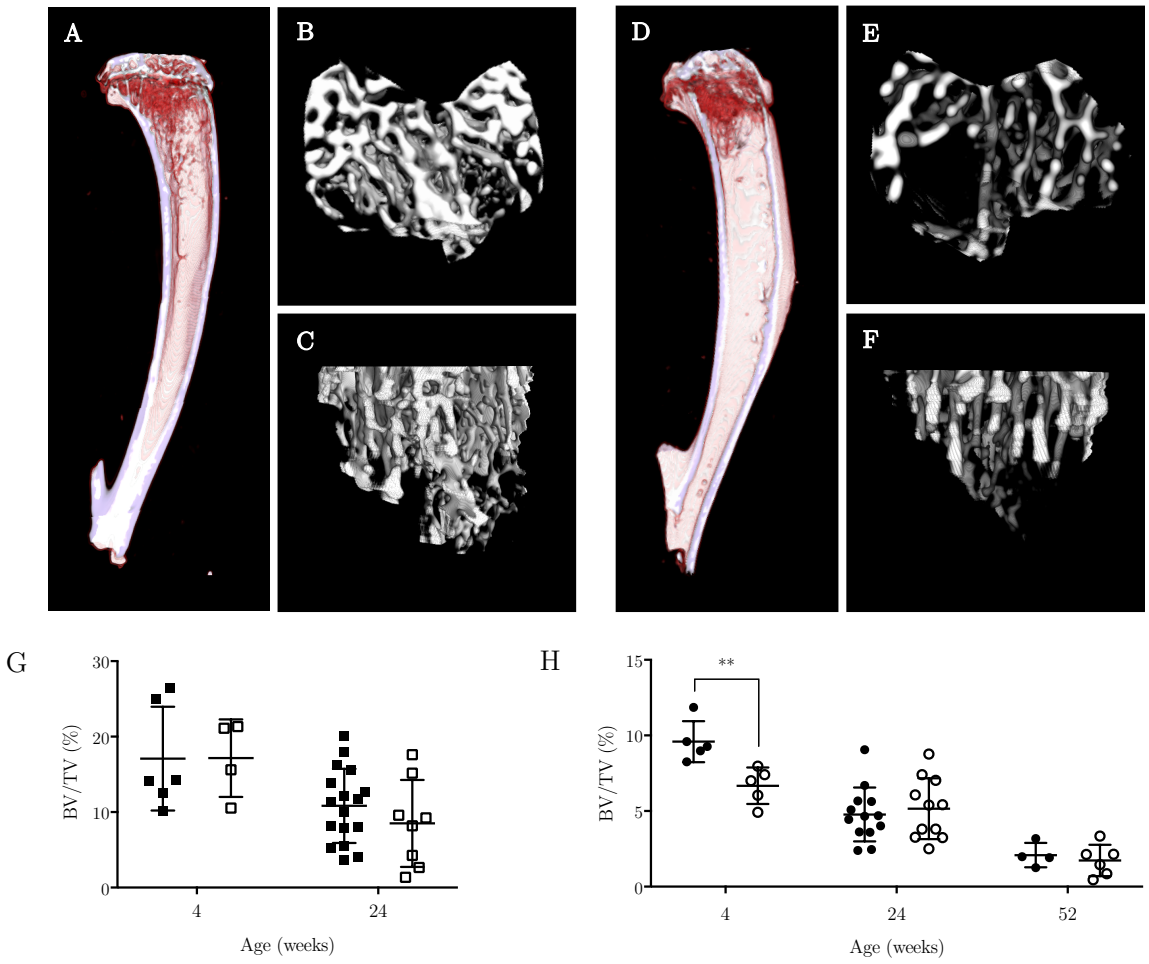
4.2.4.1 Bone microarchitecture by µCT of AdipoR2$^{-/-}$ mice

4.2.4.1.1 Young female AdipoR2$^{-/-}$ mice show reduced bone volume and altered trabecular parameters

Analysis of trabecular and cortical areas (as shown in **Figure 2.2**) of control and AdipoR2$^{-/-}$ mice was performed by µCT using the same parameters each time as described in **Section 2.1.4**

Analysis of the trabecular areas of AdipoR2$^{+/+}$ (**Figure 4.12A-C**) and AdipoR2$^{-/-}$ (**Figure 4.12D-F**) was performed in male mice at four and 24 weeks of age (**Figure 4.12G, I, K and M**) and in female mice at four, 24 and 52 weeks of age (**Figure 4.12H, J, L and N**). No significant changes in BV/TV (**Figure 4.12G**), trabecular spacing (**Figure 4.12I**), trabecular thickness (**Figure 4.12K**) or trabecular number (**Figure 4.12K**) were observed in male AdipoR2$^{-/-}$ mice as compared with age- and sex-matched AdipoR2$^{+/+}$ controls.

At four weeks old, female AdipoR2$^{-/-}$ mice consistently showed a low bone phenotype as compared with age-matched AdipoR2$^{+/+}$ controls: BV/TV (**Figure 4.12G**) and trabecular number (**Figure 4.12N**) were both significantly reduced with trabecular spacing (**Figure 4.12J**) increased. No significant change in trabecular thickness **(Figure 4.12L**) was observed in female AdipoR2$^{-/-}$ animals. These data are suggestive of a retarded rate of bone accrual in these young animals as compared with controls. In contrast, AdipoR2$^{-/-}$ mice present with no significant changes in trabecular parameters as compared with AdipoR2$^{+/+}$ controls by 24 and 52 weeks of age, suggesting no bone loss phenotype is present.



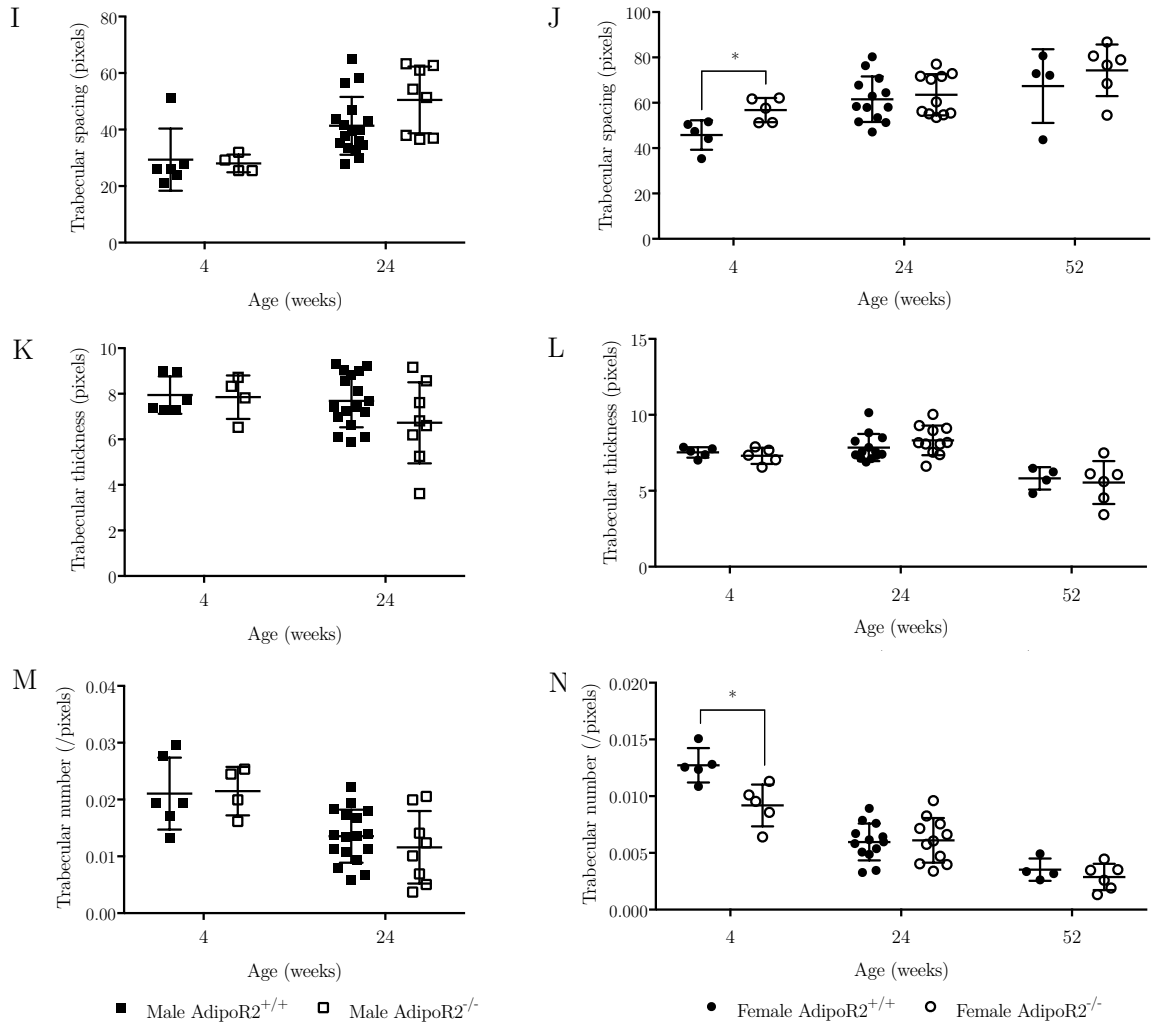


Figure 4.12: Female AdipoR2$^{-/-}$ mice show a reduced bone volume at four weeks old. (**A-F**) Representative reconstruction images of four-week-old female (**A-C**) AdipoR2$^{+/+}$ and (**D-F**) AdipoR2$^{-/-}$ mice (**A, D**) tibiae with (**B, E**) top-down and (**C, F**) side-on views of the trabecular area. (**G, I, K, M**) Male AdipoR2$^{-/-}$ mice show no significant changes in (**G**) BV/TV, (**I**) trabecular spacing, (**K**) trabecular thickness or (**M**) trabecular number at four or 24 weeks old as compared with age-matched AdipoR2$^{+/+}$ controls. (**H, J, L, N**) Female AdipoR2$^{-/-}$ mice at four weeks old only show (**H**) reduced BV/TV, (**J**) increased trabecular spacing and (**N**) reduced trabecular number as compared with age-matched AdipoR2$^{+/+}$ controls, with (**K**) no changes in trabecular thickness were observed at any age. Data presented as mean±SD, N=4-17 (biological replicates). Unpaired t-test, *=p≤0.05; **=p≤0.01.

4.2.4.1.2 Young female AdipoR2$^{-/-}$ mice show reduced bone mineral density

Male AdipoR2$^{-/-}$ mice showed no change in their BMD as compared with age- and sex-matched AdipoR2$^{+/+}$ controls (**Figure 4.13A**). In contrast, AdipoR2$^{-/-}$ female mice showed significantly reduced bone mineral density at four weeks of age as compared with age- and sex-matched AdipoR2$^{+/+}$ controls. Female 24- and 52-week-old AdipoR2$^{-/-}$ mice showed no significant BMD alteration as compared with AdipoR2$^{+/+}$ controls (**Figure 4.13B**).

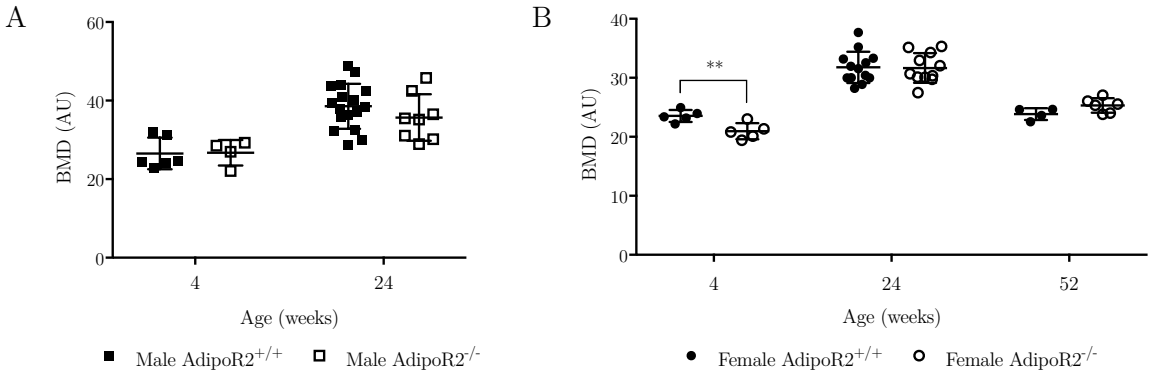


Figure 4.13: Young female AdipoR2$^{-/-}$ mice show a reduced bone mineral density. µCT analysis provides relative bone mineral density (BMD) measurements. (**A**) Male AdipoR2$^{-/-}$ mice show no changes in BMD at four or 24 weeks old as compared with AdipoR2$^{+/+}$ controls. (**B**) Female AdipoR2$^{-/-}$ mice show significantly reduced BMD as compared with age-matched AdipoR2$^{+/+}$ controls at four weeks of age only. Data presented as mean±SD, N=4-17 (biological replicates). Unpaired t-test, **=p≤0.01.

4.2.4.1.3 AdipoR2$^{-/-}$ mice show no change in cortical thickness or tissue mineral density

The cortical area analysed is shown in **Figure 2.2**. µCT analysis revealed no significant differences in the cortical thickness (**Figure 4.14C, D**) or tissue mineral density (TMD, **Figure 4.14E, F**) of four- or 24-week old male (**Figure 4.14C, E**) or four-, 24- or 52-week-old female AdipoR2$^{-/-}$ mice (**Figure 4.14D, F**) as compared with age- and sex-matched controls.

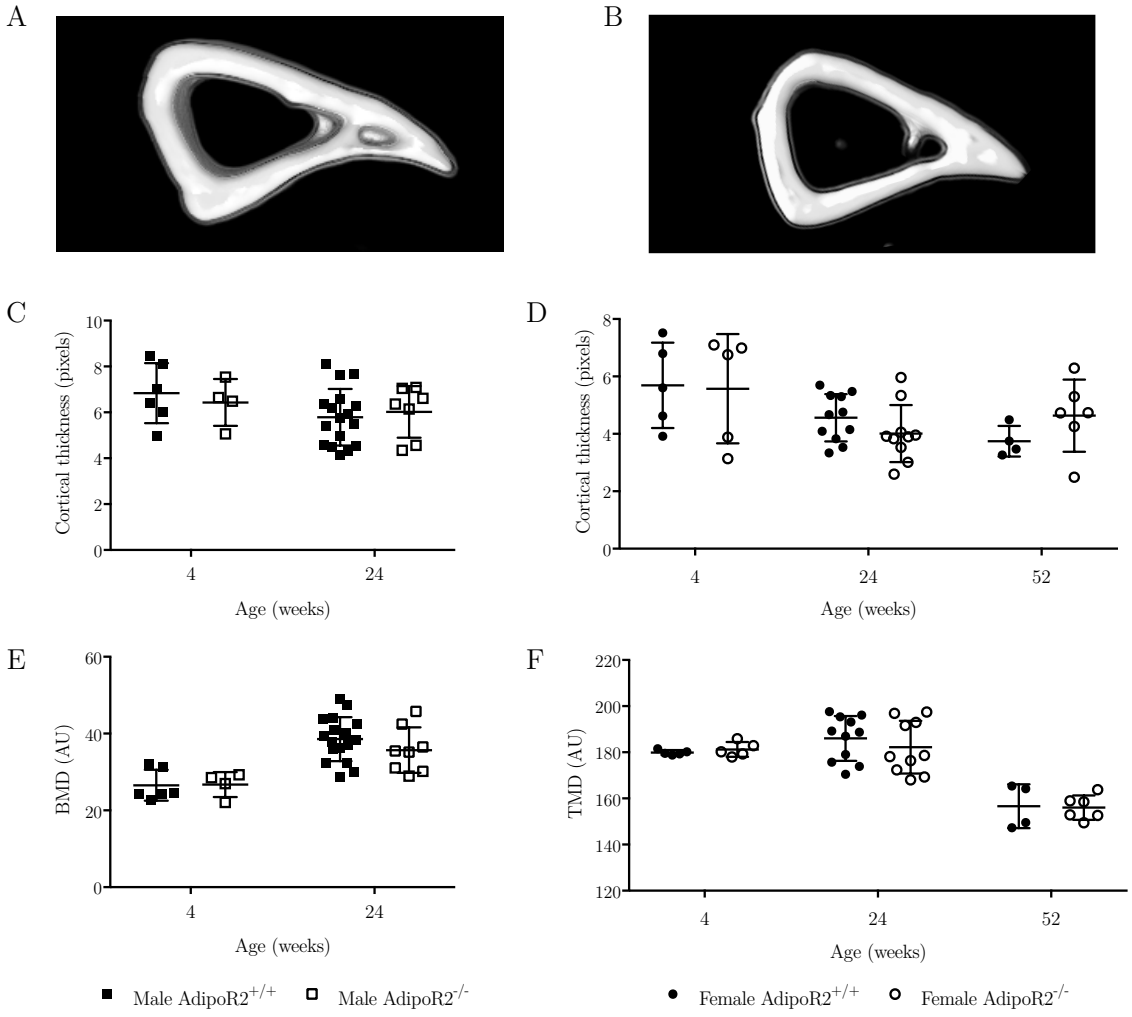
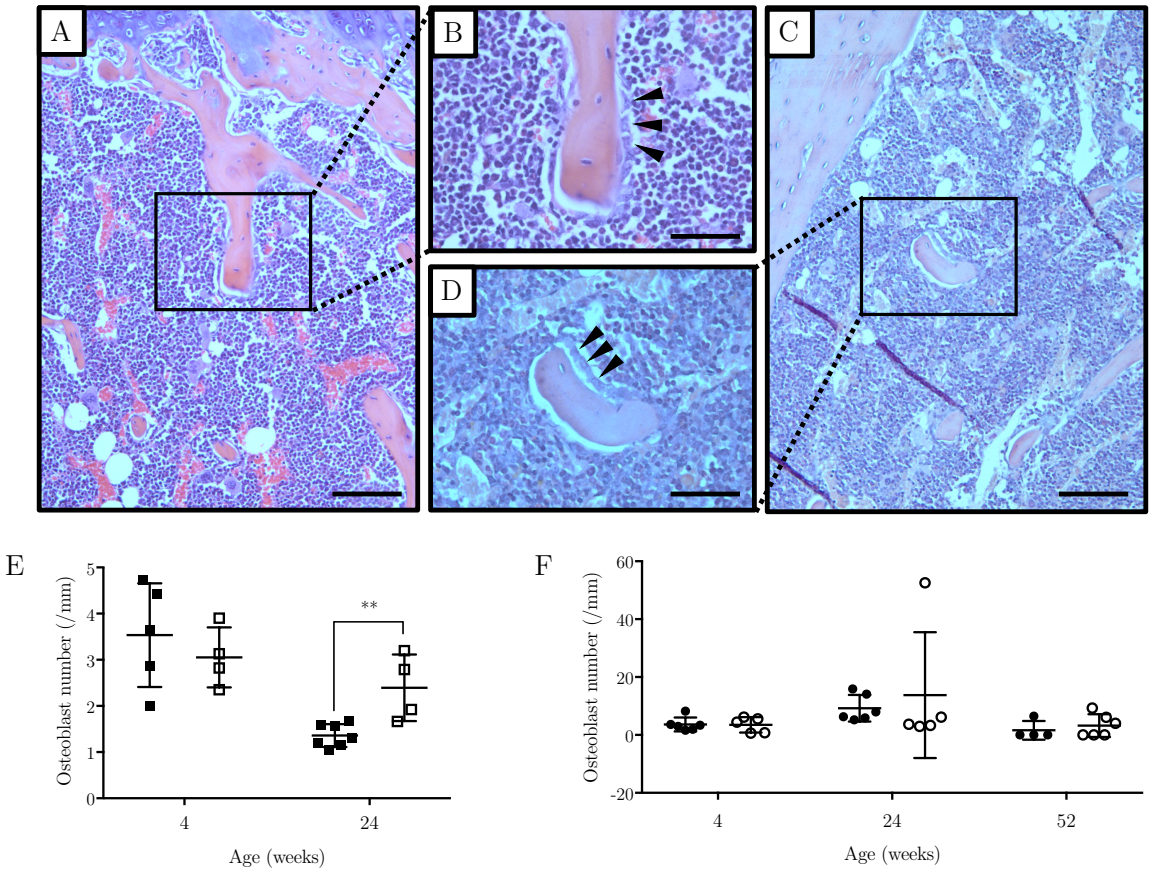


Figure 4.14: AdipoR2$^{-/-}$ mice show no changes in cortical thickness. Representative reconstruction images of four-week-old female (**A**) AdipoR2$^{+/+}$ and (**B**) AdipoR2$^{-/-}$ cortical tibial bone. (**C, E**) Male and (**D, F**) female AdipoR2$^{-/-}$ mice show no significant change in (**C**, **D**) cortical thickness or (**E**, **F**) tissue mineral density (TMD) as compared with age-matched AdipoR2$^{+/+}$ controls. Data presented as mean±SD, N=4-17 (biological replicates). Unpaired t-test, significance defined as $p \leq 0.05$.

4.2.4.2 Cellular distribution of AdipoR2$^{-/-}$ mice by histology

4.2.4.2.1 Male AdipoR2$^{-/-}$ mice show significant increases in osteoblast number and surface coverage

Osteoblast number per millimetre of trabecular bone and their average coverage of the trabecular bone surface was analysed in the area below the growth plate as shown in **Figure 2.3** in control (**Figure 4.15A, B**) and AdipoR2$^{-/-}$ (**Figure 4.15C, D**) mice. Male AdipoR2$^{-/-}$ animals showed a significant increase in osteoblast number (**Figure 4.15E**) and size (**Figure 4.15G**) at 24 weeks old only as compared with age- and sex-matched AdipoR2$^{+/+}$ controls. No significant changes were observed in osteoblast number (**Figure 4.15F**) or proportion of bone surface coverage (**Figure 4.15H**) in female AdipoR2$^{-/-}$ mice at any age studied as compared with age- and sex-matched AdipoR2$^{+/+}$ controls.



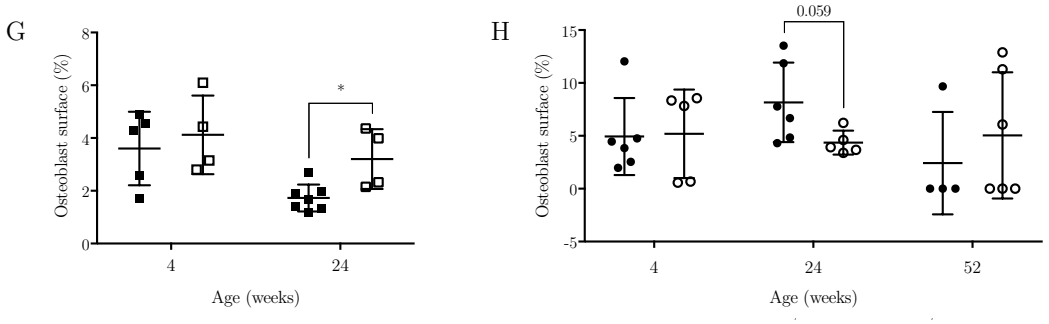


Figure 4.15: Male AdipoR2$^{-/-}$ mice show significant increase in osteoblast number and surface coverage. (**A-D**) Representative H&E-stained sections of four-week-old female (**A, B**) AdipoR2$^{+/+}$ and (**C, D**) AdipoR2$^{-/-}$ mice with osteoblasts indicated by arrows. (**E, G**) 24-week-old male AdipoR2$^{-/-}$ mice only show significant increases in osteoblast number and surface coverage as compared with age-matched AdipoR2$^{+/+}$ controls. (**F, H**) four-, 24- and 52-week-old female AdipoR2$^{-/-}$ mice show no significant differences in osteoblast number or surface coverage as compared with age-matched AdipoR2$^{+/+}$ controls. Scale bar (**A, C**) 200µm, (**B, D**) 100µm. Data presented as mean±SD, N=4-7 (biological replicates). Unpaired t-test, *=p≤0.05, **=p≤0.01.

4.2.4.2.2 Male AdipoR2$^{-/-}$ mice show significant increases in osteoclast number and surface coverage

Osteoclast number per millimetre of trabecular bone and their average relative coverage of the trabecular bone surface was analysed in the area below the growth plate as shown in **Figure 2.3**. Male AdipoR2$^{-/-}$ mice showed a significant increase in osteoclast number (**Figure 4.16E**) and proportion of bone surface coverage (**Figure 4.16G**) at 24 weeks old only as compared with age- and sex-matched AdipoR2$^{+/+}$ controls. No significant changes in osteoblast number (**Figure 4.16F**) or bone coverage (**Figure 4.16H**) were observed in female AdipoR2$^{-/-}$ mice at any age studied as compared with age- and sex-matched AdipoR2$^{+/+}$ controls.

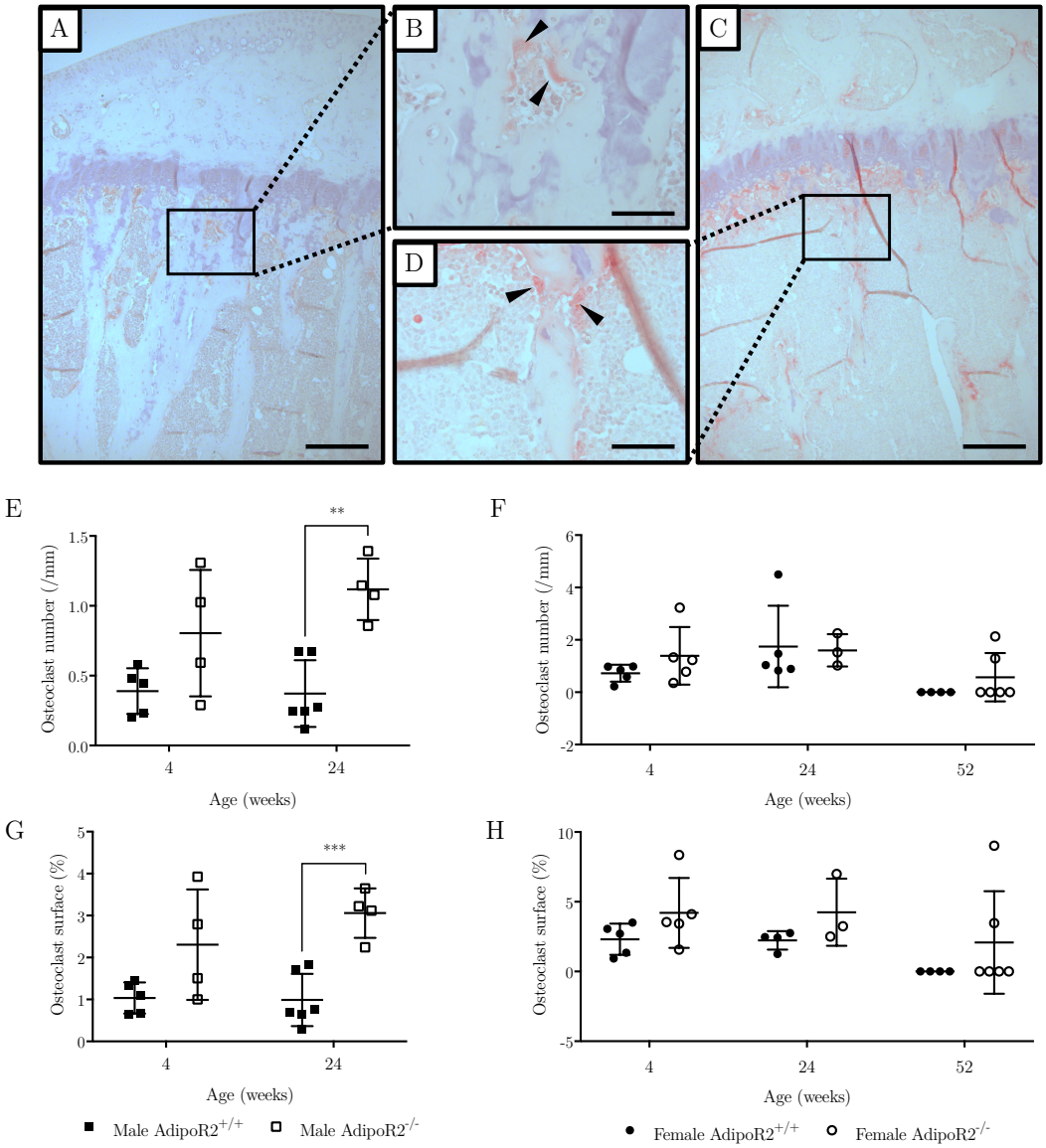
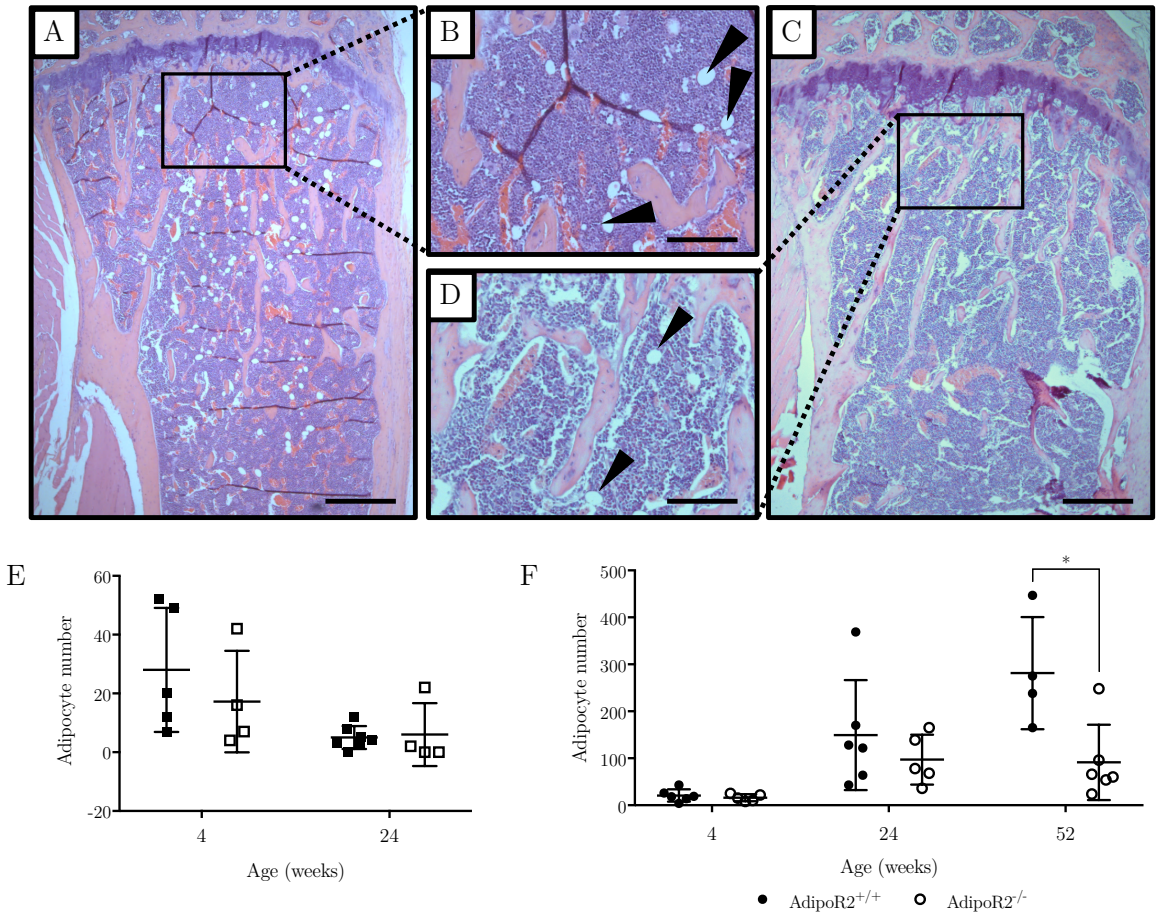


Figure 4.16: Male AdipoR2$^{-/-}$ mice show significant increase in osteoclast number and surface coverage. (**A-D**) Representative TRAP-stained sections of four-week-old female (**A, B**) AdipoR2$^{+/+}$ and (**C, D**) AdipoR2$^{-/-}$ mice with osteoclasts indicated by arrows. (**E, G**) Only 24-week-old male AdipoR2$^{-/-}$ mice show significant increases in osteoclast number and surface coverage as compared with age-matched AdipoR2$^{+/+}$ controls. (**F, H**) Four-, 24- and 52-week-old female AdipoR2$^{-/-}$ mice show no significant differences in osteoclast number or surface coverage as compared with age-matched AdipoR2$^{+/+}$ controls. Scale bar (**A, C**) 200µm, (**B, D**) 100µm. Data presented as mean±SD, N=3-6 (biological replicates). Unpaired t-test, **=p≤0.01, ***=p≤0.001.

4.2.4.2.3 Aged female AdipoR2$^{-/-}$ mice show reduced bone marrow adiposity

Adipocyte number and average perimeter as a measure of average adipocyte size was determined in the area shown in **Figure 2.3** in control (**Figure 4.17A, B**) and AdipoR2$^{-/-}$ (**Figure 4.17C, D**) mice. Male AdipoR2$^{-/-}$ mice showed no significant differences in bone marrow adiposity as compared with age-matched AdipoR2$^{+/+}$ controls (**Figure 4.17E, G**). Female AdipoR2$^{-/-}$ mice showed an age-associated decrease in adiposity and significantly reduced adipocyte number (**Figure 4.17F**) and size (**Figure 4.17H**) at 52-weeks-old as compared with age-matched AdipoR2$^{+/+}$ controls but no significant adiposity phenotype was found at four or 24 weeks old.



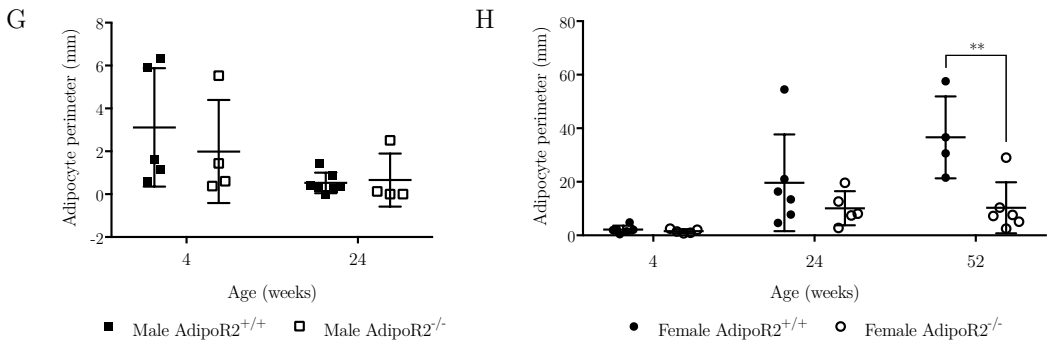


Figure 4.17: Aged female AdipoR2$^{-/-}$ mice show significantly reduced bone marrow adiposity. (**A-D**) Representative H&E-stained sections of four-week-old female (**A, B**) AdipoR2$^{+/+}$ and (**C, D**) AdipoR2$^{-/-}$ mice. (**E, G**) Male AdipoR2$^{-/-}$ mice show no significant differences in bone marrow adipocyte number or size at four weeks or 24 weeks as compared with age-matched AdipoR2$^{+/+}$ controls. (**F, H**) Female AdipoR2$^{-/-}$ mice have significantly reduced bone marrow adiposity with reduced adipocyte number and average size as compared with age-matched AdipoR2$^{+/+}$ controls at 52 weeks of age but show no significant phenotype at four or 24 weeks. Scale bar (**A, C**) 200µm, (**B, D**) 100µm. Data presented as mean±SD, N=4-7 (biological replicates). Unpaired t-test, *=p≤0.05; **=p≤0.01.

4.3 Discussion and conclusions

The work presented in this chapter aimed to provide initial information describing the skeletal phenotype associated with global deletion of AdipoR1 or AdipoR2 in a C57Bl/6 mouse line. This study was designed to make use of AdipoR1$^{-/-}$ and AdipoR2$^{-/-}$ male and female mice at three distinct ages to allow identification of sex-, age- and genotype-related phenotypic changes in bone microarchitecture, bone cell distribution and physical properties. To our knowledge, the bone phenotype of these animals has not previously been reported. Thus, this work is considered an important undertaking given the lack of clarity that still persists concerning the effect of adiponectin and its signalling via its receptors on the bone (**Section 1.4**). As hypothesised, AdipoR1$^{-/-}$ and AdipoR2$^{-/-}$ mice generally show a low bone phenotype with significant age- and sex-specific effects; in particular, young (four-week-old) and aged (52-week-old) AdipoR1$^{-/-}$ females showed a very significant skeletal phenotype as compared with age- and sex-matched controls.

The ages at which mice were studied in this chapter were chosen based on previously published observations of bone mass in C57Bl/6 mice. Four-week-old mice are extremely skeletally immature and thus provide an insight into initial bone accrual rather than subsequent bone loss. Unlike humans, bone growth and accrual continue in mice beyond their sexual maturity at six to eight weeks with skeletal maturity, including peak bone mass, reached by 24 weeks of age, making this is an ideal timepoint for the study of skeletally mature adult mice[4,315]. The age at which a mouse can reasonably be called 'aged' is difficult to define given that mice do not undergo a true menopause as humans do: while oestrogen levels are maintained during the irregular cycling observed in 32 to 52-week-old female C57Bl/6N mice, these mice are not expected to be able to continue breeding beyond 30 weeks of age[4]. 52 weeks of age was judged sufficiently aged for age-related decline in bone mass to be observed[315] and this cohort has subsequently been termed as 'aged' throughout this thesis.

Adult mice of the AdipoR1$^{-/-}$ and AdipoR2$^{-/-}$ lines showed very few significant skeletal phenotypic differences as compared with controls, with significant differences observed in very young or aged animals. An observation of reduced BV/TV and altered trabecular parameters coupled with normal cortical thickness and TMD in both lines suggests a trabecular rather than cortical phenotype. Of particular note, four- and 52-week-old AdipoR1$^{-/-}$ female mice showed very significant differences in bone microarchitecture as determined by µCT analysis and in bone marrow adiposity by histological analysis as compared with age-matched controls, whereas no significant effects were observed in the same parameters in the 24-week-old female AdipoR1$^{-/-}$ mice. This is suggestive of a dual response: a retardation in bone accrual in young animals which has been restored as compared to controls by adulthood, and an accelerated bone loss phenotype with advanced age. A temporal dual-response has previously been noted elsewhere, with six- and 12-week-old male C57Bl/6J:129/Sv mice globally deficient in adiponectin observed

to show a low bone phenotype, but a high bone mass phenotype by nine months of age[96]. Age- and genetic background-matching experiments would be necessary to compare these results directly with the results presented in this chapter, but they remain suggestive of a complex role for adiponectin in bone accrual and maintenance throughout life.

In studies that have previously made use of one timepoint only, often at ages well below that needed for skeletal maturity (six to 12 weeks)[252,254,316], it is possible that phenotypic patterns such as the one identified here could have been missed, perhaps contributing to the confusion surrounding the literature in this area. Where study designs involving more than one timepoint have been employed, age-related changes have invariably been observed: female adiponectin knockout mice showed significant reductions in trabecular bone volume at eight and 14 weeks of age, but not at 21-37 weeks of age[249]; male and female transgenic mice expressing porcine AdipoR1 (pAdipoR1) showed increased BMD at 56 weeks of age, but not at eight or 32 weeks of age[256]; and male transgenic mice overexpressing adiponectin showed significantly reduced bone mineral content at 16 weeks of age, but not at eight weeks of age[259]. Together, these data demonstrate significant age-related changes in the bone phenotype of these models, corroborating the age-related differences observed throughout the work presented in this chapter and highlighting the need for study of more than one timepoint.

The pattern of adiponectin concentration variation throughout the mouse lifespan is not well established. Adiponectin blood serum concentrations remain unchanged until around 25 weeks of age in wild type animals[317], but its changes beyond this are not well characterised. Given the significant age-related alterations in bone phenotype observed in this study, the prior evidence of age-related changes in the skeletal phenotype of adiponectin knockout animals, and the common use of circulating total adiponectin concentration as a marker in human studies, the total circulating adiponectin

concentration and its oligomeric ratios throughout the murine lifespan is an interesting point for further investigation in the future that the next chapter begins to address.

A significant sex-specific effect was observed in both the AdipoR1 and AdipoR2 lines. Female AdipoR1$^{-/-}$ mice consistently showed an altered bone phenotype as compared with controls, with very significant changes in bone microarchitecture and BMD observed by µCT which was associated with alterations in some physical properties shown by three-point bend testing in both young (four-week-old) and aged (52-week-old) models. However, these mice did not show any significant alterations in their osteoblastic or osteoclastic parameters that reflect these structural alterations. Conversely, despite a small but significant increase in the relative coverage of osteoclasts on the bone surface in young male AdipoR1$^{-/-}$ mice, the microarchitecture of the tibiae of these mice remained unaltered. When interpreting these results, the two-dimensional and subjective nature of histomorphometric analyses should be considered, but lack of significant bone cell phenotype could suggest a wider, non-bone intrinsic cause for the changes seen; this hypothesis is further explored in the next chapter.

The presence of sex-specific effects has been observed in other animal studies of adiponectin in the bone[229,234,256]. Research published in 2016 detailing a reduced bone density in 14-week-old C57Bl/6J female adiponectin knockout mice[249] was followed up by more recent data in 2018 from the same group using the same C57Bl/6J strain of mice describing an increased bone density in 14-week-old male adiponectin knockout mice[318]. While the low bone phenotype of the female adiponectin knockout mice matches the low bone phenotype observed in the female AdipoR1$^{-/-}$ and AdipoR2$^{-/-}$ mice studied in this chapter, the male mice studied do not corroborate the increased bone phenotype observed by Cornish *et al*. However, it is reasonable to assume identical housing environments for the female mice studied in 2016 and the male mice studied in 2018, and their shared genetic background is confirmed. Given the presence of an opposing

bone phenotype at the same age, this work provides significant evidence for the presence of a strong sex-specific effect in these animals, supporting the work described in this chapter. It is likely that a strong sex-specific effect explains why many studies investigating the relationship between adiponectin and the bone make use of either male or female models whether pre-clinical[253,254] or human[233,239,294]. As previously noted with age-related effects, such exclusions could contribute to the confusion in the literature.

Aside from sex-specific phenotypic observations in pre-clinical studies, the clearest evidence of an interaction between adiponectin and sex hormones occurs in women at the menopause, where adiponectin levels increase rapidly[195]. A cross-sectional study in 2010 found adiponectin to be an independent predictor of BMD in post-menopausal, but not pre-menopausal, women[319]. Interestingly, menopause has also been suggested to alter the relationship of adiponectin to oestrogen-related malignancies: a strong negative association between adiponectin and endometrial cancer risk has been observed to be reduced following menopause[320], whereas a strong negative correlation between adiponectin and breast cancer risk is observed in post-menopausal women only, with no association present in pre-menopausal women[321]. It has been hypothesised that the link between adiponectin and oestrogen alters following menopause due to adipose tissue becoming the main source of oestrogen in post-menopausal women such that non-obese women will have high adiponectin coupled with low oestrogen[294], but the exact mechanistic link between the two remains unclear.

Further, it is known that testosterone is a potent inhibitor of adiponectin production, explaining the rise in circulating adiponectin levels following castration in male mice but not female mice[250] and the generally lower circulating levels of adiponectin in males than females in both mice and humans[250,322]. This lower circulating level in males than females could underly the more subtle effect of disruption of adiponectin observed in male mice than in female mice in this chapter. Having observed the general skeletal phenotype of

the male and female models, the female models were selected for further investigation in subsequent chapters due to the presence of a stronger and more consistent skeletal phenotype.

Throughout this chapter, AdipoR1$^{-/-}$ mice consistently showed a more significant skeletal phenotype than AdipoR2$^{-/-}$ mice. As discussed, very few significant changes were observed in the male mice of either line at any timepoint studied. Adult and aged female AdipoR2$^{-/-}$ mice showed a reduced body weight and tibial length and a reduction in bone marrow adiposity but no significant change in bone volume or microarchitecture by µCT analysis, while young female AdipoR2$^{-/-}$ mice, which did show significant reductions in bone volume and changes in bone architecture by µCT, showed no alteration in bone cell distribution by histological analysis. Conversely, female AdipoR1$^{-/-}$ mice showed significant changes in gross morphology and bone microarchitecture. Most interestingly, both young and aged female AdipoR1$^{-/-}$ mice showed significant increases in bone marrow adiposity. Despite the interest in adiponectin as a coupling hormone between bone and fat and bone marrow adipocytes having been identified as significant contributors to circulating adiponectin[128], very few previous papers investigating the bone phenotype of adiponectin knockout animals have investigated and published the bone marrow adiposity of the models. One study did report the bone marrow adiposity of C57Bl/6 female adiponectin knockout mice, finding an increase in bone marrow adipocyte number in 37-week-old female adiponectin knockout mice as compared with age-matched controls, but with no significant adiposity phenotype at eight- or 21-weeks-old[249]. The same study found significant reductions in bone volume parameters by µCT analysis in the adiponectin knockout group as compared with age-matched controls[249] matching the findings of this study of AdipoR1$^{-/-}$ female C57Bl/6 mice.

The observed increase in bone marrow adiposity in young and aged AdipoR1$^{-/-}$ female mice corresponded directly with the ages at which bone volume was found to be reduced, suggesting a correlative relationship between the two parameters. This was of particular interest since bone marrow adipocytes and osteoblasts share a common progenitor cell and led to a hypothesis that a disruption of adiponectin signalling via deletion of AdipoR1 could be affecting the cell fate of these progenitors. For this reason, AdipoR1 female mice were selected for further investigation, both in this chapter via biomechanical testing, and in subsequent chapters.

Biomechanical testing provided useful insights into the physical properties of the bones of AdipoR1$^{-/-}$ females as compared with age- and sex-matched controls. Both young and aged AdipoR1$^{-/-}$ female mice showed significant changes in some parameters: young mice had reduced extension at maximum load, whereas aged mice had reduced maximum load at breakage. Some significant changes in the biomechanical properties of bones from these models are perhaps expected given the significant changes in bone microarchitecture and volume observed by µCT analysis. More interestingly, 24-week-old AdipoR1$^{-/-}$ mice, which showed no significant changes during µCT analysis, showed a reduced maximum load to breakage, extension at break and energy at break. It is clear that the quantity of the bone observed during µCT analysis does not directly correspond with the quality of the bone produced and therefore its biophysical properties in weight-bearing situations. Others have identified a lack of direct correlation between bone volume and bone performance in bend testing in C57Bl/6 female adiponectin knockout mice[249], where a low bone phenotype was associated with no significant difference between controls and knockouts in a three-point bend test, highlighting the importance of assessing the physical properties of a bone.

The work presented in this chapter found significant age-, sex- and genotype-related skeletal phenotypes associated with global deletion of AdipoR1 or AdipoR2, justifying

its use as a preliminary hypothesis-generating study. Both AdipoR1$^{-/-}$ and AdipoR2$^{-/-}$ females showed a significant low bone phenotype, particularly the young and aged cohorts. In the young and aged AdipoR1$^{-/-}$ females, this low bone phenotype was accompanied with a significant increase in bone marrow adiposity (**Figure 4.18**). Accordingly, these animals were selected for more focussed study in the next chapter with all ages studied due to the possibility of an interesting bimodal effect in the young and the aged groups.

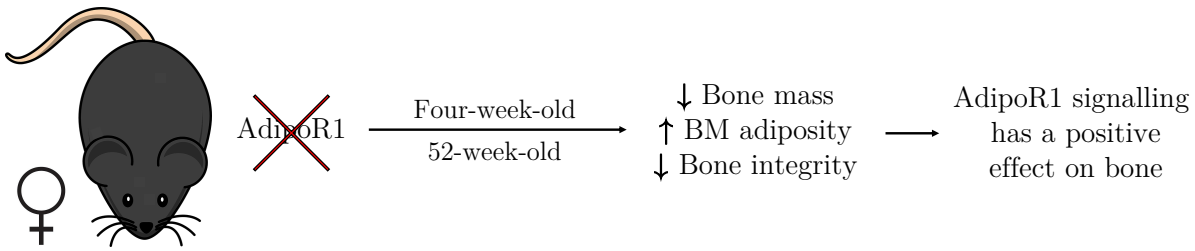


Figure 4.18: Summary of Chapter 4 key findings. Female C57Bl/6 mice globally deficient in AdipoR1 showed reduced bone mass, increased bone marrow adiposity and reduced bone integrity at four and 52 weeks of age as compared with age- and sex-matched wild type controls. This suggests adiponectin signalling via AdipoR1 has a positive effect on the bone. The investigation of these mice is continued; AdipoR2$^{-/-}$ females and males of both genotypes failed to show a significant bone phenotype.

5

Metabolomic, Adipogenic and Transcriptomic Assessment of AdipoR1$^{-/-}$ Female Mice

5.1 Introduction

5.1.1 Blood serum analytes associated with bone and fat phenotypes

Analysis of analytes circulating in the blood represents an easily accessible readout of bone health and wider phenotypic effects. To interrogate the systemic changes in bone- and adipose-related factors, blood serum analytes were measured using Luminex plates which were run on a Luminex MAGPIX Analyzer in collaboration with Dr Jennifer Hill.

These analytes were chosen based on previously published evidence or suggestion of an association of changes in their expression or circulating levels with bone mass, turnover, or BMD. Receptor Activator of Nuclear Factor Kappa-B Ligand (RANKL) is produced

by cells of the bone microenvironment, most notably osteoblasts, and binds to RANK receptors expressed on the surface of osteoclasts to induce their activation and differentiation. Osteoprotegerin (OPG) is a decoy receptor for RANKL and acts to mediate its effects[323]. Their circulating levels, particularly a ratio between them, is a commonly used readout of bone turnover in murine models and human cohort studies alike, with an increased ratio suggesting increased osteoclast activity[324,325]. Osteopontin (OPN) is a non-collagenous protein component of bone known to be involved in bone turnover while dickkopf-related protein 1 (DKK1) is a soluble inhibitor of Wnt signalling, and their circulating levels are both negative correlates of BMD in a human cohort[326,327].

Inflammatory mediators in the bone microenvironment are known to have direct effects on bone turnover. The pro-inflammatory cytokine tumour necrosis factor-α (TNFα) has been shown to promote osteoclastic activity both directly through stimulation of proliferation and activation of cells of the osteoclastic lineage and indirectly through affecting RANKL and OPG production by cells of the osteoblastic and stromal lineages[328]. Likewise, the cytokine macrophage colony stimulating factor (MCSF) is known to have potent osteoclastogenic effects[329].

Leptin is highly produced by WAT with its circulating levels correlating positively with body fat[94], fatty acid binding protein 4 (FABP4) is highly expressed by adipocytes to facilitate the transport of fatty acids into cell for storage in lipid droplets[330], and low density lipoprotein receptor (LDLR) binds to low density lipoproteins to facilitate their endocytosis[331]. Altered circulating levels of any of these fat-associated factors could indicate a significant change in fat depot size or metabolic activity.

5.1.2 Bone formation rate analysis

Bone formation rate (BFR) analysis makes use of calcein, a calcium-binding dye, which is incorporated into bone as it mineralises. Two administrations of calcein spaced 3 days apart prior to cull produces bone stained with two lines which can be visualised under fluorescence microscopy to determine mineral apposition rate (MAR), a two-dimensional measure of bone formation calculated from quantification of single-labelled bone, and BFR, a volumetric measure of bone formation calculated from quantification of the space between double labelling.

5.1.3 Osmium tetroxide staining

Osmium tetroxide staining, a recently developed tool for the study of adipose tissue, has proved particularly helpful in furthering research on BMAT due to the location of BMAT within the mineralised bone which has historically hindered its *in situ* research. Osmium tetroxide is soluble in fats and forms a black reduction with them which can then be visualised and analysed by µCT analysis due to inclusion of the heavy metal osmium into the lipid droplets[122]. Osmium-stained lipid was distinguished from compact cortical bone by thresholding, and cMAT and rMAT were defined based on location: adipose tissue in the distal tibia, defined as the end of the tibia up to the tibia-fibular junction, was classified as cMAT; adipose tissue between the tibia-fibular junction and the growth plate was classified as rMAT. Osmium tetroxide staining and subsequent µCT scanning was performed by Felix Richter.

5.1.4 RNASeq

The transcriptome is the complete set of transcripts in a cell and their quantity. RNA sequencing (RNASeq) uses deep sequencing to analyse the transcriptome, and comparative analysis between the expression profile of two groups can provide a powerful insight into the functional elements underlying an observed phenotype. In brief, the process of RNASeq involves the conversion of a population of RNA into cDNA fragments to which adaptors are attached to one or both ends before each fragment is sequenced to obtain short sequences, typically 30-400bp in length, from one (single-end sequencing) or both (pair-end sequencing) ends. After sequencing, the resulting reads are aligned to a reference genome or reference transcripts in order to produce a genome-scale transcription map encompassing the level of expression of every gene[332]. In the work presented in this chapter, single-end sequencing with 75bp fragments was used. Reads (approximately 25 million per sample) were aligned to the reference mouse genome version GRCm38 using STAR version 2.5.3a, and differential expression analysis was performed using DESeq2. RNASeq was performed by Dr Neil Ashley and bioinformatic analysis of results was performed by Dr Srinivasa Rao.

5.1.5 Phenotypic data from the IMPC

The IMPC holds general phenotyping data on the null mutant animals it produces, with a small number (approx. 7-15) of male and female null mutant animals compared with a large bank of data from many wild type animals (approx. 1500-1800). This phenotyping data is publicly available online[302]. IMPC data presented in this chapter has been downloaded as raw data and re-plotted using GraphPad Prism 7; this data is clearly indicated in the text and figure legend.

5.1.6 Chapter aims and hypothesis

The work in this chapter aims to characterise further the low bone phenotype observed in female AdipoR1$^{-/-}$ animals, with focus narrowing on the young four-week-old animals with a view to identifying candidate mechanisms underlying the observed phenotype. Within this, it was hypothesised that the phenotype observed could be mediated at least in part by whole-body, bone-extrinsic effects, so a wider consideration was given to these indirect effects alongside consideration of direct, bone-intrinsic effects.

5.2 Results

5.2.1 Analysis of fat- and bone-related blood serum analytes in AdipoR1$^{-/-}$ females

The previous chapter identified a significant change in bone phenotype of female AdipoR1$^{-/-}$ mice as compared with age-matched AdipoR1$^{+/+}$ controls; the phenotype in AdipoR2$^{-/-}$ mice and male AdipoR1$^{-/-}$ mice was much weaker, justifying further study focussing on female AdipoR1$^{-/-}$ mice. A discussion of these sex- and genotype-specific observations is included in **Section 1.3** and **Section 4.3**.

5.2.1.1 Young AdipoR1$^{-/-}$ mice show significant changes in circulating adiponectin multimer ratios

It was hypothesised that disruption of adiponectin signalling via whole-body knockout of AdipoR1 could have a significant effect on circulating adiponectin levels in the blood. Blood serum concentration of total circulating adiponectin in four-, 24- and 52-week-old

AdipoR1$^{+/+}$ and AdipoR1$^{-/-}$ mice was determined by ELISA. Total adiponectin concentrations were found to be unchanged in AdipoR1$^{-/-}$ mice at four- and 52-weeks of age but significantly increased as compared with controls at 24 weeks of age (**Figure 5.1**).

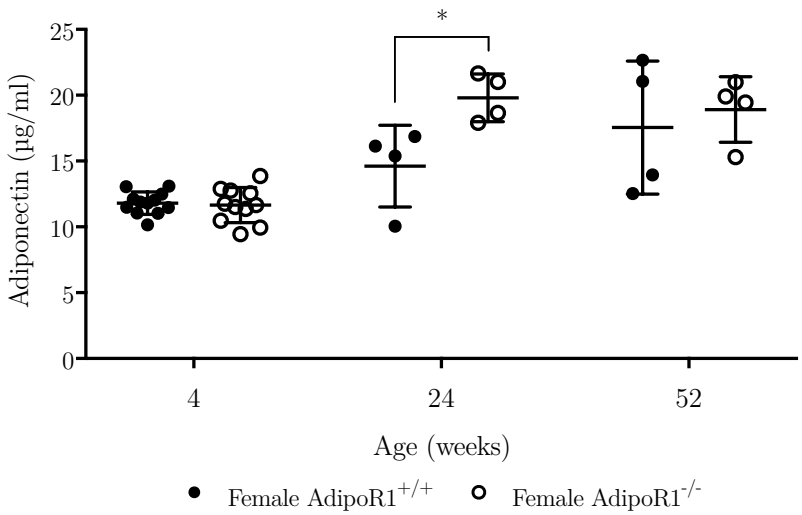
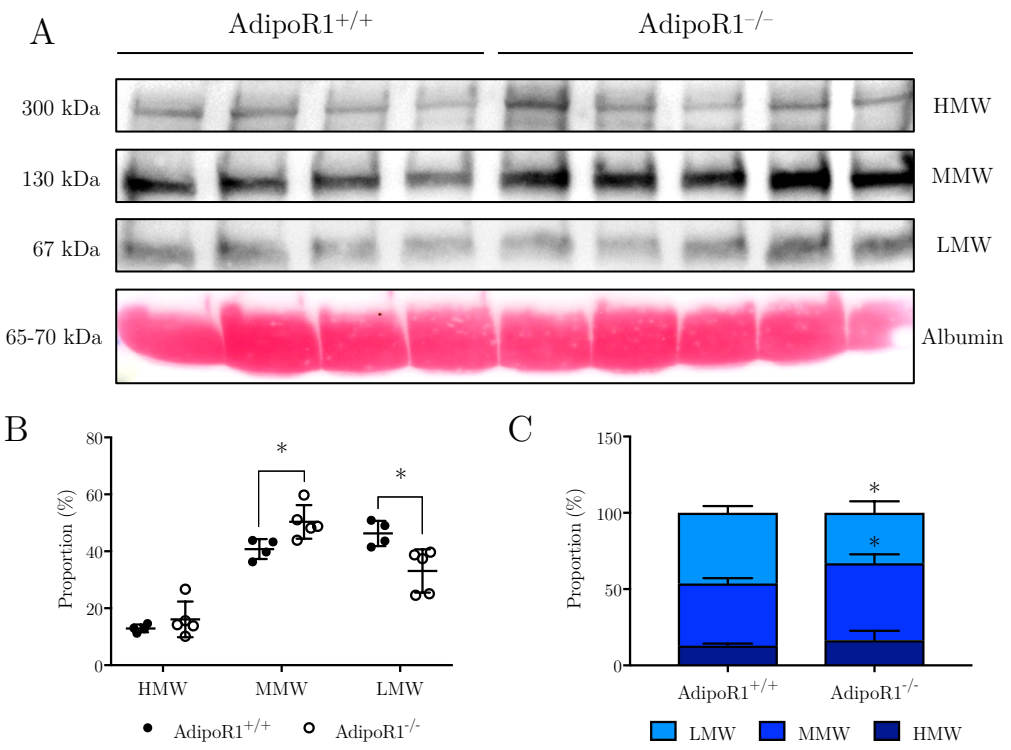


Figure 5.1: 24-week old AdipoR1$^{-/-}$ females show a significant increase in circulating adiponectin levels. Adiponectin concentration in the blood serum of AdipoR1$^{+/+}$ and AdipoR1$^{-/-}$ females was analysed at four, 24 and 52 weeks of age by ELISA. No significant differences were observed in circulating adiponectin levels in four- or 52-week-old AdipoR1$^{-/-}$ animals as compared with age-matched AdipoR1$^{+/+}$ controls, but circulating levels were significantly increased in 24-week-old AdipoR1$^{-/-}$ females. Data presented as mean±SD, N=4-11 (biological replicates). Unpaired t-test, *=p≤0.05.

As discussed in **Section 1.3.1**, adiponectin circulates in the blood in several oligomeric forms. It was considered that analysis of total circulating adiponectin could be insufficient for a comprehensive overview of alterations in adiponectin as a result of AdipoR1 deletion. To this end, the relative contribution of high molecular weight (HMW), middle molecular weight (MMW) and low molecular weight (LMW) oligomers to total circulating adiponectin was determined in the blood serum of four-week-old (**Figure 5.2A-C**), 24-week-old (**Figure 5.2D-F**) and 52-week-old (**Figure 5.2G-I**) AdipoR1$^{-/-}$ female mice as compared with age- and sex-matched AdipoR1$^{+/+}$ controls via

western blotting (**Figure 5.2A, D, G**). Densitometry analysis was used to assess the proportional contribution of each oligomeric complex to total circulating adiponectin. Ponceau S-stained albumin was used as a loading control indicator, although relative proportions only were assessed due to lack of a readily quantifiable loading control.

Four-week-old AdipoR1$^{-/-}$ females showed a significant shift in the relative contribution of adiponectin oligomers as compared with age- and sex-matched AdipoR1$^{+/+}$ controls: a significant increase in MMW adiponectin and reduction in LMW adiponectin relative to total circulating adiponectin was observed (**Figure 5.2A-C**). No significant changes in the relative contribution of adiponectin oligomers were observed in 24-week-old (**Figure 5.2D-F**) and 52-week-old (**Figure 5.2G-I**) AdipoR1$^{-/-}$ animals as compared with age- and sex-matched AdipoR1$^{+/+}$ controls.



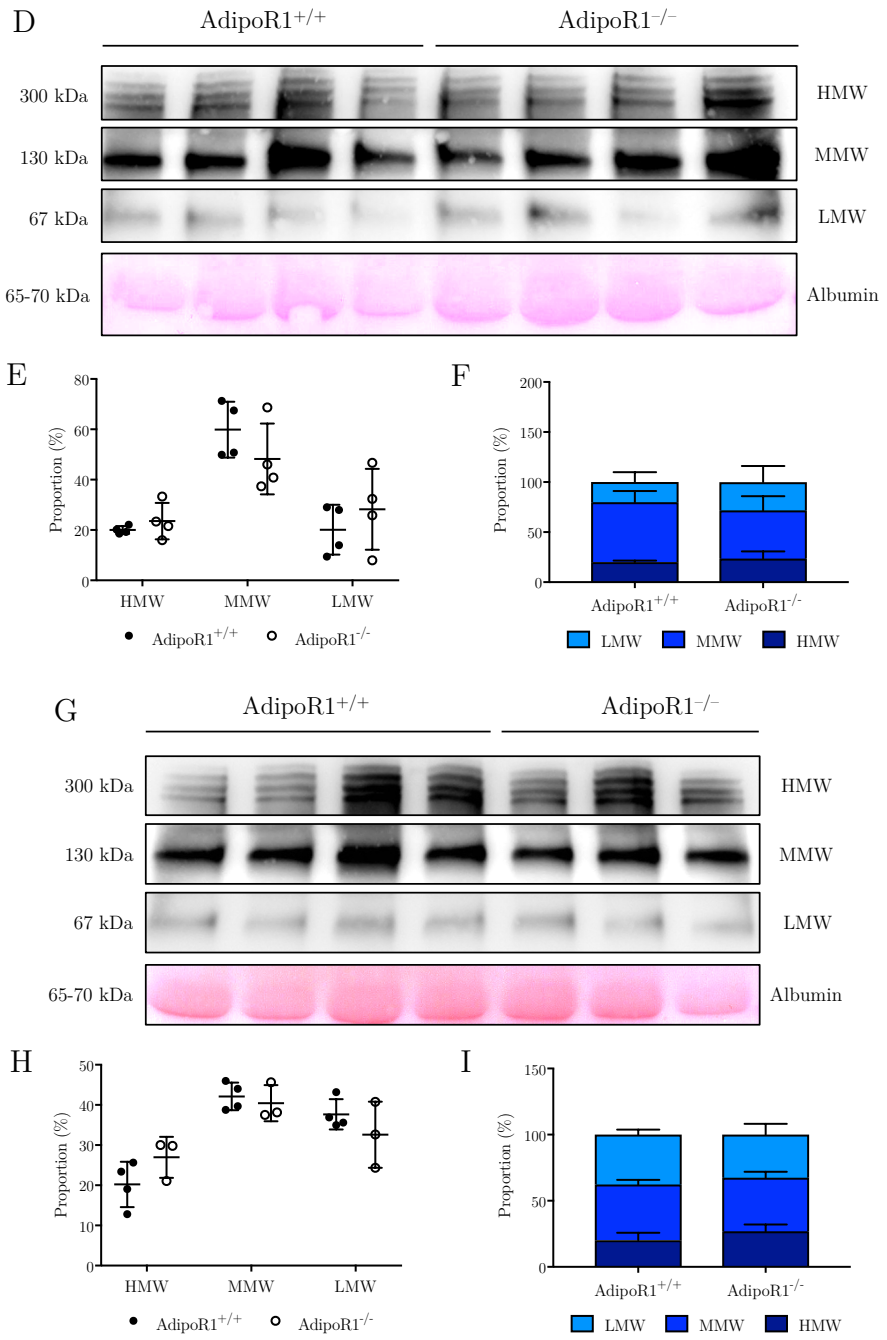
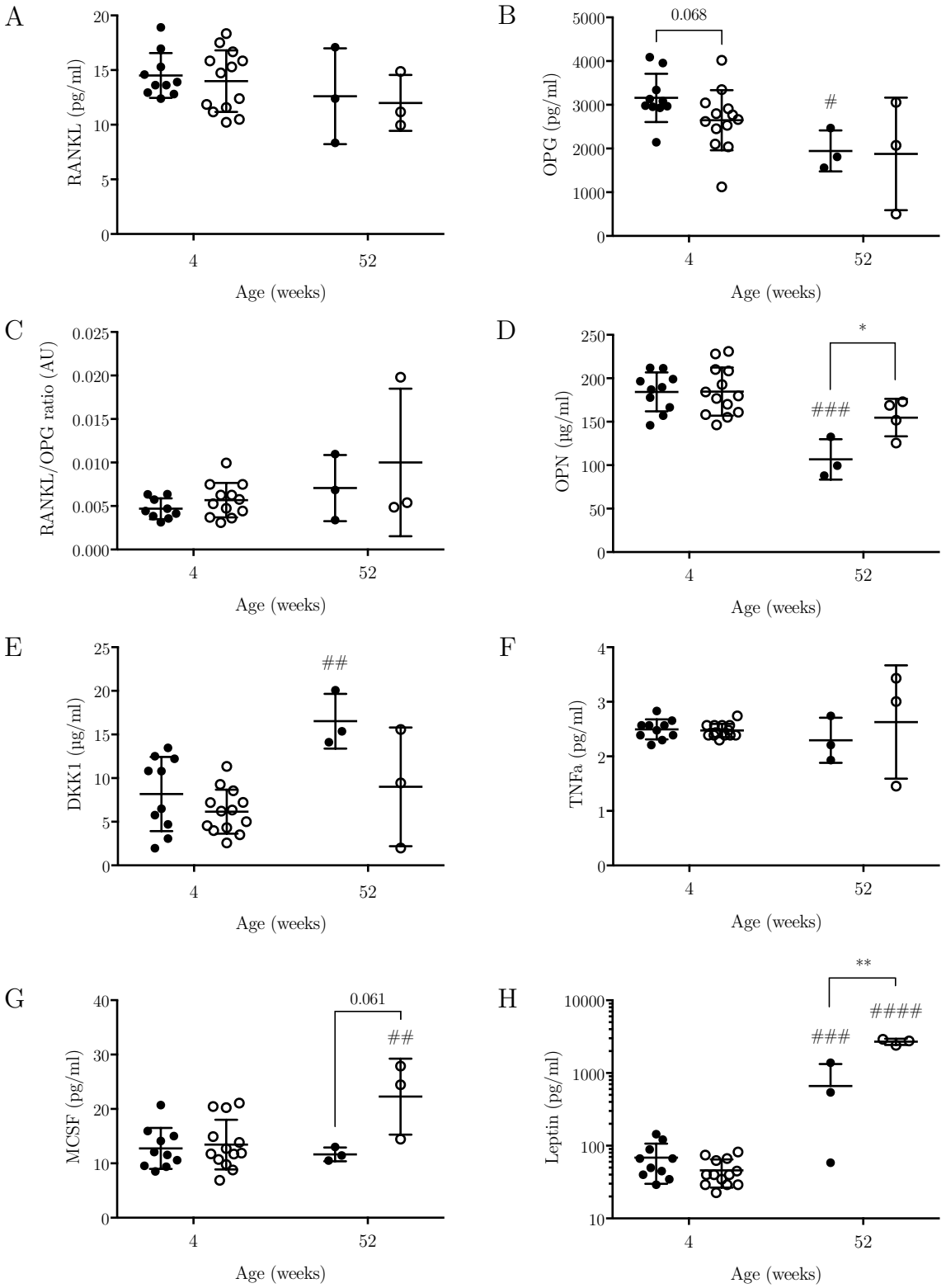


Figure 5.2: Four-week-old AdipoR1$^{-/-}$ female mice show changes to adiponectin oligomeric ratios. Blood serum of (**A-C**) four-, (**D-F**) 24- and (**G-I**) 52-week-old AdipoR1$^{+/+}$ and AdipoR1$^{-/-}$ female mice was analysed via (**A, D, G**) western blotting. Albumin was used as a loading control. (**B, C, E, F, H, I**) Densitometry analysis was used to determine the relative contribution of high molecular weight (HMW), middle molecular weight (MMW) and low molecular weight (LMW) oligomers to total circulating adiponectin. (**A-C**) A significant change in the ratio between oligomers was observed in the serum of four-week-old AdipoR1$^{-/-}$ females as compared with age- and sex- matched AdipoR1$^{+/+}$ animals, with a relative increase in MMW adiponectin and relative decrease in LMW adiponectin. (**D-I**) No significant change in the ratio between oligomers was observed in the serum of 24- and 52-week-old AdipoR1$^{-/-}$ females as compared with age- and sex- matched AdipoR1$^{+/+}$ animals. Data presented as mean±SD, N=4-5 (biological replicates). Unpaired t-test, *=p≤0.05.

5.2.1.2 AdipoR1$^{-/-}$ females show no significant differences in a screen of fat- and bone-related blood serum analytes

Following observation of a moderate genotype-associated bone phenotype particularly prevalent in females, a small screen of related blood analytes was performed. Several factors for this screen were selected based on their known effect on, or correlation with, bone health and turnover. Circulating levels of RANKL (**Figure 5.3A**), OPG (**Figure 5.3B**) and their ratio (**Figure 5.3C**) were not significantly altered between AdipoR1$^{+/+}$ and AdipoR1$^{-/-}$ mice at either age studied. Serum OPN concentrations were increased in 52-week-old AdipoR1$^{-/-}$ females as compared with age-matched controls (**Figure 5.3D**) but DKK1 levels remained unchanged (**Figure 5.3E**). Analysis of pro-inflammatory cytokines TNFα (**Figure 5.3F**) and MCSF (**Figure 5.3G**) revealed no significant difference in their circulating concentration, and although leptin was found to be significantly increased in 52-week-old AdipoR1$^{-/-}$ females (**Figure 5.3H**), the other fat-related factors FABP4 (**Figure 5.3I**) and LDLR (**Figure 5.3J**) were unaffected by genotype at either age studied. OPG, OPN, DKK1 and leptin concentrations were significantly altered between four-week-old and 52-week old AdipoR1$^{+/+}$ controls, but in leptin concentrations alone was this significant age-related difference reflected in AdipoR1$^{-/-}$ females. Similarly, MCSF, FABP4 and LDLR concentrations were significantly altered with ageing in AdipoR1$^{-/-}$ females but not AdipoR1$^{+/+}$ controls.


A
RANKL (pg/ml)
Age (weeks)
B
OPG (pg/ml)
0.068
#
Age (weeks)
C
RANKL/OPG ratio (AU)
Age (weeks)
D
OPN (µg/ml)
*
###
Age (weeks)
E
DKK1 (µg/ml)
##
Age (weeks)
F
TNFa (pg/ml)
Age (weeks)
G
MCSF (pg/ml)
0.061
##
Age (weeks)
H
Leptin (pg/ml)
**
###
####
Age (weeks)

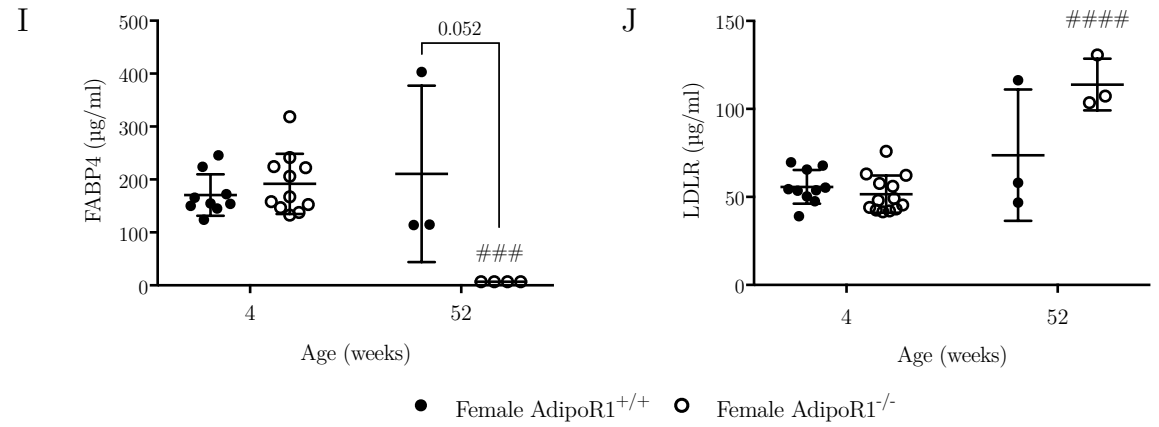


Figure 5.3: AdipoR1$^{-/-}$ females showed few significant differences in a screen of fat- and bone-related blood analytes. The blood serum of four- and 52-week-old female AdipoR1$^{+/+}$ and AdipoR1$^{-/-}$ mice was analysed by Luminex assay. No significant differences in circulating levels of (**A**) receptor activator of nuclear factor kappa-B ligand (RANKL), (**B**) osteoprotegerin (OPG) or (**C**) RANKL:OPG ratio were identified in AdipoR1$^{-/-}$ females as compared with age-matched controls. (**D**) Osteopontin (OPN) was significantly increased in 52-week-old AdipoR1$^{-/-}$ females as compared with age-matched controls, but genotype did not affect (**E**) dickkopf-related protein-1 (DKK1), (**F**) tumour necrosis factor-α (TNFα) or (**G**) macrophage colony stimulating factor (MCSF). (**H**) Leptin concentration was significantly increased in 52-week-old AdipoR1$^{-/-}$ females as compared with age-matched controls, but no significant genotype-related differences in (**I**) fatty acid binding protein-4 (FABP4) or (**J**) low density lipoprotein receptor (LDLR) concentration were detected. Data presented as mean±SD, N=3-10 (biological replicates). *=p≤0.05 and **=p≤0.01 as compared with age-matched AdipoR1$^{+/+}$ control, unpaired t-test. #=p≤0.05; ##=p≤0.01, ###=p≤0.001, ####=p≤0.0001 as compared with genotype-matched four-week-old animals, two-way ANOVA with multiple comparisons testing.

5.2.2 The low bone phenotype of young AdipoR1$^{-/-}$ females is coupled with a bone marrow-specific increase in adiposity

Thus far, young AdipoR1$^{-/-}$ female mice have been found to have the most significant and interesting genotype-related phenotype: a significantly reduced body weight, significantly lower bone volume by µCT and significantly increased bone marrow adiposity by histology have all been observed as compared with age-matched AdipoR1$^{+/+}$ controls. Consequently, focus was placed on these young AdipoR1$^{-/-}$ mice from here onwards to further interrogate the effect of AdipoR1 deletion on bone phenotype.

5.2.2.1 Young AdipoR1$^{-/-}$ females show a significant reduction in bone formation rate by calcein staining

Young AdipoR1$^{-/-}$ female mice show significantly reduced bone mass as compared with age-matched AdipoR1$^{+/+}$ controls as determined by µCT analysis (**Figure 4.3**). Given their young age, it was hypothesised that this reflected a retarded rate of bone accrual rather than increased bone loss. Bone formation rate was determined by quantification of calcein labelling in the spine (**Section 2.1.10**). AdipoR1$^{+/+}$ (**Figure 5.4A-C**) and AdipoR1$^{-/-}$ (**Figure 5.4D-F**) spines were viewed under light (**Figure 5.4A, B, D, E**) and fluorescence (**Figure 5.4C, F**) microscopy. Histomorphometry analysis revealed young AdipoR1$^{-/-}$ females to have increased trabecular spacing (**Figure 5.4G**) and reduced trabecular number (**Figure 5.4H**) in the spine, reflective of the low bone mass phenotype previously observed.

Quantification of single- and double-labelled calcein staining showed AdipoR1$^{-/-}$ females to have significantly reduced MAR (**Figure 5.4I**) and BFR (**Figure 5.4J**) as compared with AdipoR1$^{+/+}$ controls, confirming a retardation in bone accrual in these young mice.

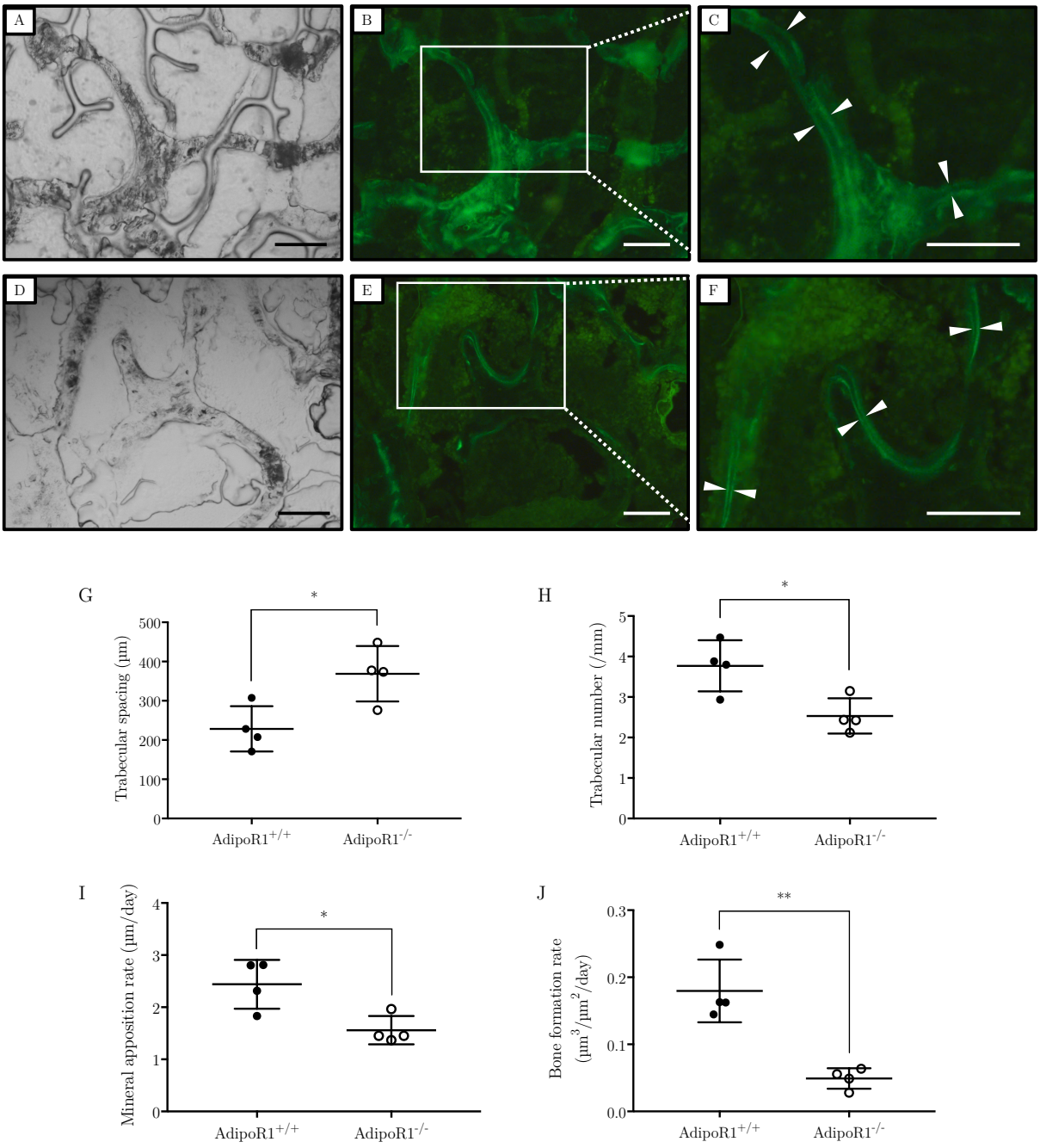
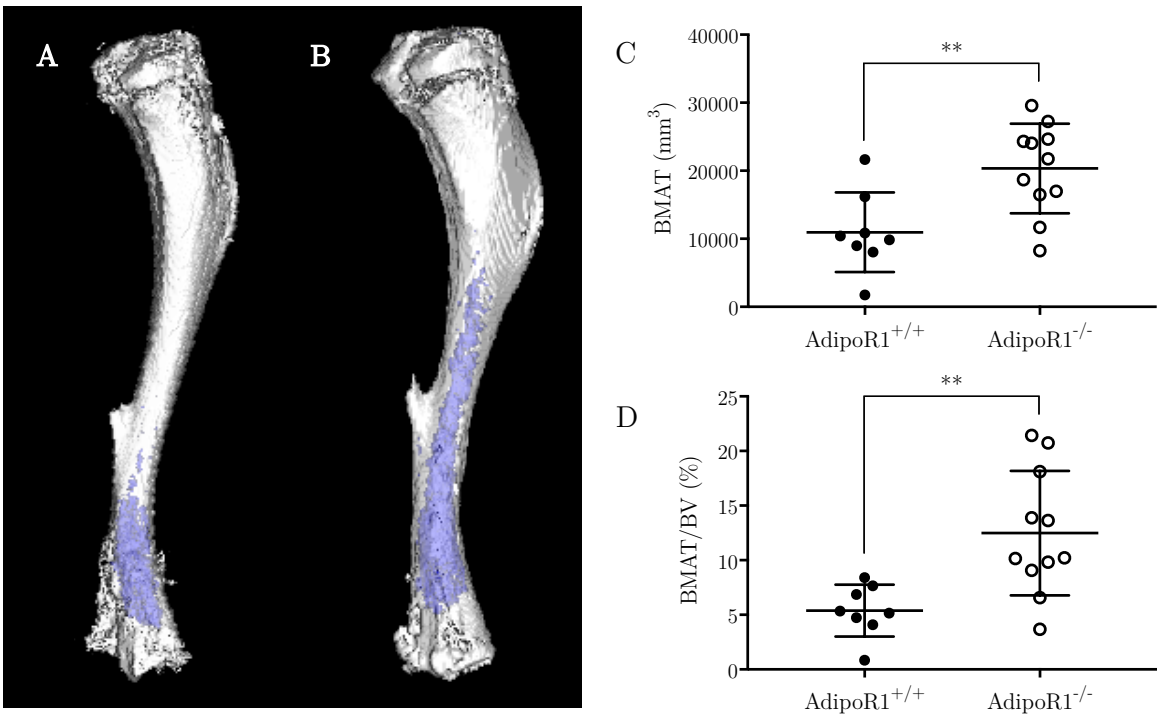


Figure 5.4: Young AdipoR1$^{-/-}$ females show a significant reduction in bone formation rate. Representative images of calcein labelled spines of four-week-old (**A-C**) AdipoR1$^{+/+}$ and (**D-F**) AdipoR1$^{-/-}$ females. (**A, D**) Brightfield images and (**B, E**) corresponding calcein labelling show (**C, F**) a reduced distance between double labelling (indicated by distance between arrows). Histomorphometric analysis was used to quantify bone volume, proportion of calcein labelling relative to bone volume surface and average distance between double labelling. Four-week-old AdipoR1$^{-/-}$ females show (**G**) significantly increased trabecular spacing and significantly reduced (**H**) trabecular number, (**I**) mineral apposition rate (MAR) and (**J**) bone formation rate (BFR) as compared with age-matched AdipoR1$^{+/+}$ controls. Scale bar: 100µm. Data presented as mean±SD, N=4 (biological replicates). Unpaired t-test, *=p≤0.05, **=p≤0.01.

5.2.2.2 Young AdipoR1$^{-/-}$ females show a significant increase in bone marrow adiposity by osmium tetroxide staining

Osmium tetroxide staining of the tibia of four-week-old AdipoR1$^{+/+}$ (**Figure 5.5A**) and AdipoR1$^{-/-}$ (**Figure 5.5B**) females was performed to produce a more comprehensive and objective measure of bone marrow adiposity in these models. Both absolute bone marrow adipose tissue (BMAT, **Figure 5.5C**) and BMAT relative to total bone volume (BMAT/BV, **Figure 5.5D**) were quantified and were both found to be significantly increased in AdipoR1$^{-/-}$ mice as compared with controls. BMAT was subcategorised as constitutive (cMAT, **Figure 5.5E**) or regulated (rMAT, **Figure 5.5F**), which are known to have distinct biological properties (see **Section 1.2.3**) and both were found to be significantly increased in AdipoR1$^{-/-}$ mice as compared with controls, with cMAT volume substantially larger than rMAT volume. No significant correlation was observed between the age at which the mouse was culled and total bone marrow fat (**Figure 5.5G**) or bone marrow fat relative to bone volume (**Figure 5.5H**) in AdipoR1$^{+/+}$ or AdipoR1$^{-/-}$ animals.



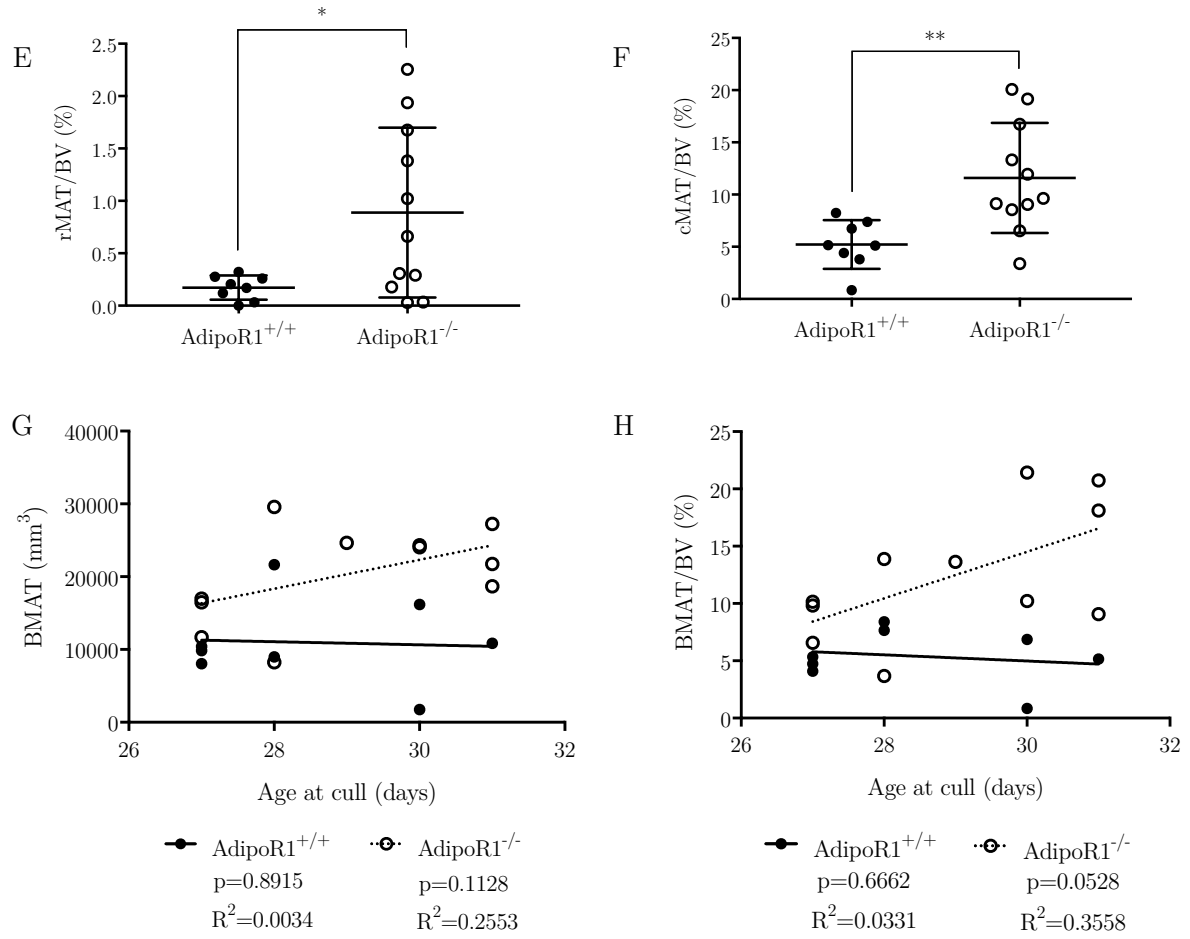


Figure 5.5: Young AdipoR1$^{-/-}$ females show increased bone marrow adiposity by osmium staining. Representative reconstruction images of µCT-scanned four-week-old female (**A**) AdipoR1$^{+/+}$ and (**B**) AdipoR1$^{-/-}$ tibia with osmium-stained bone marrow adipose (blue). As compared with age-matched AdipoR1$^{+/+}$ controls, four-week-old AdipoR1$^{-/-}$ females showed significant increases in (**C**) total bone marrow tissue (BMAT), (**D**) BMAT relative to bone volume (BMAT/BV), (**E**) regulated BMAT (rMAT) relative to BV (rMAT/BV) and (**F**) constitutive BMAT (cMAT) relative to BV (cMAT/BV). No significant correlation was observed between (**G**) total BMAT and age at cull or (**H**) BMAT/BV and age at cull. (**C-F**) Data presented as mean±SD, N=8-11 (biological replicates). Unpaired t-test. (**G**, **H**) Pearson's correlation. *=p≤0.05; **=p≤0.01.

5.2.2.3 rBMAT content correlates significantly with circulating serum adiponectin concentrations

Given the significant contribution of bone marrow adipocytes to circulating adiponectin concentrations in the blood[128], the correlation between the BMAT and circulating adiponectin was analysed. Neither total BMAT/BV (**Figure 5.6A**) nor cMAT/BV (**Figure 5.6B**) correlated significantly with serum adiponectin concentrations in control or AdipoR1$^{-/-}$ animals. However, the rMAT/BV (%) was positively correlated with serum adiponectin concentration in AdipoR1$^{-/-}$ animals, but not controls (**Figure 5.6C**).

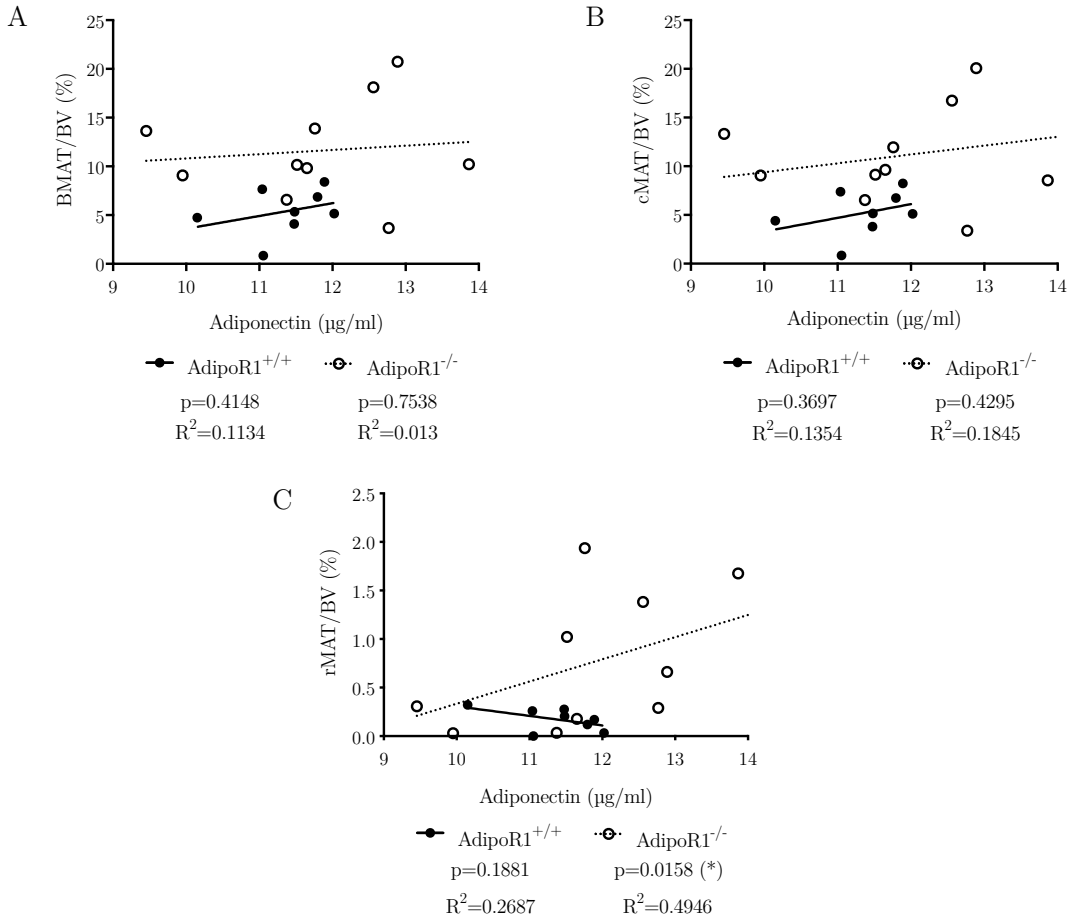


Figure 5.6: rMAT/BV correlates significantly with total circulating adiponectin in young AdipoR1$^{-/-}$ females. No significant correlation was observed between (**A**) BMAT/BV or (**B**) cMAT/BV in either control or AdipoR1$^{-/-}$ females. (**C**) A significant positive correlation exists between rMAT/BV and circulating adiponectin in AdipoR1$^{-/-}$ females but not control animals. N=8-10 (biological replicates). Pearson's correlation. *=p≤0.05.

5.2.2.4 Young AdipoR1$^{-/-}$ females show no significant difference in fat depot weight or histology

Significant increases in bone marrow adiposity in young AdipoR1$^{-/-}$ female mice have been confirmed by histological analysis and osmium tetroxide staining. To investigate whether this was an effect specific to the bone marrow or affected the wider adipose phenotype of these animals, inguinal white adipose tissue (WAT) and interscapular brown adipose tissue (BAT) were weighed and examined histologically.

Inguinal WAT (**Figure 5.7A**) was histologically indistinguishable between AdipoR1$^{+/+}$ (**Figure 5.7A1, A2)** and AdipoR1$^{-/-}$ (**Figure 5.7A3, A4**) four-week-old female mice: in both models, each adipocyte ghost contained one large lipid droplet with a nucleus pushed to the edge of the cell. No significant difference in inguinal WAT weight was observed between AdipoR1$^{+/+}$ and AdipoR1$^{-/-}$ models (**Figure 5.7C**).

Interscapular BAT (**Figure 5.7B**) was histologically similar between AdipoR1$^{+/+}$ (**Figure 5.7B1, B2**) and AdipoR1$^{-/-}$ (**Figure 5.7B3, B4**) four-week-old female mice with both showing adipocytes smaller in average size than those of WAT and which contain multiple smaller lipid droplets. By histology, the brown adipocytes of AdipoR1$^{-/-}$ mice could show slightly smaller lipid droplets as compared to AdipoR1$^{+/+}$ mice, but this was not reflected in overall weight of the interscapular BAT weight (**Figure 5.7D**) which was not significantly altered as compared with AdipoR1$^{+/+}$ controls.

A lack of significant difference in gross histological morphology or depot weight of white or brown fat suggests a bone marrow-specific effect on adiposity.

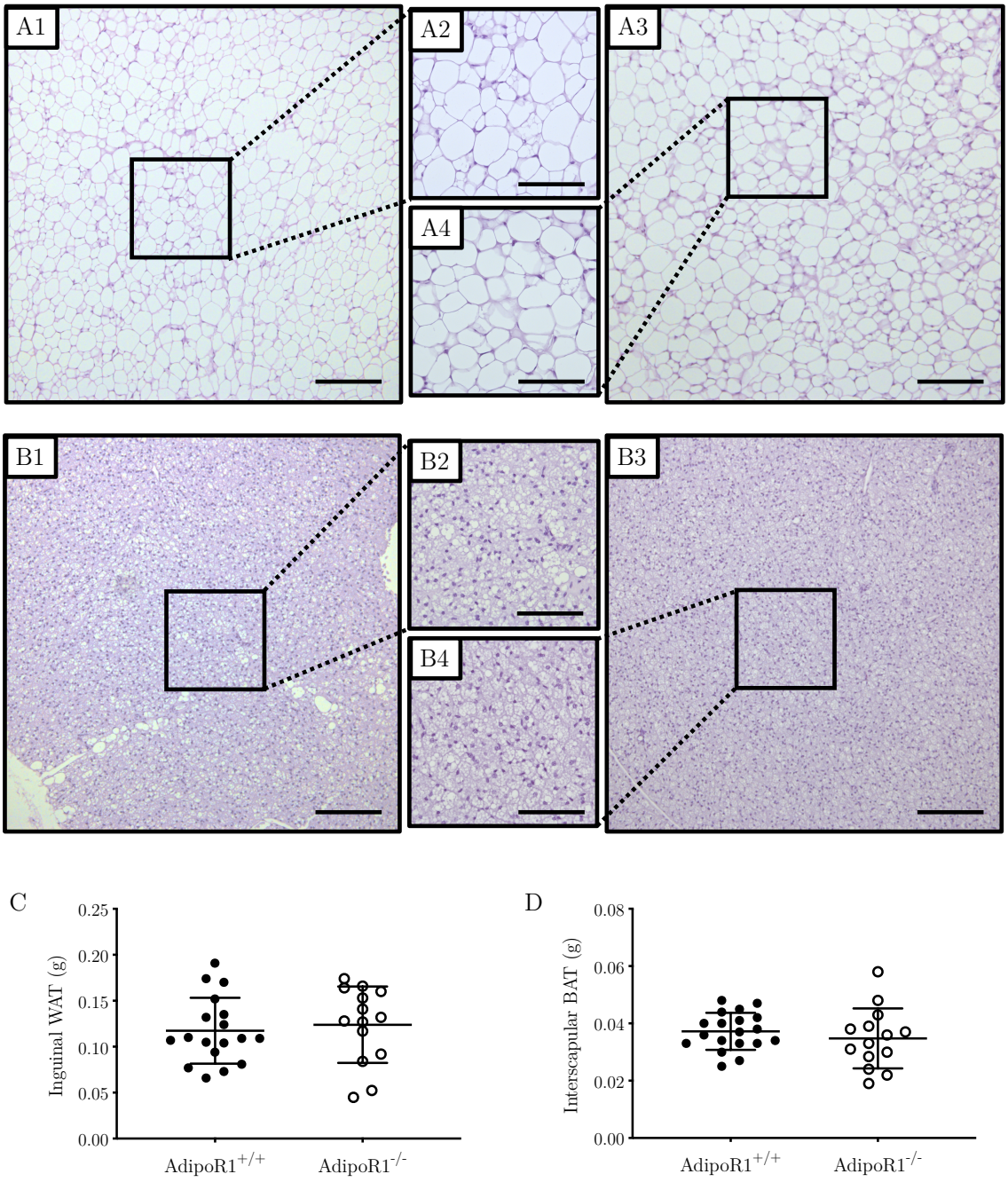


Figure 5.7: Young AdipoR1$^{-/-}$ female mice show no significant change in fat depot gross morphology or weight. Inguinal white adipose tissue (WAT) and interscapular brown adipose tissue (BAT) were excised, weighed and examined histologically by H&E staining; representative images shown. No immediately identifiable differences in the gross morphology of (**A**) inguinal WAT or (**B**) interscapular BAT were observed between four-week-old female (**1**, **2**) AdipoR1$^{+/+}$ and (**3**, **4**) AdipoR1$^{-/-}$ mice. The weight of the (**C**) inguinal WAT and (**D**) interscapular BAT depots were not significantly altered between four-week-old female AdipoR1$^{+/+}$ and AdipoR1$^{-/-}$ mice. Representative images shown. Scale bar: 200µm (**1**, **3**), 50µm (**2**, **4**); N=14-19 (biological replicates); data presented as mean±SD, N=14-19 (biological replicates); unpaired t-test, significance defined as $p \leq 0.05$.

5.2.2.5 Young AdipoR1$^{-/-}$ females show no significant difference in bone marrow plasma adiponectin concentration

Given the bone marrow-specific increased in adiposity in young AdipoR1$^{-/-}$ female mice, and bone marrow adipocytes being significant producers of adiponectin in the body[128], the concentration of local adiponectin in the bone marrow plasma was investigated in young AdipoR1$^{-/-}$ female mice despite no observed change in total circulating adiponectin (**Figure 5.1**). However, despite the observed increased bone marrow adiposity, no significant change in bone plasma adiponectin concentration was observed between young AdipoR1$^{-/-}$ females and age-matched AdipoR1$^{+/+}$ controls (**Figure 5.8**).

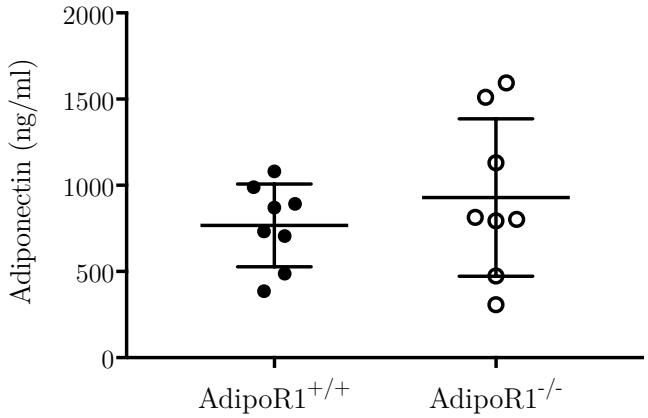


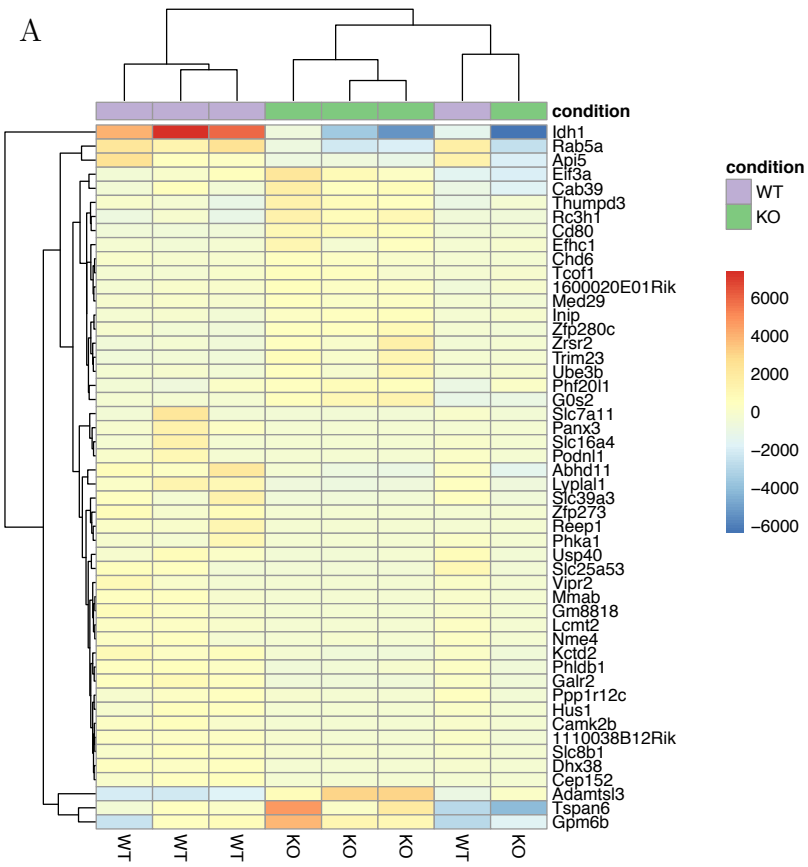
Figure 5.8: Young AdipoR1$^{-/-}$ females show no significant change in bone marrow plasma adiponectin concentration. Adiponectin concentration in the bone marrow plasma of four-week-old AdipoR1$^{+/+}$ and AdipoR1$^{-/-}$ females was analysed by ELISA. No significant difference was observed in AdipoR1$^{-/-}$ animals as compared with age-matched AdipoR1$^{+/+}$ controls. Data presented as mean±SD, N=8 (biological replicates). Unpaired t-test. Significance defined as $p \leq 0.05$.

5.2.3 RNASeq on primary MSCs

As AdipoR1$^{-/-}$ mice have been observed to have a significant increase in bone marrow adiposity alongside a significantly reduced bone volume, it was hypothesised that

alterations in mesenchymal stem cell (MSC) lineage commitment could underly these concurrent findings. To this end, primary MSCs, defined by a cell surface marker panel previously described to identify a progenitor population capable of giving rise to osteogenic progenitors and stromal marrow cells and supporting HSCs *in vivo*[55], were isolated by FACS from the bone marrow of four-week-old AdipoR1$^{+/+}$ and AdipoR1$^{-/-}$ mice before the RNA was amplified due to low cell number and subsequently sequenced via RNASeq (for full methods, see **Section 2.1.12**).

Figure 5.9A shows a heatmap of the top 50 differentially regulated genes in the MSCs of four-week-old AdipoR1$^{-/-}$ females and **Figure 5.9B** is a volcano plot showing the high and low gene expression in these cells. The principle component analysis (**Figure 5.9C**) shows significant variation between biological replicates. Pathway analysis of the differentially regulated genes did not suggest any candidate pathways that could underly the observed bone phenotype.



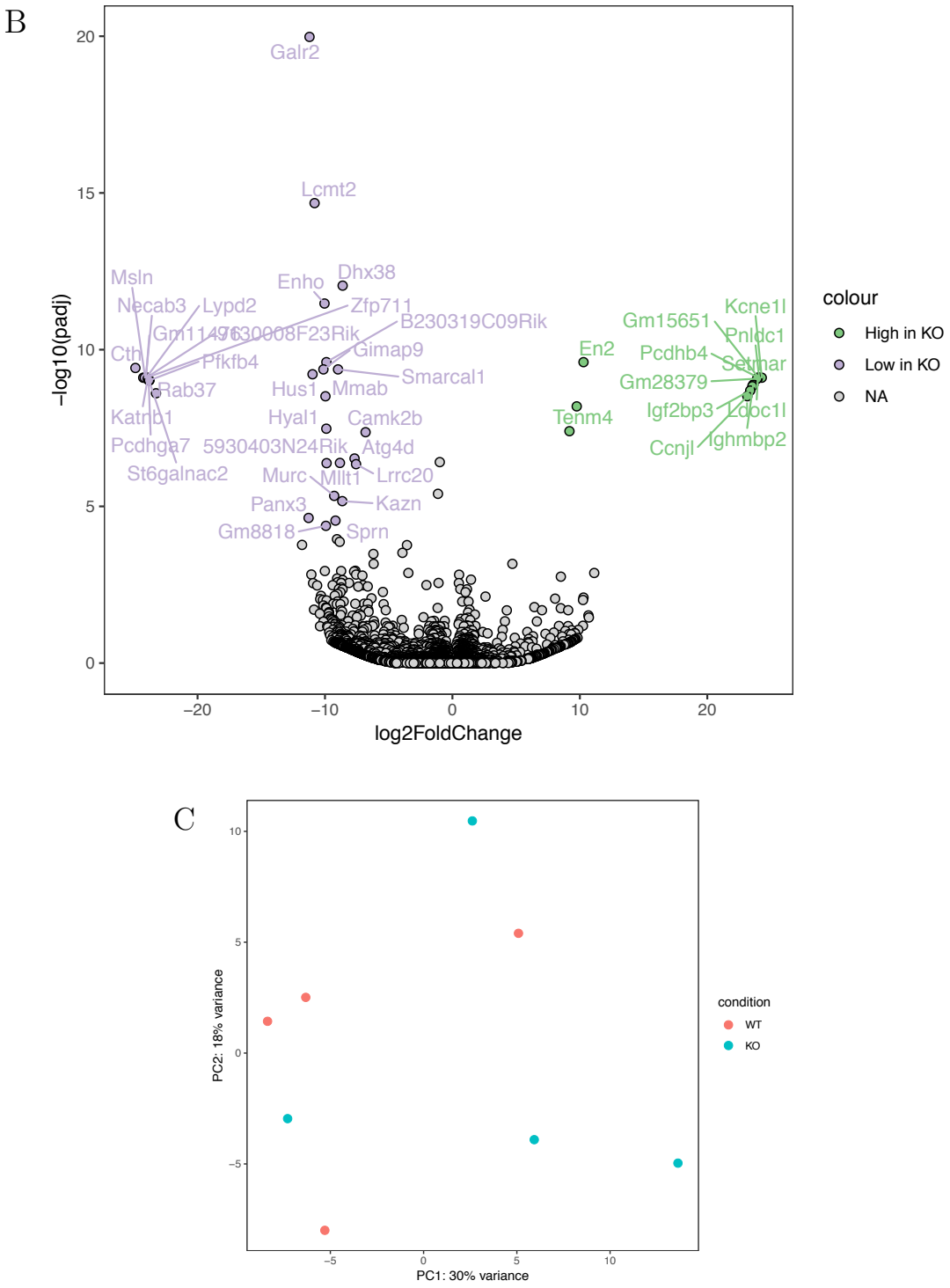


Figure 5.9: RNASeq of primary MSCs. (**A**) Heatmap showing the mean expression levels of the top 50 differentially expressed genes in four-week-old AdipoR1$^{-/-}$ female mice MSCs after p-value adjustment. (**B**) Volcano plot showing high (green) and low (pink) gene expression in four-week-old AdipoR1$^{-/-}$ female mice MSCs. (**C**) Principle component (PC) analysis showing expression variance between experimental replicates. N=4 per genotype (biological replicates). WT: AdipoR1$^{+/+}$, KO: AdipoR1$^{-/-}$.

5.2.4 Bone-extrinsic phenotyping of AdipoR1$^{-/-}$ females

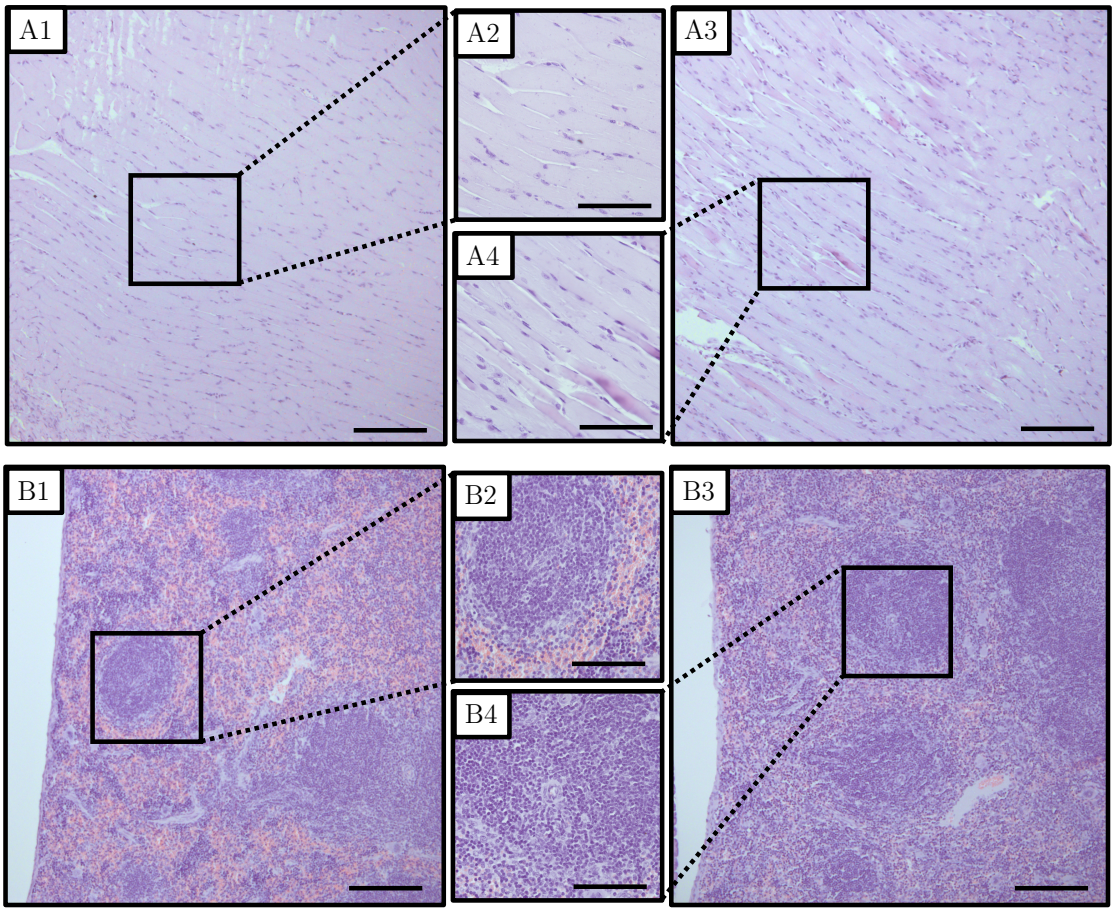
Thus far, young AdipoR1$^{-/-}$ female mice have been observed to show a delayed bone accrual by µCT analysis (**Figure 4.3**) and histologically by BFR analysis (**Figure 5.4**), a bone-marrow specific increases in adiposity (**Figure 5.7**) and altered circulating adiponectin oligomer concentrations (**Figure 5.2**) as compared with age- and sex-matched AdipoR1$^{+/+}$ controls. Despite this, no clear differences in serum analytes related to bone and fat were observed (**Figure 5.3**), and no significant pathway regulation was observed in RNASeq analysis of primary MSCs (**Figure 5.9**). It was subsequently hypothesised that due to the global knockout of AdipoR1 in these models, a bone-extrinsic effect could be mediating the observed bone phenotype indirectly. Bone-extrinsic phenotyping was performed, consisting of histological observation and blood serum analysis coupled with data collected by the IMPC.

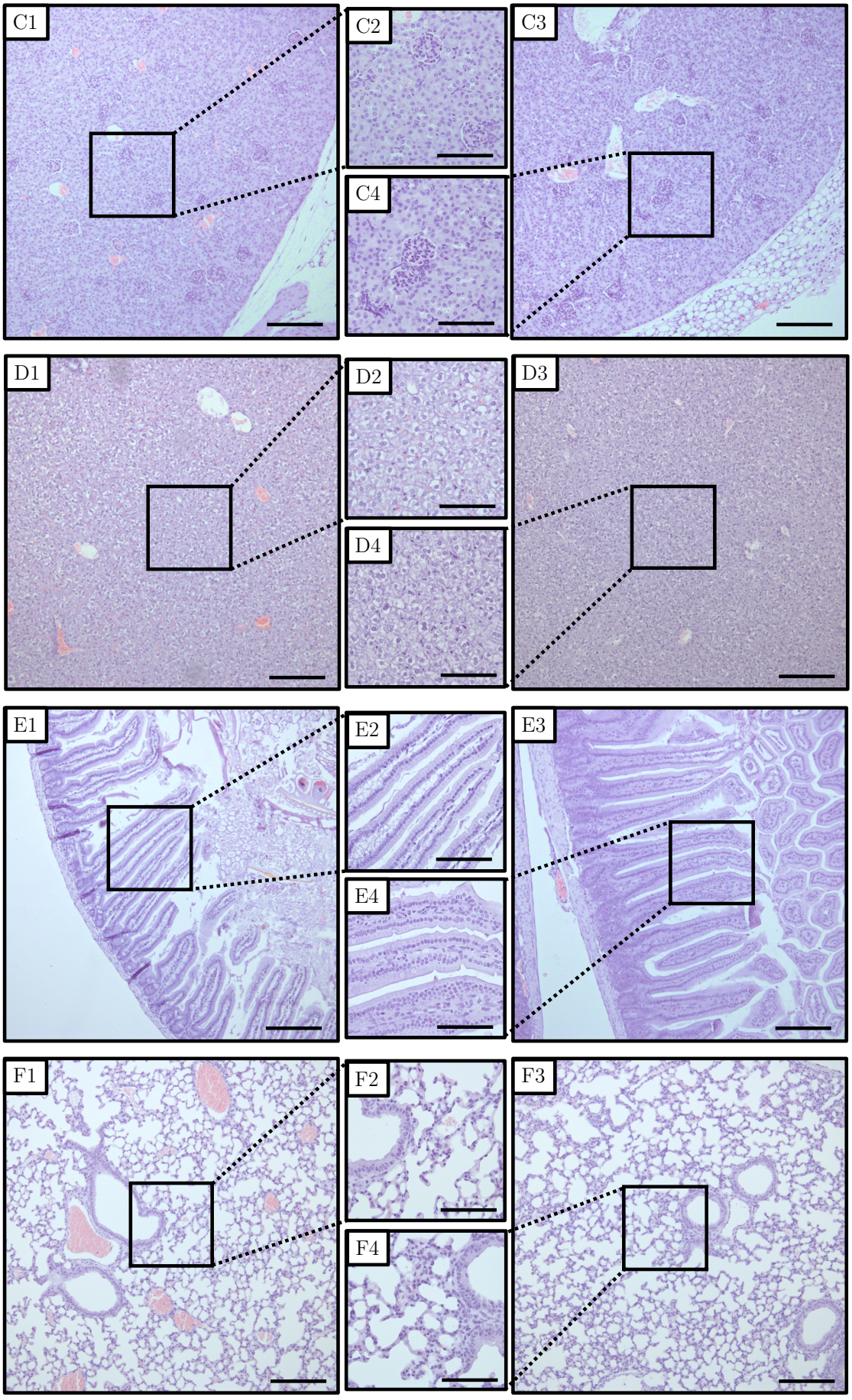
5.2.4.1 AdipoR1$^{-/-}$ females show no significant histological changes in a panel of soft tissues

A panel of soft tissues was excised from four-week-old female AdipoR1$^{+/+}$ (**Figure 5.10, 1 and 2**) and AdipoR1$^{-/-}$ (**Figure 5.10, 3 and 4**) mice for gross histological examination. Skeletal muscle (**Figure 5.10A**) was unchanged, with the typical myocyte morphology of long, large and multinucleated cells visible in the longitudinal sections from control and AdipoR1$^{-/-}$ mice. Splenic gross morphology was not significantly altered between models (**Figure 5.10B**) with both showing the typical thin connective tissue capsule and lymphatic nodules amongst the spleen pulp. The kidneys of both models show the same connective tissue capsule with healthy, intact glomeruli clearly visible (**Figure 5.10C**). Liver histology appeared unchanged by genotype (**Figure 5.10D**), although some

features of normal liver histology, like bile ducts and sinusoids, are difficult to distinguish at this magnification. A smooth and intact outer surface and a mucosal surface on which the villi are clearly visible were observed in the small intestine of both models (**Figure 5.10E**), and the models show similar lung histology (**Figure 5.10F**): larger bronchioles surrounded by vacuoles. Finally, cardiac tissue appeared similar between AdipoR1$^{+/+}$ and AdipoR1$^{-/-}$ mice (**Figure 5.10G**) with the two layers of cardiac tissue, the internal endocardium composed of connective tissues and smooth muscle and the thicker myocardium composed of cardiac muscle, both clearly visible.

Overall, identifiable features appear to be of a similar size between AdipoR1$^{+/+}$ and AdipoR1$^{-/-}$ mice in all tissues studied, with no obvious signs of gross morphological change, like abnormal development indicated by grossly altered size or shape of the organ or its cells, abnormal depositions or significant immune infiltration.




C1
C2
C3
C4
D1
D2
D3
D4
E1
E2
E3
E4
F1
F2
F3
F4

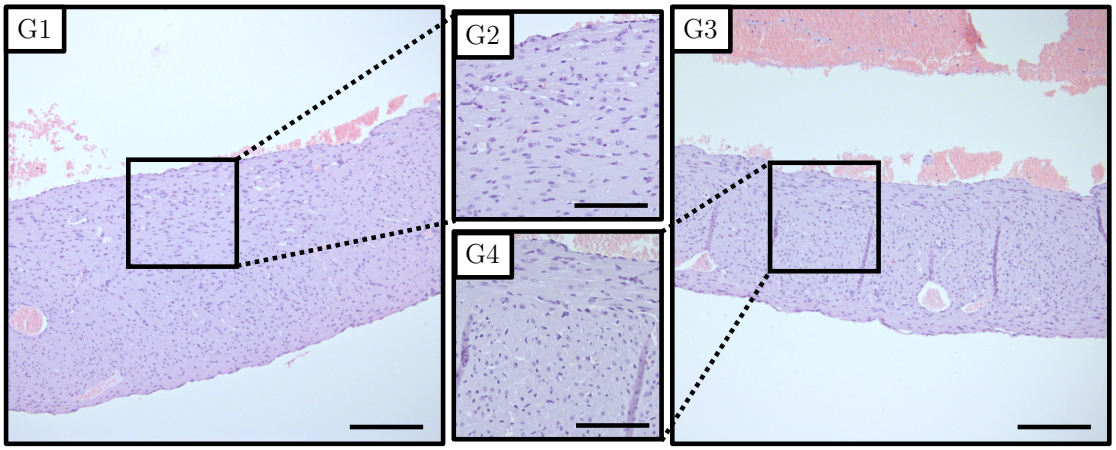


Figure 5.10: AdipoR1$^{-/-}$ females show no clear gross morphological changes in a panel of soft tissues. (**A**) Muscle, (**B**) spleen, (**C**) kidney, (**D**) liver, (**E**) small intestine, (**F**) lung and (**G**) heart were excised from four-week-old female AdipoR1$^{+/+}$ (**1**, **2**) and AdipoR1$^{-/-}$ (**3**, **4**) mice and show no clear phenotypic differences. Representative images shown, scale bar 200µm (**1**, **3**), 50µm (**2**, **4**).

5.2.4.2 AdipoR1$^{-/-}$ females have significantly altered blood chemistry profiles

Bone-extrinsic phenotyping continued making use of phenotyping data collected by the IMPC. Blood chemistry profiles were produced from 7-10 AdipoR1$^{-/-}$ female mice compared with a large bank of phenotypic data from sex- and strain-matched AdipoR1$^{+/+}$ controls (n=1500-2000). This large phenotypic screen identified reduced circulating levels of analytes directly or indirectly related to bone formation and maintenance: as compared with controls, AdipoR1$^{-/-}$ females had significant reductions in circulating serum calcium (**Figure 5.11A**) and serum alkaline phosphatase (**Figure 5.11B**), but significantly increased serum phosphorus (**Figure 5.11C**), total cholesterol (**Figure 5.11D**) and high density lipoprotein (HDL, **Figure 5.11E**).

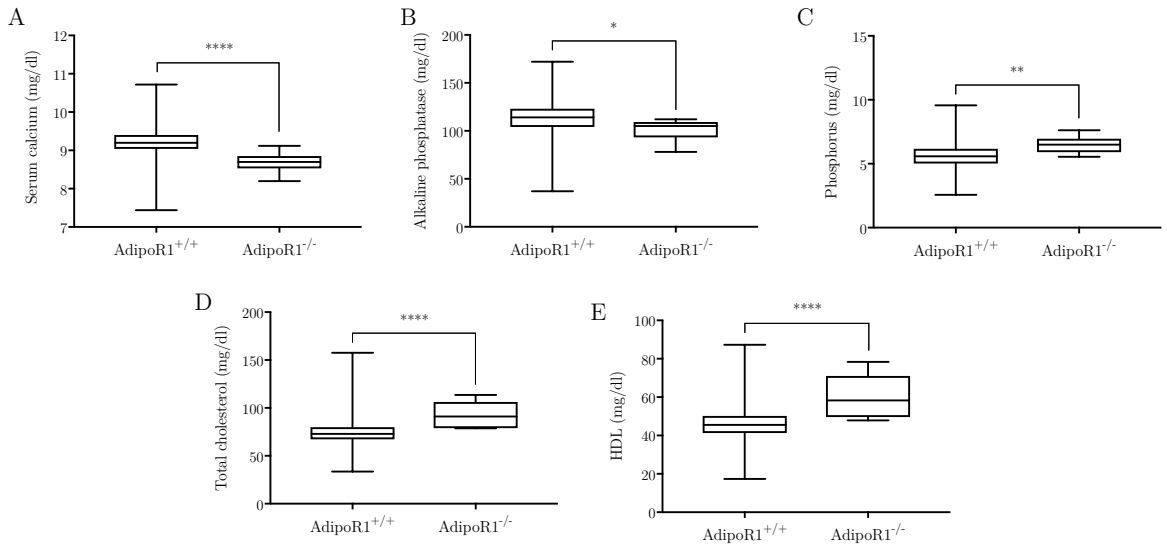


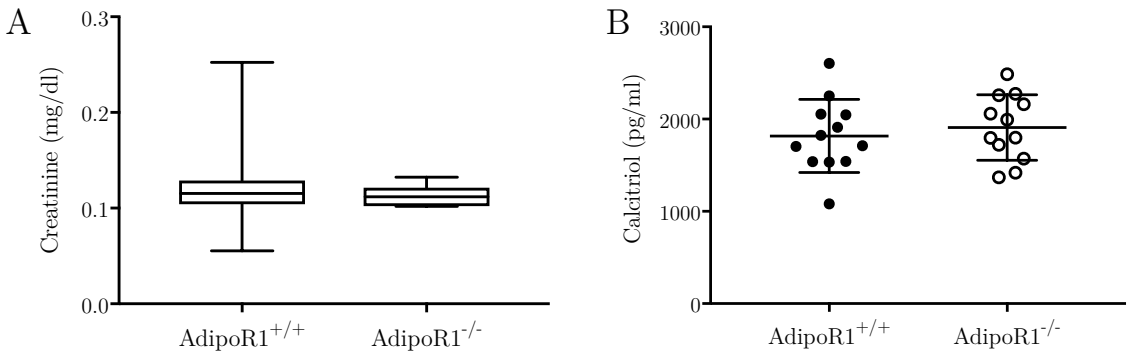
Figure 5.11: AdipoR1$^{-/-}$ females show significant differences in blood chemistry. Circulating blood serum concentrations in AdipoR1$^{-/-}$ females showed reduced (**A**) calcium and (**B**) alkaline phosphatase with significantly increased circulating (**C**) phosphorus, (**D**) total circulating cholesterol and (**E**) total high-density lipoprotein (HDL). Data taken from IMPC; AdipoR1$^{+/+}$: n=1500-2000, AdipoR1$^{-/-}$: n=7-10 (biological replicates); data presented as median±interquartile range with error bars showing maximum to minimum range. Unpaired t-test, *=p≤0.05, **=p≤0.01, ****=p≤0.0001.

5.2.4.3 AdipoR1$^{-/-}$ females show no further evidence of chronic kidney disease or hypoparathyroidism

The significant reductions in calcium, phosphate and alkaline phosphatase in the blood fit with the reduced bone phenotype previously observed. These reductions, suggestive of a metabolic issue with mineral homeostasis, coupled with increased circulating cholesterol, suggestive of an issue affecting cholesterol clearance, together suggest a wider metabolic problem. Clinically, similar altered blood chemistry profiles suggest a kidney- or parathyroid-related problem, but further parameters would need to be measured for a diagnosis. Kidney disease is associated with increased creatinine levels due to its insufficient renal excretion and its circulating levels are a commonly used clinical correlate of glomerular filtration rate[333]. Changes in calcitriol, the biologically active form of vitamin D, are associated with altered bone metabolism via the PTH-vitamin D-

FGF23 axis (see **Section 1.1.4**); indeed, its administration has been suggested for the clinical management of osteoporosis[334]. Sclerostin is an inhibitor of osteoblastic bone formation via inhibition of the Wnt signalling pathway, and its increased circulating levels are associated with fracture risk in osteoporotic patients[335]. However, sclerostin concentrations have recently been described to be increased in CKD as well, with the increased sclerostin concentration associated with the onset of cardiovascular and skeletal changes, and a return to normal levels in more advanced CKD, implicating it as an indicator of early CKD development[336].

To this end, serum concentrations of creatinine collected by the IMPC (**Figure 5.12A**) and serum calcitriol (**Figure 5.12B**) and sclerostin (**Figure 5.12C**) concentrations determined by ELISA were analysed but showed no significant differences between AdipoR1$^{+/+}$ and AdipoR1$^{-/-}$ females, suggesting no significant kidney- or parathyroid-related issue is present. However, osteocalcin serum concentrations were significantly reduced in AdipoR1$^{-/-}$ females as compared with AdipoR1$^{+/+}$ controls (**Figure 5.12D**).



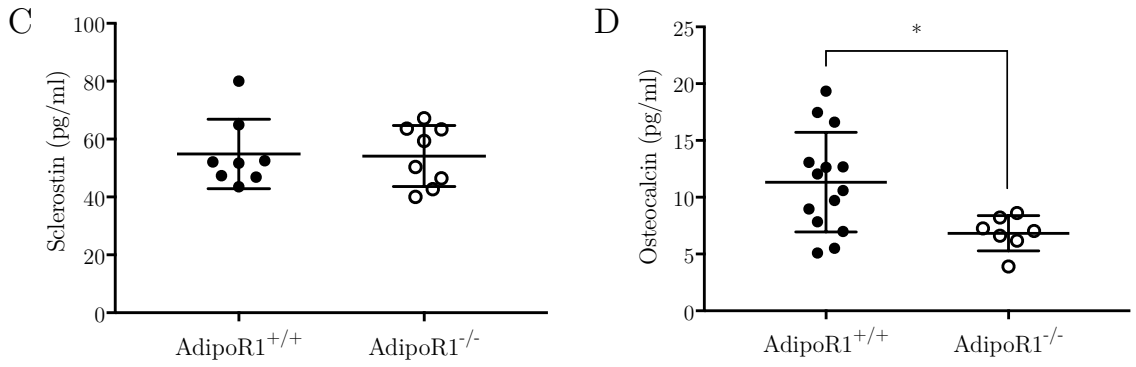


Figure 5.12: AdipoR1$^{-/-}$ females show no further evidence of chronic kidney disease (CKD) or hypoparathyrodism. (**A**) AdipoR1$^{-/-}$ females show no significant change in circulating creatinine concentration as compared with age- and sex-matched AdipoR1$^{+/+}$ controls. Data taken from IMPC; AdipoR1$^{+/+}$: n=1972, AdipoR1$^{-/-}$: n=8 (biological replicates); data presented as median±interquartile range with error bars showing maximum to minimum range; significance defined as p≤0.05. (**B**) AdipoR1$^{-/-}$ females show no significant change in circulating calcitriol concentration as compared with age- and sex-matched AdipoR1$^{+/+}$ controls by ELISA. (**C**) AdipoR1$^{-/-}$ females show no significant change in circulating sclerostin concentration as compared with age- and sex-matched AdipoR1$^{+/+}$ controls by ELISA. (**D**) AdipoR1$^{-/-}$ females show a significant reduction in circulating osteocalcin concentration as compared with age- and sex-matched AdipoR1$^{+/+}$ controls. (**B-D**) Data presented as mean±SD, N=8-14 (biological replicates). Unpaired t-test, *=p≤0.05.

5.3 Discussion and conclusions

The work in this chapter aimed to characterise further the phenotype of AdipoR1$^{-/-}$ female mice, investigating the possibility of bone intrinsic and bone extrinsic mechanisms. The young AdipoR1$^{-/-}$ mice, which showed no significant changes in osteoblast or osteoclast parameters but an increased bone marrow adiposity by histology alongside a low bone phenotype by µCT in the previous chapter, showed no alteration in their total circulating adiponectin level, but a significant decrease in the proportion of LMW adiponectin. The biological implications of this phenotype were intriguing, and further work in this chapter focussed on the investigation of these four-week-old animals only. The reduced bone formation rate determined by calcein labelling of the lumbar spine and a reduced circulating osteocalcin concentration confirmed the retarded bone accrual identified by µCT analysis (**Figure 4.3**) and suggests osteoblast function could

be affected despite osteoblast number, and therefore differentiation, considered to be unaffected in AdipoR1$^{-/-}$ animals as determined by histological analysis of osteoblast parameters (**Figure 4.6**). Osmium tetroxide staining provided objective quantification of the increased bone marrow adiposity previously observed by histology (**Figure 4.8**). A bone-intrinsic mechanism was sought using RNASeq of primary MSCs, while significant alterations in the blood chemistry profile of these animals suggest a significant contribution of a systemic indirect mechanism to the bone phenotype. Together, these results suggest alterations to adiponectin signalling via knockout of AdipoR1 has complex effects in young female mice, possibly mediated locally and systemically.

Total circulating adiponectin concentration has been observed to correlate negatively with several pathological states including diabetes and obesity (see **Section 1.3.3**). In keeping with other findings from wild type C57Bl/6 mice[317], serum adiponectin concentration in adult mice was found to be around 15-20µg/ml. As compared with age-matched controls, only the 24-week-old female AdipoR1$^{-/-}$ mice showed a significant alteration in total circulating adiponectin level. Given that this age group alone showed no significant bone phenotype by µCT in the previous chapter (**Figure 4.3**), the observed increase in blood serum adiponectin concentration could suggest that a compensatory increase in circulating adiponectin levels is necessary for these animals to overcome the retarded bone formation rate seen at a younger age. Interestingly, a significant correlation was observed between rMAT volume and adiponectin concentration in young AdipoR1$^{-/-}$, but not control, animals. This correlation implicates rMAT as a significant producer of adiponectin and the lack of correlation in controls suggests AdipoR1 knockout could disrupt a negative local feedback loop between AdipoR1 signalling and rMAT expansion in these young animals.

The ratio between the adiponectin oligomers has also been described to be affected by disease and even have direct correlation with treatment response (**Section 1.3.3**),

justifying examination of the relative contribution of HMW, MMW and LMW adiponectin to total adiponectin concentration. Disruption of AdipoR1 signalling in young female mice was found to be associated with a significant decrease in the proportion of LMW adiponectin and a significant increase in MMW adiponectin contribution. The biological significance of this shift in oligomeric ratios remains unknown, but AdipoR1 has been identified as a high affinity receptor for globular and LMW adiponectin and a low affinity receptor for MMW and HMW adiponectin[150], so these results could suggest a local positive feedback loop between AdipoR1 signalling and LMW adiponectin production by adipocytes of the bone microenvironment. Given the observation that an increase in circulating LMW adiponectin is positively associated with diabetes duration[213], future work should seek to clarify the fasted blood glucose concentration and performance during a glucose tolerance test of these young female AdipoR1$^{-/-}$ mice in order to begin to determine the practical implications of the observed differences. In addition, while the significance of altered circulating HMW adiponectin has been relatively well reported[212–214,317] and LMW contribution has been associated with disease pathology[211,213], the specific biological significance of altered MMW adiponectin concentration is unstudied. It is possible that its significant increase is more biologically relevant in this paradigm than the reduction in LMW adiponectin, but this remains unknown.

It was hypothesised that the bone marrow-specific increase in adiposity and low bone mass phenotype in these young animals could be due to the loss of AdipoR1 signalling altering lineage determination in bone-resident MSCs, skewing them towards adipogenesis and away from osteoblastogenesis. RNASeq of these cells revealed that some genes are differentially regulated in AdipoR1$^{-/-}$ mice, although the samples showed such intra-condition variation that they did not group by genotype in principle component analysis. This degree of biological variation between replicates means

interpretation of the resulting data is difficult such that no stringent conclusions can be drawn from them, and suggests that many more biological replicates would be needed in order to determine accurately the effect of AdipoR1 deletion on the expression profile of murine MSCs. Equally, these cells were defined as MSCs based on FACS sorting using previously published cell surface marker panel[55]; future work should confirm the MSC nature of these cells, either via lineage tracking *in vivo* to observe bone and adipose tissue formation from these cells, or by confirming their osteoblastic and adipogenic differentiation capacity *in vitro*. Expansion of the experimental protocol to other cells of the bone microenvironment, such as osteoblasts, may permit better characterisation of the cell-intrinsic effects of AdipoR1 knockout.

Despite these considerations and the lack of a candidate mechanism from pathway analysis, significant differential regulation of some genes is noteworthy due to their suggested involvement in osteoblast or adipocyte differentiation or function. The most highly differentially regulated gene in primary AdipoR1$^{-/-}$ MSCs is Galr2, which encodes GALR2, one of three GPCRs for galanin (GAL). GAL is a 29-30 amino acid peptide that is widely distributed in many tissues including in the central and peripheral nervous system[337], in the ligament and joint capsule[338], and in the bone marrow and cortical bone[339]. GAL and its receptors have been most significantly implicated in the central nervous system, with reported effects on regulation of neuroendocrine functions, mood and neuroinflammation[340]. In 2003, Grills *et al* reported that GAL expression was significantly upregulated in the callus of a healing rib fracture in rats as compared to baseline expression in nonfractured rib[341], implicating GAL in fracture repair for the first time. Four years later, the same group investigated the role of GAL in bone formation and bone cell expression of TNFα and GALR2 in a mouse model in which daily subcutaneous injection of a glycerol-containing vehicle onto the calvaria was used as a model of repeated mild injury[342]. Vehicle injection reduced osteoblast height and number

histologically as compared with non-injected animals, but this inhibition of osteoblasts was rescued dose-dependently following exogenous GAL treatment. Exogenous GAL treatment did not affect calvarial expression of GAL but it significantly reduced expression of Galr2, matrix metalloproteinase (MMP) 13, TNFα and IL-1β as compared with vehicle-treated control. It was concluded that GAL treatment offset the inhibition of osteoblastic activity induced by the vehicle control at least in part via its suppression of TNFα, IL-1β and MMP-13 expression and via upregulation of GALR2[342]. These results suggest a direct effect of GAL signalling via GALR2 in osteoblast-like cells to promote osteoblastic differentiation and function and that the significant downregulation of Galr2 expression in MSCs from AdipoR1$^{-/-}$ mice could underly their retarded bone formation capacity.

The energy homeostasis associated (Enho) gene encodes adropin, a peptide hormone first described in 2008 and now understood to have roles in energy homeostasis and fatty acid metabolism. Adropin overexpression is associated with reduced insulin resistance and a reduced build-up of incomplete fatty acid oxidation products in diet-induced obese mice[343] and its global deletion led to increased whole body adiposity[344]. The significant downregulation of Enho expression in the MSCs of AdipoR1$^{-/-}$ mice could underly the increased bone marrow adiposity observed. Interestingly, suppression of the intracellular recycling pathway autophagy in osteocytes has recently been described to mimic skeletal aging, with osteocyte-specific Atg7-deficient mice showing reduced osteoblast number, bone formation rate and cortical thickness[345], and the induction of autophagy has been described to regulate rat mesenchymal stem cell differentiation[346]. Together, these data indicate that the significant downregulation of Atg4d expression in AdipoR1$^{-/-}$ MSCs could be a significant mechanism regulating the bone phenotype of these animals, but the role of Atg4d is yet to be determined in cells of the bone microenvironment, warranting future investigation. Finally, AdipoR1 knockout is associated with

significantly increased expression of leucine zipper, down-regulated in cancer-1 (Ldoc1), which is widely reported as a tumour suppressor gene that is downregulated in some cancers[347–349]. Ldoc1 expression is associated with reduced Wnt5a expression in a human osteosarcoma cell line[350], and Wnt5a heterozygous deficient mice show increased bone marrow adiposity and reduced osteoblastogenesis[24]. Although the exact role of Ldoc1 in the bone microenvironment *in vivo* is yet to be determined, its upregulation in this RNASeq analysis provides another candidate mechanism for the bone phenotype observed in these mice.

How AdipoR1 deletion leads to this differential gene expression profile is yet to be determined since no previously characterised AdipoR1-responsive genes were found to be differentially regulated in this RNASeq analysis. This probably suggests that AdipoR1 signalling is distinct in this cell type or that AdipoR1 is not very active in this experimental setup. Therefore, while future work could seek to validate the discussed genes as candidate mechanisms by which AdipoR1 exerts its effects, at least in part, in MSCs of the bone microenvironment, it is suggested that a similar investigation in other cells of the bone microenvironment will be critical for further understanding.

It was next considered that the bone phenotype was mediated by a bone-extrinsic, systemic mechanism as suggested by the significant alterations in the blood chemistry profile of these animals as reported by the IMPC and in accordance with previously published evidence of opposing central and peripheral mechanisms of adiponectin action in bone[96]. Investigation of bone- and fat-related phenotypes through use of a screen of blood analytes identified very few genotype-related alterations: a significant increase in circulating OPN concentration in aged AdipoR1$^{-/-}$ animals is consistent with an observed low bone volume in these animals by µCT (**Figure 4.3**) and the lack of alteration in the RANKL/OPG axis in either age group corroborates the previously observed lack of a significant osteoblast or osteoclast phenotype by histology (**Figures 4.6** and **4.7**). Aged

animals also showed a significant increase in circulating leptin concentration, but leptin concentration remained unchanged in four-week-old female mice, possibly supporting the finding that WAT depot size is not increased in these young animals. Aside from these genotype-related findings, the significant differences in age-related changes in AdipoR1$^{+/+}$ as compared with AdipoR1$^{-/-}$ animals were observed, suggesting genotype-influenced alterations in these analytes do occur over time. It is suggested that further work is performed before firm conclusions are drawn from these results. In particular, the use of overnight fasted samples and a standardised sample collection time could provide more accurate and useful results. Food intake, and subsequently blood glucose and insulin levels, and circadian rhythms of the release of these analytes could affect the results collected; for example, the circulating level of the satiety-related hormone leptin in rats is reduced during fasting and increases post-prandially and exhibits a diurnal variation, increasing at night when rodents naturally feed[351].

The effect of food intake in these mice could be important given the roles of adiponectin signalling in the central nervous system to regulate food intake and energy expenditure via AMPK activation in the hypothalamus. Male adiponectin knockout mice have been observed to have decreased AMPK phosphorylation in the hypothalamus, decreased food intake and increased energy expenditure[352]. This AMPK activation was found to be mediated by AdipoR1: siRNA-mediated knockdown of AdipoR1 expression reduced hypothalamic AMPK phosphorylation where AdipoR2 knockdown did not, and fasting conditions increased AdipoR1 expression in the hypothalamus of wild type mice where AdipoR2 expression was unaffected[352]. Given the implication of AdipoR1 in this paradigm, it is possible that this phenotype persists in AdipoR1-deficient mice. A small reduction in total body weight in four-week-old male and female animals could indicate decreased food intake and/or increased energy expenditure as compared to controls, but this phenotype does not persist throughout life, with adult and aged animals showing no

significant change in body weight, and four-week-old females show no change in WAT or BAT depot mass.

Future work could seek to clarify whether a phenotype associated with food intake is present in these mice, and it is likely that controlling for these possible interactions by use of fasted serum for blood analyte screens is an important next step in interpreting these results. It should also be considered that several of the factors investigated in this screen are not bone-specific, meaning that significant alterations in their local concentrations may not be reflected by significant changes in their overall serum content. Future work could aim to clarify the local concentration of these analytes in the bone marrow plasma to obtain a clearer idea of the local effects of AdipoR1 deletion.

Clinically, significant alterations in blood phosphate and calcium concentrations are likely to be indicators of a problem with the parathyroid or the kidney given their role in mineral homeostasis (see **Section 1.1.4**). These AdipoR1$^{-/-}$ mice displayed hyperphosphatemia and hypocalcaemia, but normal blood sclerostin and creatinine concentrations indicate CKD is not present. This is supported by the observation of a self-resolving phenotype, with adult AdipoR1$^{-/-}$ females showing normal peak bone mass (**Figure 4.3**), and young mice showing a normal kidney histology with lack of an irregular surface due to atrophy as is seen in CKD mouse models by H&E[353], although future work could confirm this by further histological analysis of the kidney to determine whether inflammatory infiltration and fibrotic changes are present.

Although spontaneous resolution of hypoparathyroidism is rare, its clinical occurrence has been reported[354], and it also presents with hyperphosphatemia and hypocalcaemia[355]. Unlike in the kidney, where AdipoR1 expression has been reported in many of the cell types of the glomerulus[356], expression of the adiponectin receptors in the parathyroid gland has not been definitively reported or studied but transcriptomic analysis of human tissues compiled in the Human Protein Atlas, which aims to map the expression of all

protein in human cells and tissues, suggests AdipoR1 is expressed in the parathyroid gland to approximately the same level as it is in the kidney[162]. This suggests that global AdipoR1 deletion could have direct impacts on parathyroid gland function, but the reduced circulating level of calcitriol classically observed in hypoparathyroidism[357] was not observed in these mice, suggesting a parathyroid-regulated mechanism may not be significantly involved. It remains worth considering that the use of non-fasted serum could have masked a significant biological effect of AdipoR1$^{-/-}$ on calcitriol concentration: increases in blood calcium and phosphate following their post-prandial intestinal absorption will inhibit calcitriol synthesis[358] and calcitriol has a very short half-life of around 24 hours meaning that recent influences such as food intake will have an acute impact on circulating levels[359]. Future work should seek to clarify calcitriol and PTH levels in fasted serum and to establish whether the parathyroid gland shows any histological changes in a larger cohort of young AdipoR1$^{-/-}$ female mice in order to better understand the role of the PTH/calcitriol system on the whole-body metabolism of these mice.

In summary, the results presented in this chapter confirm the significant bone phenotype of young AdipoR1$^{-/-}$ female mice, but suggest that the mechanism, or mechanisms, mediating these effects is complex. The differential regulation of some candidate genes in the MSCs of AdipoR1$^{-/-}$ mice suggest bone-intrinsic changes following AdipoR1 knockout but failed to provide a candidate mechanism, and some whole-body alterations in the AdipoR1$^{-/-}$ blood chemistry profile were also observed (**Figure 5.13**). These local and systemic effects of altered adiponectin signalling via AdipoR1 ablation must be considered due to the global nature of the AdipoR1 knockout and the ubiquitous expression of AdipoR1 throughout the body.

Given the complex nature of this phenotype and the difficulties it poses in identifying candidate mechanisms underlying it, future work could utilise cell-specific knockout

models which will more accurately reflect the effect of adiponectin receptor deletion from relevant cell types and avoid issues caused by global deletion of AdipoR1$^{-/-}$. The most commonly used system of targeted gene deletion involves crossing a mouse in which the target gene to be ablated is surrounded by LoxP sites ('floxed') with a mouse in which expression of Cre recombinase is under the control of a cell-specific promoter[360]. This ensures the expression of Cre recombinase, and subsequently the excision of the target gene, specifically in the cells expressing the cell-specific marker: in particular, osteoblast-specific knockout of AdipoR1, for example using an osteocalcin-Cre system[361], is suggested for use here.

Osteoblast-specific ablation of AdipoR1$^{-/-}$ would limit the phenotype observed to bone-intrinsic effects, eliminating the confounding consideration of whole-body effects. Given the variety of biological functions to which adiponectin contributes and the ubiquitous nature of AdipoR1 expression throughout the body (**Section 1.3**), an osteoblast-specific knockout model would provide a powerful tool for more focussed investigation of this paradigm. By simplifying the model in this way, questions that can't be examined using the global knockout models presented here can be investigated; the direct effect of abrogated AdipoR1 signalling in osteoblasts on phenotypic features such as osteoblast differentiation and function, bone volume and bone marrow adiposity when all other cell types are expressing AdipoR1 as normal could be analysed, potentially facilitating mechanistic investigating in a manner not possible in the current model. Previous work using osteoblast-specific knockout of AdipoR1 in 12-week-old male mice on a C57Bl/6 J:129/Sv background has found no significant bone phenotype[96], although recapitulation of this work in these four-week-old C57Bl/6 female mice is suggested. Other conditional knockout models are considered further in **Section 7.2.2**.

Here, it was hypothesised that use of a simplified *in vitro* model of AdipoR1 manipulation in bone cells could produce a clearer understanding of the mechanistic effect of AdipoR1 knockdown or stimulation.

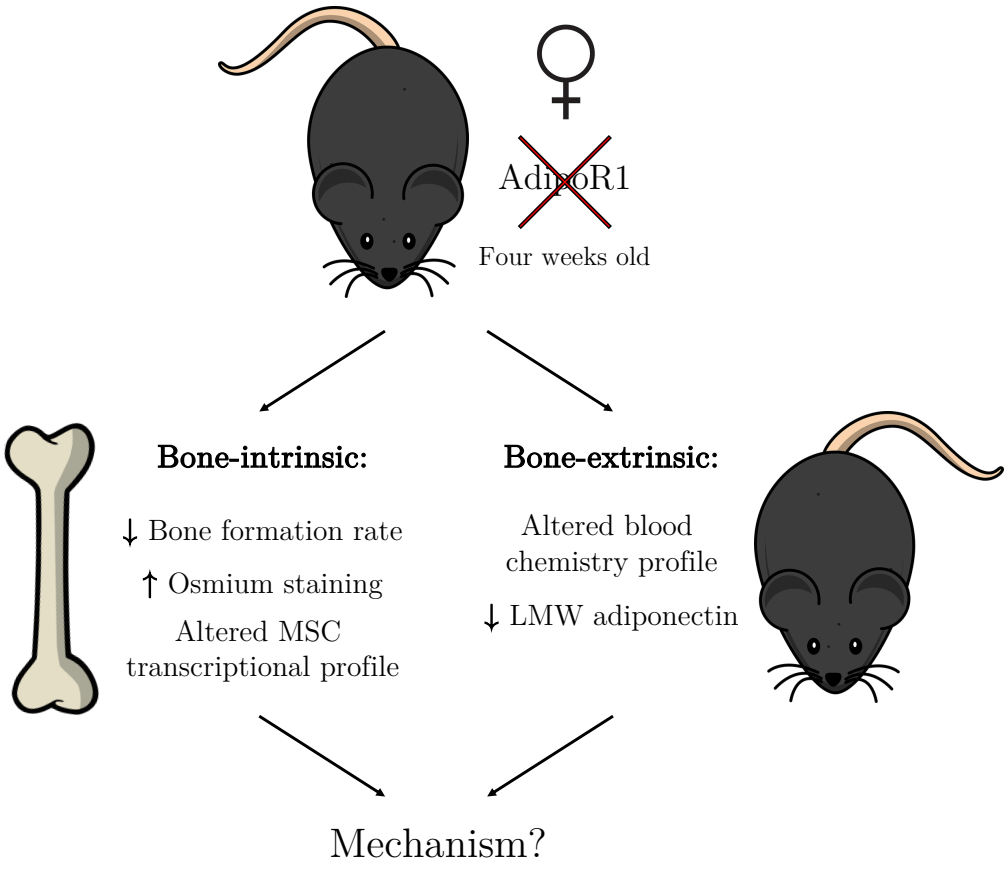


Figure 5.13: Summary of Chapter 5 key findings. Four-week-old AdipoR1$^{-/-}$ female mice are confirmed to have a significant retardation of bone formation accompanied by an increase in bone marrow adiposity. The altered transcriptional profile of MSCs suggests some candidate mechanisms for these bone-intrinsic effects of AdipoR1 deletion. Bone-extrinsic, whole-body effects are also observed, with AdipoR1$^{-/-}$ mice showing significantly altered blood chemistry profiles. The complexity of the effect caused by global AdipoR1$^{-/-}$ prevented significant insight into the mechanism underlying this phenotype. A simplified *in vitro* model is sought instead.

6

In Vitro Manipulation of AdipoR1 in Cells of the Bone Microenvironment

6.1 Introduction

6.1.1 *In vitro* cell culture and the use of cell lines

In vitro investigation of complex biological paradigms is often a starting point for the investigation of a mechanism of action. As compared with *in vivo* models, *in vitro* cell culture is quicker and cheaper, allowing high throughput screening if desired, and permitting control and manipulation of many factors that can influence cell behaviour, including cell confluency and levels of oxygen and glucose. Effects of drug treatment can be directly assessed without consideration of bioavailability or the ethical limits of repeated treatment, and the use of immortalised cell lines capable of indefinite proliferation theoretically provides a homogenous group of cells in which to work, reducing the complexity of the system being studied.

The following chapter makes use of two mouse cell lines: pre-osteoblastic 2T3 cells, and stromal ST2 cells. Given their pre-osteoblastic state, 2T3 cells were used for investigation of osteoblast-related gene expression and mineralisation. ST2 cells are bone marrow-derived stromal cells capable of differentiating to osteoblasts[362] or adipocytes[363]; in this study, they were used for investigation of osteoblast- and adipocyte-related gene expression and adipogenesis.

6.1.2 AdipoRON

AdipoRON is an orally bioavailable small molecule agonist of the adiponectin receptors. First described in 2013[223], it binds to both adiponectin receptors, although with a slightly higher affinity for AdipoR1 (K_D=1.8μM) than AdipoR2 (K_D=3.1μM), and has been characterised to show similar effects to adiponectin, including activation of the AMPK and PPARα pathways[223] at concentrations upwards of around 10μM.

6.1.3 Gene markers of osteoblastic and adipocytic differentiation

The process of osteoblastic or adipogenic differentiation can be followed by the assessment of expression of key genes. Runx2, also known as Cbfα1, is the primary molecular switch for commitment to the osteoblast line; its enforced overexpression is sufficient for osteoblastic differentiation of bone marrow stromal cells and bone formation both *in vitro* and *in vivo*[11] and its *in vivo* deletion prevents ossification[12]. Following commitment to the osteogenic line, cells undergo a three-stage differentiation process[10]. In stage 1, cells continue to proliferate, expressing early markers including collagen type I α-1 (Col1a1) and osteopontin (OPN), both structural components of bone[10]. Stage 2

involves the induction of differentiation and maturation of the extracellular matrix, marked by continued collagen production and the induction of alkaline phosphatase (ALPL) to facilitate mineralisation. Finally, during stage 3, late osteoblastic markers are expressed, particularly osteocalcin (OCN), which is involved in matrix maturation and is thought to act as an inhibitor of bone formation to prevent excessive bone production[10,364].

Adipogenic differentiation is marked by expression of peroxisome proliferator-activated receptor γ (PPARγ) and the CCAAT/enhancer binding proteins (CEBPs) such as CEBPα. Both of these genes are used here as early markers of adipogenesis[365]. Adiponectin expression, accompanied with other proteins such as fatty acid synthase (FAS) which are not tested, is responsible for the maturation of adipocytes and represents a late adipogenic marker here[365].

6.1.4 Chapter aims and hypothesis

The work presented in this chapter aimed to reproduce *in vitro* the *in vivo* phenotype of low bone volume coupled with high bone marrow adiposity described in the female AdipoR1$^{-/-}$ mice in the previous chapters. It was hypothesised that manipulation of adiponectin signalling *in vitro* would produce effects mirroring those observed *in vivo*, with addition of an exogenous agonist hypothesised to promote osteoblastogenesis and mineralisation, and stable knockdown of AdipoR1 expression hypothesised to inhibit or reduce these effects, permitting use of this model in mechanistic investigation. While it is acknowledged that a faithful recapitulation of the *in vivo* phenotype is not possible due to the exclusion of the bone-extrinsic effects discussed in the previous chapter, a simplified cellular model is used to shed light on the mechanism by which adiponectin exerted its local effects on cells of the bone microenvironment.

6.2 Results

Manipulation of AdipoR1 in the bone microenvironment began with alteration of the substrate concentration: 2T3 and ST2 cells were treated with the small molecule adiponectin receptor agonist AdipoRON in order to observe the effect of adiponectin receptor stimulation on cell viability, gene expression profiles and differentiation. Subsequent investigation involved manipulation of the receptor using lentivirus-mediated knockdown of AdipoR1 expression to assess the downstream effect of disrupted signalling via AdipoR1 on cell viability, gene expression profiles and differentiation.

6.2.1 Effect of AdipoRON treatment

6.2.1.1 AdipoRON shows dose-dependent toxicity in 2T3 and ST2 cells

2T3 and ST2 cells were plated with AdipoRON (0-50µM) for 24, 48 or 72 hours before their viability assessment by Alamar Blue assay. At each timepoint, all results were standardised to the viability of a vehicle control denoted 0µM AdipoRON.

2T3 cells showed a significant reduction in viability at all concentrations tested (20-50µM) at 24 hours, but by 48 hours only 50µM significantly reduced viability, and by 72 hours, only 40-50µM had a significant effect on viability (**Figure 6.1A**). ST2 cells had generally higher sensitivity to AdipoRON treatment than 2T3s: the significant reduction in viability of ST2s with all doses tested persisted to 48 hours of treatment, and by 72 hours, 30µM-50µM AdipoRON was still significantly affecting viability (**Figure 6.1B**). Based on these data, 30µM AdipoRON was selected as a suitable treatment concentration for further experimentation.

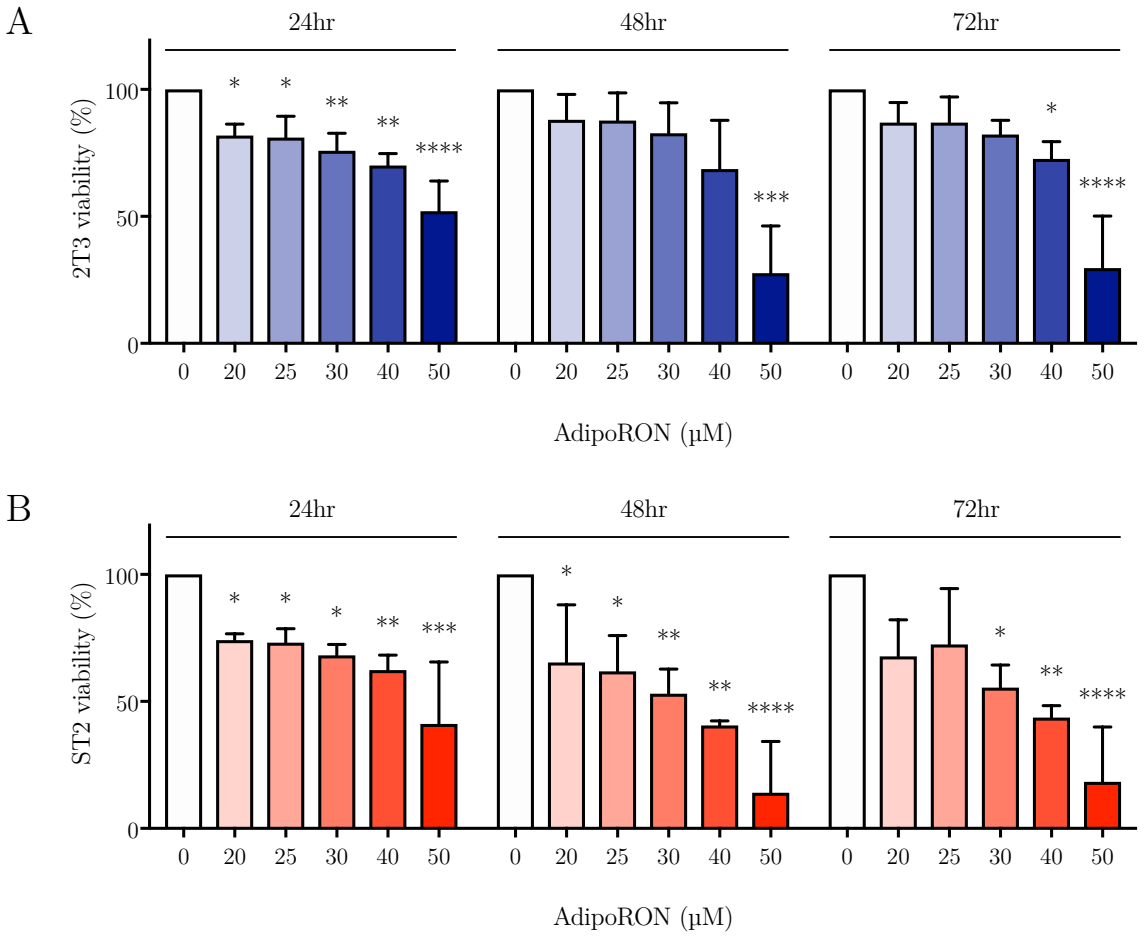


Figure 6.1: AdipoRON-treated 2T3 and ST2 cells show dose-dependent toxicity by Alamar Blue assay. Cells were plated at 5x10^4/ml for 24 hours before treatment with AdipoRON for 24, 48 or 72 hours, after which viability was determined by Alamar Blue assay. (**A**) 2T3 cells treated with 20µM AdipoRON showed significantly reduced viability at 24 hours, but only treatments of 40µM or higher maintained a significant toxicity effect at 72 hours. (**B**) ST2 cells treated with 20µM AdipoRON showed significantly reduced viability at 24 hours, but only treatments of 30µM or higher maintained a significant toxicity effect at 72 hours. Data presented as mean+SD; N=3 (biological replicates); one-way ANOVA with Dunnett's post-hoc multiple comparisons testing relative to untreated control at each timepoint; *=p≤0.05, **=p≤0.01, ***=p≤0.001.

6.2.1.2 AdipoRON-treated 2T3 and ST2 cells show few significant changes in adiponectin receptor gene expression

To test whether addition of an exogenous adiponectin receptor agonist had any significant feedback loop on receptor expression, 2T3 and ST2 cells were treated with 30µM AdipoRON for 24, 48 or 72 hours before analysis of AdipoR1 and AdipoR2

expression by qPCR. All results have been standardised to an internal housekeeping gene (GAPDH) and have been presented as fold change in expression standardised to a vehicle control.

AdipoRON treatment had no significant effect on 2T3 expression of AdipoR1 (**Figure 6.2A**) or AdipoR2 (**Figure 6.2B**) at any timepoint tested. However, AdipoR1 expression relative to vehicle control in ST2 cells was significantly increased following 24 hours of AdipoRON treatment and significantly reduced by 48 hours, with no significant effect observed by 72 hours of treatment (**Figure 6.2C**). Despite these changes in AdipoR1 expression, ST2 AdipoR2 expression remained unchanged following AdipoRON treatment (**Figure 6.2D**).

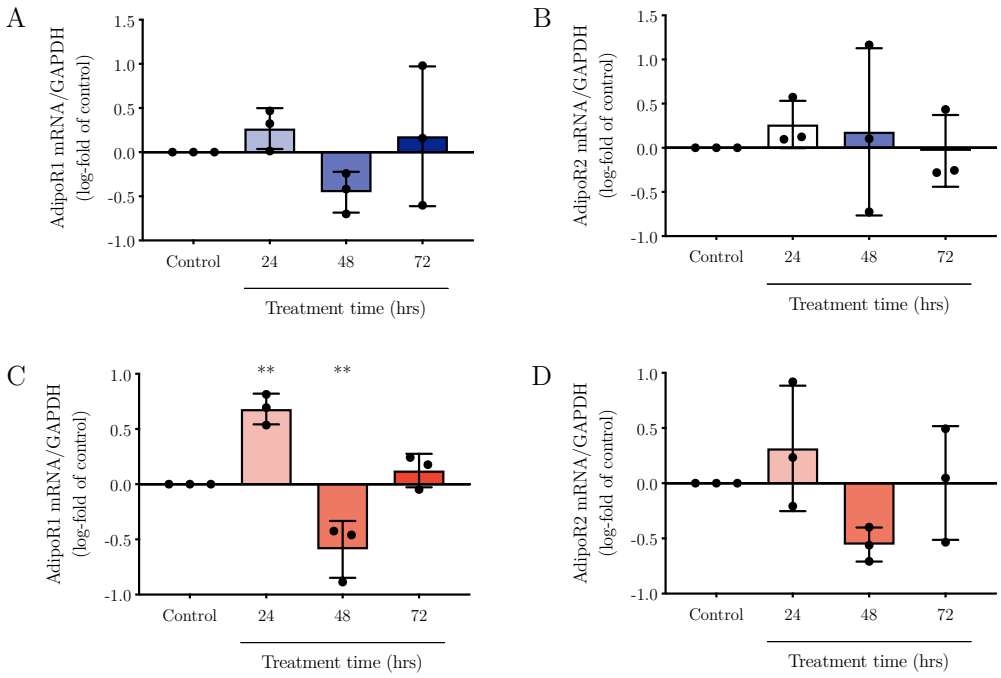


Figure 6.2: AdipoRON-treated 2T3 and ST2 cells show few significant changes in relative AdipoR1 or AdipoR2 gene expression by qPCR analysis. Cells were plated at $5x10^4$/ml for 24 hours before treatment with 30µM AdipoRON for 24, 48 or 72 hours, after which RNA was extracted and relative gene expression quantified by qPCR. (**A**, **B**) AdipoRON-treated 2T3 cells showed no significant change in relative (**A**) AdipoR1 or (**B**) AdipoR2 expression as compared to untreated control. (**C**, **D**) As compared with control, AdipoRON-treated ST2 cells showed (**C**) a significant increase in relative AdipoR1 expression at 24 hours which was significantly reduced by 48 hours treatment but unchanged by 72 hours treatment. (**D**) AdipoRON-treated ST2 cells showed no significant change in relative AdipoR2 expression as compared to untreated control. Data presented as mean+SD; N=3 (biological replicates); one-way ANOVA with Dunnett's post-hoc testing relative to untreated control at each timepoint; *=p≤0.05, ***=p≤0.001.

6.2.1.3 AdipoRON-treated 2T3 cells show significantly reduced expression of osteoblast-related genes

2T3 cells are capable of differentiating into functional mineralising osteoblasts but retain expression of some key osteoblastic genes in their undifferentiated pre-osteoblastic state. To investigate whether treatment with AdipoRON altered expression of these osteoblast-related genes, 2T3 cells were treated with 30µM AdipoRON for 24, 48 or 72 hours before analysis of relative Runx2, alkaline phosphatase (ALPL), osteopontin (OPN), collagen type I α-1 (Col1a1) and osteocalcin (OCN) expression by qPCR. All results have been standardised to an internal housekeeping gene (GAPDH) and have been presented as fold change in expression standardised to a vehicle control treated with the equivalent volume of DMSO.

AdipoRON treatment had no significant effect at any timepoint tested on expression of Runx2 (

Figure 6.3**A**), ALPL (

Figure 6.3**B**), OPN (

Figure 6.3**C**) or OCN (

Figure 6.3**E**), but a significant reduction in Col1a1 expression was observed at all three timepoints (

Figure 6.3**D**).

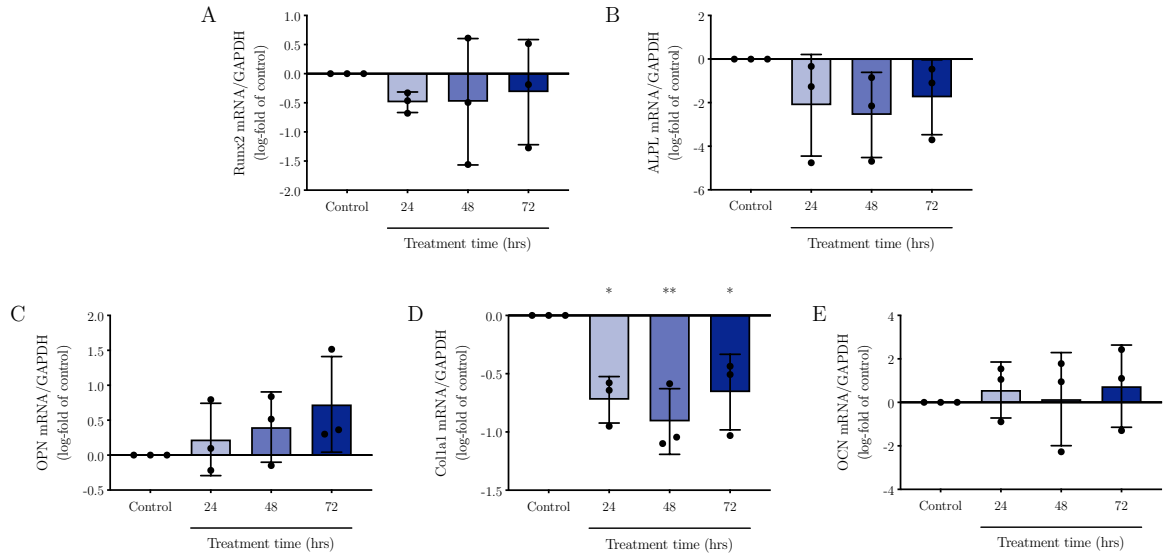


Figure 6.3: AdipoRON-treated 2T3 cells show significantly reduced expression of some osteoblast-related genes. 2T3 cells were plated at $5x10^4$/ml for 24 hours before treatment with AdipoRON for 24, 48 or 72 hours, after which RNA was extracted and relative gene expression quantified by qPCR. AdipoRON treatment did not significantly affect relative expression of Runx2 (**A**), alkaline phosphatase (ALPL, **B**), osteopontin (OPN, **C**) or osteocalcin (OCN, **E**). (**D**) AdipoRON treatment significantly reduced relative expression of collagen type I α-1 (Col1a1) at 24, 48 and 72 hours. Data presented as mean+SD; N=3 (biological replicates); one-way ANOVA with Dunnett's post-hoc multiple comparisons testing relative to untreated control at each timepoint; *=p≤0.05, **=p≤0.01, ***=p≤0.001.

6.2.1.4 AdipoRON-treated ST2 cells show significantly altered expression of some osteoblast- and adipocyte-related genes

To investigate whether treatment with AdipoRON altered expression of osteoblast- and adipocyte-related genes, ST2 cells were treated with 30μM AdipoRON for 24, 48 or 72 hours before analysis of relative Runx2, ALPL, peroxisome proliferator-activated receptor γ (PPARγ), CCAAT/enhancer-binding protein α (CEBPα) and adiponectin (AdipoQ) expression by qPCR. All results have been standardised to an internal housekeeping gene (GAPDH) and have been presented as fold change in expression standardised to a vehicle control treated with the equivalent volume of DMSO.

AdipoRON treatment had no significant effect on expression of Runx2 (**Figure 6.4A**) or ALPL (**Figure 6.4B**) at any timepoint tested). Expression of key adipogenic gene PPARγ was significantly increased following 24 and 72 hours of treatment (**Figure 6.4C**), but expression of CEBPα (**Figure 6.4D**) and AdipoQ (**Figure 6.4E**) were not changed significantly.

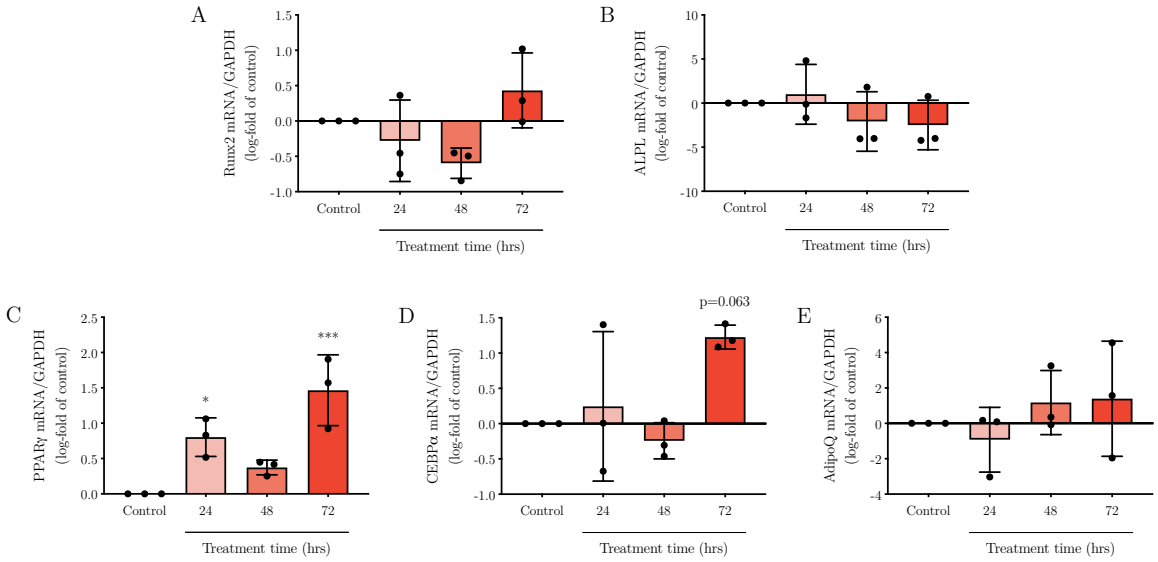


Figure 6.4: AdipoRON-treated ST2 cells show significantly altered expression of some osteoblast- and adipocyte-related genes. ST2 cells were plated at $5x10^4$/ml for 24 hours before treatment with AdipoRON for 24, 48 or 72 hours, after which RNA was extracted and relative gene expression quantified by qPCR. AdipoRON treatment did not significantly affect relative expression of Runx2 (**A**) or alkaline phosphatase (**B**). (**C**) 24 and 72 hours of AdipoRON treatment significantly increased relative expression of peroxisome proliferator-activated receptor γ (PPARγ). (**D**, **E**) AdipoRON treatment did not significantly affect relative expression of CCAAT/enhancer-binding protein α (CEBPα) or adiponectin (AdipoQ). Data presented as mean+SD; N=3 (biological replicates); one-way ANOVA with Dunnett's post-hoc multiple comparisons testing relative to untreated control at each timepoint; *=p≤0.05, **=p≤0.01, ***=p≤0.001.

6.2.1.5 AdipoRON-treated 2T3 cells show significantly reduced alkaline phosphatase activity

Following observations of reduced ALPL mRNA expression after AdipoRON treatment (

Figure 6.3**B** and **Figure 6.4B**), an ALPL enzymatic activity assay was performed in cell lysates from 2T3 cells treated with AdipoRON for 24, 48 or 72 hours to test whether reduced expression of ALPL was associated with reduced enzymatic activity. Results are presented as fold change in expression standardised to a vehicle control treated with the equivalent volume of DMSO.

While no significant effects were observed after only 24 hours of treatment, a significant reduction in ALPL activity was observed in all dosages tested (10-40µM) after 48 and 72 hours of treatment (**Figure 6.5**).

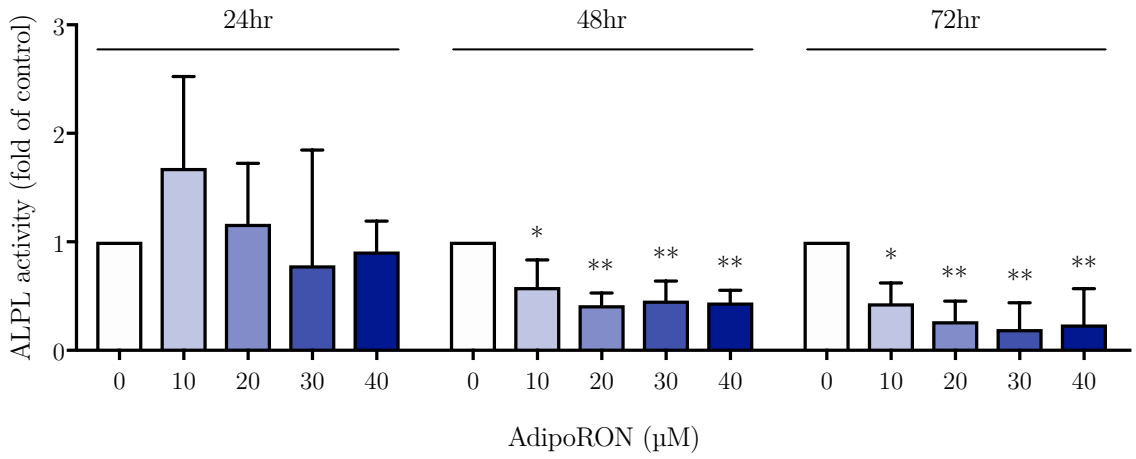


Figure 6.5: AdipoRON-treated 2T3 cells show significantly reduced alkaline phosphatase activity. 2T3 cells were plated at $5x10^4$/ml for 24 hours before treatment with AdipoRON for 24, 48 or 72 hours, after which alkaline phosphatase (ALPL) activity was measured. No significant effect of AdipoRON treatment on ALPL activity in 2T3 cells was observed at 24 hours. Treatment with 10µM-40µM AdipoRON significantly reduced 2T3 ALPL activity at 48 and 72 hours. Data presented as mean+SD; N=3 (biological replicates); one-way ANOVA with Dunnett's post-hoc multiple comparisons testing relative to untreated control at each timepoint; *=p≤0.05, **=p≤0.01.

6.2.1.6 AdipoRON-treated 2T3 cells showed no significant difference in mineralisation capacity

To test whether observed changes in gene expression and ALPL activity in 2T3 cells treated with AdipoRON had functional effects on cell differentiation, AdipoRON-treated

2T3 cells were mineralised for 16 days alongside a vehicle control. Results are presented as absolute extracted Alizarin Red concentration. Alizarin Red concentration was significantly lower in undifferentiated controls compared with differentiated vehicle controls as expected, but no significant effect of AdipoRON treatment on 2T3 mineralisation was observed (**Figure 6.6**).

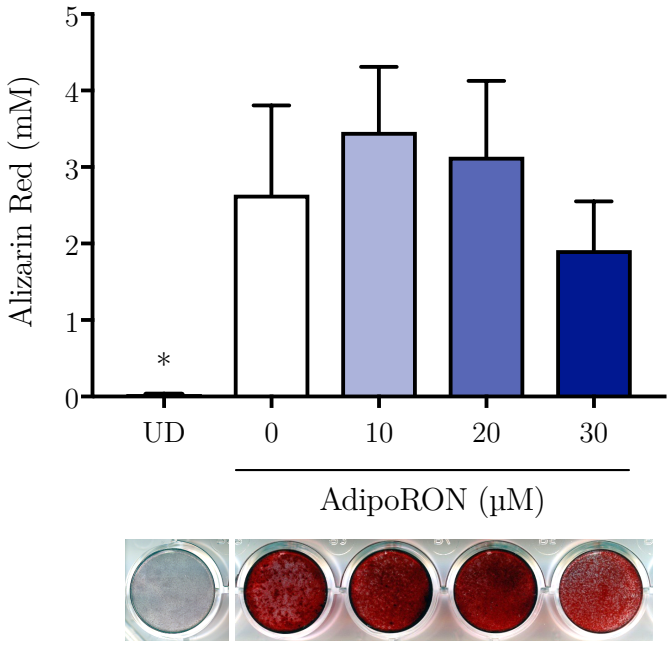


Figure 6.6: AdipoRON-treated 2T3 cells show no significant difference in mineralisation capacity. 2T3 cells were plated at $5x10^4$/ml for 24 hours before treatment with mineralisation media supplemented with AdipoRON where appropriate. Media and treatment were refreshed every three days for 16 days. Undifferentiated cells (UD) were treated every three days with basal media. After 16 days, Alizarin Red staining and quantification was performed. AdipoRON-treated 2T3 cells showed no significant difference in extracted Alizarin Red concentration as compared with differentiated untreated control. Representative images of stained well plates before dye extraction shown; image of UD well taken from different plate to stained cells due to cell peeling from over-confluency. Data presented as mean+SD; N=3 (biological replicates); one-way ANOVA with Dunnett's post-hoc multiple comparisons testing relative to mineralised untreated control; significance defined as $p \leq 0.05$.

6.2.2 Effect of stable AdipoR1 knockdown

6.2.2.1 Lentiviral knockdown of AdipoR1 does not affect AdipoR2 expression in 2T3 cells or ST2 cells

Initial work with 2T3 cells and ST2 cells with lentiviral-mediated stable knockdown of AdipoR1 expression established the extent of the knockdown and whether it affected AdipoR2 expression in a feedback loop system. Following four weeks of puromycin selection of transfected cells, baseline expression of AdipoR1 and AdipoR2 expression were assessed by qPCR. Results were standardised to an internal housekeeping gene (GAPDH) and are presented as fold change in expression standardised to an untransfected control.

Relative AdipoR1 expression in AdipoR1 knockdown (R1 KD) 2T3 cells was significantly reduced as compared with untransfected controls with a 89% knockdown level (**Figure 6.7A**); AdipoR2 expression in these cells was not significantly altered (**Figure 6.7B**). Relative AdipoR1 expression in AdipoR1 knockdown (R1 KD) ST2 cells was significantly reduced as compared with untransfected controls with a 93% knockdown level (**Figure 6.7C**); AdipoR2 expression in these cells was not significantly altered (**Figure 6.7D**).

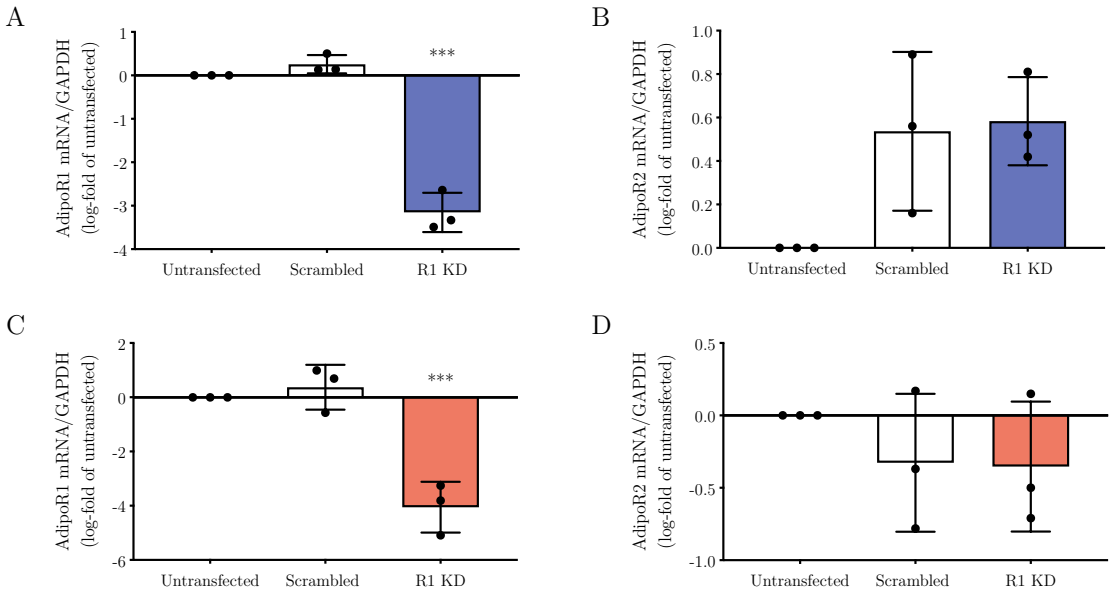


Figure 6.7: Lentiviral knockdown of AdipoR1 expression does not significantly affect AdipoR2 expression in 2T3 or ST2 cells. Following lentiviral transfection and four weeks of puromycin selection of transfected cells, baseline levels of AdipoR1 and AdipoR2 relative expression in untransfected, scrambled control transfected and AdipoR1 knockdown (R1 KD) (**A, B**) 2T3 and (**C, D**) ST2 cells were assessed by qPCR. (**A**) 2T3 relative AdipoR1 expression was significantly reduced in R1 KD cells, but (**B**) AdipoR1 knockdown had no significant effect on AdipoR2 relative expression. (**C**) ST2 relative AdipoR1 expression was significantly reduced in R1 KD cells, but (**D**) AdipoR1 knockdown had no significant effect on AdipoR2 relative expression. Data presented as mean+SD; N=3 (biological replicates); one-way ANOVA with Dunnett's post-hoc multiple comparisons testing relative to untransfected control; *=p≤0.05, ***=p≤0.001.

6.2.2.2 Lentiviral knockdown of AdipoR1 does not affect 2T3 or ST2 cell viability

Stable knockdown of AdipoR1 expression or the transfection process itself could alter 2T3 or ST2 cell viability. Viability of R1 KD cells relative to untransfected controls was determined by Alamar Blue assay at 24 and 72 hours after seeding. No significant differences in viability of 2T3 cells (**Figure 6.8A**) or ST2 cells (**Figure 6.8B**) was observed following AdipoR1 knockdown.

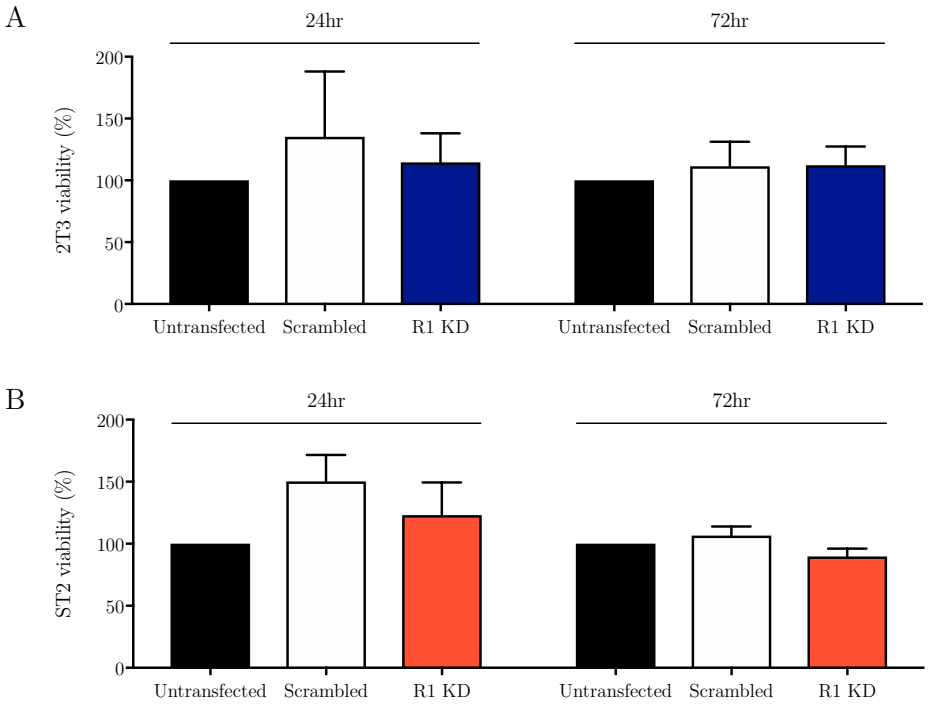


Figure 6.8: Lentiviral knockdown of AdipoR1 expression does not significantly affect cell viability by Alamar Blue assay. Following lentiviral transfection and four weeks of puromycin selection of transfected cells, untransfected, scrambled control transfected and AdipoR1 knockdown (R1 KD) (**A**) 2T3 and (**B**) ST2 cells were plated for 24 or 72 hours and their viability assessed by Alamar Blue assay. Knockdown of AdipoR1 did not significantly affect cell viability in either cell line at either timepoint tested. Data presented as mean+SD; N=3 (biological replicates); one-way ANOVA with Dunnett's post-hoc multiple comparisons testing relative to untransfected control; significance defined as $p \leq 0.05$.

6.2.2.3 Gene profile changes after osteogenic or adipogenic induction

To assess the effect of AdipoR1 knockdown in 2T3 and ST2 cells further, each line was differentiated, and gene expression assessed at baseline, during differentiation and after differentiation. 2T3 cells were differentiated into osteoblasts for 16 days, with expression quantified at zero, eight and 16 days of differentiation. ST2 cells were differentiated into adipocytes for eight days, with expression quantified at zero, four and eight days of differentiation. Due to their capacity for bilineage differentiation, expression of ST2 cell expression of osteoblast- and adipocyte-related genes was assessed during adipogenic

differentiation; osteoblastic genes only were assessed in differentiating 2T3 cells. The ST2 scrambled control was noted to have some significant effects, so an empty vector control and a second scrambled control (Scr. 2) were added alongside the original scrambled control (Scr. 1) to allow determination of whether the effect was a sequence-specific effect or was due to a general transfection effect. Results were standardised to an internal housekeeping gene (GAPDH) and are presented as fold change in expression standardised to an untransfected control.

6.2.2.3.1 AdipoR1 knockdown is maintained throughout osteoblastic differentiation of 2T3 cells

2T3 cells underwent osteogenic differentiation for up to 16 days. A significant knockdown of AdipoR1 expression was maintained in these cells throughout differentiation, with undifferentiated controls showing significantly altered AdipoR1 expression during differentiation (**Figure 6.9A**). AdipoR2 expression remained largely unaltered in 2T3 R1 KD cells during osteogenic differentiation, except midway through osteogenic differentiation where AdipoR2 expression was significantly reduced in undifferentiated cells as compared with untransfected controls (**Figure 6.9B**).

ST2 cells were differentiated to adipocytes for up to eight days. A significant reduction in AdipoR1 expression was maintained throughout differentiation (**Figure 6.9C**) while relative AdipoR2 expression was significantly reduced in undifferentiated and R1 KD cells at 8 days differentiation (**Figure 6.9D**).

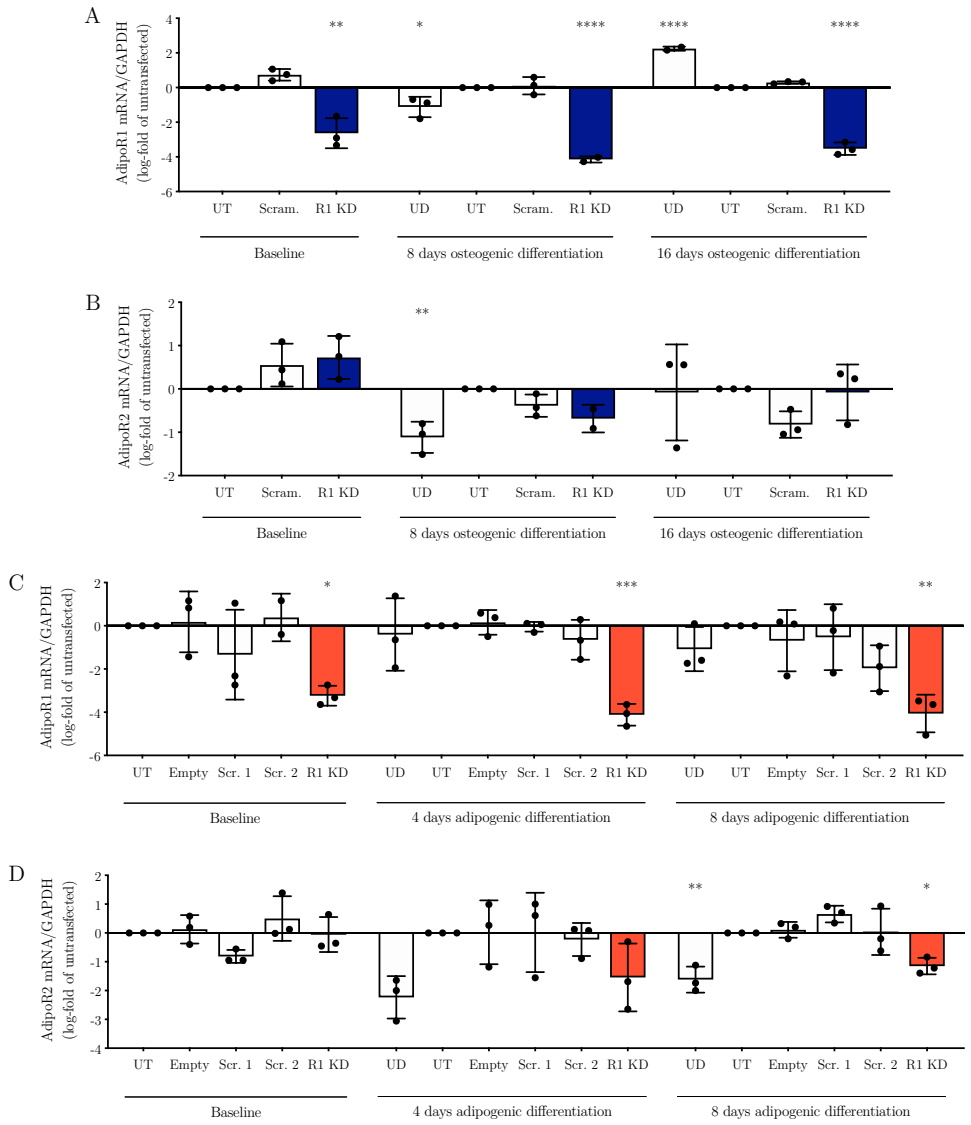


Figure 6.9: AdipoR1 knockdown is maintained in 2T3s during osteoblastic differentiation. (**A**, **B**) Untransfected (UT), scrambled control transfected (Scram.) and AdipoR1 knockdown (R1 KD) 2T3 cells were plated at $5x10^4$/ml for 24 hours before treatment with mineralisation media for up to 16 days; RNA was extracted for analysis of relative gene expression by qPCR at zero, eight or 16 days of osteoblastic differentiation. (**C**, **D**) UT, an empty vector control, two scramble control transfected (Scr. 1 and Scr. 2) and R1 KD ST2 cells were plated at $5x10^4$/ml for 24 hours before adipogenic differentiation for up to eight days; RNA was extracted for analysis of relative gene expression by qPCR at zero, four or eight days of adipogenic differentiation. (**A**) Significant knockdown of relative AdipoR1 expression was maintained in 2T3 cells for the duration of osteoblastic differentiation; at 8 and 16 days differentiation, undifferentiated (UD) cells showed significantly higher relative expression of AdipoR1 as compared to UT differentiated control. (**B**) At eight days of osteoblastic differentiation, UD 2T3 cells showed significantly reduced AdipoR2 expression but otherwise no significant effects on relative AdipoR2 expression were noted. (**C**) Relative expression of AdipoR1 in R1 KD ST2 cells was maintained significantly throughout adipogenic differentiation. (**D**) At 8 days adipogenic differentiation, relative AdipoR2 expression was reduced in UD and R1 KD cells. Data presented as mean+SD; N=3 (biological replicates); one-way ANOVA with Dunnett's post-hoc multiple comparisons testing relative to UT control at each timepoint; *=p≤0.05; **=p≤0.01; ***=p≤0.001; ****=p≤0.0001.

6.2.2.3.2 AdipoR1 knockdown in 2T3 cells is associated with reduced osteoblast-related gene expression at baseline and during osteoblastic differentiation

2T3 R1 KD cells showed no significant difference in baseline expression of Runx2, but expression was significantly reduced compared with untransfected controls midway through osteoblastic differentiation. At this time, undifferentiated controls also showed reduced Runx2 expression (**Figure 6.10A**). ALPL expression was significantly increased in R1 KD cells at baseline, but no further differences in expression were observed following induction of differentiation (**Figure 6.10B**). OPN expression was significantly lower in undifferentiated controls throughout differentiation with no further significant differences observed (**Figure 6.10C**). While Col1a1 expression was significantly increased in R1 KD cells at baseline, this difference did not persist during differentiation (**Figure 6.10D**). Finally, no significant differences in OCN expression were observed in R1 KD cells as compared with untransfected controls at baseline or during differentiation, with only undifferentiated cells at 16 days showing a reduction in OCN expression as compared with transfected controls (**Figure 6.10E**).

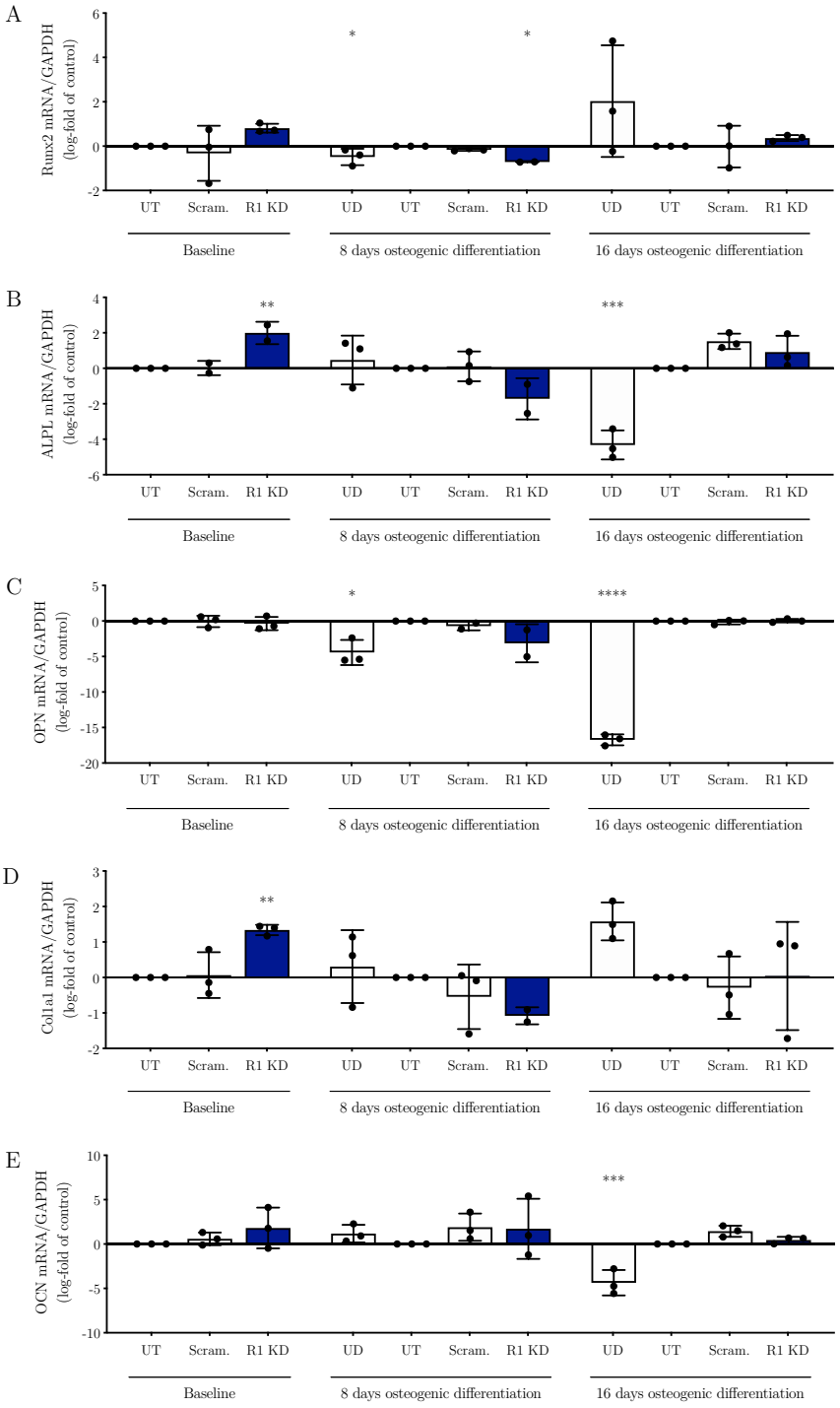


Figure 6.10: AdipoR1 knockdown in 2T3 cells is associated with altered relative expression of some osteoblast-related genes at baseline and during osteoblastic differentiation. Untransfected (UT), scrambled control transfected and AdipoR1 knockdown (R1 KD) 2T3 cells were plated at $5x10^4$/ml for 24 hours before treatment with mineralisation media for up to 16 days; RNA was extracted for analysis of relative gene expression by qPCR at zero, eight or 16 days of osteoblastic differentiation. (**A**) At eight days of osteoblastic differentiation, undifferentiated (UD) controls and R1 KD were both associated with significantly reduced expression of Runx2; no further effects on Runx2 expression were observed. (**B**) Baseline R1 KD cells showed significantly increased alkaline phosphatase (ALPL) relative expression, but during differentiation, only UD cells showed significant differences in ALPL expression as compared with

controls. (**C**) Induction of differentiation was associated with a significant increase in osteopontin (OPN) relative expression as shown by significantly lower expression of OPN in UD controls as compared with UT controls throughout differentiation. No further significant differences in OPN expression were observed. (**D**) Baseline R1 KD cells showed significantly increased collagen type I α-1 (Col1a1) relative expression, but no further significant changes in relative Col1a1 expression were seen during differentiation. (**E**) UD cells showed significantly reduced relative expression of osteocalcin (OCN) at 16 days differentiation; no further significant changes in OCN expression were observed. Data presented as mean+SD; N=3 (biological replicates); one-way ANOVA with Dunnett's post-hoc multiple comparisons testing relative to UT control at each timepoint; *=p≤0.05; **=p≤0.01; ****=p≤0.0001.

6.2.2.3.3 Baseline, but not mid-differentiation, expression of some osteoblast-related genes is increased in AdipoR1 knockdown ST2 cells

Baseline ST2 empty vector, one scrambled control (Scr. 1) and R1 KD cells all showed significantly increased expression of Runx2 at baseline as compared with untransfected control, but no differences in Runx2 expression were observed during adipogenic differentiation (**Figure 6.11A**). Similarly, R1 KD cells showed no significant change in relative ALPL expression at baseline or throughout differentiation, with undifferentiated cells at 4 days differentiation only showing significantly higher ALPL expression as compared with untransfected control (**Figure 6.11B**). PPARγ expression levels remained unchanged at baseline and throughout differentiation (**Figure 6.11C**), and expression of CEBPα was altered significantly only in day 8 undifferentiated cells (**Figure 6.11D**). AdipoQ expression was significantly lower in undifferentiated controls at 4 days differentiation and in both undifferentiated controls and R1 KD cells at 8 days differentiation (**Figure 6.11E**).

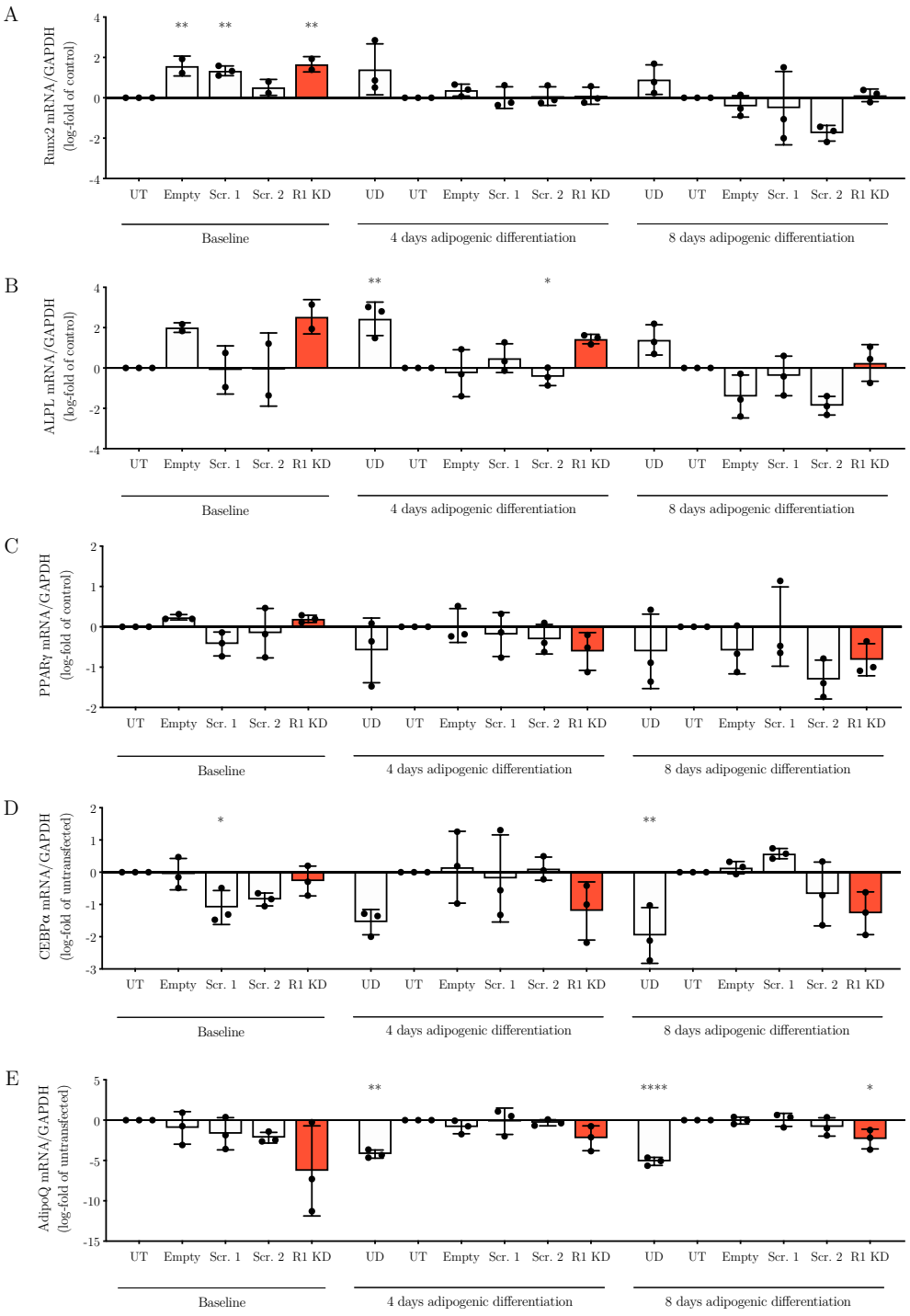


Figure 6.11: AdipoR1 knockdown in ST2 cells is associated with increased relative expression of osteoblast-related genes at baseline. Untransfected (UT), empty vector transfected, two scrambled control transfected (Scr. 1, Scr. 2) and AdipoR1 knockdown (R1 KD) ST2 cells were plated at $5x10^4$/ml for 24 hours before treatment with adipogenic media for up to eight days; RNA was extracted for analysis of relative gene expression by qPCR at zero, four or eight days of adipogenic differentiation. (**A**) At baseline, R1 KD was associated with increased relative expression of Runx2; empty transfected and one scrambled transfected control (Scr. 1) also showed significantly increased relative expression. No significant changes in Runx2 expression were observed during adipogenic differentiation. (**B**) Relative ALPL expression was significantly altered from baseline only in UD and Scr. 2 cells at 4 days

differentiation. (**C**) No significant changes in relative peroxisome proliferator-activated receptor γ (PPARγ) were observed in baseline or differentiated cells. (**D**) Baseline Scr. 1 and 8 days differentiation UD cells showed reduced relative expression of CCAAT/enhancer-binding protein α (CEBPα) relative expression. (**E**) Induction of adipogenic differentiation was associated with a significant increase in adiponectin (AdipoQ) relative expression as shown by significantly reduced expression of AdipoQ in UD controls as compared with UT controls at 4- and 8-days differentiation. At 8 days differentiation, R1 KD cells also showed significantly reduced AdipoQ expression. Data presented as mean+SD; N=3 (biological replicates); one-way ANOVA with Dunnett's post-hoc multiple comparisons testing relative to UT control at each timepoint; *=p≤0.05; **=p≤0.01.

6.2.2.4 AdipoR1 knockdown is associated with significantly increased mineralisation capacity of 2T3 cells

In order to assess the functional effects of these gene profile changes, control and R1 KD 2T3 and ST2 cells were differentiated and stained. 2T3 cells underwent osteogenic differentiation for 16 days before Alizarin Red staining; results are presented as absolute extracted Alizarin Red concentration. As expected, undifferentiated 2T3 cells had significantly lower Alizarin Red concentration than differentiated untransfected controls. R1 KD cells showed significantly increased mineralisation by Alizarin Red staining, while scrambled controls showed no significant effects (**Figure 6.12A**).

ST2 cells underwent adipogenic differentiation for eight days before Oil Red O staining; results are presented as fold change in adipocytic coverage as compared to differentiated untransfected control. Undifferentiated ST2 cells showed significantly lower Oil Red O staining than differentiated untransfected controls, indicating successful adipogenesis. However, all transfected cells (empty vector control, both scrambled controls and R1 KD) showed significantly inhibited adipogenesis, suggesting a non-specific transfection effect (**Figure 6.12B**).

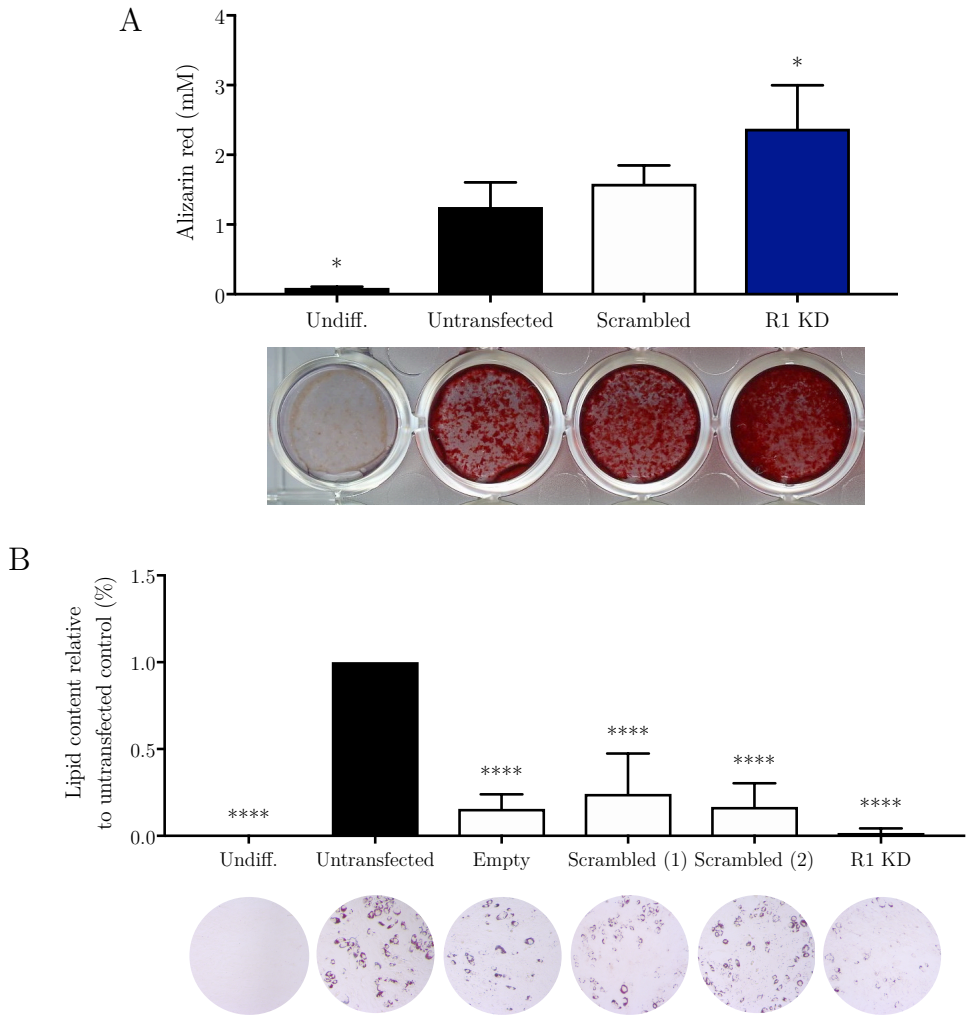


Figure 6.12: AdipoR1 knockdown in 2T3 cells increases mineralisation capacity but AdipoR1 knockdown in ST2 cells has no conclusive effect on adipogenic potential. (**A**) Representative images of Alizarin Red staining and combined quantification of extracted stain (N=3, biological replicates). Untransfected (UT), scrambled control transfected and AdipoR1 knockdown (R1 KD) 2T3 cells were plated at $5x10^4$/ml for 24 hours before treatment with mineralisation media for 16 days. Undifferentiated cells (undiff.) were treated every three days with basal media. After 16 days, Alizarin Red staining and quantification was performed. Undiff. cells showed significantly lower Alizarin Red content than differentiated UT controls; R1 KD significantly increased mineralisation and Alizarin Red content. (**B**) Representative images of Oil Red O staining and combined quantification of staining coverage (N=3, biological replicates). UT, empty vector transfected, two scrambled control transfected (Scr. 1, Scr. 2) and R1 KD ST2 cells were plated at $5x10^4$/ml for 24 hours before treatment with adipogenic media for eight days. Undiff. controls were treated with basal media each time differentiated cells were treated. After eight days, Oil Red O staining was performed, and content quantified by densitometry analysis. All differentiated transfected cells showed significant reductions in adipogenesis. Data presented as mean+SD; one-way ANOVA with Dunnett's post-hoc multiple comparisons testing relative to UT control; *=p≤0.05; ****=p≤0.0001.

6.3 Discussion and conclusions

This chapter made use of 2T3 and ST2 cells treated with the adiponectin receptor agonist AdipoRON for 24-72 hours, and of 2T3 and ST2 cells in which AdipoR1 expression had been stably knocked down using lentiviral transfection. All data concerning transfected cells is presented relative to untransfected control due to the significant effects seen in some controls, particularly in ST2 gene profiles and adipogenic differentiation, making them unsuitable for baseline comparison. While the use of the untransfected cells as the control to which results are standardised provides a stable baseline comparison, it is acknowledged that a transfected control would constitute a more biologically relevant control. The reasons underlying the significant effect observed in some controls is not understood and must be taken into consideration when interpreting these results; in particular, it is not possible to conclude the functional effect of R1 KD on ST2 adipogenesis from these data.

In contrast to the hypothesised outcome, AdipoRON treatment of 2T3 and ST2 cells had little effect on the expression of markers of the osteoblastic phenotype, with treated cells showing no change in Runx2 or ALPL expression, although 2T3 cell Col1a1 expression and ALPL activity were reduced at all timepoints of AdipoRON treatment that were tested. Meanwhile the baseline expression of some osteoblast-related genes was significantly increased in R1 KD cells, and in the 2T3 cells this was associated with a significant increase in mineralisation. Conversely, 72 hours of AdipoRON treatment of ST2 cells was associated with a significant increase in expression of the adipocytic marker PPARγ. Together, these data suggest that exogenous stimulation of the adiponectin receptors may partially inhibit osteoblastic differentiation and promote adipocytic differentiation, and a disruption of adiponectin signalling via knockdown of AdipoR1 expression increases their osteoblastic propensity.

However, the mineralisation capacity of AdipoRON-treated 2T3 cells was found to be non-significantly altered from that of the untreated cells, possibly suggesting that the significant alterations in the gene expression profile are not biologically significant. Additionally, although very few differences were seen throughout differentiation, 2T3 R1 KD cells following eight days of osteoblastic differentiation showed significant reductions in osteoblastic gene expression, suggesting disruption of adiponectin signalling reduces the osteogenic potential of these cells. In summary, the data presented in this chapter are not consistent, with some data suggesting that signalling via AdipoR1 inhibits bone formation, and other data suggesting inconclusive or even opposite effects. Many factors could be contributing to these discordant results, and a lack of previous published research in this area makes interpretation difficult, with the only previous bone-related *in vitro* results suggesting AdipoRON administration has a positive effect on bone formation via upregulation of osteoblast differentiation and mineralisation and a suppressive effect on osteoclastogenesis[255].

AdipoRON treatment was administered for between 24 and 72 hours. *In vivo*, the significant glucose-lowering effect of 50mg/kg AdipoRON following its intraperitoneal administration has been observed to last for more than eight hours in a pattern very similar to that of 3mg/kg mouse full-length adiponectin[223] despite its clearance from the blood plasma by around four hours[223], but the half-life of AdipoRON *in vitro* is not well established. The timepoints used in this study were based on previously published evidence from a variety of cell types that *in vitro* administration of AdipoRON has significant effects at 24 hours to five days of treatment[255,366,367]. In the work presented here, significant effects of AdipoRON treatment were found up to 72 hours after treatment, most noticeably the suppression of ALPL activity in 2T3 cells and ALPL expression in ST2 cells. Future work could seek to investigate the response profile of cells to AdipoRON treatment more closely. While these response profiles have been performed in an *in vivo* setting, finding that the glucose-lowering effect of AdipoRON

peaked at two hours after administration[223], similar observations have not been made *in vitro*. Given the rapidity of its *in vivo* effects, it is likely that the acute changes that occur within 24 hours of AdipoRON treatment may have been missed in present study design. A similar consideration must be made for the timepoints used during differentiation of knockdown cells: samples were extracted at baseline, mid-point and endpoint of osteogenic and adipogenic differentiation, but significant changes will have occurred between these times that are not recorded. For example, others have shown that significant increases in mouse osteoblast precursor MC3T3 Runx2 expression occur within two days of *in vitro* differentiation induction[368]. A closer study of the time course of the expression of these key genes could shed more light on the response of the knockdown cells to differentiation induction as compared with controls, and perhaps explain, at least in part, the lack of continuity within these results.

Significant changes in gene expression and cell differentiation were observed in 2T3 and ST2 AdipoR1 KD cells despite no AdipoRON being introduced to the system. It is hypothesised that these effects are mediated by alteration of signalling by the adiponectin that is present in the FBS that supplements the basal growth media in which these cells are cultured. Previous work has shown that the endogenous adiponectin in FBS consists primarily of full-length adiponectin that forms LMW, MMW and HMW oligomers and that, when purified and injected into male C57Bl/6N mice, can induce the expected glucose-lowering and insulin-sensitising effects[369]. Addition of AdipoRON alongside 15µg/ml recombinant mouse adiponectin significantly increased AMPK phosphorylation beyond adiponectin treatment alone[223], explaining the significant effects seen during AdipoRON treatment despite the presence of adiponectin in the serum. To further clarify the effects of AdipoRON, future work could make use of serum-free cultures, or charcoal-stripped FBS in which the adiponectin concentration has been greatly reduced. The removal of steroid hormones shown to be influential in oestrogen-sensitive *in vitro* settings[370] from FBS could be an important additional benefit to

consider regarding the use of charcoal-stripped FBS in future experiments, given the sex-specific effects observed in previous chapters.

Very few significant changes in the expression of the adiponectin receptors were seen in 2T3 and ST2 cells following AdipoRON treatment: at 24 hours, ST2 expression of AdipoR1 was increased, but was significantly reduced by 48 hours, suggesting the activity of a feedback loop to regulate adiponectin receptor expression in response to altered adiponectin concentrations. This phenomenon is not well reported: an *in vivo* study in 2006 found that transgenic overexpression of adiponectin in male FVB mice led to a downregulation of adiponectin at the mRNA and protein level and AdipoR2 at the mRNA level[371], but otherwise the relationships between adiponectin or adiponectin receptor agonist concentration and adiponectin receptor expression remain largely obscure. No other significant effects on receptor expression were seen in this chapter, including a lack of compensation in AdipoR2 expression following AdipoR1 knockdown, suggesting a minor biological role for this feedback loop should it exist. This is supported by the lack of a change in the circulating adiponectin concentration in the blood or level of AdipoR2 expression in the bone marrow stem cells of control and young female AdipoR1$^{-/-}$ mice that were studied in the previous chapter. Interestingly, *in vitro* knockdown of AdipoR1 or AdipoR2 in mouse myoblast-derived C2C12 cells has been seen to ameliorate AdipoRON-associated effects[366], suggesting biologically relevant effects of AdipoRON treatment are mediated through both receptors, and perhaps that a significant cross-over effect exists in the signalling pathways and outcomes of AdipoR1 and AdipoR2. Future work should seek to identify whether a rescue phenotype can be observed in 2T3 and ST2 R1 KD cells following addition of AdipoRON via a mechanism independent of receptor expression compensation.

In this chapter, *in vitro* manipulation of cells of the bone microenvironment via AdipoRON treatment and knockdown of AdipoR1 expression has shown that signalling

via AdipoR1 is likely to have a functional effect in these cells as evidenced by the significant changes in gene expression profiles and differentiation capacity when this axis is altered. The majority of this data is suggestive of an inhibitory effect of AdipoR1 signalling on bone (**Figure 6.13**), but controversies produced within the data, and the lack of a stable and significant phenotype precludes investigation of the molecular mechanisms by which these effects are mediated, preventing its application as a model for *in vitro* investigation of the mechanism underlying the bone phenotype observed *in vivo* in the previous chapters.

Future work should seek to define better these *in vitro* effects in order to produce a reliable model for the investigation of adiponectin signalling in bone cells. The use of primary MSCs and osteoblasts, particularly calvarial osteoblasts from neonatal animals, from AdipoR1$^{+/+}$ and AdipoR1$^{-/-}$ female mice would provide a significantly more robust and reliable model for the *in vitro* investigation of the effect of ablating AdipoR1 signalling than lentiviral knockdown in immortalised cell lines. Primary osteoblasts could be used to address questions concerning the effect of AdipoR1 deletion on osteoblast proliferation, differentiation and mineralisation, and differentiation of wild type and AdipoR1$^{-/-}$ primary MSCs could provide information on relative propensity for bone or fat differentiation. The use of primary mouse cells in this way would significantly strengthen this work since immortalised cell lines cannot be considered normal cells due to their limitless proliferation capacity and the permanent genetic changes introduced for immortalisation, and since the knockout would be stable and permanent, avoiding the confusion caused by transfection-related phenotypes and unstable controls.

While factors such as treatment time and the cell type used can perhaps begin to explain some of the discordance observed both within the results of this chapter and with other published literature in this area, a wider discordance between these results and the

results found *in vivo*, both human and mouse, within this thesis also exists. A discussion of these broader considerations is presented in the following chapter.

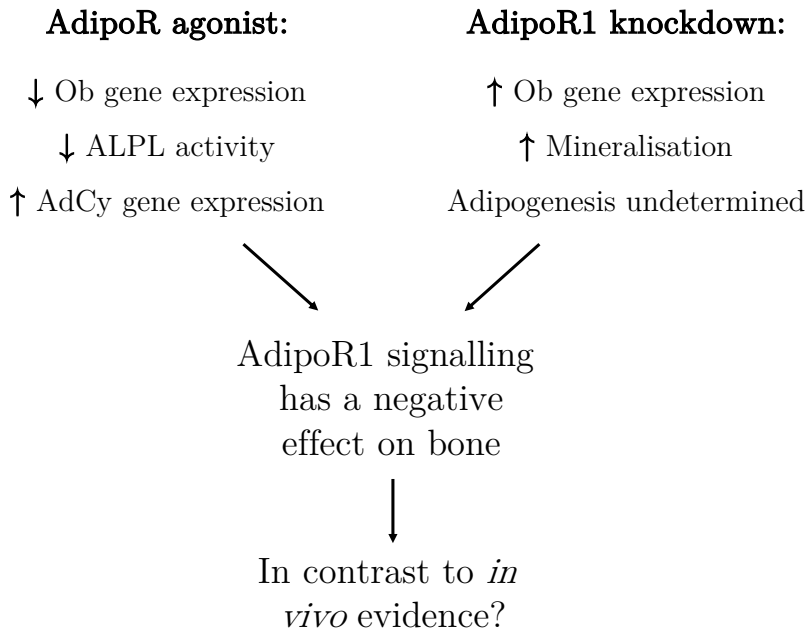


Figure 6.13: Summary of Chapter 6 key findings. Stimulation of adiponectin receptors *in vitro* reduced expression of some osteoblastic (Ob) genes and ALPL activity and increased adipocytic (AdCy) gene expression, whereas stable knockdown of AdipoR1 was associated with increased expression of some Ob genes and mineralisation. These data suggest adiponectin signalling in the cell lines tested has a negative effect on bone, in direct contrast to the *in vivo* evidence of the previous chapter, but inconsistencies in the models used prevented further mechanistic investigation. The use of primary cells and altered *in vitro* conditions are suggested for further work.

7

Discussion and Future Directions

7.1 Discussion

Diseases of the musculoskeletal (MSK) system affect the joints, bones and muscles and have a significant clinical impact: a study conducted in 2010 identified MSK disorders as one of the biggest causes of the growing burden of disability in the UK[372] and they accounted for up to 30% of GP consultations in England in 2006[373]. Financially, MSK conditions cost the NHS over £4.5 billion a year[374], but early identification and suitable management can reduce impact on quality of life for the patient and minimise downstream treatment needs for the healthcare system. In order for the identification and implementation of these management strategies, a thorough understanding of the basic mechanisms governing the maintenance of the bone in health and disease is imperative. In recent years the biological role of adipokines has begun to be studied, prompted by the hypothesis that manipulation of leptin could provide a novel therapeutic option for the treatment of obesity[375], but the significance of bone marrow adipose tissue (BMAT) has been widely overlooked. BMAT is a significant producer of adiponectin in the body[128], but despite this, the role of adiponectin in bone accrual,

maintenance and loss remains incompletely understood. It is likely that the discordant results produced to date are the result of the large variation in the models used for the study of the effect of adiponectin in the bone; this is discussed in **Section 1.4**.

Given the clinical need for an understanding of bone homeostatic mechanisms and the confusion surrounding the understanding of the role of adiponectin in this paradigm, the work in this thesis aimed to use three distinct models with which to study the relationship between adiponectin and bone. Chapter 3 utilises data collected from a large population-based cohort of post-menopausal women, Chapters 4 and 5 involve work performed on the bone phenotype of two mouse lines which carry an engineered genetic knockout of either AdipoR1 or AdipoR2, and an *in vitro* study of the direct effect of positive or negative manipulation of adiponectin signalling in cells of the bone microenvironment is presented in Chapter 6. Each chapter contains discussion of the results presented within it, and these different approaches present some supportive and conflicting results which together may point to a more complex effect of this pathway on bone biology.

In Chapter 3, post-menopausal women of the Chingford 1000 Women Study showed a significant negative correlation between circulating total adiponectin and hip BMD both cross-sectionally and five years prospectively. These findings are consistent with the majority of human population studies of the relationship between adiponectin and bone health (**Section 1.4.1**). In contrast, the bone phenotyping performed in Chapter 4 found that four-week-old female, but not male, mice deficient in AdipoR1 or AdipoR2 show a significant retardation in bone accrual; in AdipoR1$^{-/-}$ females, an accelerated bone loss phenotype following attainment of peak bone mass is also observed. These data suggest a positive effect of adiponectin on bone, with global knockout of its receptors associated with a reduced bone volume. This conclusion is consistent with other published

observations in murine models of adiponectin in bone in which the time- and sex-specificity of the effect have also been observed (**Sections 1.4.2** and **4.3**).

Further investigation of the young female AdipoR1$^{-/-}$ mice in Chapter 5 identified a significant bone marrow-specific increase in adiposity, possibly suggesting AdipoR1 deletion leads to disruption of local feedback loops between adiponectin signalling and BMAT formation. RNASeq analysis of bone marrow resident progenitor cells, identified elsewhere as early mesenchymal progenitors capable of reconstituting bone and marrow adipose tissue *in vivo*[54], identified candidate cell-intrinsic changes that could underly the observed phenotype, and an altered blood chemistry profile in these animals also suggests a significant effect of a bone-extrinsic whole-body mechanism in altering the bone phenotype, although no definitive local or systemic mechanisms were identified. In Chapter 6, *in vitro* investigation in immortalised murine cells of the bone microenvironment suggested a significant negative association between AdipoR1 signalling and bone formation, with AdipoRON stimulation of cells resulting in reduced osteoblastic gene expression, and stable knockdown of AdipoR1 associated with an increased mineralisation capacity.

Together, these results suggest circulating adiponectin levels could constitute a potential novel clinical biomarker of osteoporosis in postmenopausal women and identify adiponectin as playing a significant causative role in bone formation and maintenance. However, they provide some conflicting results: Chapters 3 and 6 identify a negative association between bone and adiponectin, whereas the mouse models used in Chapters 4 and 5 suggest this association is positive.

It should be considered that the results in Chapter 3 obtained from the Chingford 1000 Women Study are correlative, unlike the results collected in Chapters 4 and 5 in which the bone phenotypes observed in AdipoR1$^{-/-}$ or AdipoR2$^{-/-}$ are considered to be directly caused by the genotype. Thus, the data in Chapter 3 cannot support a conclusion that

increased adiponectin levels cause, either directly or indirectly, a reduction in BMD in post-menopausal women since it is not possible to exclude the possibility that a reduction in BMD could cause an increased circulating adiponectin, or that a reduction in BMD and increased adiponectin levels might both be regulated by an unidentified confounding factor or factors that were not controlled for in analyses. Despite this, the lack of causative mechanism in this data does not detract from the potential clinical application of this work: adiponectin is suggested as a potential biomarker of osteoporosis. Its cross-sectional correlation with hip BMD could provide a non-invasive and cheap readout of current osteoporotic status, but more importantly, its significant correlation with hip BMD five years prospectively could provide a marker for future osteoporotic development.

In depth *in vivo* investigation of young AdipoR1$^{-/-}$ female mice in Chapters 4 and 5 did not produce a mechanistic understanding of how AdipoR1 deletion causes the observed bone phenotype, although some potential mechanisms, both intrinsic and extrinsic to the bone, are discussed in **Section 5.3**. Previously, discrepancies between *in vitro* and *in vivo* effects of adiponectin have been reported[229,247,248] (discussed in **Section 1.4.2**) with the conclusion that adiponectin is exerting distinct effects locally and systemically. The data in Chapters 4 and 5 suggest the systemic effect of global AdipoR1 deletion on bone is negative and therefore the effect of systemic adiponectin on bone is positive; conversely, the *in vitro* investigation in Chapter 6 suggests adiponectin signalling in cells of the bone microenvironment has a direct negative effect on bone formation. However, since no definitive mechanism by which adiponectin exerts its effects have been established in this thesis, the effects associated with *in vitro* culture cannot be excluded from consideration when interpreting these results.

First, the use of cell lines should be considered a significant factor in interpreting these results. The unphysiological properties of these cells bestowed upon them during the

genetic manipulation required for their immortalisation for easier *in vitro* use can alter their phenotype, functions and responses to external stimuli and thus may not accurately represent the function of primary cells[376].

Second, the *in vitro* conditions themselves should be considered. *In vitro* cells are cultured with 20% O_2, which is close to the normal oxygen content of the air. However, despite being highly vascularised, oxygen levels in the bone range from <1-6%[377] and the bone marrow environment is one of the most hypoxic in the body[378]. Cells of the bone microenvironment usually operate in this hypoxic environment where hypoxia-inducible transcription factors are stabilised rather than degraded as they are in conditions of normoxia[378]. Stable expression of one such transcription factor, hypoxia-inducible factor 1α (HIF1α), in osteoblast precursors in prenatal mice significantly increased osteoblast population expansion and cancellous bone formation, suggesting hypoxic conditions have a positive effect on bone formation[378]. Adiponectin has been shown to mediate biological effects in a human osteosarcoma cell line via a pathway involving HIF1α activation[379]. This was found to involve signalling via the adiponectin receptors, since siRNA-mediated knockdown of AdipoR1 and AdipoR2 ameliorated the adiponectin-induced HIF1α activation, but whether this effect was primarily mediated by AdipoR1 or AdipoR2 was not established[379]. Although adiponectin-mediated activation of HIF1α has not been reported in cells of the bone microenvironment, taking this information together it can be hypothesised that it would promote bone formation. In the highly oxygenated conditions of *in vitro* culture, it is possible that the inhibition of HIF1α removes the hypoxia-induced positive effect of adiponectin signalling on bone formation that exists in the hypoxic bone environment *in vivo*.

While inhibition of HIF1α expression in normoxia in these cultured cells does not explain the significant increase in bone formation *in vitro* following AdipoR1 knockdown, it demonstrates how critical the bone microenvironment is to the normal functioning of

the cells within it. Two-dimensional culture and loss of the bone marrow niche heterogeneity have also been identified to affect cell function and remain problems to overcome in the *in vitro* modelling of the bone marrow niche[380,381].

It is possible that one or more of these *in vitro*-associated environmental alterations underlies the discrepancy between the observed positive association of adiponectin and bone *in vivo* in Chapters 4 and 5 and the negative association when studied *in vitro* in Chapter 6, rather than this representing a significant biological difference in the effect of adiponectin signalling dependant on a local or systemic modality. This cannot be concluded from the data collected and future work should seek to clarify this.

7.2 Directions for future research

7.2.1 Characterisation of the clinical utility of adiponectin as a biomarker

The most clinically relevant finding of the work presented in this thesis is the possibility that cross-sectional and five-year prospective hip BMD could be predicted by circulating total adiponectin concentration in a group at high risk of osteoporosis development. This could implicate serum adiponectin concentration as a biomarker of osteoporotic incidence and as a biological predictor of its five-year development. This is particularly important given the current lack of clinically available biomarkers for the prediction of osteoporotic development or progression, making clinical decisions about whom to treat based on their observable risk factors difficult. Previous work has identified the relationship between adiponectin and bone health as cohort-specific, particularly with regards to menopausal status in women (**Section 1.4.1**), and future work should seek to determine

whether these correlations persist in other cohorts, including pre- and peri-menopausal women and in men.

A challenging clinical consideration is the occurrence of poor responses to bisphosphonate treatment in a significant proportion of patients, defined by parameters such as occurrence of two fractures during treatment or a continued reduction in BMD[382]. It is believed that lack of adherence to the treatment regime is a problem that underlies some treatment failure, particularly since bisphosphonates are often prescribed long-term which reduces adherence[383], but even in cases of adherence, significant rates of treatment failure still persist[382]. Given the observed correlation of the HMW to LMW adiponectin ratio, rather than total adiponectin, with patient response to TZDs[215], investigation into whether the ratio of the adiponectin oligomers is correlated with patient response to bisphosphonate treatment is warranted to permit a better clinical understanding and prediction of patient response.

7.2.2 Further investigation of the effect of AdipoR1 deletion on the bone

The advent of technologies for the genetic manipulation of murine models has revolutionised pre-clinical strategies. The work presented here makes use of two mouse lines in which the bone phenotype was previously uncharacterised: global AdipoR1$^{-/-}$ or AdipoR2$^{-/-}$ mice. The global nature of this deletion makes precise determination of the mechanism by which it causes the observed bone phenotype difficult. An interesting extension of this work would involve consideration of global AdipoR1/AdipoR2 double knockout (DKO) mice. These mice have been reported to show some of the main phenotypic presentations typical of adiponectin knockout mice, including increased insulin levels and marked glucose intolerance[166], but their bone phenotype remains

unexplored. Moreover, it is suggested that comparison of the DKO bone phenotype with the bone phenotype of AdipoR2$^{-/-}$ mice could provide a different and insightful experimental setup in which to investigate further the role of adiponectin signalling via AdipoR1 in the bone.

As discussed in **Section 5.3**, the use of conditional knockout models could provide a useful further extension to this work. As well as an osteoblast-specific AdipoR1$^{-/-}$ knockout model, an adipocyte-specific AdipoR1$^{-/-}$ knockout model could also prove useful and interesting insight into the role of adiponectin in bone, and adiponectin-Cre mice have been used to knockout genes of interest in bone marrow adipose tissue[384], although adiponectin expression by all adipose tissue means this will affect WAT and BAT depots as well as BMAT. Models are beginning to identify rMAT- and cMAT-specific expression profiles, including PTRF as critical for rMAT development but not cMAT[118], and these models could reveal new opportunities for closer understanding of the role of AdipoR1$^{-/-}$ and AdipoR2$^{-/-}$ in the bone microenvironment. Similarly, specific targeting of mesenchymal stem cells using paired related homeobox 1 (Prx1)-Cre lines have been reported[385] which may also provide a more specific mechanism by which to investigate the cell-intrinsic effects of AdipoR1$^{-/-}$. This could be further aided by the use of newly developed single cell sequencing techniques: a recently published study of over 15,000 cells of the bone marrow microenvironment, including vascular, perivascular and osteoblastic cells, found vast cellular heterogeneity and provided single-cell resolution for the identification of proteins of interest, including growth factors and cytokines[386].

Inducible knockout systems make use of the application of an external stimulus, most often tetracyclin or tamoxifen, to cause the knockout to occur[387]. These systems have a significant advantage over non-inducible systems since normal development can take place before acute alteration in the expression of the gene of interest. This permits specific study of the role of the gene of interest at different developmental or cellular

differentiation stages and prevents complication of this understanding with long-standing compensatory mechanisms that could develop if the defect is present from embryonic development[229,388]. Future use of these specific and inducible knockout systems could provide a better understanding of the mechanistic involvement of adiponectin signalling via AdipoR1 in bone.

7.2.3 Clarifying the effects of *in vitro* culture on cells of the bone microenvironment

Due to the significant biological and functional differences of cell lines, future work on the effect of AdipoR1 manipulation *in vitro* must first determine whether the direct negative effect on bone formation observed in this thesis persists in cultured primary cells. The resolution of this discrepancy following use of primary cells would suggest the difference observed in this work stemmed from the use of biologically distinct cell lines. If, however, this discrepancy does continue, future work should seek to clarify that this is a true biological effect mediated by distinct local and systemic effects of adiponectin, rather than an artefact of the non-physiological *in vitro* conditions. Initially it is indicated that this should involve verification of the results in more varied *in vitro* models: the use of human and mouse cell lines is suggested alongside primary murine bone cells or MSCs. Induced pluripotent stem cell-derived osteogenic cells have recently been described[389] and represent another potential experimental setup in which to investigate the effect of AdipoR1 signalling *in vitro*. Further interrogation of the effect could involve the use of hypoxia chambers to recreate more accurately the hypoxic conditions of the bone, and charcoal-stripped FBS such that endogenous adiponectin does not affect the results obtained.

Interestingly, previous work has found the expression of some surface markers disappeared following *in vitro* culture[54]. This led the authors to conclude that their expression was induced *in vivo* by the bone marrow microenvironment and that the necessary stimuli were absent in the culture medium, demonstrating a direct effect of *in vitro* culture on cellular expression profiles. It is suggested that determination of the specific effect of *in vitro* culture via direct RNASeq comparison of primary cells that have just been extracted from an *in vivo* model with the same cell type that has undergone *in vitro* culture could provide some insight into whether the differences observed are a true biological effect.

Even if factors such as hypoxia and the changes in the expression profiles of cells following *in vitro* culture are taken into account, it is suggested that *in vitro* work is not a useful experimental paradigm for the study of the effects of adiponectin in bone since many factors, such as the two-dimensional growth surface and lack of surrounding stroma, cannot be recapitulated *in vitro*. It should also be considered that given the observed significant whole-body effects of adiponectin on bone, exclusion of these might not provide a useful insight into its biological roles and that more specific *in vivo* investigation is most likely to provide an improved understanding of the role of adiponectin and its signalling via AdipoR1 in bone.

In summary, adiponectin has powerful but complicated biological effects on the bone mediated by complex signalling pathways. While in time it could represent therapeutic possibilities, it is likely that a far deeper understanding of its overlapping and potentially conflicting effects within and without the bone and further exploration of its upstream and downstream pathways is necessary for this exciting possibility to become clinically feasible. Despite this, adiponectin is indicated here as a potential osteoporosis biomarker, an important step in the search for better diagnosis and treatment of musculoskeletal disease.

References

1. Clarke, B. Normal bone anatomy and physiology. *Clin. J. Am. Soc. Nephrol.* **3**, S131–S139 (2008).

2. Boskey, A. L. & Coleman, R. Aging and Bone. *Crit. Rev. Oral Biol. Med.* **89**, 1333–1348 (2010).

3. Berendsen, A. D. & R, O. B. Bone development. *Bone* **80**, 14–18 (2015).

4. Jilka, R. L. The relevance of mouse models for investigating age-related bone loss in humans. *Journals Gerontol. Ser. A Biol. Sci. Med. Sci.* **68**, 1209–1217 (2013).

5. Sambrook, P., Kelly, P. & Eisman, J. Bone mass and ageing. *Baillieres. Clin. Rheumatol.* **7**, 445–457 (1993).

6. Downey, P. A. & Siegel, M. I. Bone biology and the clinical implications for osteoporosis. *Phys. Ther.* **86**, 77–91 (2006).

7. Florencio-Silva, R., Sasso, G. R. D. S., Sasso-Cerri, E., Simões, M. J. & Cerri, P. S. Biology of Bone Tissue: Structure, Function, and Factors That Influence Bone Cells. *Biomed Res. Int.* **2015**, 421746 (2015).

8. Sommerfeldt, D. & Rubin, C. Biology of bone and how it orchestrates the form and function of the skeleton. *Eur. Spine J.* **10**, 86–95 (2001).

9. Hadjidakis, D. J. & Androulakis, I. I. Bone remodeling. *Ann. N. Y. Acad. Sci.* **1092**, 385–396 (2006).

10. Rutkovskiy, A., Stensløkken, K.-O. & Vaage, I. J. Osteoblast Differentiation at a Glance. *Med. Sci. Monit. Basic Res.* **22**, 95–106 (2016).

11. Zheng, H., Guo, Z., Ma, Q., Jia, H. & Dang, G. Cbfa1/osf2 Transduced Bone Marrow Stromal Cells Facilitate Bone Formation In Vitro and In Vivo. *Calcif. Tissue Int.* **74**, 194–203 (2004).

12. Komori, T. *et al.* Targeted Disruption of Cbfa1 Results in a Complete Lack of Bone Formation owing to Maturational Arrest of Osteoblasts. *Cell* **89**, 755–764 (1997).

13. Nakashima, K. *et al.* The novel zinc finger-containing transcription factor Osterix is required for osteblast differentiation and bone formation. *Cell* **106**, 17–29 (2002).

14. Manolagas, S. C. Birth and death of bone cells: Basic regulatory mechanisms and implications for the pathogenesis and treatment of osteoporosis. *Endocr. Rev.* **21**, 115–137 (2000).

15. Moorer, M. C. & Riddle, R. C. Regulation of Osteoblast Metabolism by Wnt

Signaling. *Endocrinol. Metab.* **33**, 318–330 (2018).

16. Gaur, T. *et al.* Canonical WNT signaling promotes osteogenesis by directly stimulating Runx2 gene expression. *J. Biol. Chem.* **280**, 33132–33140 (2005).

17. Canalis, E. Notch signaling in osteoblasts. *Sci. Signal.* **1**, 1–5 (2008).

18. Zorn, A. M. Antagonistic Dickkopfs. *Curr. Biol.* **11**, R592-595 (2001).

19. Li, X. *et al.* Sclerostin binds to LRP5/6 and antagonizes canonical Wnt signaling. *J. Biol. Chem.* **280**, 19883–19887 (2005).

20. Greco, T. L. *et al.* Analysis of the vestigial tail mutation demonstrates that Wnt-3a gene dosage regulates mouse axial development. *Genes Dev.* **10**, 313–324 (1996).

21. Kato, M. *et al.* Cbfa1-independent decrease in osteoblast proliferation, osteopenia, and persistent embryonic eye vascularization in mice deficient in Lrp5, a Wnt coreceptor. *J. Cell Biol.* **157**, 303–314 (2002).

22. Little, R. D. *et al.* A Mutation in the LDL Receptor-Related Protein 5 Gene Results in the Autosomal Dominant High-Bone-Mass Trait. *Am. J. Hum. Genet.* **70**, 11–19 (2002).

23. Takada, I., Kouzmenko, A. P. & Kato, S. Wnt and PPARγ signaling in osteoblastogenesis and adipogenesis. *Nat. Rev. Rheumatol.* **5**, 442–447 (2009).

24. Takada, I. *et al.* A histone lysine methyltransferase activated by non-canonical Wnt signalling suppresses PPAR-γ transactivation. *Nat. Cell Biol.* **9**, 1273–1285 (2007).

25. Abe, E. *et al.* Essential Requirement of BMPs-2/4 for Both Osteoblast and Osteoclast Formation in Murine Bone Marrow Cultures from Adult Mice: Antagonism by Noggin. *J. Bone Miner. Res.* **15**, 663–673 (2000).

26. Matsumoto, T., Kuriwaka-Kido, R., Kondo, T., Endo, I. & Kido, S. Regulation of osteoblast differentiation by interleukin-11 via AP-1 and Smad signaling. *Endocr. J.* **59**, 91–101 (2012).

27. Blair, H. C., Schlesigner, P. H., Huang, C. L. H. & Zaidi, M. Calcium Signalling and Calcium Transport in Bone. *Subcell. Biochem.* **45**, 539–562 (2007).

28. Stains, J. P., Weber, J. A. & Gay, C. V. Expression of Na+/Ca2+ exchanger isoforms (NCX1 and NCX3) and plasma membrane Ca2+ ATPase during osteoblast differentiation. *J. Cell. Biochem.* **84**, 625–635 (2002).

29. Fedde, K. N. *et al.* Alkaline Phosphatase Knock-Out Mice Recapitulate the Metabolic and Skeletal Defects of Infantile Hypophosphatasia. *J. Bone* **14**, 2015–2026 (2015).

30. Blair, H. C. *et al.* Support of bone mineral deposition by regulation of pH. *Am. J. Physiol. - Cell Physiol.* **315**, C587–C597 (2018).

31. Bonewald, L. F. The amazing osteocyte. *J. Bone Miner. Res.* **26**, 229–38 (2011).

32. Bonewald, L. F. & Johnson, M. L. Osteocytes, mechanosensing and Wnt signaling. *Bone* **42**, 606–615 (2008).

33. Sun, Y. *et al.* Failure to process Dentin Matrix Protein 1 (DMP1) into fragments leads to its loss of function in osteogenesis. *J. Biol. Chem.* **285**, 31713–31722 (2010).

34. Poole, K. E. S. *et al.* Sclerostin is a delayed secreted product of osteocytes that inhibits bone formation. *FASEB J.* **19**, 1842–1844 (2005).

35. Nakashima, T. *et al.* Evidence for osteocyte regulation of bone homeostasis through RANKL expression. *Nat. Med.* **17**, 1231–1234 (2011).

36. Tatsumi, S. *et al.* Targeted Ablation of Osteocytes Induces Osteoporosis with Defective Mechanotransduction. *Cell Metab.* **5**, 464–475 (2007).

37. Stenbeck, G. Formation and function of the ruffled border in osteoclasts. *Semin. Cell Dev. Biol.* **13**, 243–249 (2002).

38. Grigoriadis, A. E. *et al.* c-Fos: A Key Regulator of Osteoclast Macrophage Lineage Determination and Bone Remodeling. *Science (80-.).* **266**, 443–448 (1994).

39. Matsuo, K. *et al.* Nuclear factor of activated T-cells (NFAT) rescues osteoclastogenesis in precursors lacking c-Fos. *J. Biol. Chem.* **279**, 26475–26480 (2004).

40. Arai, A. *et al.* Fos plays an essential role in the upregulation of RANK expression in osteoclast precursors within the bone microenvironment. *J. Cell Sci.* **125**, 2910–2917 (2012).

41. Xu, F. & Teitelbaum, S. L. Osteoclasts: New Insights. *Bone Res.* **1**, 11–26 (2013).

42. Boyle, W. J., Simonet, W. S. & Lacey, D. L. Osteoclasts Differentation and Activation. *Nature* **423**, 337–342 (2003).

43. Díez-Pérez, A. *et al.* Effects of teriparatide on hip and upper limb fractures in patients with osteoporosis: A systematic review and meta-analysis. *Bone* **120**, 1–8 (2019).

44. Hanley, D. A., Adachi, J. D., Bell, A. & Brown, V. Denosumab: Mechanism of action and clinical outcomes. *Int. J. Clin. Pract.* **66**, 1139–1146 (2012).

45. Vesprey, A. & Yang, W. Pit Assay to Measure the Bone Resorptive Activity of Bone Marrow-derived Osteoclasts. *Bio-Protocol* **6**, 1–10 (2016).

46. Hughes, D. E. *et al.* Estrogen promotes apoptosis of murine osteoclasts mediated byTGFb. *Nat. Med.* **2**, 1132–1136 (1996).

47. Kumar, R., Godavarthy, P. S. & Krause, D. S. The bone marrow microenvironment in health and disease at a glance. *J. Cell Sci.* **131**, jcs201707 (2018).

48. Friedenstein, A. J., Chailakhjan, R. K. & Lalykina, K. S. The development of fibroblast colonies in monolayer ultures of guinea-pig bone marrow and spleen cells. *Cell Tissue Kinet.* **3**, 393–403 (1970).

49. Caplan, A. I. Mesenchymal Stem Cells. *J. Orthop. Res.* **9**, 641–650 (1991).

50. Sacchetti, B. *et al.* Self-Renewing Osteoprogenitors in Bone Marrow Sinusoids Can Organize a Hematopoietic Microenvironment. *Cell* **131**, 324–336 (2007).

51. Delorme, B. *et al.* Specific lineage-priming of bone marrow mesenchymal stem cells provides the molecular framework for their plasticity. *Stem Cells* **27**, 1142–1151 (2009).

52. Cook, D. & Genever, P. *Regulation of Mesenchymal Stem Cell Differentiation. In: Transcriptional and Translational Regulation of Stem Cells: Advances in Experimental Medicine and Biology*. (Springer Dordrecht, 2013).

53. Augello, A. & De Bari, C. The regulation of differentiation in mesenchymal stem cells. *Hum. Gene Ther.* **21**, 1226–1238 (2010).

54. Jones, E. A. *et al.* Isolation and characterization of bone marrow multipotential mesenchymal progenitor cells. *Arthritis Rheum.* **46**, 3349–3360 (2002).

55. Hu, X. *et al.* Identification of a common mesenchymal stromal progenitor for the adult haematopoietic niche. *Nat. Commun.* **7**, 1–14 (2016).

56. Cohen Jr, M. M. The New Bone Biology: Pathologic, Molecular and Clinical Correlates. *Am. J. Med. Genet. Part A* **140A**, 2646–2706 (2006).

57. Rodan, G. A. & Martin, T. J. Therapeutic approaches to bone diseases. *Science (80-.).* **289**, 1508–1514 (2000).

58. Arias, C. F., Herrero, M. A., Echeverri, L. F., Oleaga, G. E. & López, J. M. Bone remodeling: A tissue-level process emerging from cell-level molecular algorithms. *PLoS One* **13**, e0204171 (2018).

59. Verborgt, O., Gibson, G. J. & Schaffler, M. B. Loss of osteocyte integrity in association with microdamage and bone remodeling after fatigue in vivo. *J. Bone Miner. Res.* **15**, 60–67 (2000).

60. Sims, N. A. & Martin, T. J. Coupling the activities of bone formation and resorption: a multitude of signals within the basic multicellular unit. *Bonekey Rep.*

3, 481–490 (2014).

61. Raggatt, L. J. & Partridge, N. C. Cellular and molecular mechanisms of bone remodeling. *J. Biol. Chem.* **285**, 25103–25108 (2010).

62. Tunyogi-Csapo, M. *et al.* Cytokine-controlled RANKL and osteoprotegerin expression by human and mouse synovial fibroblasts. *Arthritis Rheum.* **58**, 2397–2408 (2008).

63. Wang, R. *et al.* Regulation of activation-induced receptor activator of NF-κB ligand (RANKL) expression in T cells. *Eur. J. Immunol.* **32**, 1090–1098 (2002).

64. Eriksen, E. F., Melsen, F. & Mosekilde, L. Reconstruction of the resorptive site in iliac trabecular bone: A kinetic model for bone resorption in 20 normal individuals. *Metab. Bone Dis. Relat. Res.* **5**, 235–242 (1984).

65. Tang, Y. *et al.* TGF-B1-induced migration of bone mesenchymal stem cells couples bone resorption and formation. *Nat. Med.* **15**, 757–765 (2009).

66. Howard, G. A., Bottemiller, B. L., Turner, R. T., Rader, J. I. & Baylink, D. J. Parathyroid hormone stimulates bone formation and resorption in organ culture: Evidence for a coupling mechanism. *Proc. Natl. Acad. Sci. U. S. A.* **78**, 3204–3208 (1981).

67. Pederson, L., Ruan, M., Westendorf, J. J., Khosla, S. & Oursler, M. J. Regulation of bone formation by osteoclasts involves Wnt/BMP signaling and the chemokine sphingosine-1-phosphate. *Proc. Natl. Acad. Sci. U. S. A.* **105**, 20764–20769 (2008).

68. Krum, S. A. *et al.* Estrogen protects bone by inducing Fas ligand in osteoblasts to regulate osteoclast survival. *EMBO J.* **27**, 535–545 (2008).

69. Baum, M. The bone kidney axis. *Curr. Opin. Pediatr.* **26**, 177–179 (2014).

70. Damasiewicz, M. J. & Nickolas, T. L. Rethinking Bone Disease in Kidney Disease. *JBMR Plus* **2**, 309–322 (2018).

71. Hruska, K. A., Mathew, S., Lund, R., Qiu, P. & Pratt, R. Hyperphosphatemia in chronic kidney disease. *Kidney Interational* **74**, 148–157 (2008).

72. Tomasello, S. Secondary hyperparathyroidism and target organs in chronic kidney disease. *Diabetes Spectr.* **21**, 19–25 (2008).

73. Gesta, S., Tseng, Y. H. & Kahn, C. R. Developmental Origin of Fat: Tracking Obesity to Its Source. *Cell* **131**, 242–256 (2007).

74. Luo, L. & Liu, M. Adipose tissue in control of metabolism. *J. Endocrinol.* **231**, R77–R99 (2016).

75. Song, Z., Xiaoli, A. M. & Yang, F. Regulation and metabolic significance of de

novo lipogenesis in adipose tissues. *Nutrients* **10**, 1383 (2018).

76. Berry, D. C., Stenesen, D., Zeve, D. & Graff, J. M. The developmental origins of adipose tissue. *Development* **140**, 3939–3949 (2013).

77. Park, A., Kim, W. & Bae, K. Distinction of white, beige and brown adipocytes derived from mesenchymal stem cells. *World J. Stem Cells* **6**, 33 (2014).

78. Seale, P. *et al.* PRDM16 controls a brown fat/skeletal muscle switch. *Nature* **454**, 961–967 (2008).

79. Rosen, E. D. *et al.* PPAR-Gamma Is Required for the Differentiation of Adipose Tissue In Vivo and In Vitro. *Mol. Cell* **4**, 611–617 (1999).

80. Tontonoz, P., Hu, E. & Spiegelman, B. M. Stimulation of Adipogenesis by PPARy2, a Lipid-Activated in Fibroblasts Transcription Factor. *Cell* **79**, 1147–1156 (1994).

81. Tamori, Y., Masugi, J., Nishino, N. & Kasuga, M. Role of Peroxisome Proliferator–Activated Receptor gamma in Maintenance of the Characteristics of Mature 3T3-L1 Adipocytes.pdf. *Diabetes* **51**, 2045–2055 (2002).

82. Rosen, E. D. *et al.* C/EBPa induces adipogenesis through PPARγ: a unified pathway. *Genes Dev.* **16**, 22–26 (2002).

83. Kang, S. *et al.* Wnt signaling stimulates osteoblastogenesis of mesenchymal precursors by suppressing CCAAT/enhancer-binding protein α and peroxisome proliferator-activated receptor γ. *J. Biol. Chem.* **282**, 14515–14524 (2007).

84. Ross, D. A., Rao, P. K. & Kadesch, T. Dual Roles for the Notch Target Gene Hes-1 in the Differentiation of 3T3-L1 Preadipocytes. *Mol. Cell. Biol.* **24**, 3505–3513 (2004).

85. Nichols, A. M. *et al.* Notch pathway is dispensable for adipocyte specification. *Genesis* **40**, 40–44 (2004).

86. Wang, E. A., Israel, D. I., Kelly, S. & Luxenberg, D. P. Bone morphogenetic protein-2 causes commitment and differentiation in C3H10T1/2 and 3T3 cells. *Growth Factors* **9**, 57–71 (1993).

87. Rosen, E. D. & MacDougald, O. A. Adipocyte differentiation from the inside out. *Nat. Rev. Mol. Cell Biol.* **7**, 885–896 (2006).

88. Veldhuis-Vlug, A. G. & Rosen, C. J. *Clinical implications of bone marrow adiposity*. *Journal of Internal Medicine* **283**, (2018).

89. Jeanson, Y., Carrière, A. & Casteilla, L. A new role for browning as a redox and stress adaptive mechanism? *Front. Endocrinol. (Lausanne).* **6**, 158–169 (2015).

90. Cook, K. S., Groves, D. L., Min, H. Y. & Spiegelman, B. M. A developmentally regulated mRNA from 3T3 adipocytes encodes a novel serine protease homologue. *Proc. Natl. Acad. Sci. U. S. A.* **82**, 6480–6484 (1985).

91. Cook, K. S. *et al.* Adipsin: a circulating serine protease homolog secreted by adipose tissue and sciatic nerve. *Science (80-.).* **237**, 402–405 (1987).

92. Zhang, Y. *et al.* Positional cloning of the mouse obese gene and its human homologue. *Nature* **372**, 425–432 (1994).

93. Ronti, T., Lupattelli, G. & Mannarino, E. The endocrine function of adipose tissue: An update. *Clin. Endocrinol. (Oxf).* **64**, 355–365 (2006).

94. Pan, W. W. & Myers, M. G. Leptin and the maintenance of elevated body weight. *Nat. Rev. Neurosci.* **19**, 95–105 (2018).

95. Takeda, S. *et al.* Leptin regulates bone formation via the sympathetic nervous system. *Cell* **111**, 305–317 (2002).

96. Kajimura, D. *et al.* Adiponectin regulates bone mass via opposite central and peripheral mechanisms through FoxO1. *Cell Metab.* **17**, 901–915 (2013).

97. Turner, R. T. *et al.* Peripheral leptin regulates bone formation. *J. Bone Miner. Res.* **28**, 22–34 (2013).

98. Thomas, T. *et al.* Leptin acts on human marrow stromal cells to enhance differentiation to osteoblasts and to inhibit differentiation to adipocytes. *Endocrinology* **140**, 1630–1638 (1999).

99. Yue, R., Zhou, B. O., Shimada, I. S., Zhao, Z. & Morrison, S. J. Leptin Receptor Promotes Adipogenesis and Reduces Osteogenesis by Regulating Mesenchymal Stromal Cells in Adult Bone Marrow. *Cell Stem Cell* **18**, 782–796 (2016).

100. Zhang, K. *et al.* Preservation of high-fat diet-induced femoral trabecular bone loss through genetic target of TNFα. *Endocrine* **50**, 239–249 (2015).

101. Wang, C. *et al.* Interleukin-6 gene knockout antagonizes high-fat-induced trabecular bone loss. *J. Mol. Endocrinol.* **57**, 161–170 (2016).

102. Cawthorn, W. P., Heyd, F., Hegyi, K. & Sethi, J. K. Tumour necrosis factor-α inhibits adipogenesis via a β-catenin/TCF4(TCF7L2)-dependent pathway. *Cell Death Differ.* **14**, 1361–1373 (2007).

103. Huang, R. L. *et al.* IL-6 potentiates BMP-2-induced osteogenesis and adipogenesis via two different BMPR1A-mediated pathways article. *Cell Death Dis.* **9**, 144–158 (2018).

104. Ruan, H. *et al.* Profiling gene transcription in vivo reveals adipose tissue as an immediate target of tumor necrosis factor-α: Implications for insulin resistance.

Diabetes **51**, 3176–3188 (2002).

105. Senn, J. J. *et al.* Suppressor of cytokine signaling-3 (SOCS-3), a potential mediator of interleukin-6-dependent insulin resistance in hepatocytes. *J. Biol. Chem.* **278**, 13740–13746 (2003).

106. Scarpace, P. J. & Zhang, Y. Leptin resistance: A prediposing factor for diet-induced obesity. *Am. J. Physiol. - Regul. Integr. Comp. Physiol.* **296**, R493-500 (2009).

107. Symonds, M. E., Aldiss, P., Pope, M. & Budge, H. Recent advances in our understanding of brown and beige adipose tissue: The good fat that keeps you healthy [version 1; referees: 2 approved]. *F1000Research* **7**, 1129 (2018).

108. Villarroya, F., Cereijo, R., Villarroya, J. & Giralt, M. Brown adipose tissue as a secretory organ. *Nat. Rev. Endocrinol.* **13**, 26–35 (2017).

109. Foster, M. T. *et al.* Subcutaneous adipose tissue transplantation in diet-induced obese mice attenuates metabolic dysregulation while removal exacerbates it. *Physiol. Rep.* **1**, 1–12 (2013).

110. Cannon, B. & Nedergaard, J. Brown Adipose Tissue: Function and Physiological Significance. *Physiol. Rev.* **84**, 277–359 (2004).

111. Horowitz, M. C. *et al.* Bone marrow adipocytes. *Adipocyte* **6**, 193–204 (2017).

112. Symonds, M. E. Brown adipose tissue growth and development. *Scientifica (Cairo).* **2013**, 51–66 (2013).

113. Gill, J. A. & La Merrill, M. A. An emerging role for epigenetic regulation of Pgc-1α expression in environmentally stimulated brown adipose thermogenesis. *Environ. Epigenetics* **3**, 1–7 (2017).

114. Nisoli, E., Tonello, C., Benarese, M., Liberini, P. & Carruba, M. O. Expression of nerve growth factor in brown adipose tissue: Implications for thermogenesis and obesity. *Endocrinology* **137**, 495–503 (1996).

115. Sun, K. *et al.* Brown adipose tissue derived VEGF-A modulates cold tolerance and energy expenditure. *Mol. Metab.* **3**, 474–483 (2014).

116. Mahdaviani, K., Chess, D., Wu, Y., Shirihai, O. & Aprahamian, T. Autocrine Effect of Vascular Endothelial Growth Factor-A is Essential for Mitochondrial Function in Brown Adipocytes. *Metabolism* **65**, 26–35 (2016).

117. Vijgen, G. H. E. J. *et al.* Brown adipose tissue in morbidly obese subjects. *PLoS One* **6**, e17247 (2011).

118. Scheller, E. L. *et al.* Region-specific variation in the properties of skeletal adipocytes reveals regulated and constitutive marrow adipose tissues. *Nat.*

Commun. **6**, 7808 (2015).

119. Krings, A. *et al.* Bone marrow fat has brown adipose tissue characteristics, which are attenuated with aging and diabetes. *Bone* **50**, 546–552 (2012).

120. Li, Q., Wu, Y. & Kang, N. Marrow adipose tissue: Its origin, function, and regulation in bone remodeling and regeneration. *Stem Cells Int.* **2018**, 7098456 (2018).

121. Li, Y., Meng, Y. & Yu, X. The Unique Metabolic Characteristics of Bone Marrow Adipose Tissue. *Front. Endocrinol. (Lausanne).* **10**, 1–13 (2019).

122. Scheller, E. L. *et al.* Use of osmium tetroxide staining with microcomputerized tomography to visualize and quantify bone marrow adipose tissue in vivo. *Methods Enzymol.* **537**, 123–139 (2014).

123. Scheller, E. L. *et al.* Bone marrow adipocytes resist lipolysis and remodeling in response to β-adrenergic stimulation. *Bone* **118**, 32–41 (2019).

124. Suchacki, K. J. & Cawthorn, W. P. Molecular Interaction of Bone Marrow Adipose Tissue with Energy Metabolism. *Curr. Mol. Biol. Reports* **4**, 41–49 (2018).

125. Pino, A. M., Miranda, M., Figueroa, C., Rodríguez, J. P. & Rosen, C. J. Qualitative aspects of bone marrow adiposity in osteoporosis. *Front. Endocrinol. (Lausanne).* **7**, 139 (2016).

126. Kim, T. Y. & Schafer, A. L. Diabetes and bone marrow adiposity. *Curr. Osteoporos. Rep.* **14**, 337–344 (2016).

127. Georgiou, K. R. *et al.* Attenuated Wnt/β-catenin signalling mediates methotrexate chemotherapy-induced bone loss and marrow adiposity in rats. *Bone* **50**, 1223–1233 (2012).

128. Cawthorn, W. P. *et al.* Bone marrow adipose tissue is an endocrine organ that contributes to increased circulating adiponectin during caloric restriction. *Cell Metab.* **20**, 368–375 (2014).

129. Walsh, J. S. & Vilaca, T. Obesity, Type 2 Diabetes and Bone in Adults. *Calcif. Tissue Int.* **100**, 528–535 (2017).

130. Naveiras, O. *et al.* Bone-marrow adipocytes as negative regulators of the haematopoietic microenvironment. *Nature* **460**, 259–263 (2009).

131. Spindler, T. J., Tseng, A. W., Zhou, X. & Adams, G. B. Adipocytic cells augment the support of primitive hematopoietic cells in Vitro but have no effect in the bone marrow niche under homeostatic conditions. *Stem Cells Dev.* **23**, 434–441 (2014).

132. Ambrosi, T. H. *et al.* Adipocyte Accumulation in the Bone Marrow during Obesity and Aging Impairs Stem Cell-Based Hematopoietic and Bone Regeneration. *Cell*

Stem Cell **20**, 771–784 (2017).

133. Hardaway, A. L., Herroon, M. K., Rajagurubandara, E. & Podgorski, I. Marrow adipocyte-derived CXCL1 and CXCL2 contribute to bone osteolysis in metastatic prostate cancer. *Clin. Exp. Metastasis* **32**, 353–368 (2015).

134. Takeshita, S., Fumoto, T., Naoe, Y. & Ikeda, K. Age-related marrow adipogenesis is linked to increased expression of RANKL. *J. Biol. Chem.* **289**, 16699–16710 (2014).

135. Yang, Y. *et al.* Effect of zoledronic acid on vertebral marrow adiposity in postmenopausal osteoporosis assessed by MR spectroscopy. *Skeletal Radiol.* **44**, 1499–1505 (2015).

136. Duque, G. & Rivas, D. Alendronate has an anabolic effect on bone through the differentiation of mesenchymal stem cells. *J. Bone Miner. Res.* **22**, 1603–1611 (2007).

137. Elbaz, A., Wu, X., Rivas, D., Gimble, J. M. & Duque, G. Inhibition of fatty acid biosynthesis prevents adipocyte lipotoxicity on human osteoblasts in vitro. *J. Cell. Mol. Med.* **14**, 982–991 (2010).

138. Taipaleenmäki, H., Abdallah, B. M., AlDahmash, A., Säämänen, A. M. & Kassem, M. Wnt signalling mediates the cross-talk between bone marrow derived pre-adipocytic and pre-osteoblastic cell populations. *Exp. Cell Res.* **317**, 745–756 (2011).

139. Martin, P. J. *et al.* Adipogenic RNAs are transferred in osteoblasts via bone marrow adipocytes-derived extracellular vesicles (EVs). *BMC Cell Biol.* **16**, 10 (2015).

140. Liu, L. F., Shen, W. J., Ueno, M., Patel, S. & Kraemer, F. B. Characterization of age-related gene expression profiling in bone marrow and epididymal adipocytes. *BMC Genomics* **12**, 212 (2011).

141. Tencerova, M. *et al.* High-Fat Diet–Induced Obesity Promotes Expansion of Bone Marrow Adipose Tissue and Impairs Skeletal Stem Cell Functions in Mice. *J. Bone Miner. Res.* **33**, 1154–1165 (2018).

142. Scheller, E. L., Burr, A. A., MacDougald, O. A. & Cawthorn, W. P. Inside out: Bone marrow adipose tissue as a source of circulating adiponectin. *Adipocyte* **5**, 251–269 (2016).

143. Scherer, P. E., Williams, S., Fogliano, M., Baldini, G. & Lodish, H. F. A novel serum protein similar to C1q, produced exclusively in adipocytes. *J. Biol. Chem.* **270**, 26746–26749 (1995).

144. Hu, E., Liang, P. & Spiegelman, B. M. AdipoQ is a novel adipose-specific gene dysregulated in obesity. *J. Biol. Chem.* **271**, 10697–10703 (1996).

145. Maeda, K. *et al.* cDNA cloning and expression of a novel adipose specific collagen-like factor, apM1 (adipose most abundant gene transcript 1). *Biochem. Biophys. Res. Commun.* **221**, 286–289 (1996).

146. Nakano, Y., Tobe, T., Choi-Miura, N. H., Mazda, T. & Tomita, M. Isolation and characterization of GBP28, a novel gelatin-binding protein purified from human plasma. *J. Biochem.* **120**, 803–812 (1996).

147. Achari, A. E. & Jain, S. K. Adiponectin, a therapeutic target for obesity, diabetes, and endothelial dysfunction. *Int. J. Mol. Sci.* **18**, 1321–1337 (2017).

148. Tsao, T. S. Assembly of adiponectin oligomers. *Reviews in Endocrine and Metabolic Disorders* **15**, 125–136 (2014).

149. Shapiro, L. & Scherer, P. E. The crystal structure of a complement-1q family protein suggests an evolutionary link to tumor necrosis factor. *Curr. Biol.* **8**, 335–340 (1998).

150. Yamauchi, T. *et al.* Cloning of adiponectin receptors that mediate antidiabetic metabolic effects. *Nature* **423**, 760–762 (2003).

151. Chandran, M., Phillips, S. A., Ciaraldi, T. & Henry, R. R. Adiponectin: More than just another fat cell hormone? *Diabetes Care* **26**, 2442–2450 (2003).

152. Kadowaki, T. & Yamauchi, T. Adiponectin and adiponectin receptors. *Endocr. Rev.* **26**, 439–451 (2005).

153. Tsao, T. S. *et al.* Role of Disulfide Bonds in Acrp30/Adiponectin Structure and Signaling Specificity: Different oligomers activate different signal transduction pathways. *J. Biol. Chem.* **278**, 50810–50817 (2003).

154. Hampe, L. *et al.* Regulation and quality control of adiponectin assembly by endoplasmic reticulum chaperone ERp44. *J. Biol. Chem.* **290**, 18111–18123 (2015).

155. Halberg, N. *et al.* Systemic fate of the adipocyte-derived factor adiponectin. *Diabetes* **58**, 1961–1970 (2009).

156. Richards, A. A. *et al.* Sialic acid modification of adiponectin is not required for multimerization or secretion but determines half-life in circulation. *Mol. Endocrinol.* **24**, 229–239 (2010).

157. Kim, J. *et al.* Extracellular conversion of adiponectin hexamers into trimers. *Biosci. Rep.* **32**, 641–652 (2012).

158. Schraw, T., Wang, Z. V., Halberg, N., Hawkins, M. & Scherer, P. E. Plasma adiponectin complexes have distinct biochemical characteristics. *Endocrinology*

149, 2270–2282 (2008).

159. Peake, P. W., Kriketos, A. D., Campbell, L. V., Shen, Y. & Charlesworth, J. A. The metabolism of isoforms of human adiponectin: studies in human subjects and in experimental animals. *Eur. J. Endocrinol.* **153**, 409–417 (2005).

160. Ušaj, M. M. *et al.* Yeast Saccharomyces cerevisiae adiponectin receptor homolog Izh2 is involved in the regulation of zinc, phospholipid and pH homeostasis. *Metallomics* **7**, 1338–1351 (2015).

161. Yamauchi, T., Iwabu, M., Okada-Iwabu, M. & Kadowaki, T. Adiponectin receptors: A review of their structure, function and how they work. *Best Pract. Res. Clin. Endocrinol. Metab.* **28**, 15–23 (2014).

162. ADIPOR1. *The Human Protein Atlas* (2019). Available at: https://www.proteinatlas.org/ENSG00000159346-ADIPOR1/tissue. (Accessed: 16th September 2019)

163. ADIPOR2. *The Human Protein Atlas* (2019). Available at: https://www.proteinatlas.org/ENSG00000006831-ADIPOR2/tissue. (Accessed: 16th September 2019)

164. Berner, H. S. *et al.* Adiponectin and its receptors are expressed in bone-forming cells. *Bone* **35**, 842–849 (2004).

165. Kim, M. J. *et al.* Increased adiponectin receptor-1 expression in adipose tissue of impaired glucose-tolerant obese subjects during weight loss. *Eur. J. Endocrinol.* **155**, 161–165 (2006).

166. Yamauchi, T. *et al.* Targeted disruption of AdipoR1 and AdipoR2 causes abrogation of adiponectin binding and metabolic actions. *Nat. Med.* **13**, 332–339 (2007).

167. Rasmussen-Torvik, L. J. *et al.* The association of SNPs in ADIPOQ, ADIPOR1, and ADIPOR2 with insulin sensitivity in a cohort of adolescents and their parents. *Hum. Genet.* **125**, 21–28 (2009).

168. Damcott, C. M. *et al.* Genetic Variation in Adiponectin Receptor 1 and Adiponectin Receptor 2 Is Associated With Type 2 Diabetes in the Old Order Amish. **54**, 2245–2250 (2005).

169. Mao, X. *et al.* APPL1 binds to adiponectin receptors and mediates adiponectin signalling and function. *Nat. Cell Biol.* **8**, 516–523 (2006).

170. Ryu, J. *et al.* APPL1 potentiates insulin sensitivity by facilitating the binding of IRS1/2 to the insulin receptor. *Cell Rep.* **7**, 1227–1238 (2014).

171. Wang, C. *et al.* Yin-Yang regulation of adiponectin signaling by APPL isoforms

in muscle cells. *J. Biol. Chem.* **284**, 31608–31615 (2009).

172. Cheng, K. K. Y. *et al.* The adaptor protein APPL2 inhibits insulin-stimulated glucose uptake by interacting with TBC1D1 in skeletal muscle. *Diabetes* **63**, 3748–3758 (2014).

173. Zhou, L. *et al.* Adiponectin Activates AMP-activated Protein Kinase in Muscle Cells via APPL1 / LKB1-dependent and Phospholipase C / Ca 2 / Ca 2 / Calmodulin-dependent Protein Kinase Kinase-dependent Pathways *. *J. Biol. Chem.* **284**, 22426–35 (2009).

174. Salminen, A., Hyttinen, J. M. T. & Kaarniranta, K. AMP-activated protein kinase inhibits NF-κB signaling and inflammation: Impact on healthspan and lifespan. *J. Mol. Med.* **89**, 667–676 (2011).

175. Marcinko, K. & Steinberg, G. R. The role of AMPK in controlling metabolism and mitochondrial biogenesis during exercise. *Exp. Physiol.* **99**, 1581–1585 (2014).

176. Chopra, I., Li, H. F., Wang, H. & Webster, K. A. Phosphorylation of the insulin receptor by AMP-activated protein kinase (AMPK) promotes ligand-independent activation of the insulin signalling pathway in rodent muscle. *Diabetologia* **55**, 783–794 (2012).

177. Chen, M. B. *et al.* Impaired activation of AMP-kinase and fatty acid oxidation by globular adiponectin in cultured human skeletal muscle of obese type 2 diabetics. *J. Clin. Endocrinol. Metab.* **90**, 3665–3672 (2005).

178. Schultze, S. M., Hemmings, B. A., Niessen, M. & Tschopp, O. PI3K/AKT, MAPK and AMPK signalling: Protein kinases in glucose homeostasis. *Expert Rev. Mol. Med.* **14**, (2012).

179. Berg, A. H., Combs, T. P., Du, X., Brownlee, M. & Scherer, P. E. The adipocyte-secreted protein Acrp30 enhances hepatic insulin action. *Nat. Med.* **7**, 947–953 (2001).

180. Gao, H. *et al.* Evidence of a causal relationship between adiponectin levels and insulin sensitivity: A mendelian randomization study. *Diabetes* **62**, 1338–1344 (2013).

181. Xin, X., Zhou, L., Reyes, C. M., Liu, F. & Dong, L. Q. APPL1 mediates adiponectin-stimulated p38 MAPK activation by scaffolding the TAK1-MKK3-p38 MAPK pathway. *Am. J. Physiol. - Endocrinol. Metab.* **300**, E103–E110 (2011).

182. Ono, K. & Han, J. The p38 signal transduction pathway Activation and function. *Cell. Signal.* **12**, 1–13 (2000).

183. Devchand, P. R. *et al.* The PPARa-leukotriene B4 pathway to inflammation control. *Nature* **384**, 39–43 (1996).

184. Tsuchida, A. *et al.* Preoxisome Proliferator-Activated Receptor (PPAR) alpha Activation Increases Adiponectin Receptors and Reduces Obesity-Related Inflammation in Adipose Tissue. *Diabetes* **54**, 3358–3370 (2005).

185. Parker-Duffen, J. L. *et al.* Divergent roles for Adiponectin receptor 1 (adipor1) and AdipoR2 in mediating revascularization and metabolic dysfunction in vivo. *J. Biol. Chem.* **289**, 16200–16213 (2014).

186. Bjursell, M. *et al.* Opposing effects of adiponectin receptors 1 and 2 on energy metabolism. *Diabetes* **56**, 583–593 (2007).

187. Inukai, K. *et al.* Regulation of adiponectin receptor gene expression in diabetic mice. *Am. J. Physiol. - Endocrinol. Metab.* **288**, E876–E882 (2005).

188. Beylot, M., Pinteur, C. & Peroni, O. Expression of the adiponectin receptors AdipoR1 and AdipoR2 in lean rats and in obese Zucker rats. *Metabolism.* **55**, 396–401 (2006).

189. Almabouada, F. *et al.* Adiponectin Receptors Form Homomers and Heteromers Exhibiting Distinct Ligand Binding and Intracellular Signaling. *J. Biol. Chem.* **288**, 3112–3125 (2013).

190. Hug, C. *et al.* T-cadherin is a receptor for hexameric and high-molecular-weight forms of Acrp30/adiponectin. *Proc. Natl. Acad. Sci. U. S. A.* **101**, 10308–13 (2004).

191. Parker-Duffen, J. L. *et al.* T-cadherin is essential for adiponectin-mediated revascularization. *J. Biol. Chem.* **288**, 24886–24897 (2013).

192. Denzel, M. S. *et al.* T-cadherin is critical for adiponectin-mediated cardioprotection in mice. *J. Clin. Invest.* **120**, 4342–4352 (2010).

193. Obata, Y. *et al.* Relationship between serum adiponectin levels and age in healthy subjects and patients with type 2 diabetes. *Clin. Endocrinol. (Oxf).* **79**, 204–210 (2013).

194. Mankowska, A., Nowak, L. & Sypniewska, G. Adiponectin and Metabolic Syndrome in Women at Menopause. *EJIFCC* **19**, 173–84 (2009).

195. Koh, S. J. *et al.* Influence of age and visceral fat area on plasma adiponectin concentrations in women with normal glucose tolerance. *Clin. Chim. Acta* **389**, 45–50 (2008).

196. Jürimäe, J. & Jürimäe, T. Plasma adiponectin concentration in healthy pre- and postmenopausal women: relationship with body composition, bone mineral, and metabolic variables. *Am. J. Physiol. Endocrinol. Metab.* **293**, E42-7 (2007).

197. Alzmon, G. *et al.* Adiponectin Levels and Genotype: A Potential Regulator of Life Span in Humans. **63**, 447–453 (2008).

198. Otabe, S. *et al.* Overexpression of human adiponectin in transgenic mice results in suppression of fat accumulation and prevention of premature death by high-calorie diet. *Am. J. Physiol. - Endocrinol. Metab.* **293**, E210–E218 (2007).

199. Yu, J. G. *et al.* The Effect of Thiazolidinediones on Plasma Adiponectin Levels in Normal , Obese , and Type 2 Diabetic Subjects. *Diabetes* **51**, 2968–2974 (2002).

200. Ouchi, N. *et al.* Novel modulator for endothelial adhesion molecules: adipocyte-derived plasma protein adiponectin. *Circulation* **100**, 2473–2746 (1999).

201. Iwahashi, H. *et al.* Plasma Adiponectin Levels in Women with Anorexia Nervosa. *Horm. Metab. Res.* **35**, 537–540 (2003).

202. Esfahani, M., Movahedian, A., Baranchi, M. & Goodarzi, M. T. Adiponectin: an adipokine with protective features against metabolic syndrome. *Iran. J. Basic Med. Sci.* **18**, 430–442 (2015).

203. Li, S., Shin, H. J., Ding, E. L. & van Dam, R. M. Adiponectin Levels and Risk of Type 2 Diabetes. *Jama* **302**, 179–188 (2009).

204. Chow, W. S. *et al.* Hypoadiponectinemia as a predictor for the development of hypertension: A 5-year prospective study. *Hypertension* **49**, 1455–1461 (2007).

205. Kondo, H. *et al.* Association of adiponectin mutation with type 2 diabetes: A candidate gene for the insulin resistance syndrome. *Diabetes* **51**, 2325–2328 (2002).

206. Zhang, H., Mo, X., Hao, Y. & Gu, D. Association between polymorphisms in the adiponectin gene and cardiovascular disease: A meta-analysis. *BMC Med. Genet.* **13**, 40 (2012).

207. Arita, Y. *et al.* Paradoxical decrease of an adipose-specific protein, adiponectin, in obesity. *Biochem. Biophys. Res. Commun.* **257**, 79–83 (1999).

208. Ye, R. & Scherer, P. E. Adiponectin, driver or passenger on the road to insulin sensitivity? *Mol. Metab.* **2**, 133–141 (2013).

209. Parida, S., Siddharth, S. & Sharma, D. Adiponectin, obesity, and cancer: Clash of the bigwigs in health and disease. *Int. J. Mol. Sci.* **20**, 2519 (2019).

210. Veluri, G. *et al.* Serum adiponectin levels in patients with rheumatoid arthritis. *Indian J. Rheumatol.* **14**, 119–122 (2019).

211. Li, P. *et al.* Low-molecular-weight adiponectin is more closely associated with disease activity of rheumatoid arthritis than other adiponectin multimeric forms. *Clin. Rheumatol.* **34**, 1025–1030 (2015).

212. De Rosa, A. *et al.* Adiponectin oligomers as potential indicators of adipose tissue improvement in obese subjects. *Eur. J. Endocrinol.* **169**, 37–43 (2013).

213. Hamilton, M. P. *et al.* Adiponectin and cardiovascular risk profile in patients with type 2 diabetes mellitus: Parameters associated with adiponectin complex distribution. *Diabetes Vasc. Dis. Res.* **8**, 190–194 (2011).

214. Daniele, A. *et al.* Adiponectin oligomerization state and adiponectin receptors airway expression in chronic obstructive pulmonary disease. *Int. J. Biochem. Cell Biol.* **44**, 563–569 (2012).

215. Pajvani, U. B. *et al.* Complex Distribution, Not Absolute Amount of Adiponectin, Correlates with Thiazolidinedione-mediated Improvement in Insulin Sensitivity. *J. Biol. Chem.* **279**, 12152–12162 (2004).

216. Nagai, R. *et al.* Succination of protein thiols during adipocyte maturation: a biomarker of mitochondrial stress. *J. Biol. Chem.* **282**, 34219–34228 (2007).

217. Frizzell, N. *et al.* Succination of thiol groups in adipose tissue proteins in diabetes: succination inhibits polymerization and secretion of adiponectin. *J. Biol. Chem.* **284**, 25772–25781 (2009).

218. Pajvani, U. B. *et al.* Structure-function studies of the adipocyte-secreted hormone Acrp30/adiponectin: Implications for metabolic regulation and bioactivity. *J. Biol. Chem.* **278**, 9073–9085 (2003).

219. Kubota, N. *et al.* Disruption of adiponectin causes insulin resistance and neointimal formation. *J. Biol. Chem.* **277**, 25863–25866 (2002).

220. Nawrocki, A. R. *et al.* Mice lacking adiponectin show decreased hepatic insulin sensitivity and reduced responsiveness to peroxisome proliferator-activated receptor gamma agonists. *J. Biol. Chem.* **281**, 2654–2660 (2006).

221. Yano, W. *et al.* Molecular mechanism of moderate insulin resistance in adiponectin-knockout mice. *Endocr. J.* **55**, 515–522 (2008).

222. Maeda, N. *et al.* Diet-induced insulin resistance in mice lacking adiponectin/ACRP30. *Nat. Med.* **8**, 731–737 (2002).

223. Okada-Iwabu, M. *et al.* A small-molecule AdipoR agonist for type 2 diabetes and short life in obesity. *Nature* **503**, 493–499 (2013).

224. Kim, Y. *et al.* The adiponectin receptor agonist AdipoRon ameliorates diabetic nephropathy in a model of type 2 diabetes. *J. Am. Soc. Nephrol.* **29**, 1108–1127 (2018).

225. Choi, S. R. *et al.* Adiponectin receptor agonist AdipoRon decreased ceramide, and lipotoxicity, and ameliorated diabetic nephropathy. *Metabolism.* **85**, 348–360

(2018).

226. Fairaq, A., Shawky, N. M., Osman, I., Pichavaram, P. & Segar, L. AdipoRon, an adiponectin receptor agonist, attenuates PDGF-induced VSMC proliferation through inhibition of mTOR signaling independent of AMPK: Implications toward suppression of neointimal hyperplasia. *Pharmacol. Res.* **119**, 289–302 (2017).

227. Liu, X. H., Pan, J. P., Bauman, W. A. & Cardozo, C. P. AdipoRon prevents myostatin-induced upregulation of fatty acid synthesis and downregulation of insulin activity in a mouse hepatocyte line. *Physiol. Rep.* **7**, 1–12 (2019).

228. Akimoto, M., Maruyama, R., Kawabata, Y., Tajima, Y. & Takenaga, K. Antidiabetic adiponectin receptor agonist AdipoRon suppresses tumour growth of pancreatic cancer by inducing RIPK1/ERK-dependent necroptosis. *Cell Death Dis.* **9**, 1–18 (2018).

229. Naot, D., Musson, D. S. & Cornish, J. The Activity of Adiponectin in Bone. *Calcif. Tissue Int.* **100**, 486–499 (2017).

230. Jürimäe, J., Rembel, K., Jürimäe, T. & Rehand, M. Adiponectin is Associated with Bone Mineral Density in Perimenopausal Women. *Horm. Metab. Res.* **37**, 297–302 (2005).

231. Michaelsson, K. *et al.* Serum adiponectin in elderly men does not correlate with fracture risk. *J Clin Endocrinol Metab* **93**, 4041–4047 (2008).

232. Zoico, E. *et al.* Relation between adiponectin and bone mineral density in elderly post-menopausal women: Role of body composition, leptin, insulin resistance, and dehydroepiandrosterone sulfate. *J. Endocrinol. Invest.* **31**, 297–302 (2008).

233. Ozkurt, B. *et al.* The relationship between serum adiponectin level and anthropometry, bone mass, osteoporotic fracture risk in postmenopausal women. *Jt. Dis. Relat. Surg.* **20**, 78–84 (2009).

234. Barbour, K. E. *et al.* Adipokines and the risk of fracture in older adults. *J. Bone Miner. Res.* **26**, 1568–1576 (2011).

235. Kontogianni, M. D., Dafni, U. G., Routsias, J. G. & Skopouli, F. N. Blood Leptin and Adiponectin as Possible Mediators of the Relation Between Fat Mass and BMD in Perimenopausal Women. *J. Bone Miner. Res.* **19**, 546–551 (2004).

236. King, G. A., Deemer, S. E. & Thompson, D. L. Relationship between leptin, adiponectin, bone mineral density, and measures of adiposity among pre-menopausal hispanic and caucasian women. *Endocr. Res.* **35**, 106–117 (2010).

237. Komorita, Y. *et al.* Serum adiponectin predicts fracture risk in individuals with type 2 diabetes: the Fukuoka Diabetes Registry. *Diabetologia* **60**, 1922–1930

(2017).

238. Kanazawa, I. *et al.* Relationships between serum adiponectin levels versus bone mineral density, bone metabolic markers, and vertebral fractures in type 2 diabetes mellitus. *Eur. J. Endocrinol.* **160**, 265–273 (2009).

239. Doherty, A. L. *et al.* Adiponectin is a candidate biomarker of lower extremity bone density in men with chronic spinal cord injury. *J. Bone Miner. Res.* **29**, 251–9 (2014).

240. Okuno, S. *et al.* Serum adiponectin and bone mineral density in male hemodialysis patients. *Osteoporos. Int.* **23**, 2027–2035 (2012).

241. Misra, M. *et al.* Relationships between serum adipokines, insulin levels, and bone density in girls with anorexia nervosa. *J. Clin. Endocrinol. Metab.* **92**, 2046–2052 (2007).

242. Sayers, A. *et al.* Adiponectin and Its Association With Bone Mass Accrual in Childhood. **25**, 2212–2220 (2010).

243. Rhie, Y. J., Lee, K. H., Chung, S. C., Kim, H. S. & Kim, D. H. Effects of body composition, leptin, and adiponectin on bone mineral density in prepubertal girls. *J. Korean Med. Sci.* **25**, 1187–1190 (2010).

244. Carrasco, F. *et al.* Changes in bone mineral density, body composition and adiponectin levels in morbidly obese patients after bariatric surgery. *Obes. Surg.* **19**, 41–46 (2009).

245. Zhang, Z.-L. *et al.* Association between SNP and haplotypes in PPARGC1 and adiponectin genes and bone mineral density in Chinese nuclear families. *Acta Pharmacol. Sin.* **28**, 287–295 (2007).

246. Kim, H. Y. *et al.* Association of ADIPOR1 polymorphisms with bone mineral density in postmenopausal Korean women. *Exp. Mol. Med.* **44**, 394–402 (2012).

247. Shinoda, Y. *et al.* Regulation of bone formation by adiponectin through autocrine/paracrine and endocrine pathways. *J. Cell. Biochem.* **99**, 196–208 (2006).

248. Williams, G. A. *et al.* In vitro and in vivo effects of adiponectin on bone. *Endocrinology* **150**, 3603–3610 (2009).

249. Naot, D. *et al.* Reduced bone density and cortical bone indices in female adiponectin-knockout mice. *Endocrinology* **157**, 3550–3561 (2016).

250. Gui, Y., Silha, J. V. & Murphy, L. J. Sexual dimorphism and regulation of resistin, adiponectin, and leptin expression in the mouse. *Obes. Res.* **12**, 1481–1491 (2004).

251. Glatt, V., Canalis, E., Stadmeyer, L. & Bouxsein, M. L. Age-related changes in

trabecular architecture differ in female and male C57BL/6J mice. *J. Bone Miner. Res.* **22**, 1197–1207 (2007).

252. Tu, Q. *et al.* Adiponectin inhibits osteoclastogenesis and bone resorption via APPL1-mediated suppression of Akt1. *J. Biol. Chem.* **286**, 12542–53 (2011).

253. Oshima, K. *et al.* Adiponectin increases bone mass by suppressing osteoclast and activating osteoblast. *Biochem. Biophys. Res. Commun.* **331**, 520–526 (2005).

254. Mitsui, Y. *et al.* Hyperadiponectinemia enhances bone formation in mice. *BMC Musculoskelet Disord* **12**, 18 (2011).

255. Wu, X. *et al.* An Adiponectin Receptor Agonist Reduces Type 2 Diabetic Periodontitis. *J. Dent. Res.* **98**, 313–321 (2019).

256. Lin, Y. Y. *et al.* Adiponectin receptor 1 regulates bone formation and osteoblast differentiation by GSK-3β/β-catenin signaling in mice. *Bone* **64**, 147–54 (2014).

257. Wang, F. *et al.* Deficiency of Adiponectin Protects against Ovariectomy-Induced Osteoporosis in Mice. *PLoS One* **8**, e68497 (2013).

258. Wang, Q. *et al.* Adiponectin exerts its negative effect on bone metabolism via OPG/RANKL pathway: an in vivo study. *Endocrine* **47**, 845–853 (2014).

259. Ealey, K. N., Kaludjerovic, J., Archer, M. C. & Ward, W. E. Adiponectin is a negative regulator of bone mineral and bone strength in growing mice. *Exp. Biol. Med.* **233**, 1546–1553 (2008).

260. FVB Mouse Strain datasheet. *The Jackson Laboratory* (2019).

261. C57BL/6 Mouse Strain Datasheet. *The Jackson Laboratory* (2019). Available at: https://www.criver.com/products-services/find-model/c57bl6-mouse?region=3611. (Accessed: 3rd September 2019)

262. Ziemke, F. & Mantzoros, C. S. Adiponectin in insulin resistance: Lessons from translational research. *Am. J. Clin. Nutr.* **91**, 258S-261S (2010).

263. Kanazawa, I. *et al.* Adiponectin and AMP kinase activator stimulate proliferation, differentiation, and mineralization of osteoblastic MC3T3-E1 cells. *BMC Cell Biol.* **8**, 51 (2007).

264. Luo, X.-H. *et al.* Adiponectin stimulates human osteoblasts proliferation and differentiation via the MAPK signaling pathway. *Exp. Cell Res.* **309**, 99–109 (2005).

265. Huang, C. Y. *et al.* Adiponectin increases BMP-2 expression in osteoblasts via AdipoR receptor signaling pathway. *J. Cell. Physiol.* **224**, 475–483 (2010).

266. Hyun, W. L. *et al.* Adiponectin stimulates osteoblast differentiation through

induction of COX2 in mesenchymal progenitor cells. *Stem Cells* **27**, 2254–2262 (2009).

267. Pu, Y. *et al.* Adiponectin Promotes Human Jaw Bone Marrow Stem Cell Osteogenesis. *J. Dent. Res.* **95**, 769–775 (2016).

268. Luo, X.-H. *et al.* Adiponectin stimulates RANKL and inhibits OPG expression in human osteoblasts through the MAPK signaling pathway. *J. Bone Miner. Res.* **21**, 1648–1656 (2006).

269. Erben, R. G. Embedding of bone samples in methylmethacrylate: An improved method suitable for bone histomorphometry, histochemistry, and immunohistochemistry. *J. Histochem. Cytochem.* **45**, 307–313 (1997).

270. Picelli, S. *et al.* Full-length RNA-seq from single cells using Smart-seq2. *Nat. Protoc.* **9**, 171–181 (2014).

271. Hart, D., Mootoosamy, I., Doyle, D. & Spector, T. The Relationship Between Osteoarthritis and Osteoporosis in the General Population: The Chingford Study. *Ann. Rheum. Dis.* **53**, 158–162 (1994).

272. Reginster, J. Y. & Burlet, N. Osteoporosis: A still increasing prevalence. *Bone* **38**, S4–S9 (2006).

273. Hernlund, E. *et al.* Osteoporosis in the European Union: Medical management, epidemiology and economic burden: A report prepared in collaboration with the International Osteoporosis Foundation (IOF) and the European Federation of Pharmaceutical Industry Associations (EFPIA). *Arch. Osteoporos.* **8**, 136 (2013).

274. Osteoporosis: assessing the risk of fragility fracture, clinical guidelines. *NICE Guideline* 6 (2012).

275. Cauley, J. A. Estrogen and bone health in men and women. *Steroids* **99**, 11–15 (2015).

276. Felson, D. T., Zhang, Y., Hannan, M. T. & Anderson, J. J. Effects of weight and body mass index on bone mineral density in men and women: the Framingham study. *J. Bone Miner. Res.* **8**, 567–573 (1993).

277. Sozen, T., Ozisik, L. & Calik Basaran, N. An overview and management of osteoporosis. *Eur. J. Rheumatol.* **4**, 46–56 (2017).

278. NICE. Osteoporosis: Prevention of fragility fractures. *Clinical Knowledge Summaries* (2016). doi:2016

279. Kennel, K. A. & Drake, M. T. Adverse Effects of Bisphosphonates: Implications for Osteoporosis Management. *Mayo Clin. Proc.* **84**, 632–638 (2009).

280. Bauer, D. C. Osteoporosis Treatment After Hip Fracture: Bad News and Getting

worse. *JAMA Netw. Geriatr.* **1**, e80844 (2018).

281. Black, D. M. & Rosen, C. J. Postmenopausal Osteoporosis. *N. Engl. J. Med.* **364**, 254–262 (2016).

282. Leibson, C. L., Tosteson, A. N. A., Gabriel, S. E., Ransom, J. E. & Melton, L. J. Mortality, disability, and nursing home use for persons with and without hip fracture: a population-based study. *J. Am. Geriatr. Soc.* **50**, 1644–1650 (2002).

283. Kuo, T. R. & Chen, C. H. Bone biomarker for the clinical assessment of osteoporosis: Recent developments and future perspectives. *Biomark. Res.* **5**, 5–13 (2017).

284. Upadhyay, J., Farr, O. M. & Mantzoros, C. S. The role of leptin in regulating bone metabolism. *Metabolism* **64**, 105–113 (2015).

285. Lawson, E. A. *et al.* Hormone predictors of abnormal bone microarchitecture in women with anorxia nervosa. *Bone* **46**, 458 (2010).

286. Cirmanová, V., Bayer, M., Stárka, L. & Zajíčková, K. The effect of leptin on bone - An evolving concept of action. *Physiol. Res.* **57**, S143–S151 (2008).

287. Thomas, T. *et al.* Role of serum leptin, insulin, and estrogen levels as potential mediators of the relationship between fat mass and bone mineral density in men versus women. *Bone* **29**, 114–120 (2001).

288. Lenchik, L. *et al.* Adiponectin as a novel determinant of bone mineral density and visceral fat. *Bone* **33**, 646–651 (2003).

289. Biver, E. *et al.* Influence of adipokines and ghrelin on bone mineral density and fracture risk: A systematic review and meta-analysis. *J. Clin. Endocrinol. Metab.* **96**, 2703–2713 (2011).

290. Gupta, V., Mishra, S., Mishra, S., Kumar, S. & Gupta, V. Association of Leptin:Adiponectin ratio and metabolic risk markers in postmenopausal women. *Immunol. Lett.* **196**, 63–67 (2018).

291. Rueda-Clausen, C. F. *et al.* The presence of abdominal obesity is associated with changes in vascular function independently of other cardiovascular risk factors. *Int. J. Cardiol.* **139**, 32–41 (2010).

292. Ashizawa, N. *et al.* Serum leptin-adiponectin ratio and endometrial cancer risk in postmenopausal female subjects. *Gynecol. Oncol.* **119**, 65–69 (2010).

293. Fuggle, N. R. *et al.* Relationships between markers of inflammation, grip strength and bone mineral density: findings from the Hertfordshire Cohort Study. *Osteoporos. Int.* **29**, 1581–1589 (2018).

294. Richards, J. B., Valdes, A. M., Burling, K., Perks, U. C. & Spector, T. D. Serum

adiponectin and bone mineral density in women. *J. Clin. Endocrinol. Metab.* **92**, 1517–1523 (2007).

295. Patel, I. & Zaro, S. Diagnosis and management of osteoporosis. *SAGE Journals* **5**, 509–519 (2012).

296. Kanis, J. A. *et al.* Overview of fracture prediction tools. *J. Clin. Densitom.* **20**, 444–450 (2017).

297. Aso, Y. *et al.* Comparison of serum high-molecular weight (HMW) adiponectin with total adiponectin concentrations in type 2 diabetic patients with coronary artery disease using a novel enzyme-linked immunosorbent assay to detect HMW adiponectin. *Diabetes* **55**, 1954–1960 (2006).

298. Perlman, R. L. Mouse Models of Human Disease: An Evolutionary Perspective. *Evol. Med. Public Heal.* 170- (2016). doi:10.1093/emph/eow014

299. Why are mice considered excellent models for humans? *The Jackson Laboratory* Available at: https://www.jax.org/why-the-mouse/excellent-models. (Accessed: 21st August 2019)

300. Lacey, D. L. *et al.* Osteoprotegerin ligand is a cytokine that regulates osteoclast differentiation and activation. *Cell* **93**, 165–176 (1998).

301. Blake, J. A., Bult, C. J., Kadin, J. A., Richardson, J. E. & Eppig, J. T. The mouse genome database (MGD): Premier model organism resource for mammalian genomics and genetics. *Nucleic Acids Res.* **39**, D842–D848 (2011).

302. Gene: Adipor1. *IMPC phenotyping* Available at: https://www.mousephenotype.org/data/genes/MGI:1919924. (Accessed: 21st August 2019)

303. Gene: Adipor2. *IMPC phenotyping* Available at: https://www.mousephenotype.org/data/genes/MGI:93830. (Accessed: 21st August 2019)

304. The Function of Human Genetic Variation: IMPC Strategy 2021-2030. *The International Mouse Phenotyping Consortium* Available at: https://www.mousephenotype.org/wp-content/uploads/2019/05/IMPC_Strategy_2021-30.pdf. (Accessed: 21st August 2019)

305. Zurita, E. *et al.* Genetic polymorphisms among C57BL/6 mouse inbred strains. *Transgenic Res.* **20**, 481–489 (2011).

306. Sluch, V. M. *et al.* ADIPOR1 is essential for vision and its RPE expression is lost in the Mfrp rd6 mouse. *Sci. Rep.* **8**, 14339 (2018).

307. Boskey, A. L., Wright, T. M. & van der Meulen, M. C. H. Guidelines for describing mouse skeletal phenotype. *J. Orthop. Res.* **21**, 1–5 (2003).

308. Jiang, Y. *et al.* Application of micro-CT assessment of 3-D bone microstructure in preclinical and clinical studies. *J. Bone Miner. Metab.* **23**, 122–131 (2005).

309. Feldkamp, L. A., Goldstein, S. A., Parfitt, A. M., Jesion, G. & Kleerekoper, M. The Direct Examination of Three-Dimensional Bone Architecture In Vitro by Computed Tomography. *J. Bone Miner. Res.* **4**, 3–11 (1989).

310. Kuhn, J. L., Goldstein, S. A., Feldkamp, L. A., Goulet, R. W. & Jesion, G. Evaluation of a microcomputed tomography system to study trabecular bone structure. *J. Orthop. Res.* **8**, 833–842 (1990).

311. Bouxsein, M. L. *et al.* Guidelines for assessment of bone microstructure in rodents using micro-computed tomography. *J. Bone Miner. Res.* **25**, 1468–1486 (2010).

312. Fischer, A. H., Jacobson, K. A., Rose, J. & Zeller, R. Hematoxylin and eosin staining of tissue and cell sections. *Cold Spring Harb. Protoc.* **3**, 1–3 (2008).

313. Oksztulska-Kolanek, E., Znorko, B., Michałowska, M. & Pawlak, K. The biomechanical testing for the assessment of bone quality in an experimental model of chronic kidney disease. *Nephron* **132**, 51–58 (2016).

314. Jepson, K. J., Silva, M. J., Vashishth, D., Guo, X. E. & van de Meulen, M. C. H. Establishing biomechanical mechanisms in mouse models: practical guidelines for systematically evaluating phenotypic changes in the diaphyses of long bones. *J. Bone Miner. Res.* **30**, 951–966 (2015).

315. Somerville, J. M., Aspden, R. M., Armour, K. E., Armour, K. J. & Reid, D. M. Growth of C57Bl/6 Mice and the Material and Mechanical Properties of Cortical Bone from the Tibia. *Calcif. Tissue Int.* **74**, 469–475 (2004).

316. Lin, Y. Y., Chen, C. Y. & Ding, S. T. Adiponectin receptor 1 resists the decline of serum osteocalcin and GPRC6A expression in ovariectomized mice. *PLoS One* **12**, 6–13 (2017).

317. Lubbers, E. R. *et al.* Adiponectin in mice with altered growth hormone action: links to insulin sensitivity and longevity? *J. Endocrinol.* **216**, 363–374 (2013).

318. Williams, G. A. *et al.* Adiponectin knock-out mice have increased trabecular number and bone volume at 14 weeks of age. *Orthop. Proc.* **91-B**, (2018).

319. Wu, N. *et al.* Relationships between serum adiponectin, leptin concentrations and bone mineral density, and bone biochemical markers in Chinese women. *Clin. Chim. Acta* **411**, 771–775 (2010).

320. Dal Maso, L. *et al.* Circulating adiponectin and endometrial cancer risk. *J. Clin.*

Endocrinol. Metab. **89**, 1160–1163 (2004).

321. Mantzoros, C. *et al.* Adiponectin and breast cancer risk. *J. Clin. Endocrinol. Metab.* **89**, 1102–1107 (2004).

322. Song, H. J. *et al.* Gender differences in adiponectin levels and body composition in older adults: Hallym aging study. *BMC Geriatr.* **14**, 1–8 (2014).

323. Boyce, B. F. & Xing, L. The RANKL/RANK/OPG pathway. *Curr. Osteoporos. Rep.* **5**, 98–104 (2007).

324. Vega, D., Maalouf, N. M. & Sakhaee, K. The role of receptor activator of nuclear factor-κB (RANK)/RANK ligand/osteoprotegerin: clinical implications. *J. Clin. Endocrinol. Metab.* **92**, 4514–4521 (2007).

325. Cao, J., Venton, L., Sakata, T. & Halloran, B. P. Expression of RANKL and OPG correlates with age-related bone loss in male C57BL/6 mice. *J. Bone Miner. Res.* **18**, 270–277 (2003).

326. Cho, E. H., Cho, K. H., Lee, H. A. & Kim, S. W. High serum osteopontin levels are associated with low bone mineral density in postmenopausal women. *J. Korean Med. Sci.* **28**, 1496–1499 (2013).

327. Butler, J. S. *et al.* The role of Dkk1 in bone mass regulation: Correlating serum Dkk1 expression with bone mineral density. *J. Orthop. Res.* **29**, 414–418 (2011).

328. Boyce, B. F. *et al.* TNFα and pathologic bone resorption. *Keio J. Med.* **54**, 127–131 (2005).

329. Hodge, J. M., Kirkland, M. A. & Nicholson, G. C. Multiple roles of M-CSF in human osteoclastogenesis. *J. Cell. Biochem.* **102**, 759–768 (2007).

330. Furuhashi, M., Saitoh, S., Shimamoto, K. & Miura, T. Fatty Acid-Binding Protein 4 (FABP4): Pathophysiological insights and potent clinical biomarker of metabolic and cardiovascular diseases. *Clin. Med. Insights Cardiol.* **8**, 23–33 (2014).

331. Goldstein, J. L. & Brown, M. S. History of discovery: the LDL receptor. *Arterioscler. Thromb. Vasc. Biol.* **29**, 431–438 (2009).

332. Wang, Z., Gerstein, M. & Snyder, M. RNA-Seq: a revolutionary tool for transcriptomics. *Nat. Rev. Genet.* **10**, 57–63 (2009).

333. Sandilands, E. A., Dhaun, N., Dear, J. W. & Webb, D. J. Measurement of renal function in patients with chronic kidney disease. *Br. J. Clin. Pharmacol.* **76**, 504–515 (2013).

334. Liao, R. X., Yu, M., Jiang, Y. & Xia, W. Management of osteoporosis with calcitriol in elderly Chinese patients: A systematic review. *Clin. Interv. Aging* **9**, 515–526 (2014).

335. Ardawi, M. S. M. *et al.* High serum sclerostin predicts the occurrence of osteoporotic fractures in postmenopausal women: the center of excellence for osteoporosis research study. *J. Bone Miner. Res.* **27**, 2592–2602 (2012).

336. Brandenburg, V. M. *et al.* Sclerostin in chronic kidney disease-mineral bone disorder think first before you block it! *Nephrol. Dial. Transplant.* **34**, 408–414 (2019).

337. Merchenthaler, I., López, F. J. & Negro-Vilar, A. Anatomy and physiology of central galanin-containing pathways. *Prog. Neurobiol.* **40**, 711–769 (1993).

338. Ackermann, P. W., Finn, A. & Ahmed, M. Sensory neuropeptidergic pattern in tendon, ligament and joint capsule. A study in the rat. *Neuroreport* **10**, 2055–2060 (1999).

339. Qinyang, W., Lindgren, U. J. & Hultenby, K. Distribution of galanin in bone and joint tissues. *Anat. Embryol. (Berl).* **209**, 227–231 (2005).

340. Fuxe, K. *et al.* On the existence and function of galanin receptor heteromers in the central nervous system. *Front. Endocrinol. (Lausanne).* **3**, 127 (2012).

341. McDonald, A. C., Schuijers, J. A., Shen, P. J., Gundlach, A. L. & Grills, B. L. Expression of galanin and galanin receptor-1 in normal bone and during fracture repair in the rat. *Bone* **33**, 788–797 (2003).

342. McDonald, A. C., Schuijers, J. A., Gundlach, A. L. & Grills, B. L. Galanin treatment offsets the inhibition of bone formation and downregulates the increase in mouse calvarial expression of TNFα and GalR2 mRNA induced by chronic daily injections of an injurious vehicle. *Bone* **40**, 895–903 (2007).

343. Onay-Besikci, A., Altarejos, J. Y. & Lopaschuk, G. D. gAd-globular head domain of adiponectin increases fatty acid oxidation in newborn rabbit hearts. *J. Biol. Chem.* **279**, 44320–44326 (2004).

344. Kumar, K. G. *et al.* Adropin deficiency is associated with increased adiposity and insulin resistance. *Obesity* **20**, 1394–1402 (2012).

345. Onal, M. *et al.* Suppression of autophagy in osteocytes mimics skeletal aging. *J. Biol. Chem.* **288**, 17432–17440 (2013).

346. Zhang, G. Y. *et al.* MicroRNA-9 promotes the neuronal differentiation of rat bone marrow mesenchymal stem cells by activating autophagy. *Neural Regen. Res.* **10**, 314–320 (2015).

347. Ogawa, R. *et al.* Identification of candidate genes involved in the radiosensitivity of esophageal cancer cells by microarray analysis. *Dis. Esophagus* **21**, 288–297 (2008).

348. Zhao, S. *et al.* LDOC1 inhibits proliferation and promotes apoptosis by repressing NF-κB activation in papillary thyroid carcinoma. *J. Exp. Clin. Cancer Res.* **34**, 146 (2015).

349. Duzkale, H. *et al.* LDOC1 mRNA is differentially expressed in chronic lymphocytic leukemia and predicts overall survival in untreated patients. *Blood* **117**, 4076–4084 (2011).

350. Yong, B. C. *et al.* LDOC1 regulates Wnt5a expression and osteosarcoma cell metastasis and is correlated with the survival of osteosarcoma patients. *Tumor Biol.* **39**, 1–10 (2017).

351. Saladin, R. *et al.* Transient increase in obese gene expression after food intake or insulin administration. *Nature* **377**, 527–529 (1995).

352. Kubota, N. *et al.* Adiponectin stimulates AMP-activated protein kinase in the hypothalamus and increases food intake. *Cell Metab.* **6**, 55–68 (2007).

353. Tani, T., Orimo, H., Shimizu, A. & Tsuruoka, S. Development of a novel chronic kidney disease mouse model to evaluate the progression of hyperphosphatemia and associated mineral bone disease. *Sci. Rep.* **7**, 2233 (2017).

354. Ostlere, L. & Reeve, J. A case of resolving idiopathic hypoparathyroidism. *Postgrad. Med. J.* **67**, 179–182 (1991).

355. Brandi, M. L. *et al.* Management of hypoparathyroidism: Summary statement and guidelines. *J. Clin. Endocrinol. Metab.* **101**, 2273–2283 (2016).

356. Kim, Y. & Park, C. W. Mechanisms of adiponectin action: Implication of adiponectin receptor agonism in diabetic kidney disease. *Int. J. Mol. Sci.* **20**, 1782 (2019).

357. Bilezikian, J. P. *et al.* Management of hypoparathyroidism: Present and future. *J. Clin. Endocrinol. Metab.* **101**, 2313–2324 (2016).

358. Hassoon, A., Michos, E. D., Miller, E. R., Crisp, Z. & Appel, L. J. Effects of different dietary interventions on calcitriol, parathyroid hormone, calcium, and phosphorus: Results from the DASH trial. *Nutrients* **10**, 367 (2018).

359. Wootton, A. M. Improving the measurement of 25-hydroxyvitamin D. *Clin. Biochem. Rev.* **26**, 33–36 (2005).

360. Kim, H., Kim, M., Im, S.-K. & Fang, S. Mouse Cre-LoxP system: general principles to determine tissue-specific roles of target genes. *Lab. Anim. Res.* **34**, 147–159 (2018).

361. Zhang, M. *et al.* Osteoblast-specific knockout of the insulin-like growth factor (IGF) receptor gene reveals an essential role of IGF signaling in bone matrix

mineralization. *J. Biol. Chem.* **277**, 44005–44012 (2002).

362. Otsuka, E., Yamaguchi, A., Hirose, S. & Hagiwara, H. Characterization of osteoblastic differentiation of stromal cell line ST2 that is induced by ascorbic acid. *Am. J. Physiol. - Cell Physiol.* **277**, C132-138 (1999).

363. Ding, J., Nagai, K. & Woo, J. Insulin-dependent adipogenesis in stromal ST2 cells derived from murine bone marrow. *Biosci. Biotechnol. Biochem.* **67**, 314–321 (2003).

364. Zoch, M. L., Clemens, T. L. & Riddle, R. C. New Insights into the Biology of Osteocalcin. *Bone* **82**, 42–49 (2016).

365. Moseti, D., Regassa, A. & Kim, W. K. Molecular regulation of adipogenesis and potential anti-adipogenic bioactive molecules. *Int. J. Mol. Sci.* **17**, 124 (2016).

366. Ito, R. *et al.* Activation of adiponectin receptors has negative impact on muscle mass in C2C12 myotubes and fast-type mouse skeletal muscle. *PLoS One* **13**, 1–18 (2018).

367. Yamashita, T. *et al.* An orally-active adiponectin receptor agonist mitigates cutaneous fibrosis, inflammation and microvascular pathology in a murine model of systemic sclerosis. *Sci. Rep.* **8**, 1–14 (2018).

368. Wang, Y. G. *et al.* Functional differences between AMPK α1 and α2 subunits in osteogenesis, osteoblast-associated induction of osteoclastogenesis, and adipogenesis. *Sci. Rep.* **6**, 1–14 (2016).

369. Wang, Y. *et al.* Proteomic and functional characterization of endogenous adiponectin purified from fetal bovine serum. *Proteomics* **4**, 3933–3942 (2004).

370. Cao, Z. *et al.* Effects of resin or charcoal treatment on fetal bovine serum and bovine calf serum. *Endocr. Res.* **34**, 101–108 (2009).

371. Bauche, I. B. *et al.* Adiponectin downregulates its own production and the expression of its AdipoR2 receptor in transgenic mice. *Biochem. Biophys. Res. Commun.* **345**, 1414–1424 (2006).

372. Murray, C. J. L. *et al.* UK health performance: findings of the Global Burden of Disease Study 2010. *Lancet* **381**, 997–1020 (2013).

373. Department of Health. *A joint responsibility: doing it differently*. (2006).

374. Health Education England and NHS England. *Musculoskeletal core capabilities framework for first point of contact practitioners*. (2018).

375. Farooqi, I. S. *et al.* Beneficial effects of leptin on obesity, T cell hyporesponsiveness, and neuroendocrine/metabolic dysfunction of human congenital leptin deficiency. *J. Clin. Invest.* **110**, 1093–1103 (2002).

376. Kaur, G. & Dufour, J. M. Cell lines: valuable tools or useless artifacts? *Spermatogenesis* **2**, 1–5 (2012).

377. Johnson, R. W., Sowder, M. E. & Giaccia, A. J. Hypoxia and bone metastatic disease. *Curr. Osteoporos. Rep.* **15**, 231–238 (2017).

378. Regan, J. N. *et al.* Up-regulation of glycolytic metabolism is required for HIF1α-driven bone formation. *PNAS* **111**, 8673–8678 (2014).

379. Lee, H. P. *et al.* Adiponectin promotes VEGF-A-dependent angiogenesis in human chondrosarcoma through PI3K, Akt, mTOR, and HIF-α pathway. *Oncotarget* **6**, 36746–36761 (2015).

380. Abarrategi, A. *et al.* Modeling the human bone marrow niche in mice: From host bone marrow engraftment to bioengineering approaches. *J. Exp. Med.* **215**, 729–743 (2018).

381. Duval, K. *et al.* Modeling physiological events in 2D vs. 3D cell culture. *Physiology* **32**, 266–277 (2017).

382. Diez-Perez, A. *et al.* Treatment failure in osteoporosis. *Osteoporos. Int.* **23**, 2769–2774 (2012).

383. Vieira, H. P. *et al.* Bisphosphonates adherence for treatment of osteoporosis. *Int. Arch. Med.* **6**, 24 (2013).

384. Zhou, B. O. *et al.* Bone marrow adipocytes promote the regeneration of stem cells and hematopoiesis by secreting SCF. *Nat. Cell Biol.* **19**, 891–903 (2017).

385. Simic, P. *et al.* SIRT1 regulates differentiation of mesenchymal stem cells by deacetylating β-catenin. *EMBO Mol. Med.* **5**, 430–440 (2013).

386. Tikhonova, A. N. *et al.* The bone marrow microenvironment at single-cell resolution. *Nature* **569**, 222–228 (2019).

387. Zhang, J. *et al.* Conditional gene manipulation: Cre-ating a new biological era. *J. Zhejiang Univ. Sci. B* **13**, 511–524 (2012).

388. Elefteriou, F. & Yang, X. Genetic mouse models for bone studies-Strengths and limitations. *Bone* **49**, 1242–1254 (2011).

389. Wu, Q. *et al.* Deriving osteogenic cells from induced pluripotent stem cells for bone tissue engineering. *Tissue Eng.* **23**, 1–8 (2017).